

This item is held in Loughborough University's Institutional Repository (<https://dspace.lboro.ac.uk/>) and was harvested from the British Library's EThOS service (<http://www.ethos.bl.uk/>). It is made available under the following Creative Commons Licence conditions.



For the full text of this licence, please go to:  
<http://creativecommons.org/licenses/by-nc-nd/2.5/>

**AERATION**  
**BY**  
**PLUNGING LIQUID JET**

**BY**

**AFZAL AHMED, B.E.( Mech. )**

**A DOCTORAL THESIS**

**Submitted in partial fulfilment of the requirements  
for the award of  
degree of Doctor of Philosophy of the Loughborough University of Technology**

**September, 1974**

**Supervisors:**

**J.Glover**

**Department of Chemical Engineering**

**R.Q.Hepherd**

**National Institute of Agricultural Engineering, Silsoe**



**by Afzal Ahmed**

To:

*Faheda*  
*(my wife)*

*Ibrahim*

*Salma*

*Shama*

*Bilal*

*— my family*

### ACKNOWLEDGEMENTS

The author thanks the following persons and institutions:

- |   |   |
|---|---|
| Mr. J. GLOVER   | for encouragement, friendly guidance and valuable suggestions.  |
| Mr. R. Q. HEPHERD   | for the facilities and valuable suggestions during the work at National Institute of Agricultural Engineering (NIAE), Silsoe. |
| Prof. D. C. FRESHWATER  | for encouragement and facilities for research work.   |
| The British Council   | for financial support during the years 1970-72.   |
| Agricultural Research Council   | for financial support during the years 1972-74.   |
| Pakistan Council of Scientific and Industrial Research (PCSIR)        | for granting the study leave.   |
| Mr. M. HUGHES   | for assistance in analytical work.  |
| Technical staff of Department of Chemical Engineering and NIAE Silsoe | for engineering assistance.   |
| Mrs. A. BEAVEN  | for typing this dissertation nicely.  |
| Author's parents and past teachers                                    | for their efforts and advice.   |
| Author's family   | for patience.   |



### Summary

The air entrainment and oxygen transfer aspects of a plunging aqueous jet have been studied for biological and non-biological systems having properties close to water. Cylindrical nozzles (9.5 - 38.1 mm diameter ( $d_n$ )) and annular nozzles were used and the liquid pool was about one  $m^3$ .

The air entrainment data for cylindrical jet lengths greater than 0.66 m is correlated by the equation:

$$En = 8.7 \times 10^{-5} (Re_j)^{0.77} (We)^{0.15}$$

where En (entrainment ratio) is the ratio of air entrainment rate ( $m^3/s$ ) to jet liquid flow rate ( $m^3/s$ ). The oxygen transfer was measured by the sulphite method under conditions (determined in this work) where maximum oxygen transfer takes place through gas film and the reaction is virtually instantaneous at the interface. Under these conditions, the oxygen transfer by entrainment (J) in kg/h is correlated with the power of the jet ( $P_j$ ) in kW by the equation

$$J = 4 P_j$$

The aeration efficiency of the plunging jet system ( $4 \text{ kgO}_2/\text{kW h} - \text{SO}_3^-$  system) is comparable with those of commercial aeration units. The oxygen transfer in a biological system gives a different correlation:

$$\frac{J_{\text{biol}}^*}{d_n} = 1.96 \times 10^{-2} (P_j)^{0.72}$$

where  $J_{\text{biol}}^*$  is in kg/s,  $d_n$  in m, and  $P_j$  in kW. Moreover, in the biological system the oxygen transfer is directly proportional to the

air entrainment rate and is unaffected by suspended solids; also, the oxygen transfer rate is greater than that in tap water. Mean bubble diameters (1.5 to 6.6 mm), bubble retention time (1 to 9.5 s) and the interfacial area per unit volume of gas hold up ( $5 \text{ cm}^{-1}$ ) all calculated from the sulphite data are in close agreement with the reported values.

The biological system when aerated produced foam which caused loss of liquid and a reduction in the oxygen transfer rate. In continuous operation the foam problems were overcome by using a concealed jet and periodic use of a liquid spray to suppress the foam. Nearly the same (41 and 45 %) reduction in COD and the same (20 - 25%) increase in suspended solids of waste was obtained with short (28 hours) and long (10 days) retention times. The kg COD removed / kW h was in the range 3.3 to 4.9 and the kg BOD removed / kW h was 2.3.

It is concluded that the plunging jet system has a valuable potential as a gas-liquid contactor for waste treatment, chemical and fermentation processes.

NOTATIONS

$a$	interfacial area per unit volume, $m^{-1}$
$A$	total interfacial area, $m^2$
$B_L$	liquid phase reactant concentration, $kg/m^3$
$c$	oxygen concentration at the cell surface, $kg/m^3$
$C$	concentration of oxygen (or absorbing gas) in the liquid, $kg/m^3$
$C_{SO_3}$	sodium sulphite concentration in feed in continuous reactor, $kg/m^3$
$C'$	apparent saturation concentration, equation 6.9, $kg/m^3$
$C'_{SO_3}$	sodium sulphite concentration in product in continuous reactor at steady state, $kg/m^3$
$C^*$	concentration of dissolved oxygen (or gas) at interface, in equilibrium with oxygen (or gas) at interface or saturation concentration, $kg/m^3$ .
$\bar{C}$	equilibrium concentration of dissolved oxygen in liquid in slow reactions, $kg/m^3$
$\hat{C}$	concentration of oxygen in air, $kg/m^3$
$C_c$	concentration of dissolved oxygen corrected to standard conditions or any other conditions signified by symbol $c$ , $kg/m^3$
$C_c^*$	saturation concentration of oxygen corrected to standard conditions or any other conditions signified by symbol $c$ , $kg/m^3$
$C_i$	concentration of dissolved oxygen in the feed, $kg/m^3$
$C_L$	concentration of dissolved oxygen (or absorbing gas) in the bulk liquid, $kg/m^3$
$d_b$	bubble diameter, m or mm
$\bar{d}_b$	average bubble diameter, m or mm
$\bar{d}_{bm}$	mean bubble diameter, m or mm



$d_j$	cylindrical jet diameter at nozzle end ( $= d_n$ ), m or mm
$d_j^*$	envelope diameter of plunging jet, m or mm
$d_{ji}$	inside diameter of annular jet at nozzle end ( $= d_{ni}$ ), m or mm
$d_{jo}$	outside diameter of annular jet at nozzle end ( $= d_{no}$ ), m or mm
$d_n, d_{ni}, d_{no}$	cylindrical and annular nozzle diameters, m or mm
$D$	diffusivity of oxygen (or absorbing gas), $m^2/s$
$D_l$	diffusivity of liquid phase reactant, $m^2/s$
$\bar{D}$	turbulent diffusivity of the absorbing gas equation 2.6, $m^2/s$
$E_n = \frac{Q_a}{Q_l}$	Entrainment ratio stoichiometric coefficient, dimensionless
$g$	gravitational acceleration, $9.8 m/s^2$
$h$	maximum penetration depth of bubbles, m.
$H$	distance between the nozzle and tank liquid surface, m.
$H_e = \frac{P^*}{C^*}$	Henry's law constant, $atm m^3/kg$
$J$	oxygen transfer rate, due to entrainment, $kg/s$
$J^*$	measured oxygen transfer rate, $kg/s$
$\bar{J}$	oxygen or gas mass transfer rate per unit interfacial area, $kg/m^2s$
$K$	oxygen transfer coefficient $s^{-1}$
$K'$	aeration efficiency, $kgO_2/kW h$
$K_g$	gas-film mass transfer coefficient, $m/s$ or $kg/m^2s atm.$
$K_L$	liquid-film mass transfer coefficient, $m/s$
$\dot{K}_L$	chemical mass transfer coefficient, $m/s$
$l_j$	length of liquid jet, m
$l_n$	length of nozzle defined in Fig. 9.2, m or mm.
$m$	mass of gas diffusing into the liquid, kg

$n$	bubble frequency, $s^{-1}$
$N$	number of bubbles
$OC$	oxygenation capacity $kgO_2/m^3s$
$(OC)_c$	oxygenation capacity corrected to standard conditions or any other condition specified by symbol $c$ .
$P$	partial pressure of oxygen (or absorbing gas) in the bulk of gas phase, atm.
$P^*$	partial pressure of oxygen (or absorbing gas) at the interface, atm.
$P'$	barometric pressure, mm Hg.
$\hat{P}$	measured power consumption, W or kW
$P_j$	power of jet, W or kW
$q$	feed or product rate, $m^3/s$
$Q_a$	air entrainment rate, $m^3/s$
$Q_b$	air boundary layer entrainment rate, $m^3/s$
$Q_c$	captured air entrainment rate, $m^3/s$
$Q_f$	fluid entrainment rate, $m^3/s$
$Q_l$	jet liquid flow rate $m^3/s$
$r$	respiration rate, $kg/m^3 s$ or $kg/s$
$r'$	sulphite oxidation rate, $kmol/m^3s$
$\bar{r}$	reaction rate per unit volume of liquid, $kg/m^3s$
$R$	off-centricity of plunge point, m.
$Re_j$	$= \frac{V_j d_n \ell_l}{\eta_l}$ jet Reynolds number
$Re_{lj}$	$= \frac{V_j l_j \ell_a}{\eta_a}$ jet length Reynolds number
$s$	surface renewal rate, $s^{-1}$
$S$	liquid sample, ml.
$t$	time, s
$t_b$	bubble retention time, s.

$t_R$	reaction time, s
$T$	temperature $^{\circ}\text{K}$ or $^{\circ}\text{C}$
$u$	dilution factor
$U$	bubble rise velocity, m/s
$v$	liquid volume per unit interfacial area, m.
$u'$	volume of iodine to which sample is added, ml.
$V$	liquid volume, $\text{m}^3$
$V_e$	minimum entrainment velocity, m/s
$V_g$	gas hold up volume, $\text{m}^3$
$V_j$	velocity of jet, m/s
$w \times u$	per cent dry matter of liquid in waste sample
$W$	mean of thiosulphate titrations on product samples at steady-state, ml.
$W_e = \frac{\rho_a \cdot v_j^2 \cdot d_n}{\sigma}$	Weber number.
$W_l$	liquid mass flow rate, kg/s
$W_o$	mean of thiosulphate titrations on feed samples, ml.
$x$	per cent oxygen saturation
$x'$	apparent saturation concentration as per cent of actual saturation concentration.
$\dot{x}$	distance along axis perpendicular to gas-liquid interface, m or mm.
$x$	fraction of dry suspended solids in waste liquid.
$\bar{x}$	value of $x$ at $t = 0$
$x^*$	measured value of per cent oxygen concentration
$y$	normality of thiosulphate solution, N
$\dot{y}$	per cent dry matter of waste liquid
$z$	normality of iodine solution, N
$\dot{z}$	fraction of dry dissolved solids in waste liquid.

Greek Symbols

$\alpha$	fraction of oxygen absorbed
$\alpha'$	$= K_L a_{\text{waste}} / K_L a_{\text{water}}$
$\beta$	$= C^*_{\text{waste}} / C^*_{\text{water}}$
$\theta$	jet angle to liquid surface, degrees.
$\rho$	density, $\text{kg/m}^3$
$\eta$	viscosity, $\text{N s/m}^2$
$\sigma$	surface tension, $\text{N/m}$
$\epsilon$	error
$\lambda$	thickness of liquid film, m or mm.
$\delta$	distance of interface from reaction plane, m or mm.
$\xi$	chemical enhancement factor equation 3.18.
$\psi$	gas hold up ratio.

Subscripts

a	air
l	liquid
f	fluid



CONTENTS

Page:

ACKNOWLEDGEMENTS	(iii)
SUMMARY	(iv)
1. INTRODUCTION	1
1.1 STATEMENT OF PROBLEM	3
1.2 STRUCTURE OF THESIS	4
2. PHYSICAL MASS TRANSFER FROM GAS TO LIQUID PHASE	8
2.1 THEORIES OF MASS TRANSFER FROM GAS TO LIQUID PHASE	8
2.1.1 Two-film Theory	8
2.1.2 Higbie's Model	10
2.1.3 Danckwerts' Model	10
2.1.4 Dobbins' Model	10
2.1.5 Kishinevski's Model	11
2.2 EFFECT OF PHYSICAL PROPERTIES OF LIQUID ON MASS TRANSFER	12
2.2.1 Viscosity	12
2.2.2 Presence of Surface Active Agents	13
2.2.3 Presence of Suspended Solids	16
2.2.4 Temperature	17
3. MASS TRANSFER WITH CHEMICAL REACTION IN LIQUID PHASE	19
3.1 SLOW REACTION	21
3.2 FAST REACTION	23
3.3 INSTANTANEOUS REACTION	24
4. AERATION OF BIOLOGICAL SYSTEM	30
4.1 MASS TRANSFER IN BIOLOGICAL SYSTEM	31
4.2 AERATION DEVICES	36
4.2.1 Compressed Air Aerators	36
4.2.1.1 Porous diffusers	36
4.2.1.2 Sparger units	37
4.2.1.3 Coarse bubble aerator	38
4.2.1.4 Impingement aerator	38
4.2.1.5 Danjes system	40



CONTENTS (contd.)	Page :
4.2.1.6 Ejector system	40
4.2.1.7 Inka system	40
4.2.1.8 Performance of air diffusion units	42
4.2.2 Mechanical Aerators	44
4.2.2.1 Vortair aerator	44
4.2.2.2 Simplex Hi-Cone aerator	44
4.2.2.3 Simcar cone aerator	48
4.2.2.4 BSK turbine aerator	48
4.2.2.5 Turbine-sparger aerator	48
4.2.2.6 Brush aerator	51
4.2.2.7 Oxidation ditch	53
4.2.2.8 Suction aerator	54
4.2.2.9 Plunging jet aerator	54
4.2.2.10 Vortex or Waldhof system	54
4.2.2.11 Carrousel system	57
4.2.2.12 Performance of mechanical aerators	59
4.3 PROBLEMS ASSOCIATED WITH AERATION DEVICES	59
4.3.1 Air Diffusion Units	59
4.3.2 Mechanical Aerators	60
4.4 ECONOMIC CONSIDERATIONS IN AERATION PROCESSES	61
5. PREVIOUS WORK ON GAS ENTRAINMENT AND MASS TRANSFER IN A PLUNGING JET REACTOR	63
5.1 INSTABILITY OF A TURBULENT LIQUID JET	63
5.2 MECHANISM OF GAS ENTRAINMENT BY LIQUID JET PLUNGING INTO A LIQUID POOL	64
5.3 RELATION OF JET PARAMETERS WITH ENTRAINMENT RATE	71
5.4 BUBBLE SIZE DISTRIBUTION IN A PLUNGING JET SYSTEM	79
5.5 MASS TRANSFER IN A PLUNGING JET REACTOR	80
5.6 DISCUSSION	83
6. MEASUREMENT OF OXYGEN TRANSFER RATE IN AN AERATION PROCESS	85
6.1 UNSTEADY-STATE AERATION OF DEOXYGENATED TAP WATER	88
6.2 STEADY-STATE AERATION OF DEOXYGENATED TAP WATER	88
6.3 MEASUREMENT OF AERATION UNDER PROCESS CONDITIONS	89

CONTENTS (contd.)	Page :
6.4 SODIUM SULPHITE OXIDATION METHOD	91
7. A LITERATURE SURVEY ON SULPHITE OXIDATION	93
8. OXIDATION OF CATALYSED SODIUM SULPHITE SOLUTION IN 100 LITRES QVF VESSEL	100
8.1 EXPERIMENTAL	101
8.1.1 Apparatus for Continuous and Batch Experiments	101
8.1.2 Apparatus for Experiments with Pure Oxygen	103
8.2 EXPERIMENTAL PROCEDURE	104
8.2.1 Procedure for Continuous Experiments	106
8.2.2 Procedure for Batch Experiments	108
8.2.3 Procedure for Experiments with Pure Oxygen	112
8.3 RESULTS AND DISCUSSION	117
8.3.1 Effect of Sulphite Concentration on Oxygen Transfer Rate	117
8.3.2 Effect of Impurities in Tap Water on Oxygen Transfer Rate	117
8.3.3 Effect of the Presence of Sodium Sulphate on Oxygen Transfer Rate in Sulphite Solution	119
8.3.4 Effect of pH on Oxygen Transfer Rate	119
8.3.5 Effect of Catalyst Concentration on Oxygen Transfer Rate	119
8.3.6 Effect of Oxygen Pressure on Oxygen Transfer Rate	122
8.3.7 Effect of Stirrer Speed on Oxygen Transfer Rate	125
8.3.8 Mechanism of Oxygen Transfer	125
8.3.9 The Valid Conditions for Sulphite Method for Measurement of Aeration	127
8.4 100 LITRES QVF VESSEL AS A JET-VORTEX AERATOR	128
9. AIR ENTRAINMENT BY PLUNGING LIQUID JET	130
9.1 EXPERIMENTAL	130
9.2 RESULTS AND DISCUSSION	145
9.2.1 Effect of Jet Velocity on Air Entrainment Rate	146
9.2.2 Effect of Nozzle Diameter on Entrainment Rate	146
9.2.3 Effect of Jet Length on Entrainment Rate	146
9.2.4 Air Flow Through Inner Tube of Annular Nozzle	149
9.2.5 Correlation of Air Entrainment with Power of Jet	149
9.2.6 Comparison of Results with the Data of Other Workers	152
9.2.7 Dimensionless Equation for Air Entrainment	164



## CONTENTS (contd.)

Page:

10.	PLUNGING LIQUID JET REACTOR	168
10.1	EXPERIMENTAL	169
10.2	MIXING IN THE REACTOR	169
10.2.1	Experimental Procedure	170
10.2.2	Results and Discussion	171
10.3	LIQUID FLOW PATTERN IN THE AERATION TANK FOR DIFFERENT JET POSITIONS	173
10.3.1	Flow Pattern Due to Plunging Central and Vertical Jet	176
10.3.2	Flow Pattern Due to Plunging Angular and Central Jet	176
10.3.3	Flow Pattern Due to Plunging Angular and Off-centred Jet	179
10.3.4	Flow Pattern Due to Plunging Vertical and Off-centred Jet.	179
10.4	OXYGEN MASS TRANSFER IN PLUNGING LIQUID JET REACTOR	180
10.4.1	Experimental Procedure	180
10.4.2	Oxygen Transfer by Entrainment	183
10.4.3	Results and Discussion	184
10.4.3.1	Effect of jet length on oxygen transfer rate	184
10.4.3.2	Effect of jet positions on oxygen transfer rate	187
10.4.3.2.1	Effect of centred and off-centred vertical jet on the oxygen transfer rate	188
10.4.3.2.2	Effect of centred angular jets on the oxygen transfer rate	188
10.4.3.2.3	Effect of off-centred and angular jets on oxygen transfer rate	188
10.4.3.3	Effect of Velocity and diameter of jet on the oxygen transfer rate	191
10.4.4	Correlation of Oxygen Transfer Rate with Jet Velocity and Nozzle Diameter	194
10.4.5	Correlation of Oxygen Transfer with Power of Jet	198
10.4.6	Determination of Average Bubble Diameter	204
11.	AERATION OF BIOLOGICAL SYSTEM IN PLUNGING LIQUID JET REACTOR	219
11.1	FOAM PROBLEM	219
11.1.1	Causes of Foaming	219
11.1.2	Foam Control	222
11.1.2.1	Mechanical methods	222

CONTENTS (contd.)	Page:
11.1.2.2 Chemical methods	223
11.1.2.3 Foam control in this work	224
11.2 OXYGEN TRANSFER IN BIOLOGICAL SYSTEM	229
11.2.1 Experimental	229
11.2.2 Measurement of Oxygen Transfer Coefficient	235
11.2.3 Results and Discussion	240
11.2.3.1 Effect of suspended solids on oxygen transfer rate	240
11.2.3.2 Effect of jet velocity and nozzle diameter on oxygen transfer rate	243
11.2.4 Correlation of Oxygen Transfer with Power of Jet	245
11.2.5 Comparison of Oxygen Transfer in Tap Water, Sulphite Solution, and Biological System	247
11.2.6 Correlation of Oxygen Transfer Rate with Entrainment Rate	251
11.3 PERFORMANCE OF PLUNGING JET REACTOR AS CONTINUOUS BIOLOGICAL REACTOR	252
11.3.1 Experimental	252
11.3.2 Results and Discussion on the Performance of Plunging Jet Reactor as a Biological Continuous Reactor	263
11.4 TECHNOLOGICAL POTENTIAL OF PLUNGING JET REACTOR	286
CONCLUSIONS	289
RECOMMENDATIONS FOR FURTHER WORK	294
BIBLIOGRAPHY	296
APPENDICES	
I CALCULATION OF OXYGEN TRANSFER RATES BY IODOMETRIC TITRATION OF SAMPLES FROM SULPHITE OXIDATION EXPERIMENTS	307
II DIMENSIONAL ANALYSIS AS APPLIED TO ENTRAINMENT PHENOMENON	311
III CALCULATION OF AVERAGE BUBBLE DIAMETER	317
IV METHODS FOR DETERMINATION OF POLLUTION PARAMETERS	319
V EXPERIMENTAL RESULTS IN TABULAR FORM	327
VI PLATES	357

**AERATION**  
**BY**  
**PLUNGING LIQUID JET**

## Chapter 1

i



## 1. INTRODUCTION

The subject of this thesis is the aeration of a liquid pool by a plunging liquid jet. The term aeration specifies the oxygen mass transfer aspects of the aeration system.

It is well known that when a liquid jet impacts on to the surface of a liquid pool it entrains the surrounding air into the pool in the form of bubbles. Although this entrainment phenomenon is a process occurring in nature with a resulting enhancement of the gas liquid interfacial area, little has been done towards the understanding and industrial exploitation of this phenomenon.

Note that entrainment phenomenon has detrimental effects in some industrial processes: pouring and filling of molten glass, molten metal, cosmetics, paints and food products. Similarly, air entrainment in bottle filling operations is a problem; often bottles filled with bubble free liquids are desired. The air entrained in bottles when filling with viscous liquids is difficult to remove. Lin and Donnelly (63) studied the entrainment phenomenon to find the velocity below which the entrainment does not occur; hence their work relates to the aspect, where the avoidance of the entrainment is important.

Sometimes the entrainment is a desirable phenomenon. The enhancement of this phenomenon could have great potential as a gas liquid contacting device in chemical, fermentation, and waste treatment processes.

The potential of this phenomenon as an efficient gas-liquid contacting method was first realized by Mertes (73) who registered

a US patent for this invention in 1938. He showed that the oxidation in a plunging jet system is 4 times more than that obtained with a spray nozzle and 2 times more than that obtained by bubbling the air at the bottom of the tank. Several other claims have been made as regards the superiority of this method over the conventional gas-liquid contacting methods and will be described later.

The obvious advantages of aeration by the plunging jet invites its application to the fermentation, and especially waste treatment processes since the treatment of waste has no returns to waste producing agencies. The advantages other than the simplicity are:-

- (a) The free oxygen from the air is used.
- (b) The jet does both the job of aeration and mixing.

Note that nature has also chosen in different forms this method for the self purification of river streams. The intensive aeration caused by the water falls and the aeration due to numerous hydraulic jumps experienced by the river streams during their flow on uneven grounds are the excellent examples of aeration by entrainment. Böhnke (10) has reported that in West Germany this method was applied on a large scale for the treatment of waste water obtained from a community of 25,000 inhabitants. The aeration was accomplished by multiple angular liquid jets, which also maintained the circulation of the liquid in a ditch constructed with a return flow.

A great interest has grown during the past few years towards the understanding of the entrainment mechanism and the prediction



of the entrainment rates. There had been constant creative efforts to design better experimental techniques for measurement of entrainment rates; however, more emphasis has been given to the mechanism and measurement of the entrainment rates than to the oxygen mass transfer aspects of the system. In this author's opinion, the oxygen mass transfer studies should be given priority because of their practical value.' Also, the diameters of jets used in the previous investigations were so small that the results obtained with these jets pose the question of scale-up for practical systems. The results so far reported are inconsistent in many respects and this will be described later. In addition, the oxygen mass transfer in biological systems with reference to the plunging jet system has not yet been studied. Therefore, a systematic study on oxygen mass transfer aspects with reference to air entrainment is needed; hence, the present work was undertaken to satisfy this need.

#### 1.1 STATEMENT OF THE PROBLEM

The purpose of this work was to investigate how the jet parameters affected the air entrainment and oxygen mass transfer rates in a plunging jet aeration system containing biological or non biological liquids; to explore the potential of the system as a gas liquid contacting device for chemical processes and as an aeration device for fermentation and waste treatment processes.

This study is limited to the liquids whose physical properties can be assumed equal to that of water under practical situations.

## 1.2 STRUCTURE OF THE THESIS

To present the work in a logical sequence, the text is divided into 11 chapters. The logic of the matter presented in a chapter is maintained through its sections. The relevance of each chapter with reference to the structure of the thesis is discussed below.

Chapters 2 to 4 summarise the background knowledge of the theories on (1) physical mass transfer; (2) mass transfer with chemical reaction; and (3) mass transfer in a biological system. Chapter 4 also discusses various aeration devices. The knowledge gained from these chapters will help in understanding some important results presented later. Similarly, the knowledge of various aeration devices — regarding construction, performance, and problems — will help in appreciating the potential of a plunging jet aeration system.

Chapter 5 reviews all the previous work on the mechanism of entrainment, prediction of entrainment rate, and mass transfer in a plunging jet aeration system.

The various methods for the measurement of oxygen mass transfer are described in chapter 6. From here the widely used sulphite method was chosen. Therefore it was necessary to deal with sulphite oxidation in detail; hence, chapter 7 presents a literature survey on sulphite oxidation. The literature survey revealed, the sulphite method should be investigated further. So, in the beginning, the objective was to determine the valid conditions under which the sulphite method could be used to



measure aeration. Chapter 8 presents this part of the investigation, and gives the valid conditions under which the oxygen mass transfer studies should be carried out in an aeration system.

Chapter 9 deals with the study of air entrainment in terms of the jet parameters; and, finally, gives dimensionless correlation for the estimation of entrainment rate.

Then chapter 10 presents qualitatively the mixing and flow patterns produced by the jets in different positions. Chapter 10 also contains the study on oxygen mass transfer aspects and the correlation of oxygen mass transfer with the power of the jet. The knowledge of the air entrainment and oxygen transfer rates at certain jet conditions led to the determination of bubble sizes and some other factors.

The mass transfer studies in the biological system are presented in chapter 11. The aeration of the biological system results in a foam problem. So, this chapter begins with a discussion on foam problem at some length and then gives its solution. Next, the effect of jet parameters on the oxygen transfer rate is presented. A correlation of oxygen transfer with the power of jet is also derived. A comparison of the oxygen transfer rate in the sulphite system, biological system, and the tap water is also made. In practice, the jet aeration system will work as a continuous aeration system; so finally, a study of the performance of the jet aeration system as a continuous biological reactor at short (28 hours) and long residence time (10 days) is presented.

Main conclusions from this study are drawn. Truly speaking, no research work can ever be complete; instead, it illuminates some more research problems. Hence, the author gives some suggestions stemming from this work, which could be the basis for further research. A bibliography is added which gives the references of all the authors whose ideas and findings were either referred to or used in the preparation of this dissertation, and the author acknowledges these references.

Finally, six appendices are included which contain derivation of dimensionless equation for the air entrainment, calculation of average bubble diameter, standard methods for the analytical work carried out in this investigation, the experimental results in tabular form, and the photographs referred to in the text.

## Chapter 2

## 2. PHYSICAL MASS TRANSFER FROM GAS TO LIQUID PHASE

This chapter is a brief account of existing theories on physical mass transfer from gas to liquid phase.

Also, the effect of the physical nature of the liquid on the transfer process has been reviewed.

### 2.1 THEORIES OF MASS TRANSFER FROM GAS TO LIQUID PHASE

Whenever two phases not in chemical equilibrium with one another are brought together, mass transfer between the two phases takes place until chemical equilibrium is reached. Mass transfer takes place through the interface and various models have been proposed to account for the overall rate of mass transfer.

#### 2.1.1 Two-Film Theory

Lewis and Whitman (62) in 1924 proposed the two-film theory in which it is assumed that there are thin stagnant films of gas and liquid at the gas-liquid interface and a steady-state gas transfer occurs by molecular diffusion through these films. For a less soluble gas, the gas film offers negligible resistance and the liquid film is almost saturated with the gas at the interface. Moreover, the liquid beneath the film is assumed to be mixed at such a rate that the concentration of gas in the bulk remains uniform. Mathematically, the steady-state rate of gas transfer  $(\frac{dm}{dt})$  across the liquid film of thickness  $\lambda$  is given by:

$$\frac{dm}{dt} = D A \frac{(C^* - C_L)}{\lambda} \quad 2.1$$



where  $D$  is diffusivity of the absorbing gas,  $A$  is the total gas-liquid interfacial area,  $C^*$  is the saturation concentration of the absorbing gas in the liquid, and  $C_L$  is the concentration of the absorbing gas in the bulk liquid.  $\left(\frac{C^* - C_L}{\lambda}\right)$  is the driving concentration gradient.

Since  $K_L = D/\lambda$ , therefore, equation 2.1 can be written as:

$$\frac{dm}{dt} = K_L A (C^* - C_L) \quad 2.2$$

Also:  $m = C_L \cdot V$ ,

where  $V$  is volume of the bulk liquid. Hence, equation 2.2 can be written again as:

$$\frac{dC_L}{dt} = K_L a (C^* - C_L) \quad 2.3$$

where  $a = A/V$ , and is called as specific interfacial area.

The principal objection to this theory is the assumption of steady-state rate of transfer and stagnant films which is no longer valid in turbulent liquids. In a turbulent liquid the liquid film at the interface is being continuously replaced by the liquid below it. The concentration of dissolved gas in the fresh film is uniform and equal to the bulk concentration. The interface concentration of this film increases during its exposure by unsteady-state molecular diffusion until the concentration gradient approaches the constant value of  $\left(\frac{C^* - C_L}{\lambda}\right)$ .

### 2.1.2 Higbie's Model

Higbie (49), in 1935, approached this unsteady-state transfer and developed a model by applying equations of transient molecular diffusion in liquids of infinite depth and assuming that the time of renewal of all the surface elements is the same.

### 2.1.3 Danckwerts' Model

Danckwerts (27) modified Higbie's model and assumed that the distribution of all the surface elements is completely a random function. Applying this assumption, Danckwerts showed that the transfer rate of gas into a turbulent liquid is given by

$$J = \sqrt{D s} A (C^* - C_L) \quad 2.4$$

where  $s$  is the surface renewal rate and can be defined as the average frequency with which any particular vertical element is mixed.

### 2.1.4 Dobbins' Model

Dobbins (33) reported that the results obtained from aeration of rivers and streams still support the concept of laminar surface film and hence Danckwerts' model is inadequate when applied to turbulent deep mass of liquids. From this it follows that the concept of a stagnant film at the interface should not be abandoned. It may be assumed that the film exists in a statistical sense, the film being always present, with the liquid of which it is composed being continuously replaced by the liquid below it. Based on this assumption, Dobbins developed a model which combined the random exchange function with the boundary conditions of a liquid film of



finite thickness. Dobbins showed that the mass transfer coefficient can be expressed by the equation

$$K_L = \sqrt{Ds} \coth \sqrt{\frac{s \lambda^2}{D}} \quad 2.5$$

#### 2.1.5 Kishinevski's Model

Kishinevski (58) disagreed with the assumption of laminar surface film and showed by experiments that in a turbulent liquid the gas transfer is controlled by turbulent diffusivity rather than by the diffusivity of the transferring gas. Kishinevski expresses  $K_L$  as

$$K_L = \frac{2}{\sqrt{\pi}} \sqrt{(\bar{D} + D)s} \quad 2.6$$

where  $\bar{D}$  is turbulent diffusivity,

$D$  is molecular diffusivity of the gas,

$s$  is surface renewal rate.

However, Dobbins disagreed with the Kishinevski's theory since he found in his experiments that  $K_L$  was dependent on diffusivity of gas under turbulent conditions.

## 2.2 EFFECT OF PHYSICAL PROPERTIES OF LIQUID ON MASS TRANSFER

### 2.2.1 Viscosity

Theoretical models have been developed to consider the effect of viscosity on mass transfer coefficient. Those interested in these models should see Calderbank et al. (22), Moo-Young and Hirose (76), Wellek and Huang (128), Hirose and Moo-Young (52), Shiotsuka and Kawase (108) and the references cited by these authors.

Calderbank et al. (22) experimentally determined liquid phase mass transfer coefficient,  $K_L$ , using  $\text{CO}_2$  bubbles in three Newtonian liquids (covering a wide range of viscosities) and one non-Newtonian liquid. The Newtonian liquids were distilled water, 90.6% (1.8 poise) and 99% (7.75 poise) aqueous glycerol solutions. The non-Newtonian liquid was 1% aqueous solution of polyox (polyethylene oxide), which was pseudoplastic. For non-Newtonian liquid

$$\tau = K_u \dot{\gamma}^{n'} \quad 2.7$$

where  $\tau$  is shear stress,  $\dot{\gamma}$  is shear rate,  $K_u$  and  $n'$  are constants.

For 1% polyox solution,  $K_u = 0.87$  and  $n' = 0.54$ . The surface tension and density of these liquids were nearly same as that of water.

Generally speaking, for Newtonian liquids the results of Calderbank et al. show that the liquid film mass transfer coefficient decreases with the increase of viscosity, and for non-Newtonian liquids the decrease is rather less compared to glycerol solutions. For example, for 10 mm diameter bubbles,  $K_L$  in

distilled water decreases to 60% for 90.6% glycerol solution, 80% for 99% glycerol solution, and 4% for 1% polyox solution.

For non-Newtonian liquids, Hirose and Moo-Young (52) have theorized and proved by experiments that the mass transfer coefficient is enhanced for pseudoplastic ( $n' < 1$ ) and depressed for dilatants ( $n' > 1$ ). This was also confirmed by Dang et al. (30). Similarly, Wellek and Huang (128) say that the mass transfer rate increases as the fluid becomes more pseudoplastic, but did not give any physical explanation of this behaviour.

#### 2.2.2 Presence of Surface-Active Agent (SAA)

Hauser (46) mentioned that the surface-active agents are materials which naturally concentrate at the surface of a liquid and reduce surface energy by reducing the surface tension.

Mancy and Barlage (68) gave a detailed account of the effect of SAA on gas absorption. Generally speaking, the effect of increasing the concentration is a rapid decrease in the gas transfer coefficient,  $K$  ( $= K_L a$ ), at low SAA concentration followed by a slow increase in  $K$  as reported by Deindoerfer and Gaden (29). Most fermentors employ antifoam agents to suppress foaming. Addition of a small amount of antifoam (0.1%) causes a large (up to 50%) reduction in  $K$  (29). At higher antifoam concentrations, the gas transfer coefficient,  $K$ , increases slightly due to the higher interfacial area per unit volume resulting from the formation of smaller bubbles (29, 68).

Mancy and Barlage (68), Eckenfelder et al. (37,39), McKeown and Okun (72) studied the effect of SAA concentration on the



liquid-film mass transfer coefficient  $K_L$ . They found that the effect is the same as that on  $K$ : an initial rapid decrease in  $K_L$  followed by a slow increase in  $K_L$ . However, Mancy and Barlage (68), Eckenfelder and Ford (37) disagreed with the second part since they found that  $K_L$  remains constant after decreasing to a minimum value. Table 2.1 shows the maximum reduction in liquid-film coefficient and equivalent SAA concentration for various SAA. McKeown and Okum (72) report that the concentration at which maximum reduction in  $K_L$  occurs is in the range of critical micelle concentration, which is defined below.

SAA concentrates at the gas-liquid interface and decreases  $K_L$  by resisting the molecular diffusion. There exists a maximum concentration of SAA on the interface at which complete surface coverage occurs. Any further addition of SAA will cause SAA molecules to aggregate in the bulk. This maximum concentration of SAA is called "critical micelle concentration" (37).  $K_L$  decreases until critical micelle concentration is reached as expected (37, 72), then further increase in SAA has no effect on  $K_L$ .

Turbulence also influences the degree to which the SAA affects  $K_L$  and  $K$ . Under poor mixing conditions, the presence of SAA on the interface decreases  $K_L$  by resisting molecular diffusion. Because of the reduced frequency of renewal, the life of the surface element is quite sufficient to permit the creation of the surfactant film at the interface. In contrast to this, when mixing is intensive, the life of the surface element becomes so short that the SAA adsorption equilibrium is not established at the interface, and therefore the effect of SAA disappears (37).

TABLE 2.1

Maximum Reduction in  $K_L$  and  
Equivalent SAA Concentration  
for Various SAA.

SAA	SAA Concentration 'mg/lt'	Maximum Reduction in $K_L$ '%'	Investigator
Sodium Lauryl Sulphate	10-30	44	ECKENFELDER and BARNHART (39)
Pepton	1000	51	" (39)
N-Heptanoic Acid	20-40	67	" (39)
Alkyl Benzene Sulphonate	8	67	McKEOWN and OKUN (72)
Triton X-100	4-10	58	" (72)

Eckenfelder and Ford (37) have reported the value of K obtained with some aerators (spargers, cone aerators) under intensive mixing and in the presence of SAA exceeded the value obtained with tap water under identical experimental conditions. The reason for this increase is not quite clear.

### 2.2.3 Presence of Suspended Solids (SS)

The effect of the presence of suspended solids on mass transfer is controversial. Mancy and Okun (69) say that the presence of suspended solids creates thicker boundary layer and a smaller frequency of surface renewal; hence, the net effect of adding suspended solids is the reduction of gas transfer coefficient. The results reported by Deindoerfer and Gaden (29), and Von der Kroon (127) also agree with this view. They noted 85 % reduction in the oxygen transfer in a suspension of mycelium at a concentration of 13.4 gm dry tissue/lit. An opposite conclusion was reached by Poon and Campbell (90), who studied the effect of several soluble and insoluble substances on the oxygen transfer in a diffused aeration system, and found that the low concentrations of suspended solids enhance the rate of oxygen transfer. In addition, they also found that the smaller particles have more effect on transfer rate than the larger particles.

When the mixing is good, the effect of SS on gas transfer coefficient is minimized as reported by Bowers (11), and Brierley and Steel (12). At higher degrees of mixing, the gas transfer coefficient is not affected by the presence of solids (127). These findings have been confirmed in this work and will be described later.

#### 2.2.4 Temperature

The gas transfer coefficient increases with the temperature by about 2 % per degree C, from 0 to 30°C as reported by Truesdale and Vandyke (118). If the value of the transfer coefficient at a datum temperature (20°C) is known, then the coefficient at any temperature T is given by

$$K_{\text{at } T} = K_{\text{at } 20} \bar{\theta}^{(T-20)} \quad 2.8$$

where  $\bar{\theta} = 1.024$  according to Lister and Boon (66).

## Chapter 3



### 3. MASS TRANSFER WITH CHEMICAL REACTION IN LIQUID

The ways in which the phenomenon of gas absorption will be affected when the absorbing gas is continuously reacting with a dissolved reactant in the liquid are considered in this chapter, based on standard texts by Astarita (2), Danckwerts (28), and Sherwood and Pigford (106).

In an absorption process, the gas diffuses through the gas film towards the gas-liquid interface. The equilibrium conditions are assumed at the interface. Finally, the dissolved gas at the interface diffuses into the bulk of liquid and undergoes a chemical reaction with the dissolved reactant B. Because of reaction, the depletion of both dissolved gas and the reactant B develops the concentration gradients for both reactants in the liquid bulk.

Except the process of diffusion through the gas film, all the other steps take place simultaneously and thus mutually interfere. In addition, all the processes pertaining to liquid phase take place in series with the process of diffusion through the gas film. In the special case when the gas film is rate controlling, the overall rate becomes independent of chemical kinetics. In this case, the absorption process may be regarded as a simple mass transfer phenomenon not being influenced by reaction rate. The chemical reaction may enhance the transfer rate within the liquid phase and the gas film still being the rate controlling (2). When the reaction in the liquid phase is rate controlling the analysis of the problem is complicated by

the mutual interference of several factors in the liquid phase. In the following, the relative influence of these factors on oxygen transfer rate when the conditions in the liquid phase are rate controlling are discussed.

In penetration theory, the mass transfer with chemical reaction is given by:

$$D \frac{\partial^2 C}{\partial x^2} = \frac{\partial C}{\partial t} + \bar{r} \quad 3.1$$

and in film theory it is given by:

$$D \frac{\partial^2 C}{\partial x^2} = \bar{r} \quad 3.2$$

where  $\bar{r}$  is the reaction rate per unit volume of the liquid.

Astarita (2) introduced the concept of diffusion time and reaction time. It will be shown later how these concepts help in distinguishing different reaction regimes. Astarita (2) defined the "equivalent diffusion time" by the equation:

$$K_L^2 = \frac{D}{\tau_D} \quad 3.3$$

Physically the equivalent diffusion time is defined as the average life of surface elements or, in other words, the interval of time among successive mixing processes which make the concentration within the liquid elements uniform. The second concept of reaction time is defined as the length of time during which an appreciable amount of reaction takes place (2). An important difference between the diffusion and the reaction times is that the diffusion time is the time actually available for the unsteady-state diffusion within the surface elements and thus depends upon the

hydrodynamic conditions, whereas the reaction time is the time required by the reaction to occur.

### 3.1 SLOW REACTION

In slow reactions the diffusion time is much less than the reaction time. It is assumed that the depletion of reactant B at the interface is negligible as compared to its bulk concentration. In this case the reaction rate would depend upon the concentration of the dissolved gas. The reaction time ( $t_R$ ) is calculated at interface concentration. When the reaction is slow, the average life of surface elements is much less than the time required by the reaction to take place appreciably even if the surface elements are saturated with the dissolved gas. It means that the reaction does not take place during the diffusion time. Under these conditions  $\bar{r}$  will be equal to zero in equation 3.1. The resulting equation represents the unsteady molecular diffusion of gas. From this it follows that in slow reaction regimes the absorption rate does not depend on the reaction rates and therefore the chemical mass transfer coefficient becomes equal to physical mass transfer coefficient (2). Thus,

$$\dot{K}_L = K_L \quad 3.4$$

Under these conditions, the function of chemical reaction is to consume the physically dissolved component in the bulk and to keep its concentration to an equilibrium value  $\bar{C}$ . When steady state conditions are reached the reaction rate becomes equal to the absorption rate and the following equation applies:



$$\bar{J} = K_L (C^* - C_L) = v \bar{r} \quad 3.5$$

where  $\bar{J}$  is absorption or gas transfer rate per unit interfacial area. The term  $(C^* - C_L)$  is employed as the concentration gradient for physical absorption, whereas the difference  $(C^* - \bar{C})$  is the overall driving force (2). The overall driving force can be broken into two parts so that first part  $(C^* - C_L)$  is used in diffusion and the second part  $(C_L - \bar{C})$  is used in reaction. The relative magnitude of the two parts in which the driving force is broken up depends upon the relative specific rates of the two processes.

In the slow reaction when the reaction rate is high enough so that it keeps the concentration of dissolved gas practically equal to equilibrium value  $\bar{C}$ , then the overall driving force is entirely used up by the diffusion process. This condition is called a "diffusional regime" and the absorption rate is given by:

$$\bar{J} = K_L (C^* - \bar{C}) \quad 3.6$$

When the reaction is so fast that it consumes practically all the dissolved oxygen in the bulk, then the absorption rate is given by

$$\bar{J} = K_L C^* \quad 3.7$$

In a diffusional regime the chemical reaction does not influence the value of  $K_L$ , but it keeps the concentration of dissolved gas equal to equilibrium value of  $\bar{C}$ .

If the reaction is so slow that the overall driving force is entirely used up by the reaction, then the reaction is said to be in a "kinetic regime":  $(C^* - C_L)$  is much less than  $(C_L - \bar{C})$ .



Under this condition the liquid phase is almost saturated everywhere with the dissolved gas. In this case, the absorption rate is given by

$$\bar{J} = v \bar{r} \quad 3.8$$

### 3.2 FAST REACTION

When an appreciable amount of reaction takes place during the life of surface elements the reaction is said to be fast reaction. Thus, the diffusion time ( $t_D$ ) is much greater than the reaction time ( $t_R$ ). The value of  $\frac{\partial C}{\partial t}$  becomes negligible as compared to higher value of  $\bar{r}$  and therefore equation 3.1 reduces to

$$D \frac{\partial^2 C}{\partial \dot{x}^2} = \bar{r} (C) \quad 3.2$$

with the boundary conditions,

$$\dot{x} = 0 \quad C = C^* \quad 3.9$$

$$C = C_L \quad \frac{\partial C}{\partial \dot{x}} = 0 \quad 3.10$$

In fast reaction regime, the absorption process is independent of the hydrodynamic conditions. From penetration theory, this means that when the average life of surface elements is greater than the reaction time, the consideration of average life time of surface elements is immaterial. When viewed by film theory, this would mean that as long as the thickness of the film is greater than the depth required by the reaction to reduce the concentration gradient to a negligible value, it does not matter how thick the film is. For detailed analysis on fast reaction refer Astarita (2) and Sherwood and Pigford (106) and Danckwerts (28).

### 3.3 INSTANTANEOUS REACTION

The term instantaneous reaction in the liquid film implies that the absorbing gas and the liquid phase reactant B cannot coexist at the common point in the liquid. The assumption that the concentration of reactant B is uniform throughout the liquid is no longer valid as it does not exist at the interface.

First, the reaction takes place at the interface. The reaction products produced at the interface diffuse into the liquid. Because of reaction the liquid is depleted of reactant B at the interface. Thus, a concentration gradient is set up and the reactant B diffuses towards the interface from the bulk. The rapid removal of reactant B at the interface makes it necessary for the absorbing gas to diffuse further into the liquid elements or film in order to meet the coming reactant B. Soon the equilibrium conditions are reached so that the rate of diffusion of gas is equal, mole for mole, to the rate of diffusion of reactant B from the liquid bulk. Under these conditions a reaction plane is formed where both the diffusing components react. The concentration of both reactants at the reaction zone is zero. The absorbing gas diffuses from gas-liquid interface to the reaction plane. Between the reaction plane and interface the concentration of reactant B is zero. Similarly, the reactant B diffuses from the bulk towards the reaction plane and the concentration of dissolved gas in the bulk is zero. The various diffusional steps which bring about the instantaneous reaction are shown in Fig. 3.1.

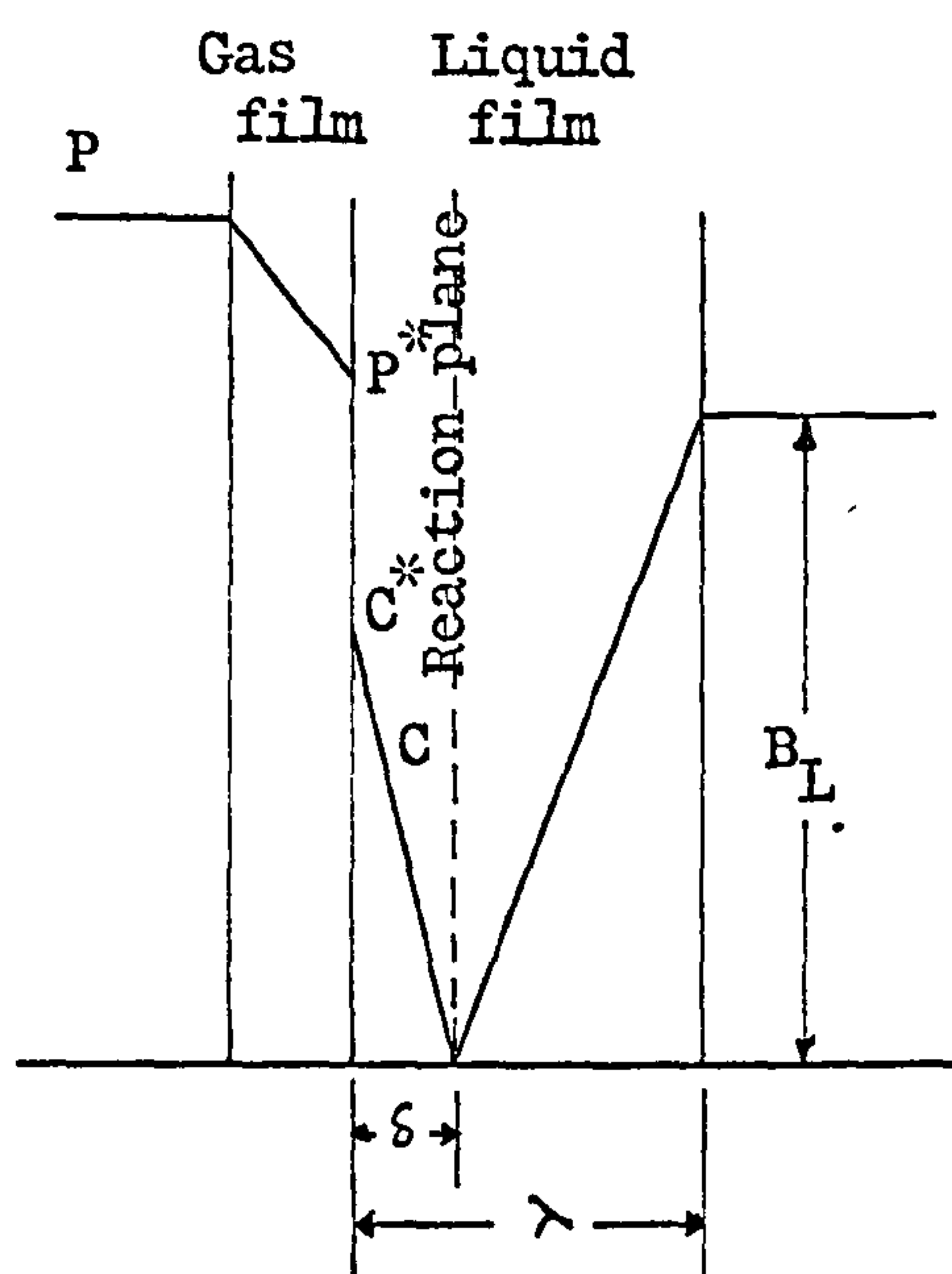


Figure 3.1. Concentration gradients of reactants in instantaneous reaction.

The diffusion of gas through the gas film is given by:

$$\bar{J} = K_g (P - P^*). \quad 3.11$$

Since the stoichiometric condition is required at the reaction plane, the film thickness is divided into two parts in such a way that the stoichiometric balance at the reaction plane is fulfilled. Thus,

$$D_1 \frac{B_L}{\lambda - \delta} = f D \frac{C^*}{\delta} \quad 3.12$$

where

$D_1$  is diffusivity of the reactant B

$B_L$  is bulk concentration of reactant B,

$\delta$  is distance of reaction plane from the interface,

$f$  is stoichiometric constant.

Also

$$\bar{J} = D \frac{C^*}{\delta} \quad 3.13$$

Since the absorbing gas diffuses physically up to the reaction plane, the equilibrium conditions at the interface may be assumed to follow Henry's law, therefore,

$$P^* = H_e C^* \quad 3.14$$

where  $H_e$  is Henry's law constant.

By eliminating  $\delta$ ,  $C^*$  and  $P^*$  from equations 3.11 to 3.14, it can be shown that

$$\bar{J} = \frac{\left(\frac{D_1}{D}\right) \frac{B_L}{f} + \frac{P}{H_e}}{\frac{\lambda}{D} + \frac{1}{H_e K_g}} \quad 3.15$$



Considering gas film resistance as negligible, equation 3.15 reduces to

$$\bar{J} = \frac{\left(\frac{D_1}{D}\right) \frac{B_L}{f} + C^*}{\frac{\lambda}{D}} \quad 3.16$$

The mass transfer coefficient due to chemical reaction is given by:

$$\dot{K}_L = \frac{D}{\lambda} \left(1 + \frac{D_1}{D} \frac{B_L}{f C^*}\right) \quad 3.17$$

The enhancement due to chemical reaction,  $\zeta$ , is given by

$$\zeta = \frac{\dot{K}_L}{K_L} = 1 + \frac{D_1}{D} \frac{B_L}{f C^*} \quad 3.18$$

The effect of chemical reaction is simply to enhance the absorption rate by a constant factor which is independent of hydrodynamic conditions in the liquid phase.

When the equation 3.15 is solved for  $P^*$  the resulting relation is given by

$$P^* = \frac{K_g P - \left(\frac{D_1 B_L}{\lambda f}\right)}{K_g + \frac{D}{\lambda H_e}} > 0 \quad 3.19$$

Since  $P^*$  cannot be negative and it will be either equal to zero or greater than zero therefore from equation 3.19

$$B_L < \frac{\lambda K_g P f}{D_1} \quad 3.20$$

when  $B_L$  is greater than  $\frac{\lambda K_g P f}{D_1}$ , the  $P^*$  approaches zero and the reaction takes place at the interface. Gas transfer takes place at maximum rate given by

$$\bar{J} = K_g P \quad 3.21$$

and is independent of concentration of reactant B at the interface as long as  $B_L$  is greater than  $\frac{\lambda K_g P f}{D_1}$  .

## Chapter 4

#### 4. AERATION OF BIOLOGICAL SYSTEM

In a biological system aerobic micro-organisms, dispersed in the liquid phase, are grown by supplying to them the essential nutrients, food (substrate), and dissolved oxygen.

There is no problem in providing food and nutrients to the micro-organisms as these can be easily dissolved in substantial quantities in water, but the problem lies with the oxygen because of its low solubility in water. Oxygen, in fact, is needed to bring about the biochemical reaction, which results in the production of new cells and removal of the substrate.

Thus, large quantities of oxygen can only be transferred to the liquid by continuously generating large gas-liquid interfacial area in a given volume of liquid. The rate of generation of interfacial is directly dependent on the oxygen demand of the micro-organisms.

Gas-liquid contacting devices called aerators are employed to cope with the oxygen demand of the biological systems in fermentation and waste treatment processes. Several versions of these aeration devices are described in detail later in this chapter. The practical problems associated with some of the commonly used aeration devices have also been discussed in this chapter.



#### 4.1 MASS TRANSFER IN BIOLOGICAL SYSTEM

The preceding discussion emphasises the importance of the phenomenon of oxygen mass transfer from the gas phase to the cell material. The theory of physical mass transfer (2.1) and the theory of mass transfer with chemical reaction still apply to the biological system.

The process of oxygen transfer from gas phase to cell material in a biological system takes place through following successive resistances in series according to Richards (95):

- $\frac{1}{K_1}$  gas-film resistance between gas and interface;
- $\frac{1}{K_2}$  gas-liquid interface resistance;
- $\frac{1}{K_3}$  liquid-film resistance between interface and the bulk liquid;
- $\frac{1}{K_4}$  liquid path resistance;
- $\frac{1}{K_5}$  liquid-film resistance around the cell or cell clump;
- $\frac{1}{K_6}$  intercellular or intrac lump resistances;
- $\frac{1}{K_7}$  resistance to reaction of oxygen with the respiratory enzymes.

The sum of all these resistances where they are present gives the overall resistance to oxygen transfer to cell material.

In addition, the rate of oxygen transfer across these resistances will also depend upon their respective oxygen concentration gradients and the available area for the diffusion of oxygen. Under steady conditions, the rate of oxygen transfer at all these stages will be equal. The oxygen concentration at all these stages will be equal. The oxygen concentration at all these stages will

be in decreasing order, so that it will be maximum in the gas phase and minimum within the cell. The individual values of oxygen concentration across each resistance will adjust itself so that the same oxygen transfer rate exists at all stages.

At one of these stages at which resistance is very high or the area very low, the concentration gradient will be as large as possible; but in spite of this, the maximum rate at which oxygen can be transferred across this stage will be lower than that possible for other stages. This stage will then become the transfer rate determining step in the process.

Usually the first three resistances are grouped together and represented by a single resistance  $K$ .

The remaining resistances  $\frac{1}{K_4}$ ,  $\frac{1}{K_5}$ ,  $\frac{1}{K_6}$ , and  $\frac{1}{K_7}$  apply not only to the oxygen transfer into the cell, but also to the transfer of any nutrient present in the medium. The resistance  $\frac{1}{K_4}$  is of no more importance in relation to the others; since, even a mild agitation of the liquid phase will execute the transfer process much more rapidly than the diffusion processes controlling the transfer at other stages. The liquid film  $\frac{1}{K_5}$  and inter-cellular or intrac lump resistance  $\frac{1}{K_6}$  can be changed by:

- (a) The degree of agitation,
- (b) Increasing the relative velocity between cell and liquid medium,
- (c) Breaking the clumps and dispersing the component organisms.

Calderbank (20) has shown that oxygen transfer from liquid to the micro-organism is very rapid as compared to oxygen transfer

from gas to liquid phase. However, if clumps of micro-organisms (few mm) are formed, then the oxygen transfer from liquid to cell might become rate limiting.

Finn (40) says that agitation in excess of that required to keep the solids in suspension will not improve the oxygen transfer from liquid to cell material. This is because the cell will move with the liquid. What is, in fact, required is the increase of relative motion between the liquid and the cells.

The reaction resistance  $\frac{1}{K_7}$  is in no way related to the degree of agitation of the biological system; however, the agitation helps in rapid removal of the waste product from the vicinity of the cell which would otherwise reduce the reactivity of the respiratory enzymes.

Oxygen uptake rate is independent of the dissolved oxygen concentration above the critical oxygen concentration. Thus, in the presence of growing organisms, the dissolved oxygen concentration will decrease linearly until the critical oxygen concentration is reached; thereafter, it will decrease non-linearly.

The lack of dependence of the oxygen uptake rate of micro-organisms on dissolved oxygen concentration is surprising in the light of the fact that the oxygen transfer rate through various resistances before oxygen reaches the cell is governed by the oxygen concentration gradient. However, Winzler (133) reports that the oxygen transfer from cell wall into the interior of cell is a process that might be controlled by surface enzyme activity or by diffusion.



It seems likely that in the presence of sufficient oxygen at the cell wall, some sort of dynamic equilibrium would be set up between oxygen molecules free at the surface and those absorbed on it. Hinshelwood (50) suggests this equilibrium can be expressed in the form of an adsorption equation such as the Langmuir isotherm. According to this isotherm:

$$\text{Rate of oxygen adsorption} = \frac{K_{10} c}{1 - K_{10} c} \quad 4.1$$

where  $c$  is the oxygen concentration at cell wall and  $K_{10}$  is constant.

The change from independency to dependency is, in fact, much more abrupt than that accounted for by Langmuir isotherm itself. and in practice a more complex expression may need to be applied.

In an actively respiring biological system, the oxygen which is being transferred to the liquid is continuously utilized by the micro-organisms. If the oxygen demand balances its supply, then the dissolved oxygen concentration in the liquid would be zero and the maximum oxygen transfer would take place at the maximum efficiency of the system. In practice, the dissolved oxygen concentration is not allowed to drop below the critical value of 0.1 atmosphere. (minimum oxygen concentration at individual cell surface to give maximum oxygen uptake rate). However, Hirose et al. (51) found in an experiment on bacterial fermentation that agitation-aeration conditions were optimum at zero dissolved oxygen concentration.

Tsao (119) found that the liquid-film mass transfer coefficient  $K_L$  increased by about 35% as a result of the biological reaction. In his experiments with biological reaction, the oxygen transfer



coefficient was measured by determining the rate of substrate consumption. He proposed the existence of two mass transfer mechanisms occurring simultaneously; one physical absorption (two-film theory), and the second direct absorption of oxygen from air by the cells concentrated at the interface.

So far as oxygen transfer from air to liquid is concerned, it will be influenced by:

- (a) The physical conditions of the interface.
- (b) The bubble dynamics.

A biological liquid is a complex liquid containing suspended solids (micro-organisms and inert solids), colloids, surface-active agents, and dissolved organic substances. Also, the liquid is, usually, non-Newtonian. These factors tend to reduce the oxygen transfer through the interface when compared to the air-water system.

On the other hand, factors such as:

- (a) Increase in the bubble retention time due to high viscosity;
- (b) Increase in the gas hold up due to foaming; and
- (c) Formation of smaller, non-coalescing bubbles due to film elasticity; and
- (d) Turbulence in the liquid;

all tend to increase the oxygen transfer. These factors would counteract the factors which reduce the oxygen transfer; and when predominant, may make up, or even increase, the oxygen transfer rate as compared to the air-water system. For instance, under intensive turbulent conditions, the reducing effect of

surface-active agents and suspended solids on oxygen transfer is diminished (2.2.2).

The increase of oxygen transfer rate in waste liquor over that in tap water was also found in this work and will be described in (11.2.5).

## 4.2 AERATION DEVICES

### 4.2.1 Compressed Air Aerators

In these systems air is compressed and introduced below the surface of the liquid in a tank and dispersed in the form of bubbles. The oxygen transfer takes place from the bubble surface. The rising bubbles also impart turbulence in the tank liquid.

Various commonly used compressed air units are described below.

#### 4.2.1.1 Porous diffusers

The air can be fed to an aeration tank in the form of fine bubbles by means of a porous diffuser. In principle, when the air is pumped through a porous diffuser (having pores less than 1 mm diameter) it emerges at the pores in the form of bubbles which grow and then detach when the buoyancy forces of the bubbles exceed the surface tension forces holding the bubbles at the pores. Since the pore size is small, smaller total surface tension forces are encountered and hence fine bubbles are produced. However, for aeration devices having large openings, as discussed in the following sections, the air emerges from the unit in individual

large bubbles, or as a continuous chain of bubbles which break into stable bubbles during ascent as reported by Bewtra and Nicholas (9).

The commercial units consist of:

- (a) Plates or tubes constructed of silicon dioxide or aluminium dioxide, held in a porous mass with ceramic binder, shown in Fig. 4.1, page 39.
- (b) Saran or Nylon wrapped tubes or bags.

Eckenfelder and Moore (38) report that the bubble sizes in these units are from 2 to 2.5 mm diameter. The bubble size for small pores is considerably greater than the pore size. When the bubbles are formed slowly, the bubble size depends on pore size, but does not increase with the latter at the same rate. Seeliger (103) reports that with 0.025 mm pores, the bubble diameter was 0.5 mm, and with 0.3 mm pores a good 2 mm. Moreover, with the increase of air feed rate it increased up to an ultimate value of 5 to 6 mm, which did not appear to depend on pore size.

#### 4.2.1.2 Sparger units

A sparger contains four horizontal large diameter (usually 5 to 6.25 mm) orifices, with common air inlet and releases air through these orifices at high velocity (Eckenfelder and Ford (37)). The spargers are mounted on air header located along the side of the tank wall. During operation, a row of spargers produces a turbulent wall of air-water mixture. This wall has relatively low density. The liquid away from this low density wall flows towards it and imparts turbulence.



#### 4.2.1.3 Coarse bubble aerator

Coarse bubbles are obtained from openings of the order of 50 mm diameter according to Von Der Emde (126).

It is claimed that the oxygenation efficiency of coarse bubble aeration can be increased by dividing the coarse bubbles by baffles as shown in Fig. 4.2. The tests have shown that this device has enabled the coarse bubble aeration units to achieve the same efficiency as that for medium bubble aeration (126).

#### 4.2.1.4 Impingement aerator

In this unit, shown in Fig. 4.3, the air is diffused through a cup-shaped bowl mounted on an air header inside the tank. A nozzle mounted on a water header which is above the air header directs a high velocity jet above the bowl. The jet divides the air bubbles released within the bowl into extremely fine bubbles. The fineness of the bubbles depends upon the flow rate of the nozzles (Eckenfelder and Moore (38)).

The power required for pumping impingement water varies from 8 to 15 per cent of the total power for aeration (38) and decreases at higher air release rates per bowl.

The impingement aerators do not clog because of large orifice diameter. The head loss is low and there is no build up of back pressure.



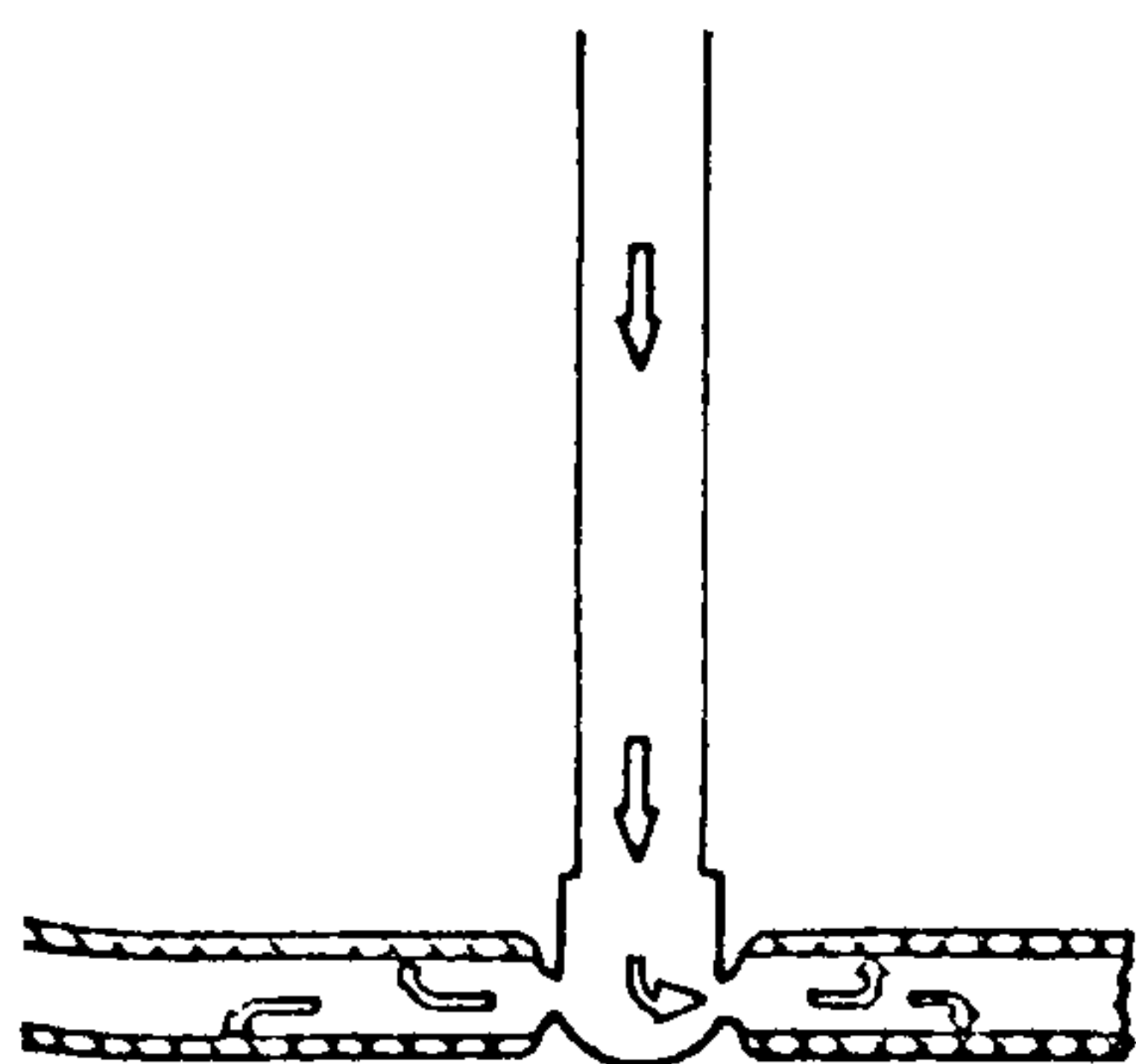


Figure 4.1. A sectional view of porous ceramic diffuser (38)

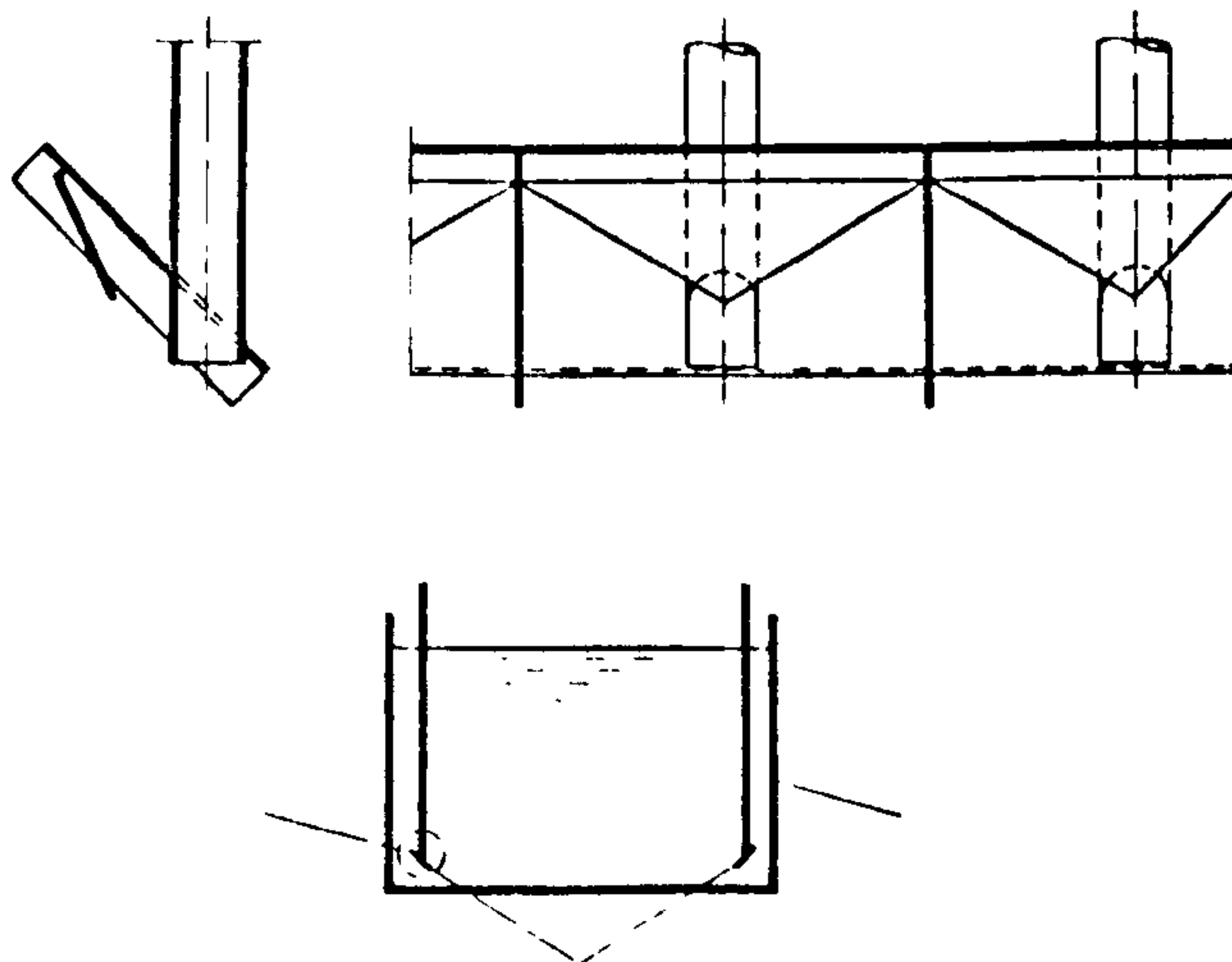


Figure 4.2. Coarse bubble aeration device (126).

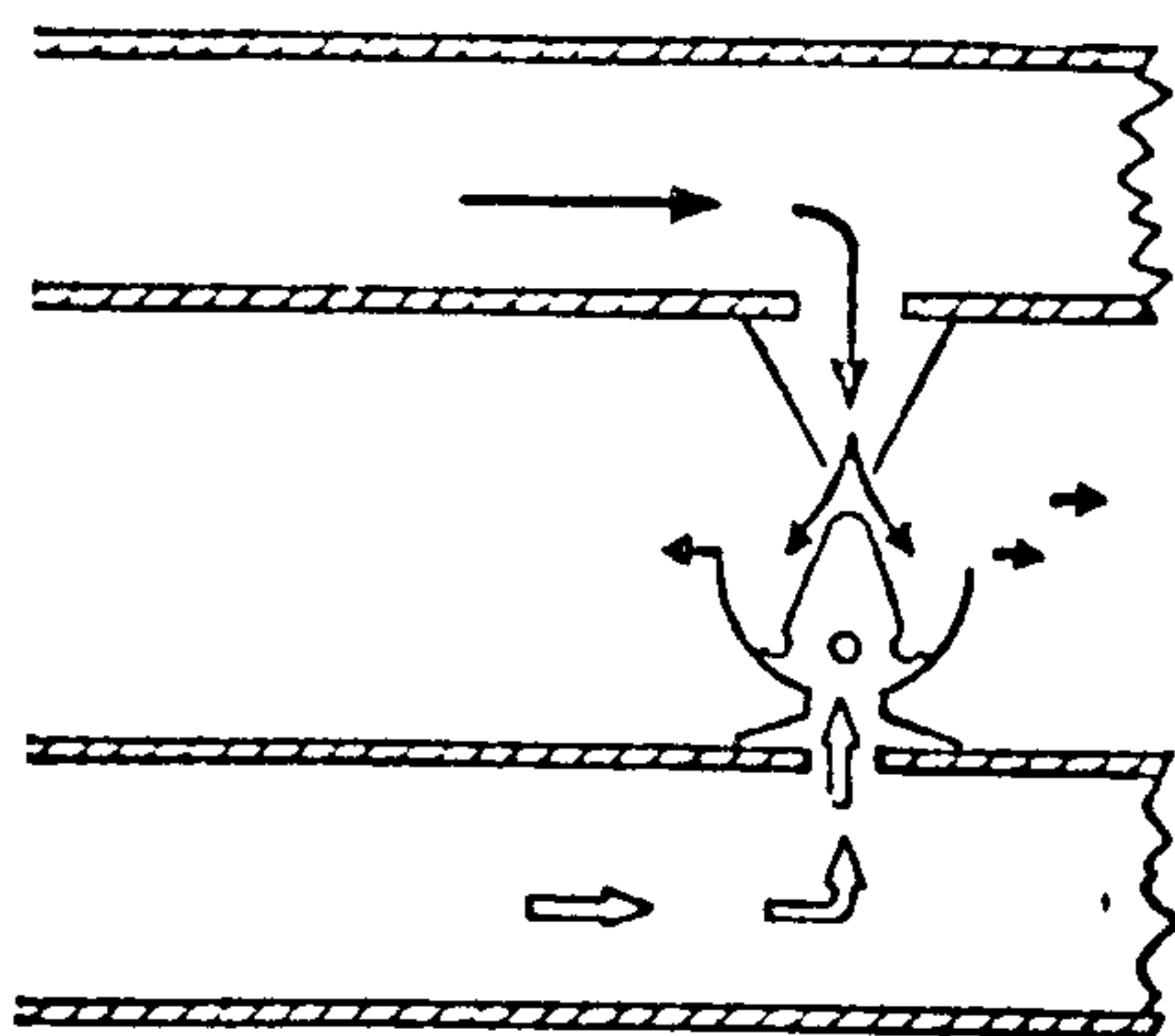


Figure 4.3. Impingement aerator (38).

#### 4.2.1.5 Danjes system

In this unit porous diffuser tubes are adjusted to a moving bridge as shown in Fig. 4.4. The bridge moves horizontally with a low velocity (e.g. 0.2 m/s), as reported by Von Der Emde (126). The baffles fitted to the bridge in front of the tube force the water to flow in the upper part of the tank. The moving water diverts the vertical path of the rising bubbles. As a result of this, the retention time of bubbles is increased and high oxygen transfer is obtained.

#### 4.2.1.6 Ejector system

The liquid is pumped through an ejector unit, which entrains the atmospheric air or the air supplied by a blower as shown in Fig. 4.5.

Morgan and Bewtra (78) report that the oxygen transfer in this system is a function of nozzle velocity and the volume of air entrained.

#### 4.2.1.7 Inka system

In this unit stainless steel pipes in the form of a grating are placed about a metre below the liquid surface. These pipes are perforated from the underside and are located between a tank wall and a baffle as shown in Fig. 4.6.

A large quantity of air under low pressure imparts a spiral flow within the tank and maintains sludge in suspension.

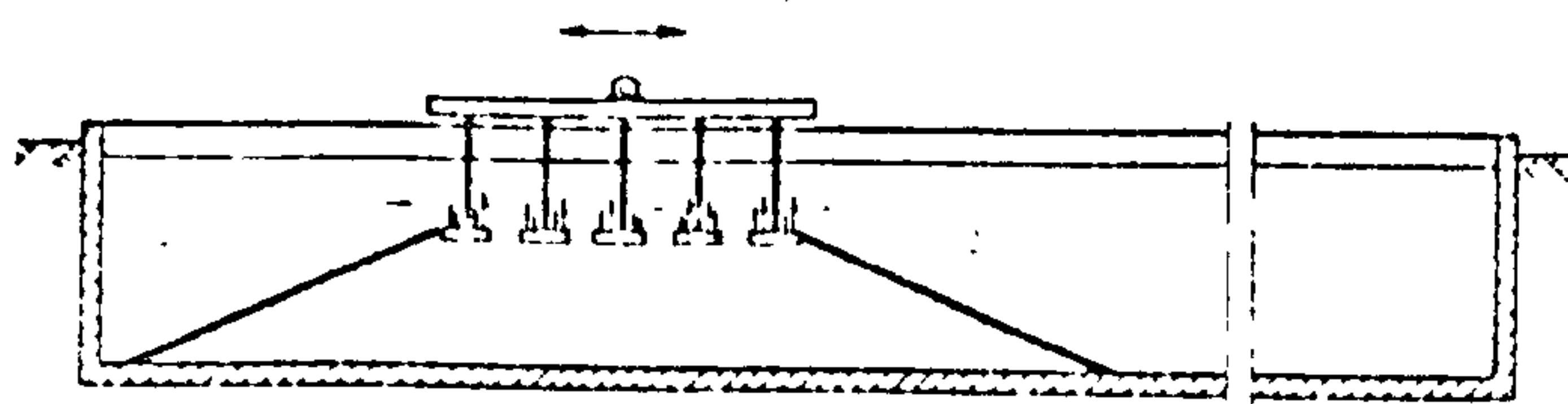


Figure 4.4. Danjes system (126).

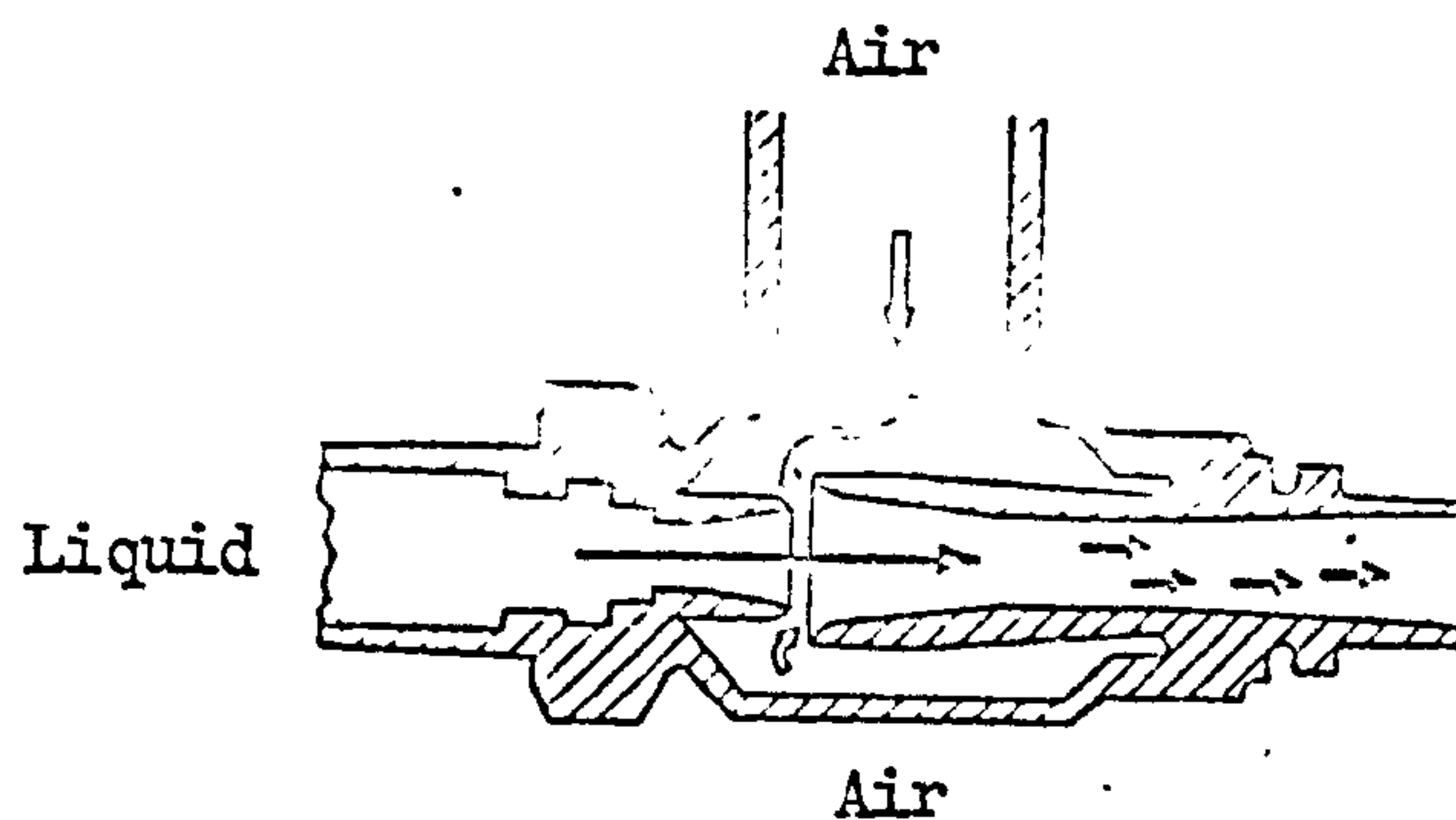


Figure 4.5. Ejector aeration system.

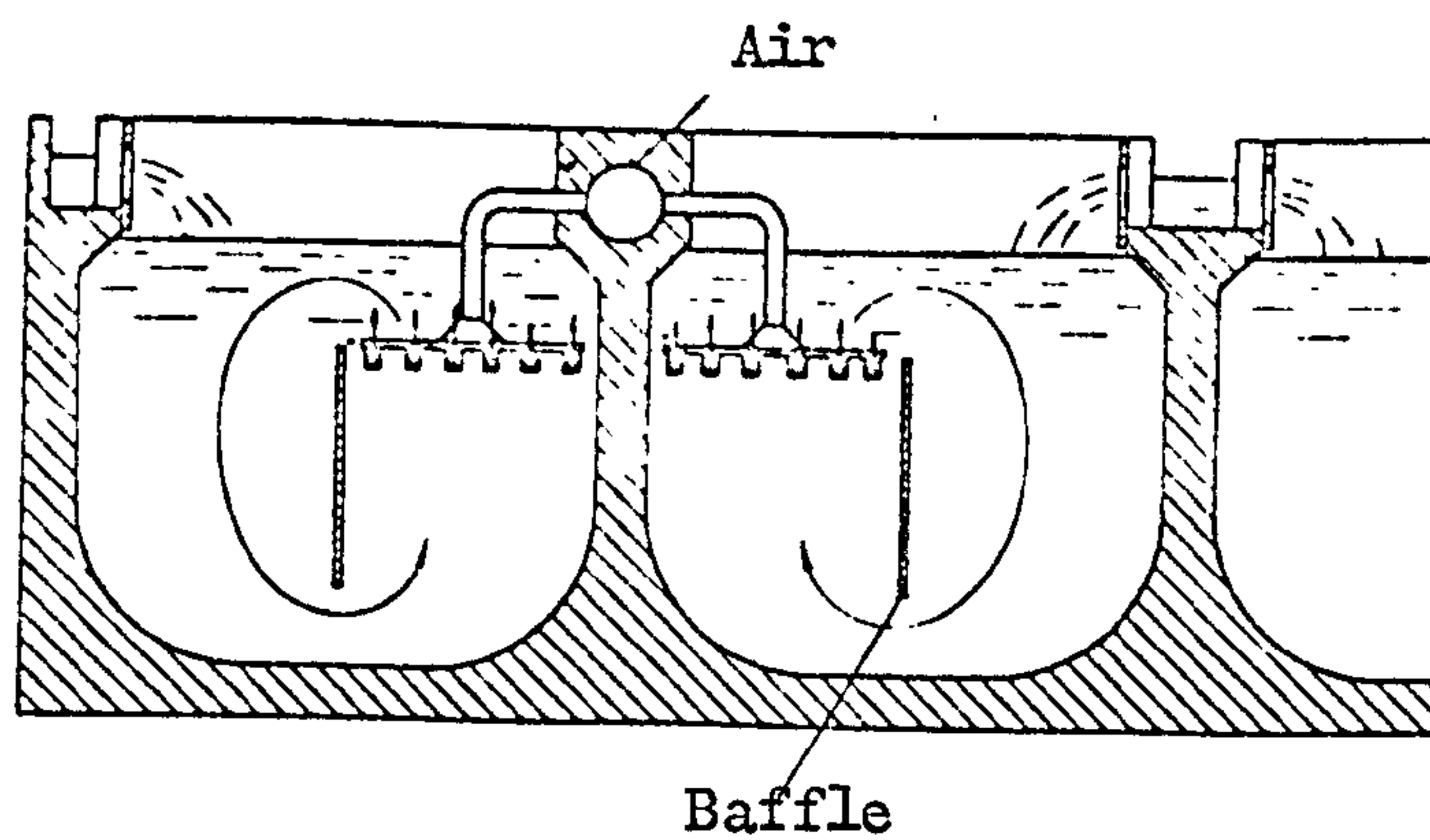


Figure 4.6. Inka system (156).

#### 4.2.1.8 Performance of compressed air aerators

The weight of oxygen transferred by an aeration device per kilowatt hour of energy consumed is commonly known as its "aeration efficiency". In the case of compressed air aerators, the ratio of the weight of oxygen absorbed to the weight of oxygen supplied expressed as a percentage is called the "per cent oxygen absorption".

The aeration efficiencies of various units described in preceding sections are shown in Table 4.1. With the exception of perforated and open end pipe aerators ( $1 \text{ kg O}_2/\text{kW hr}$ ) the aeration efficiencies of other systems lie between 2 to  $5 \text{ kg O}_2/\text{kW h}$ . The low aeration efficiency of the perforated and the open end pipe aerators is expected as a result of medium and coarse bubble formation: as the bubble diameter increases, the interfacial area per unit volume of liquid decreases for a constant air feed rate. Seeliger (103) says that the oxygen transfer rate in fine bubble aeration is more than that in coarse bubble aeration. He reports that variation from coarse to fine bubble aeration varied the oxygen absorption from 5 to 11%. Similarly, Lamb (60) reports that the oxygen transfer rate increases linearly with the increase in the submergence depth of the aeration device. When the submergence depth was increased from 1 to 4 m, he observed an increase from 5 to 14% and 2 to 8% with diffuser units and nozzle units respectively: the air feed rates were  $1.8 \times 10^{-3} \text{ m}^3/\text{s}$  air-per-porous-tube and 4.5 to  $9 \times 10^{-3} \text{ m}^3/\text{s}$  per nozzle diffuser. The performance as regards the degree of turbulence imparted by the rising bubbles and tank geometry are less well established.



TABLE 4.1                      Aeration Efficiencies of Various Aeration Methods Under Optimum Conditions

Aeration Method	Liquid Used in Test	Depth of Tank m <sup>†</sup>	Aeration Efficiency kgO <sub>2</sub> /kW h	Reference
Porous diffusers *	WD	4	1.8 - 2.2	WHEATLAND ( 132 )
Perforated Pipes *	WD	4	1.0	WHEATLAND ( 132 )
Open ended pipes *	ED	2.6	1.0	WHEATLAND ( 132 )
Danjes system	-	-	3 - 5	SCHERB ( 102 )
Ejector system	-	-	3	THAER ( 116 )
Inka system ‡	WD	3	1.8 - 1.9	WHEATLAND ( 132 )
Simplex Hi-cone (1.8 m dia.)	WD	5.5	1.7 - 1.8	WHEATLAND ( 132 )
Simcar cone	W	-	2.4 <sup>‡</sup>	KAYSER ( 57 )
B.S.K. turbine (1.2 m dia.)	-	-	3	WHEATLAND ( 132 )
Turbine and sparger	E	-	2.3	VON DER EMDE ( 126 )
Kessener brush	ED	2.9	1.6	WHEATLAND ( 132 )
Fuchs	-	-	15	THAER ( 116 )
Plunging liquid jet (angular jet - 70°)	DW	-	3 - 4	BOHNKE ( 10 )
Plunging liquid jet (pilot scale)	SO <sub>3</sub> system	1	4	AHMED and GLOVER ( 1 )
Plunging liquid jet (lab.scale)	W	-	2.8	HAUXWELL ( 47 )

W Clean water

WD Water + 5 mg/lit. anionic detergent.

ED Sewage effluent containing 3 to 5 mg/lit. of anionic detergent.

DW Domestic waste

\* Near floor of tank.

† Submerged 60 cm.

‡ Minimum value calculated from manufacturer's data.

## 4.2.2 Mechanical Aerators

### 4.2.2.1 Vortair aerator

Fig. 4.7 shows a vortair aerator. It employs a flat circular plate. On one side of the plate short vertical blades are fitted radially with one end lying on the periphery of the plate. This aerator is also known as turbine aerator.

The turbine rotates a few inches below the liquid surface, and pumps the liquid through the blades. The discharged liquid produces a hydraulic jump around the turbine. The hydraulic jump causes intense agitation and aeration - by entraining atmospheric air.

Weston and Stack (131) report that when the top plate of the turbine is free of the liquid during operation, air is sucked down past the top plate of the turbine because of formation of a low pressure region behind the radial vanes. The air is carried away by the liquid - being pumped through the blades - in the form of bubbles.

Often this aerator is mounted on floats or piers for the aeration of lagoons and streams.

Oxygen transfer rate by vortair aerator depends upon diameter, speed, and submergence of the turbine. With the decrease of the submergence, the oxygen transfer rate increases and the power input decreases. However, at zero submergence, the oxygen transfer rate drops with a slight decrease in the input power (131). Eckenfelder and Ford (37) report that 40 to 60% of the total oxygen transfer takes place in the spray zone, and the rest in the turbulent zone. Also, the oxygen transfer

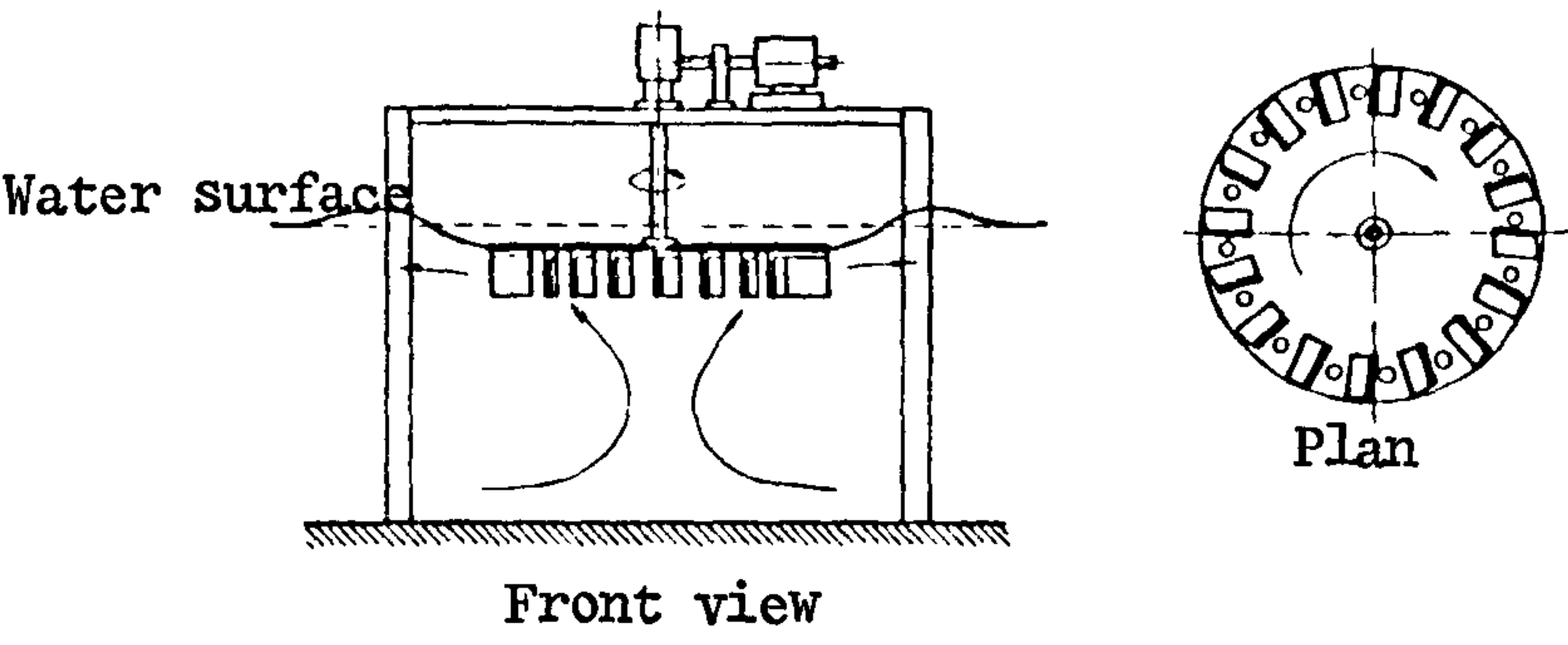


Figure 4.7. Vortair aerator.

rate increases with the increase of surface area of the tank (37).

#### 4.2.2.2 Simplex Hi-Cone aerator

A Simplex Hi-Cone aerator (Fig. 4.8) employs a cone, which revolves over a vertical draft tube. The revolving cone draws the liquid through the draft tube and sprays it over the liquid surface.

The liquid elements at the surface flow towards the tank wall in a spiral pattern, then flow downwards along the tank wall. After reaching the tank bottom the liquid flows towards the uptake of the draft tube. The rotation of the cone imparts a spiral motion in the liquid elements and hence creates a vortex in the tank. Knop and Kalbskopf (59) report that the vertical flow of the liquid contributes to the aeration by entraining air bubbles. The vortex is beneficial as it breaks large bubbles into smaller bubbles (59).

Like the Vortair aerator, the oxygen transfer in the Simplex Hi-Cone aerator is a function of the diameter, the speed, and the submergence depth of the cone.

Von Der Emde (126) and Hurwitz et al. (54) say that, at higher cone speeds, the insignificant increase in the oxygen transfer rate indicates the existence of an optimum speed for maximum aeration efficiency.

At zero free-board, the maximum oxygen transfer rate and pumping capacity are obtained for a given speed. As the free-board increases - submergence depth decreases - both the oxygen transfer rate and the pumping capacity decrease (126).



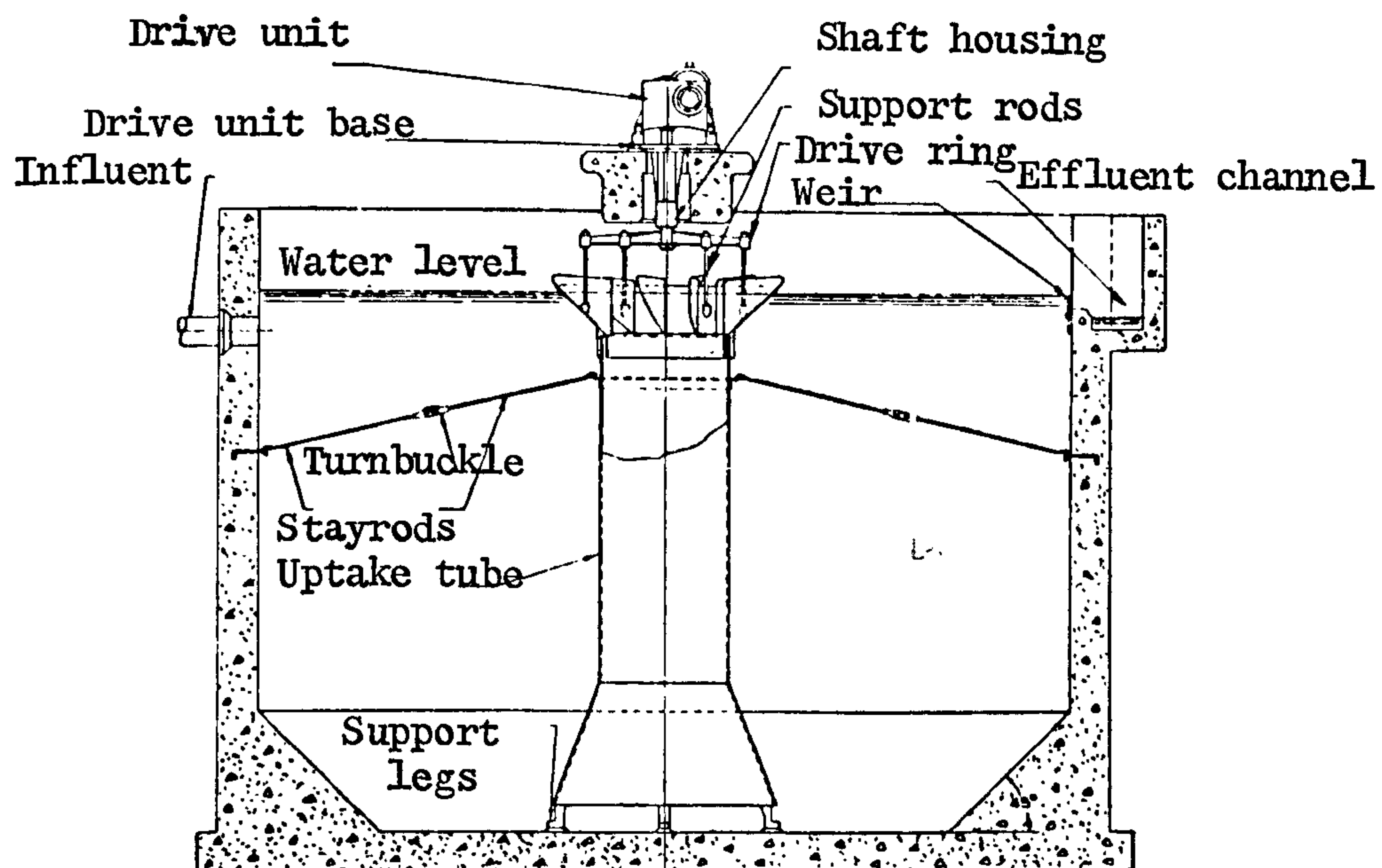


Figure 4.8. Simplex Hi-Cone aerator.

Eckenfelder (36) reports that, under optimum submergence conditions, the aeration efficiency remains nearly the same over a wide range of impeller diameters.

#### 4.2.2.3 Simcar cone aerator

Fig.4.9 shows a Simcar cone aerator which employs an inverted cone. Underneath this cone, blades made of steel strips are fitted. At the cone base, the blades take the form of an angle iron and extend outwards beyond the periphery a short distance. The Simcar cone does not use a draft tube. Like the Simplex Hi-Cone the oxygen transfer rate increases with the increase of the submergence and vice versa (126). However, the power input increases as the submergence increases (126). In Simcar cone aeration the aeration efficiency improves at higher speeds (126).

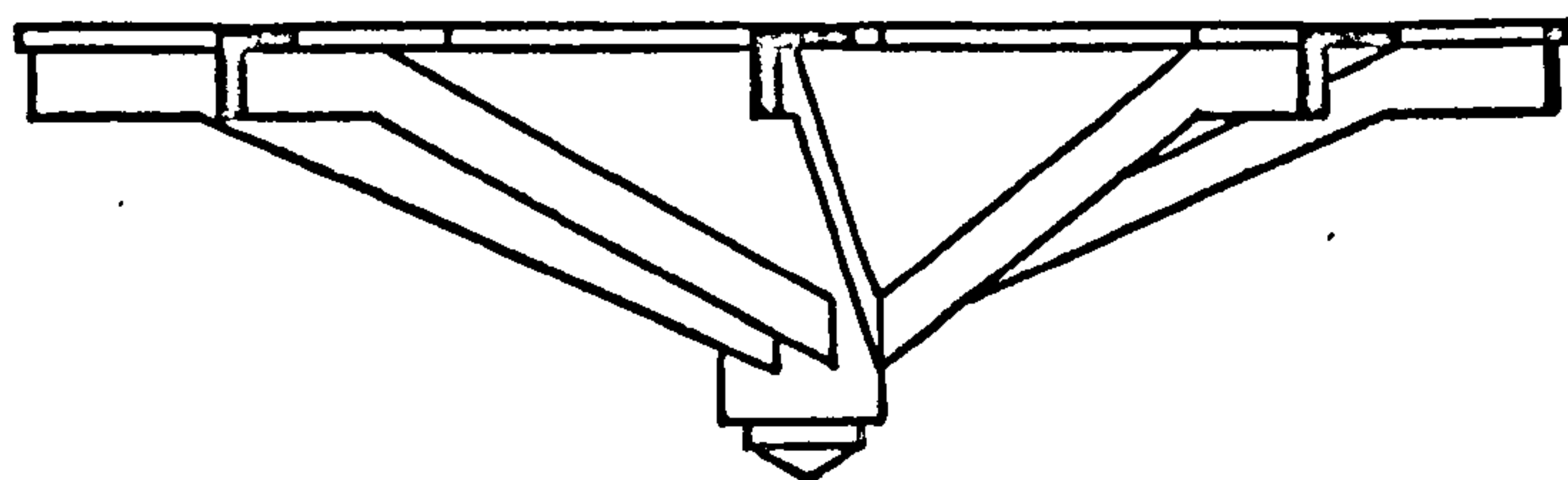
#### 4.2.2.4 BSK turbine aerator

Figure 4.10 shows a BSK turbine unit. As the turbine rotates, air and water are drawn through their respective passages, then discharged through the guide vanes.

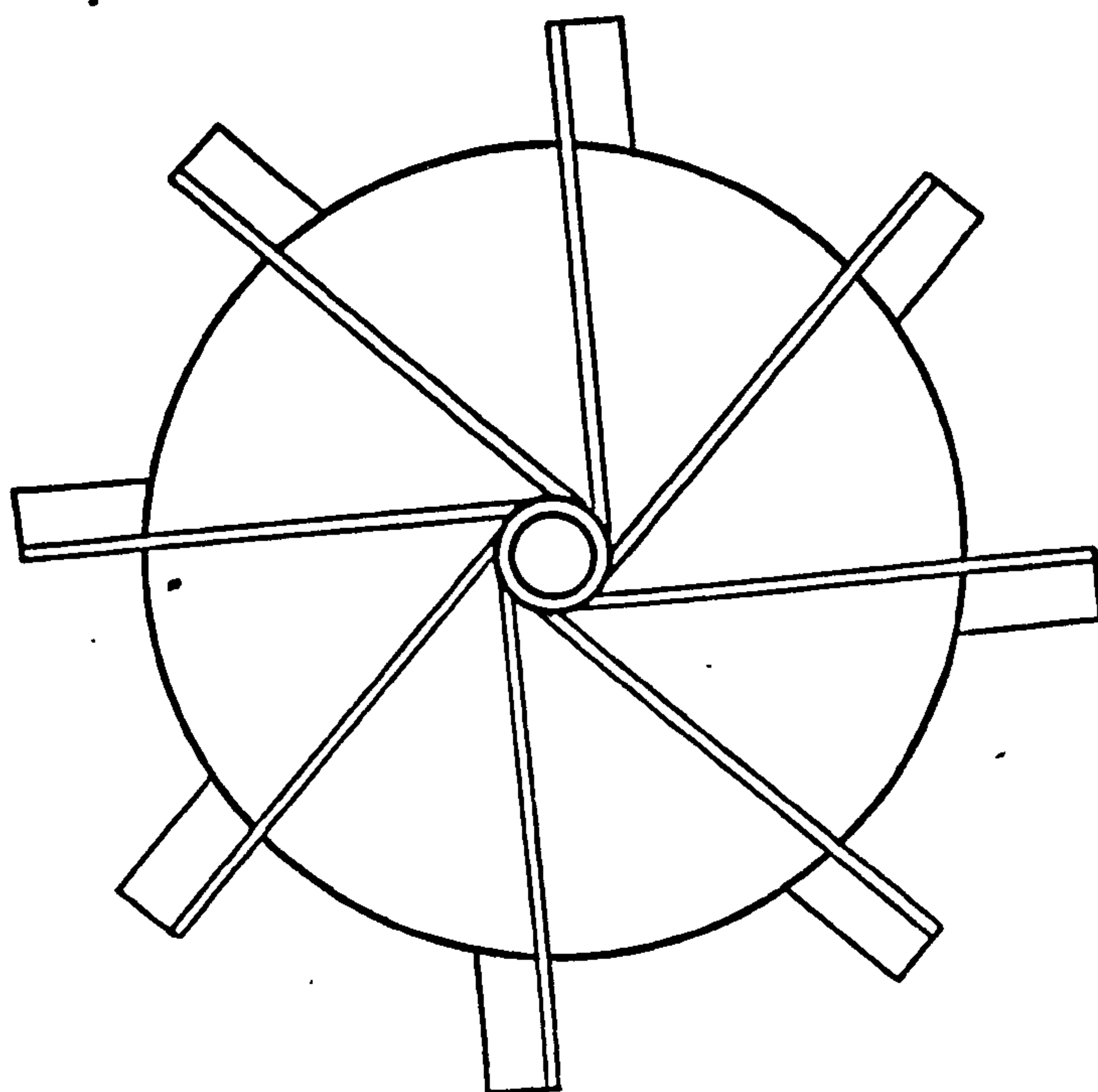
The aeration efficiency and the power input increase slightly with the increase of the submergence depth (126).

#### 4.2.2.5 Turbine-sparger aerator

In this aeration unit, a turbine rotates just above a sparger ring through which air is blown. The air released from the sparger is dispersed within the tank, in the form of small bubbles, by shearing and pumping action of the turbine.



Front view



Bottom view

Figure 4.9. Simcar cone aerator.

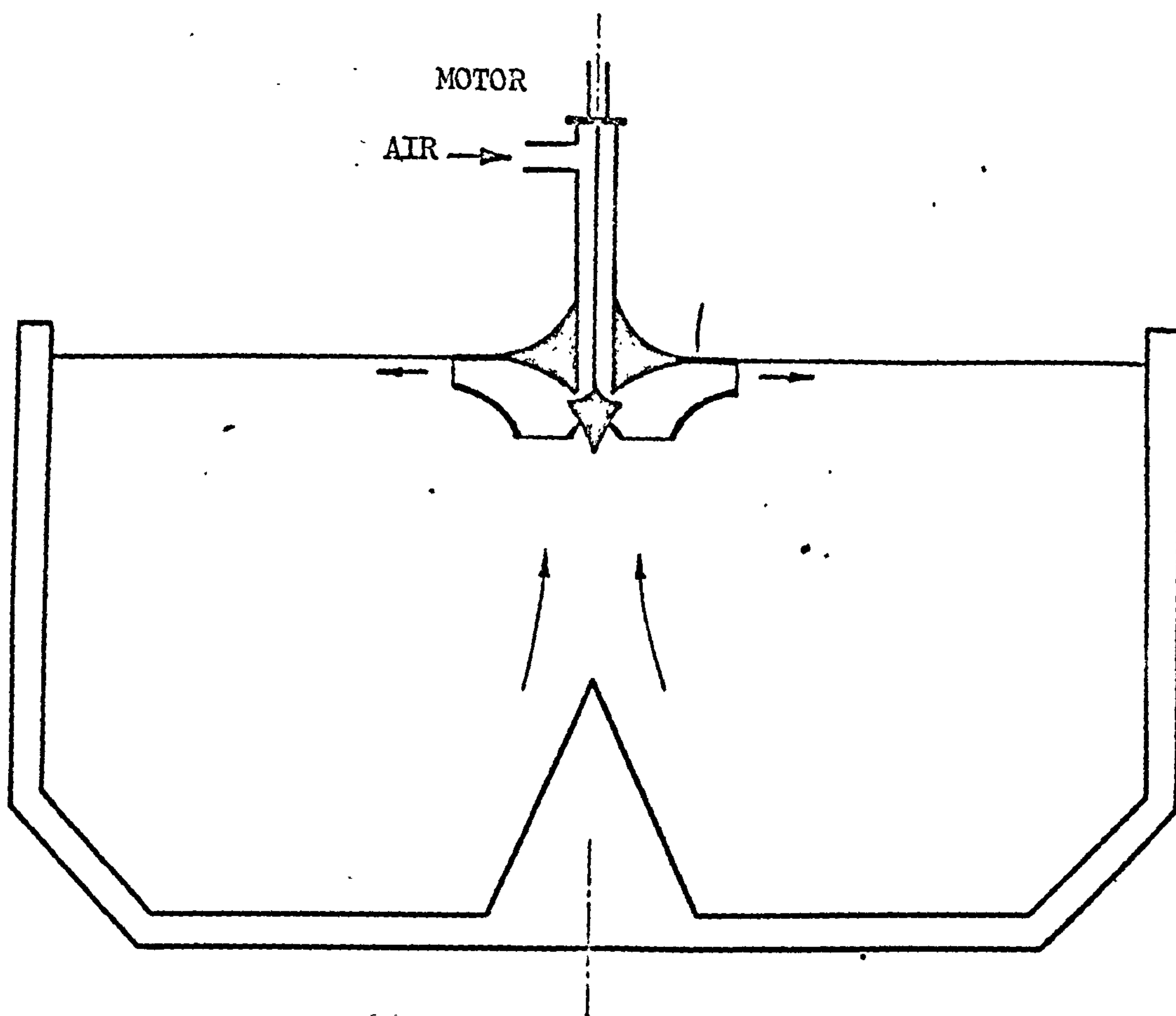


Figure 4.10. BSK turbine aerator.



A modification of this unit is a dual-turbine-sparger unit, in which one turbine is used to create surface aeration while the other is used to disperse the air bubbles and ensure good mixing conditions within the tank. Buelتمان et al. (15) say that this modification improves the aeration efficiency of the system; however, at higher air feed rates the flooding occurs, and the oxygen transfer rate decreases.

#### 4.2.2.6 Brush aerator

In this unit, a long brush-like rotor rotates over the surface of the liquid in the tank (Fig. 4.11, p.52). It sprays the liquid on the liquid surface and maintains the liquid circulation. Knop and Kalbskopf (59) and Pasveer (85) report that research on this aeration system has led to the development of various types of rotors, differing only in their constructional details. These include: Kessener brush; Mammoth rotors; Angle iron rotors; Cage iron rotors (85, 59).

The circulation in the tank is improved by using two baffles, one beneath the rotor, called the suction baffle, and the other opposite the rotor called the pressure baffle (Fig. 4.11). The liquid pumped by the rotor flows down the pressure baffle, whereas the liquid within the tank flows towards the suction baffle; then it is pumped by the rotor.

Pasveer (85) says that the oxygen transfer rate in angle iron rotor and cage iron rotor aeration is four times more than that obtained in conventional Kessener brush aeration.

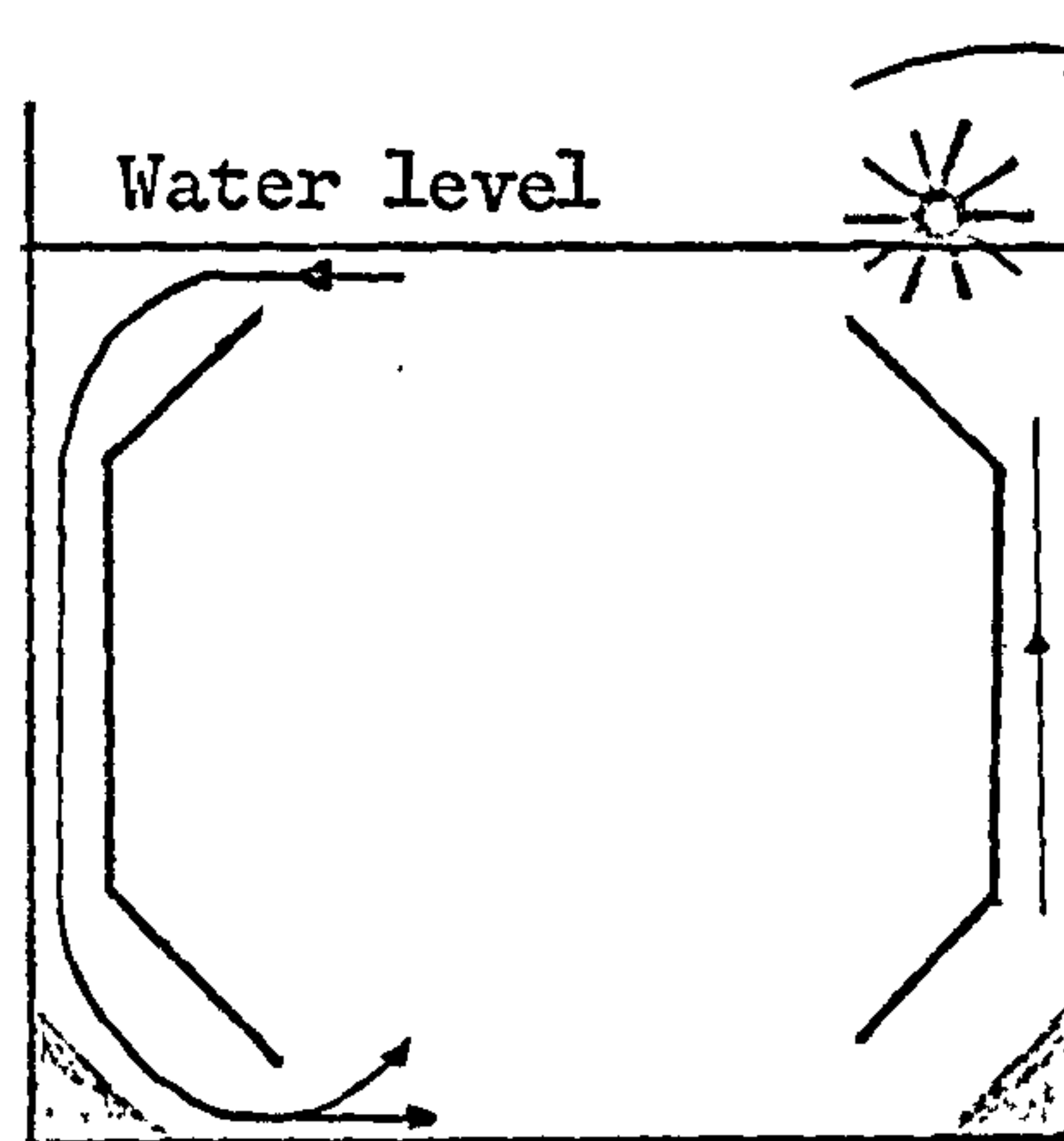


Figure 4.11. Brush aerator.

The oxygen transfer depends upon the diameter of the brush and takes place entirely in the vicinity of the brush (85). Von Der Emde (125) observed that with the increase of rpm the aeration efficiency increases to a maximum value of  $1.2 \text{ kg O}_2 / \text{kW h}$  and then decreases with further increase of rpm. He explained that the aeration efficiency decreases at higher speeds because the interfacial area generation increases faster than the circulation rate. Von Der Emde found that the oxygen transfer rate increased linearly with the increase of immersion depth up to an immersion depth of 12 and 14 cm (brush diameter 52 cm). Also the energy consumption increased linearly with the immersion depth so that the aeration efficiency remained approximately constant at a given speed.

Up to the limiting ratio between turbulence and circulation, the energy consumption increases with second power while the oxygen transfer rate increases with 2.6 power of rpm or peripheral velocity (125).

#### 4.2.2.7 Oxidation ditch

The system in which aeration is carried out in a ditch constructed in the ground is called an "oxidation ditch". The mixing is poor in oxidation ditches because of the low liquid velocities. To improve mixing the ditches are often constructed with a return flow.

One advantage of the oxidation ditch is that the accumulation of the sludge solids renders the treatment insensitive to high organic loadings as reported by Pasveer (85).

#### 4.2.2.8 Suction aerator

Several versions of suction aerator exist:

- (a) Hollow mixer aerator: Zlokarnik and Judat (138, 139, 140) have described these units as consisting of hollow mixing impellers connected to a hollow shaft (Fig. 4.12). The air is drawn from the atmosphere in the impeller ducts via the hollow shaft, and is dispersed in the liquid through holes in the impeller ducts.
- (b) Fuchs mixing aerator: Popel (91,92) and Thaer (116) have described this aerator which is shown in Fig. 4.13. The liquid flows towards the turbine from the bottom of the tank. The liquid combines with the air sucked through the axial tube; and the air-liquid mixture is pumped along the guide shield towards the outside. (The aeration efficiency for Fuchs aerator is claimed to be 15 kg O<sub>2</sub>/kW h (91, 92, 116)).

#### 4.2.2.9 Plunging jet aerator

The aeration by a plunging liquid jet on to a liquid pool has recently been utilized. This method has been applied in West Germany for the treatment of waste water as reported by Bohnke (10).

#### 4.2.2.10 Vortex or Waldhof system

Brown and Peterson (13) and Chain et al. (24) have described this aeration unit used in fermentation processes (Fig. 4.14). A rotating impeller below a draft tube contained in a vessel imparts vortex motion to the liquid. As a result



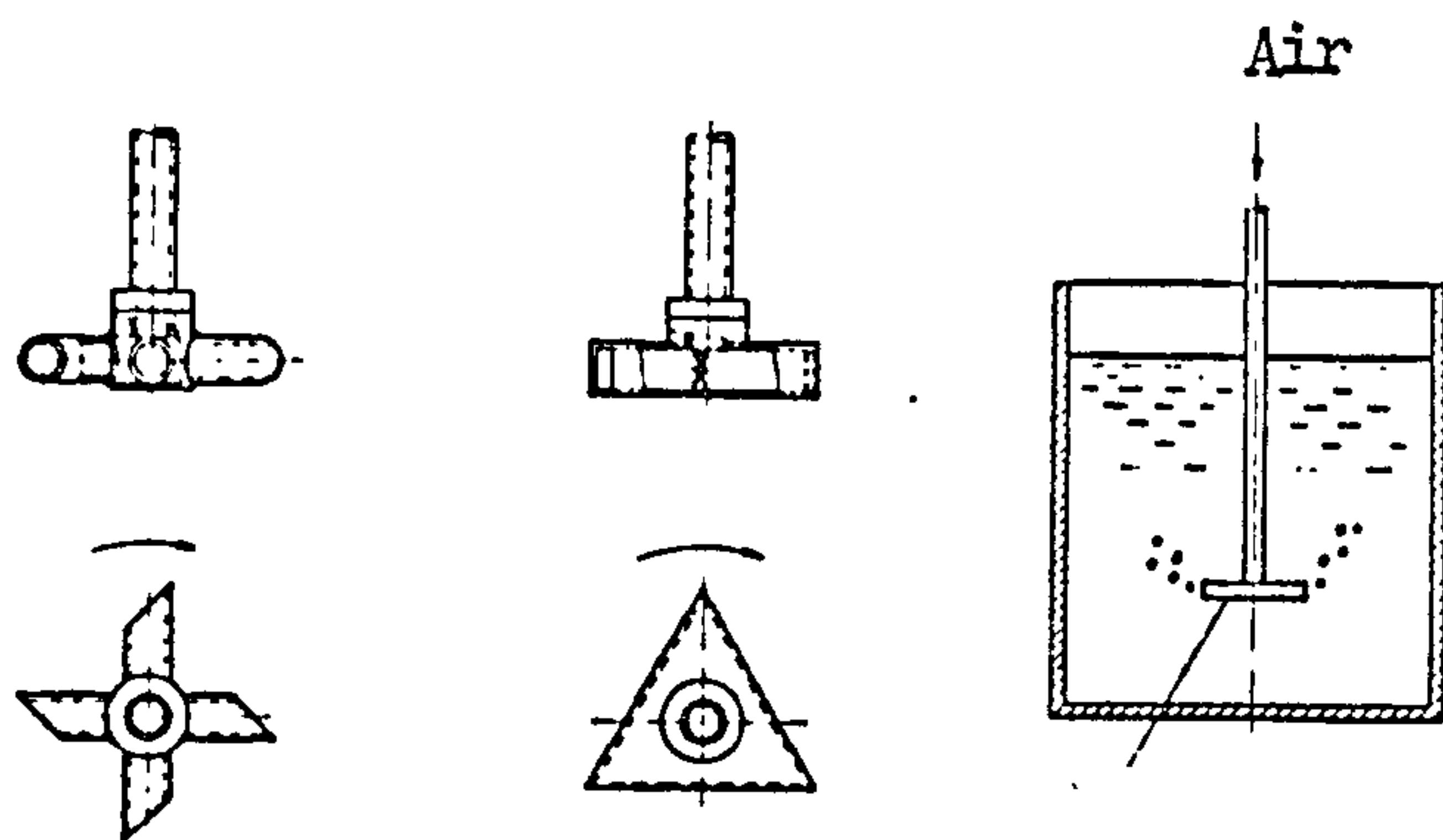


Figure 4.12. Hollow mixer aerators.

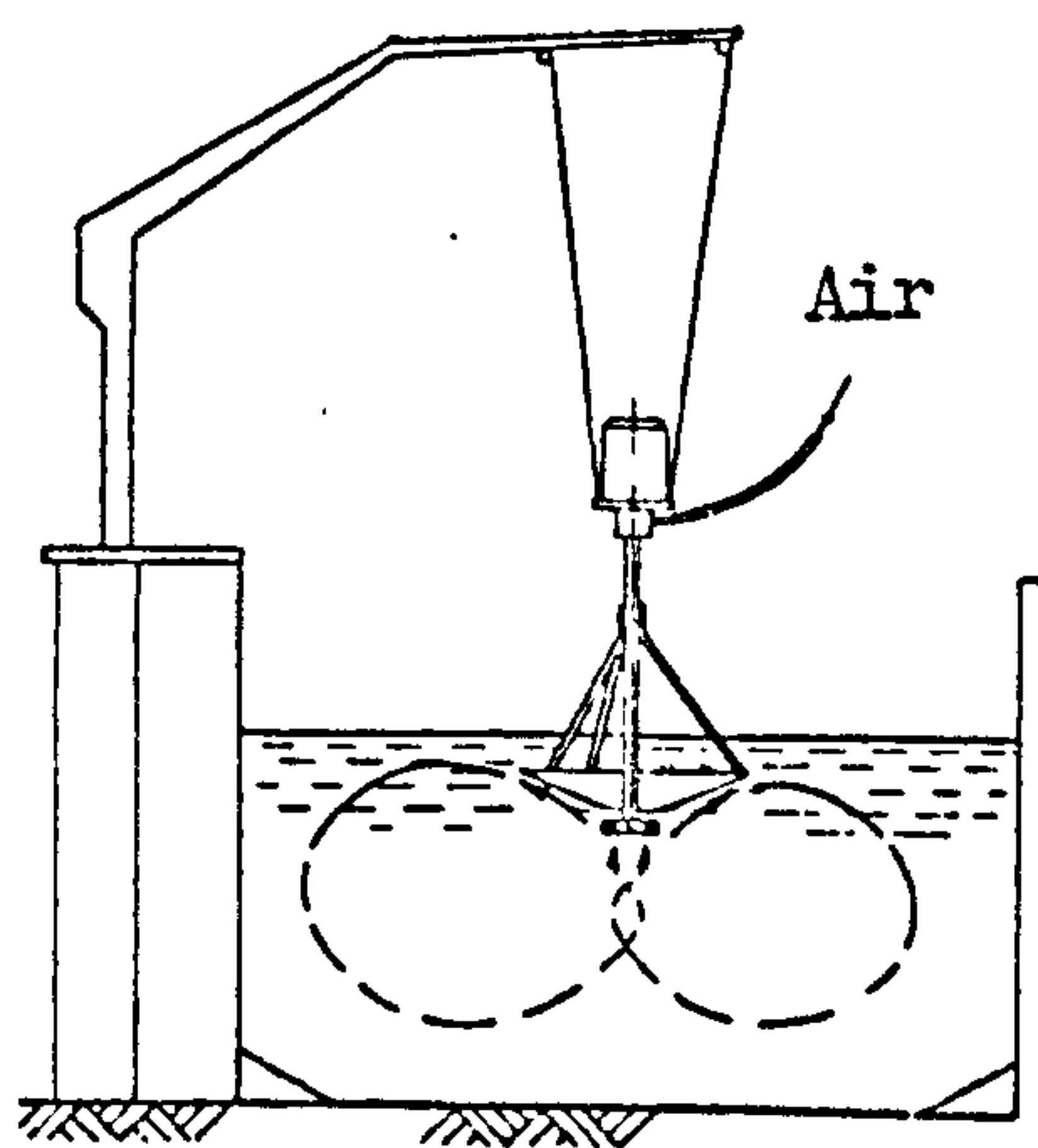


Figure 4.13. Fuchs aerator.

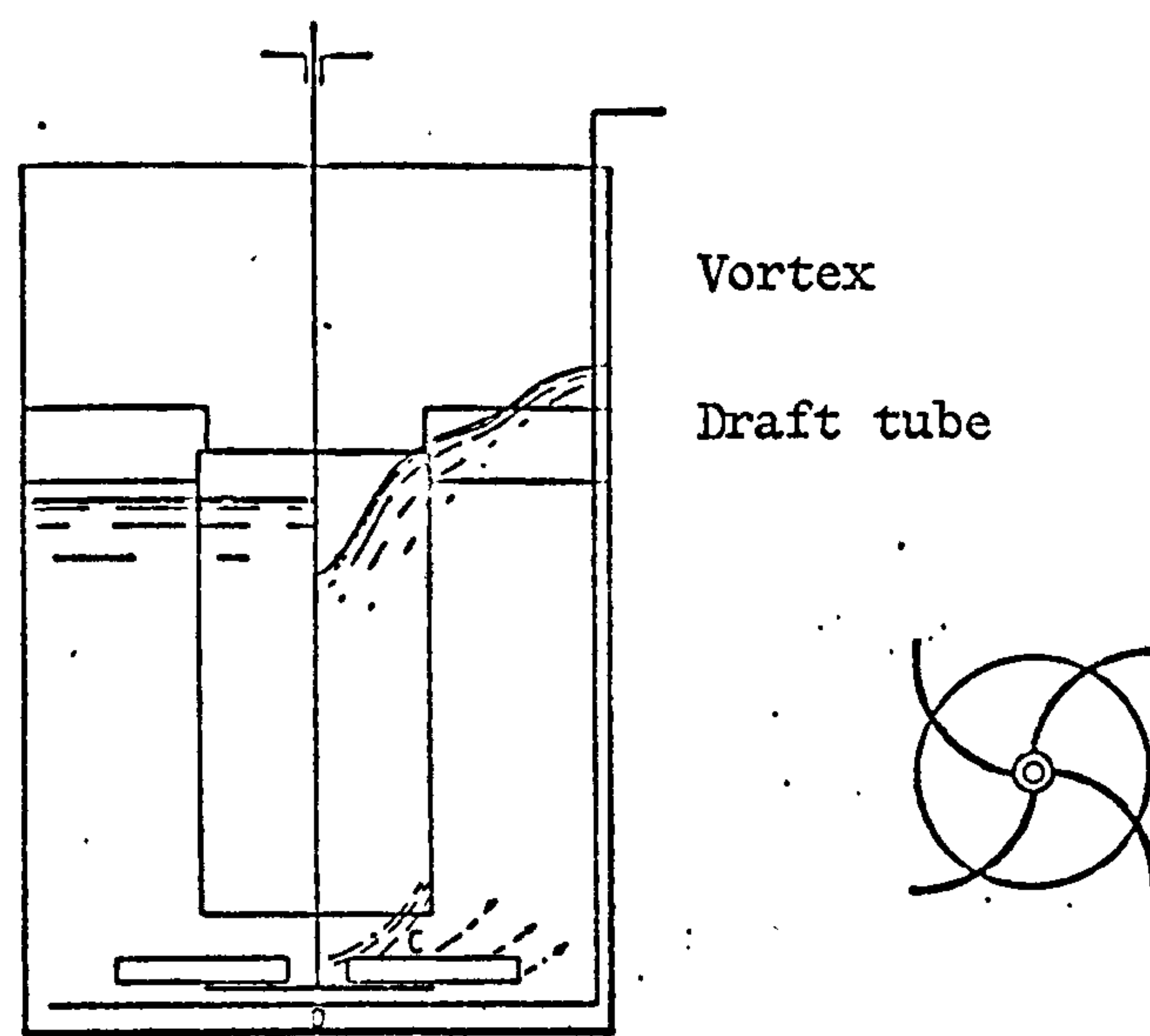


Figure 4.14. Waldhof system.

of the vortex, the liquid level at the vessel wall rises, and the liquid spills into the draft tube. When the amount of the liquid reaching the impeller is less than the impeller pumping capacity, air is also entrained by the impeller suction and is dispersed in the liquid in the form of bubbles.

#### 4.2.2.11 Carrousel system

Sometimes in practice the oxygen requirement is so low that a considerable part of the total energy of aeration would be employed for mixing and the rest for oxygenation. This would result in an uneconomic plant operation. An economic way for efficient transfer of oxygen in this situation is to concentrate oxygen supply in a small volume of the tank. The small volume corresponds to that required for optimum supply of oxygen. The problem of maintaining the sludge in suspension can be solved by somehow tapping a part of turbulence from the small volume which is sufficient enough to keep the circulation in a larger tank. Zeper and De Man (137) describe that the practical solution of this problem has led to the development of Carrousel system (Fig. 4.15).

In this system a surface aerator transfers the oxygen in a small volume of tank. A spiral flow pattern is developed along the vertical tube of the aerator. The dividing wall in the tank intercepts the spiral flow. As a result of this, the aerator pumps the liquid along one side of the dividing wall and sucks the liquid along the other side of the wall.

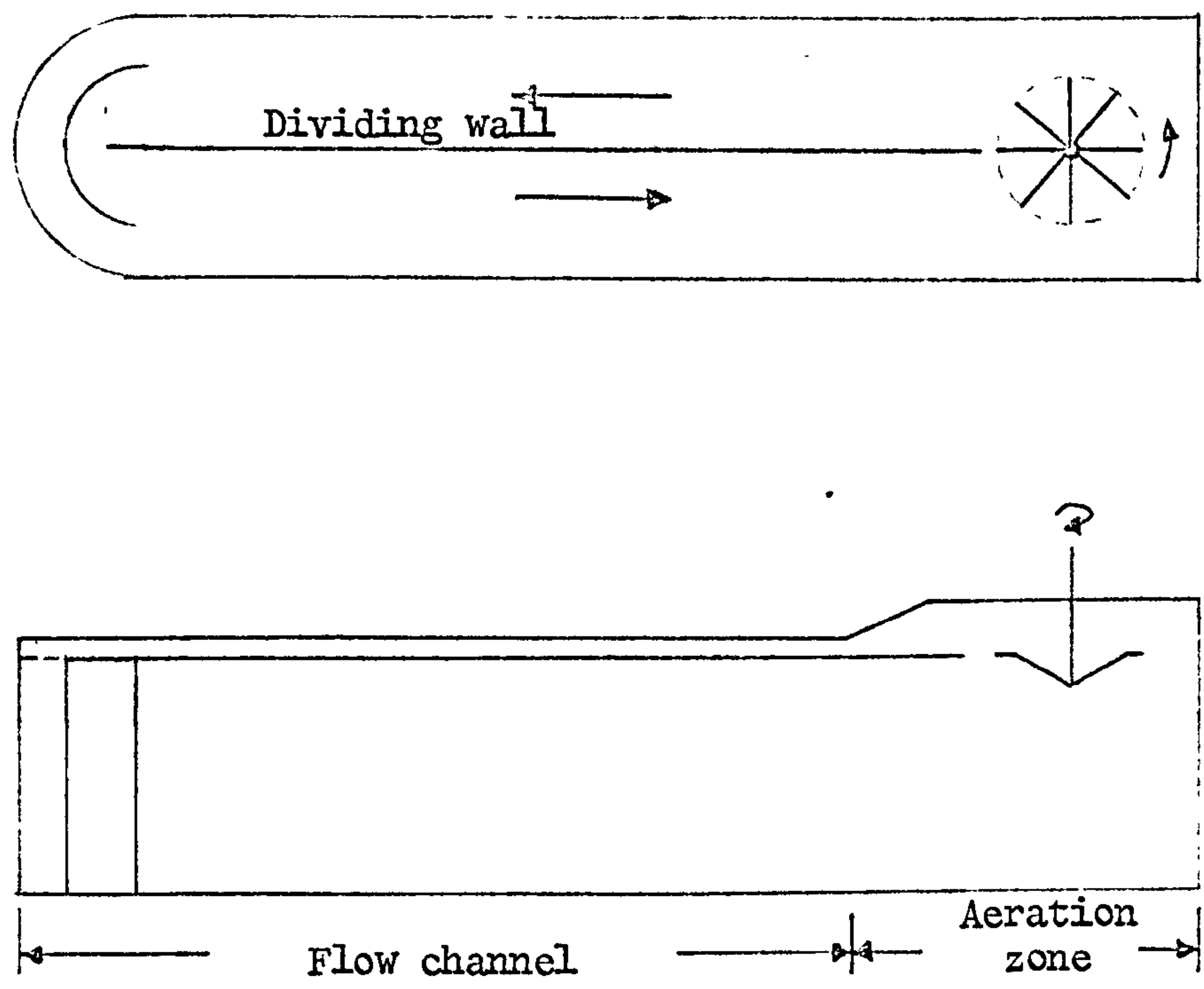


Figure 4.15 Basic form of Carrousel.



#### 4.2.2.12 Performance of mechanical aerators

Generally, the performance of mechanical aerators is characterised by efficient oxygen transfer, and good mixing. Large quantities of liquid are circulated through the intense-aeration zone. These aerators keep solids in suspension, and provide good mixing in large tanks (Eckenfelder and O'Connor (35)). Tests on some of these aerators have shown that 40 to 60% of the total oxygen is transferred in the intense aeration zone while the remainder is transferred in the turbulent mixing zone, as reported by Eckenfelder and Ford (37). In addition, the performance of the aerator improves when the water is jet sprayed instead of being finely sprayed (Knop and Kalbskopf (59)).

The aeration efficiencies for various mechanical aerators are shown in Table 4.1. With the exceptions of Fuchs aerator (15 kg  $O_2$ /kW h), perforated and open end pipe aerator (1 kg  $O_2$ /kW h), the aeration efficiency of all aerators generally lie within the range 2 to 4 kg  $O_2$ /kW h.

### 4.3 PROBLEMS ASSOCIATED WITH AERATION DEVICES

Commercial waste treatment plants create some operational problems in practice. Some such problems reported in literature are described below.

#### 4.3.1 Air Diffusion Units

In this case a considerable part of the operational cost is used in pumping the air, under pressure, through the diffusion units. In practice, as reported by Imhoff (55), it is found that

only 5 to 11 per cent of the total oxygen supplied is actually transferred to the liquid phase. The absorption efficiency increases in fine bubble aeration units: saran wrapped tubes; porous diffuser tubes. However, these units are highly susceptible to clogging. The frequent clogging results in a rapid increase in power and maintenance costs; also, the air must be filtered prior to pumping into these units. The clogging is rare in medium and coarse bubble aeration; however, the aeration efficiency of this system is very low ( $1 \text{ kg O}_2/\text{kW h}$ ).

#### 4.3.2 Mechanical Aerators

The oxygen transfer increases with the increase of speed of surface aeration. Spray diameter also increases with speed; hence the speed is limited by the tank width. Eckenfelder and Ford (37) say that the surface aerators when used in large lagoons and streams do not establish complete mixing. At larger depth, the surface aerator which does not use a draft tube will create the turbulence within the upper section, and will leave the lower section inadequately mixed.

As pointed out earlier in a brush aeration system all the oxygen is transferred in the vicinity of the brush (Pasveer (85)). In a field test on a Kessener brush aerator without baffles, it was observed that only one-third of the upper part had an excess oxygen, whereas, in the lower portion oxygen content was practically zero as reported by Von Der Emde (125). As a result of the poor mixing conditions in the lower part, considerable amounts of sludge settled at the tank bottom. The poor mixing can be

explained by the fact that the liquid pumped by the rotor flows back quickly towards the suction side of the rotor. It gives little chance to the liquid in the lower part to flow towards the suction side of the rotor. As mentioned in 4.2.2.6, the circulation in the brush aeration system is improved by using the suction and pressure baffles.

#### 4.4 ECONOMIC CONSIDERATIONS IN AERATION PROCESSES

An investment of capital in treatment of waste has no returns to the waste producing agencies. This emphasises the fact that the treatment and disposal of waste should be accomplished at a minimum cost.

The capital cost and the operating cost of an aerobic waste treatment plant are directly related to the total oxygen demand of the waste. The cost of dewatering, handling and disposal of sludge are additional costs and may become a significant proportion of the total operational cost. Power consumed in aeration is usually a considerable proportion of the operating cost; thus, consideration of aeration efficiency of a treatment plant is of prime importance.

## Chapter 5



## 5. PREVIOUS WORK ON GAS ENTRAINMENT AND MASS TRANSFER IN PLUNGING JET REACTOR

This chapter presents a chronological review of the previous work on the gas entrainment and the mass transfer aspects of a plunging liquid jet aeration system. Air had always been the gas medium, however, for some mass transfer studies  $\text{CO}_2$ ,  $\text{O}_2$  and  $\text{N}_2$  were also used. To avoid intermingling of different aspects, the chapter is divided into sections. Each section is devoted to a particular aspect of the phenomenon and only the work related to this aspect is reviewed in that section.

Before dealing with the actual topic of the chapter the instability of a turbulent liquid jet is briefly described; because the characteristics of a jet have a direct bearing on the phenomenon of gas entrainment.

The existing theories on the mechanism of gas entrainment are reviewed, followed by a summary of the empirical and theoretical correlations, derived by various authors to calculate the air entrainment rate. Correlations for maximum penetration depth of bubbles are then presented. Finally, the mass transfer aspects of the plunging jet system are reviewed. The chapter is closed by a brief discussion.

### 5.1 INSTABILITY OF TURBULENT LIQUID JET

A jet of liquid issuing from a nozzle is not always stable for all of its length. The disturbances in the jet stream grow along the jet length, and at some lengths may become strong enough to disintegrate the jet. The length of the jet from the nozzle exit to the break up point is called the "continuous length". The

relationship of the continuous length of a formed jet with the jet velocity is linear until a maximum is approached (Fig. 5.1). Beyond this maximum the continuous length decreases approximately hyperbolically with the further increase of jet velocity (Tyler and Richardson (120))

The disturbances along the jet stream due to induced turbulence and/or the action of air friction forces, produce surface irregularities at low jet velocities, while spreading and disintegration of jet at high jet velocities.

It will be shown later that these surface irregularities of the jet at low jet velocities and the spreading

of the jet at high jet velocities, play a major role in the process of air entrainment by plunging jet.

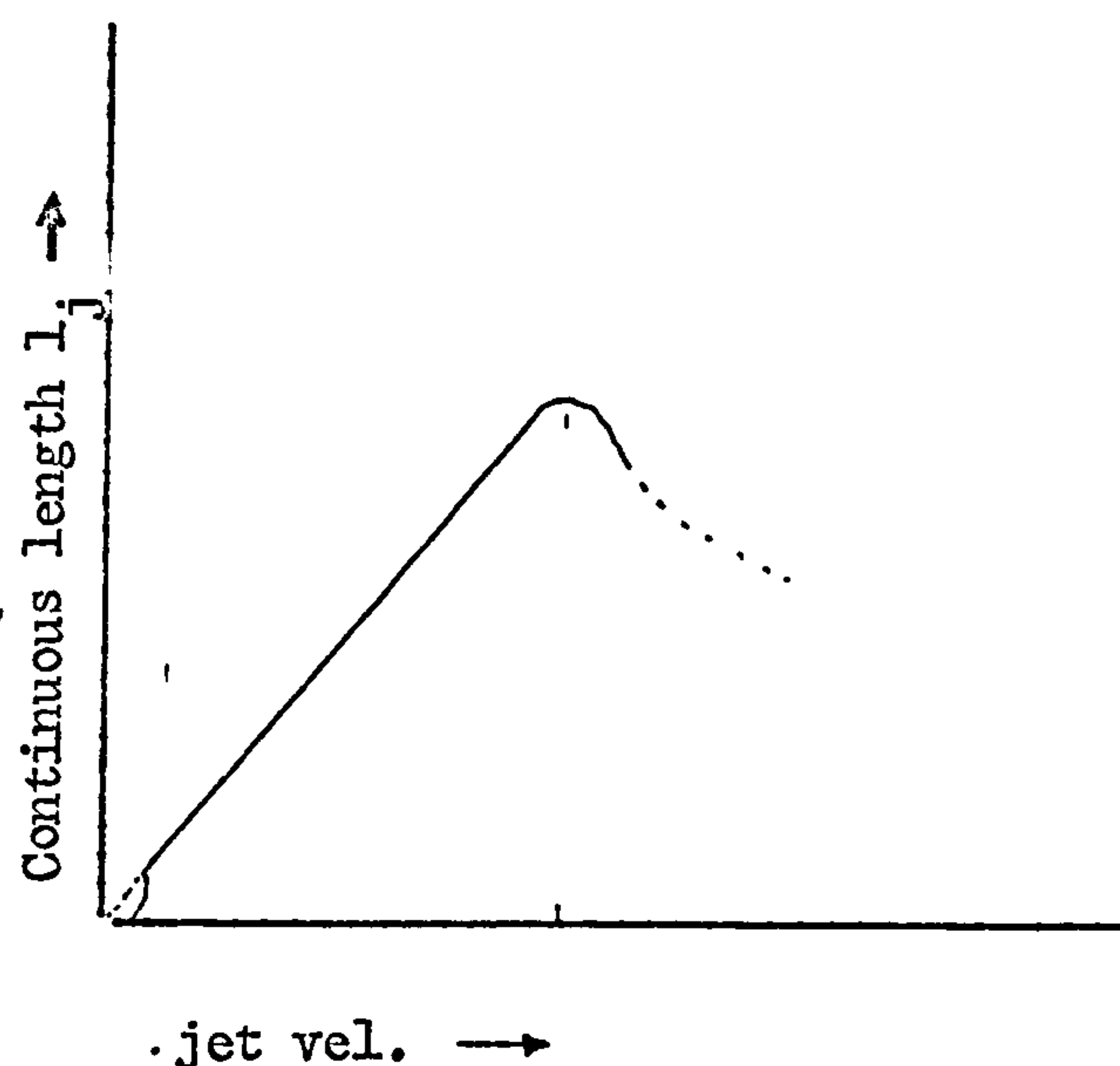


Figure 5.1: Relationship of continuous length with jet vel. showing the maximum continuous length or break-up length.

## 5.2 MECHANISM OF GAS ENTRAINMENT BY A LIQUID JET PLUNGING INTO A LIQUID POOL

This section reviews the literature on the mechanism of air entrainment by a liquid jet plunging into a pool of liquid. The literature on this subject is scarce but a good effort has been made during the past few years in this regard. The authors who have studied the mechanism of entrainment are: Mertes; Lin and Donnelly; De Frate and Rush; McCarthy et al.; Robertson et al.;

Van De Sande and Smith. Some authors studied only the laminar jets, and some only the turbulent jets, while the rest studied the whole course of entrainment mechanism from laminar to turbulent jets. All the authors agree that there is not a single mechanism that rules the process of air entrainment both in laminar and turbulent regions. This point will become clearer from the following detailed review on the work of the above authors.

Mertes (73) first realized the technological potential of the process of an entrainment by the plunging jet. He used the entrained gas to oxidize iron impurities in zinc sulphate liquor. Mertes claimed that the air entrainment is due to the formation of a gas film around the jet. The film is dragged down by the jet below the liquid surface and then sheared by the jet into bubbles.

With laminar jets Lin and Donnelly (63) also observed the existence of a gas film around the jet at the plunge point. The average length of this film varied from 0 to 4.5 mm. From their observations they conclude that the air entrainment in the laminar jets takes place through the gas film and the disintegration of the jet in the liquid pool causes the subsequent detachment of the film in the liquid pool.

At the higher jet velocities ( $Re_j > 1500$ ) the gas film was not observed. Lin and Donnelly did not investigate the mechanism for turbulent jets, but suggested that the entrainment with this mode is probably due to instability of the jet.



McCarthy et al. (71) observed plunging water jets with 30  $\mu$  second flash photographs at the plunge point and came out with a mechanism of air entrainment different from that described by Lin and Donnelly. They studied the entrainment mechanism for various jet velocities, ranging from very low (laminar) to high value (turbulent). They observed that at low jet velocities a funnel-like indent is caused by the jet in the liquid surface at the plunge point. They called this indent the "induction trumpet" because of its appearance. The liquid surface of the "induction trumpet" forms the walls of a venturi, and the entrainment takes place on the principle of a simple jet ejector pump mechanism. Large scale random fluctuations were noted in the rate of entrainment. The reason for these fluctuations is explained as follows. The "induction trumpet" is, in fact, a vortex and its vorticity is amplified whenever the moving vortices in the liquid bath merged with it. This results in a sudden increase in entrainment and hence the random fluctuations which were noticed.

The process of entrainment seems to be an intermittent process since the bubbles emerge from the throat of the "induction trumpet" in distinct masses (71).

With further increase of the velocity the jet surface becomes rough. An additional phenomenon of direct occlusion of bubbles between the jet surface and the trumpet wall surface comes into play. In this case no fluctuations in the rate of air entrainment were observed.

If the velocity is increased further (turbulent jet) the jet breaks up and the trumpet is completely disrupted. The air



entrainment is governed by cavity formation and closure about each separate drop with further increase in the entrainment rate.

De Frate and Rush (31) studied the mechanism of air entrainment solely by turbulent jets. They claim that the turbulent jets entrain air because of the presence of large disturbances and dilations along the jet length. In the absence of these disturbances, entrainment does not occur. De Frate and Rush report three modes of entrainment when the jet velocity varies from a low to a higher value.

At low jet velocity (turbulent jet) a shallow indent is formed around the jet. The bubbles disperse from the base of this indent. Initially, the entrainment is due to dilations which follow each other in quick succession at the plunge point. A dilation momentarily deepens the indent, whereupon air is trapped in the indent by the next dilation.

As the velocity of the jet increases further, the jet becomes varicose or sinuous and the indent at the plunge point is replaced by an oscillating cavity. This is the second mode of entrainment. When a drop or dilated jet segment fills the neck of the contracting cavity, the air is trapped in the cavity and is then dispersed into the pool.

The third mode is characterized at very high jet velocities, and with this mode of entrainment the cavity does not collapse and is sometimes stabilized by a swirl.

Robertson et al. (97) found that the gas film is formed when the viscosity of the jet liquid is greater than  $5 \times 10^{-2}$  poise whereas the jet of lower liquid viscosity produced the induction

trumpet at the plunge point. This coincides with the finding of McCarthy et al. (71).

Most recently (1974) Van De Sande. (121) studied the mechanism of entrainment for both laminar and turbulent jets. According to Van De Sande at low jet velocities (laminar) the movements in the elements of the receiving liquid at the plunge point are responsible for the air entrainment. These movements are caused by the disturbances in the stream. Fig. 5.2 shows the course of air entrainment at the low jet velocity due to a disturbance in the jet stream.

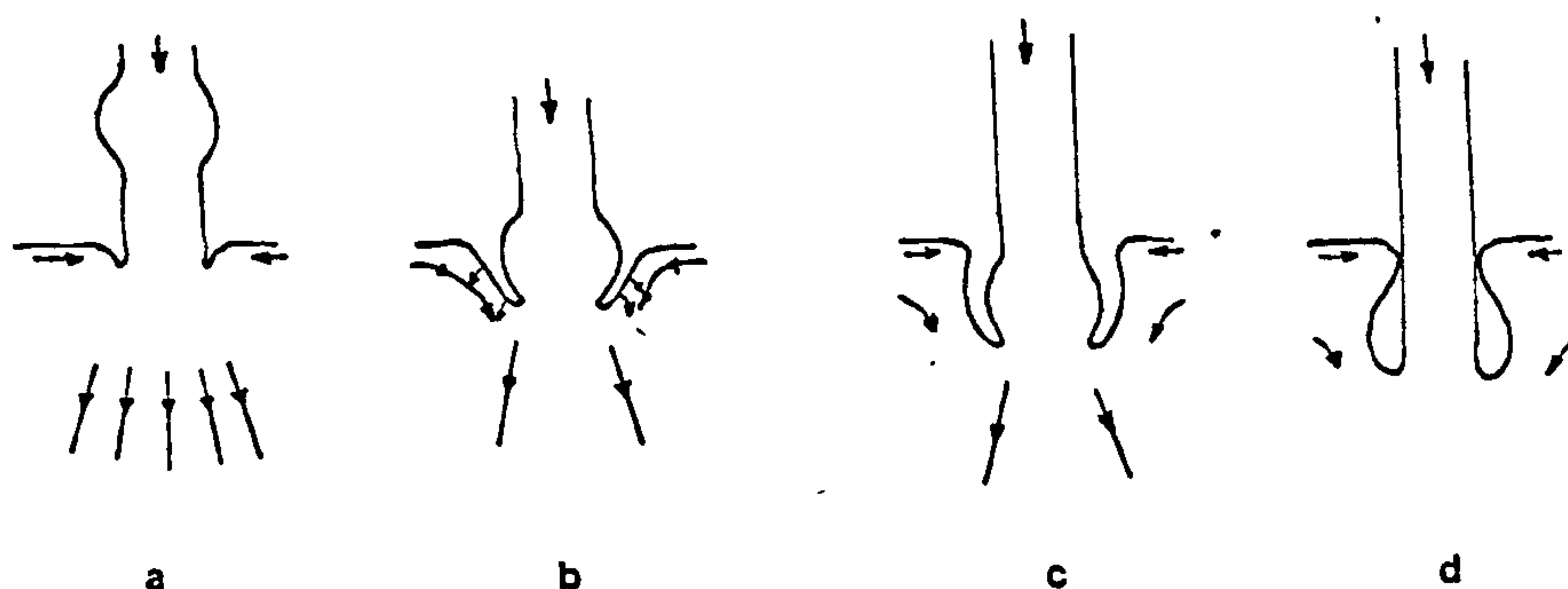


Figure 5.2. Process of the air entrainment by a disturbance in the jet stream at the low jet velocity.

The liquid elements in the vicinity of the plunge point flow towards the plunge point as shown by arrows. Arrival of a disturbance at the plunge point depresses the liquid elements adjacent to the plunge point. As the disturbance penetrates further, the cavity caused by the depression gets deeper. When the disturbance sinks into the liquid, the side-ways movement of the liquid surface elements close the cavity. The air so captured is later broken up into bubbles by the shearing action of the jet.



At high jet velocities (turbulent) the entrainment process is continuous. Air friction forces become important. The surrounding air is captured inside the rough surface of the jet. The air boundary layer is also carried along with the jet. The jet hits the liquid surface, and carries the captured and the boundary layer air a long distance into the liquid.

With a further increase in velocity, the jet is destroyed by the air friction force, and atomisation of the jet occurs. The separate liquid drops hit the liquid surface causing air filled cavities.

While studying the history of the entrained bubbles, Hauxwell (47) revealed some fascinating aspects - which none of the other authors have pointed out - regarding the behaviour of these bubbles. Like other authors, he also observed the formation of an induction trumpet or cavity at the plunge point of the jet. In his study he found that the bubbles are driven rapidly to their maximum depth of penetration. The bubble penetration velocity approaches approximately the jet velocity. After reaching the maximum penetration depth the bubbles tend to accumulate in the form of a swarm. The swarm seemed to be entrapped by the diverging submerged jet stream. Also, the size of bubble swarm increased with the increase of jet liquid flow rate. Photographs showed that the bubbles could be trapped in the bubble swarm for periods exceeding 10 seconds. At the jet velocities near the minimum entrainment velocity, the bubbles may be trapped in the jet stream envelope for periods exceeding five minutes. Within the bubble swarm turbulence is relatively high. Moreover, the bubbles are in a vibratory state, oscillating back and forth, up and down.

As the bubble detaches itself from the jet stream envelope, it rises to the liquid surface through the peripheral regions of the bubble swarm and burst at the surface releasing the air to atmosphere. However, sometimes rising bubbles are caught by liquid eddies just below the liquid surface and these surface bubbles are dragged to the jet stream envelope by the liquid flow patterns generated by the jet. In this way some of the entrained bubbles are recirculated in the system. However, the majority of the rising bubbles burst at the liquid surface. Hauxwell did not mention about the coalescence of the bubbles; however, coalescence is expected as a result of collision of entrained bubbles especially within the turbulent two phase cone.

From the preceding review it is clear that the process of entrainment is a complex process. Entrainment is not only dependent upon the jet parameters, but also upon the conditions of the jet surface itself. For instance, the disintegration of the jet surface in the forms of drops, would cause additional entrainment due to the impinging drops or the train of drops. Also, the level of induced turbulence in the jet stream would affect the entrainment.

Despite these complications, attempts have been made to quantify the entrainment process, particularly the work of Van De Sande (121) is admirable. These attempts are summarized in the following section.



### 5.3 RELATION OF JET PARAMETERS WITH ENTRAINMENT RATE

It was pointed out earlier that Mertes (73) was the first who studied the phenomenon of air entrainment by a plunging jet.

Since then there was silence until 1950 when Shirley (107) carried out experiments to study the effect of flow characteristics of the plunging jet on air entrainment rate. In fact, his aim was to seek an explanation for the entrainment by surface waves in open channels. He obtained data for various jet sizes at varying jet angles ranging from 45 to 67 degrees. The data for vertical jets was obtained by extrapolation of the data for angular jets.

Shirley drew the following important conclusions from his work:

- (a) The air entrainment rate is not a direct function of jet diameter and jet velocity alone, but is also influenced by the characteristics of the liquid.
- (b) The minimum entrainment velocity (velocity of the jet at the onset of entrainment) is governed by the jet surface roughness and the turbulence in the liquid pool. The minimum entrainment velocity is reduced by enhancement of either or both factors.

Ohyama et al. (80) studied the effect of jet parameters ( $d_j$ ,  $V_j$ ,  $l_j$ ) on the air entrainment rate. They used vertical jets in their experiments. Finally they correlated their data by the relationship shown in Table 5.1, which shows the empirical and theoretical correlations developed by various authors for the prediction of the air entrainment rates.

TABLE 5.1                      Various Correlations for the Prediction of Air Entrainment Rates

Investigator	Correlation	
OHIYAMA et al. ( 80 )	$En^a = \left(\frac{V_j}{g l_j}\right)^{2-0.447} \left(\frac{d_n V_j l_1}{\eta_1}\right)^{1.33} \left(\frac{\eta_1}{\sqrt{\sigma} l_1 d_n}\right)^{2.18} \left(\frac{l_j}{d_n}\right)^{0.281}$	5.1
LIN and DONNELLY ( 63 )	$\left(\frac{d_j^* V_e}{\sigma}\right)^2 = 10 \left(\frac{V_e d_j^* l_1}{\eta_1}\right)^{0.74}$	5.2
where $d_j^*$ is jet diameter at plunge point, and $V_e$ is minimum entrainment velocity.		
SZEKELY ( 115 )	$En = \frac{4}{d_j} \left(\frac{3 \eta_a l_j}{l_a^2 V_j}\right)^{0.5} + 1.73 d_j \left(\frac{\eta_a l_j}{l_a^2 V_j}\right)^{0.5}$	5.3
De FRATE and RUSH ( 31 )	$En = \frac{l_a V_j^2 l_j}{\sigma} \times 10^{-6}$	5.4
HENDERSON et al. ( 48 )	$En = \left(\frac{d_j}{d_n}\right)^{2*} - 1$	5.5
CIBOROWSKI and BIN ( 25 )	$En = 4.06 \times 10^4 d_n^4 \left(\frac{1}{g l_j \times 10^3}\right)^4 \left(V_j^2 - \frac{30}{d_n l_1}\right) - A \left(\frac{l_j}{d_n}\right)^{1.8}$	5.6
where $u^* = 47.9 d_n - 1.603$ , $d_n$ is in m, $l_j$ is in m, and $V_j$ is in m/s A is a constant.		

<sup>a</sup> Entrainment ratio:— Ratio of air entrainment rate to jet liquid flow rate.

TABLE 5.1 (continued)

Investigator	Correlation	
VAN DE SANDE and SMITH ( 123)	(a) For $2 < V_j < 5 \text{ m/s}$ , and $Q_a > 1.5 \times 10^{-5} \text{ m}^3/\text{s}$	5.7
	$Q_a = 0.015 \left( \frac{d_j^2 V_j^{1.05}}{\sin^{1.5} \theta} \right)^{\frac{3}{4}}$	
	where $\theta$ is jet angle to liquid surface.	
	(b) For jets near or beyond the break up length	5.8
	$Q_a = 0.85 \times 10^{-5} + 21 \times 10^{-5} \left( \frac{1}{2} \xi_1 \frac{\pi}{4} d_j^2 V_j^3 \right)$	
	(c) For high velocity jets ( $We > 10$ , $Re_{1j} < 5 \times 10^5$ )	5.9
	$Q_a = Q_c + Q_b$	
	$Q_c = \frac{\pi}{4} V_j d_n^2 (1.56 \times 10^{-2} We^{\frac{1}{3}} Re_{1j}^{\frac{1}{3}} - 1)$	5.10
	$Q_b$ is obtained from Fig. 5.3.	



As pointed out in the introduction, the occurrence of air entrainment in some industrial processes (pouring of molten metal or glass, etc.) is an undesirable phenomenon. Thus, knowledge of the jet velocity at the onset of entrainment is important in these pouring and filling operations.

Lin and Donnelly (63) also investigated the effect of jet velocity and found that the minimum entrainment velocity is a function of the jet diameter at the plunge point and the viscosity of the liquid. They developed a correlation to predict the minimum entrainment velocity (Table 5.1).

De Frate and Rush (31) working with turbulent jets found that the air entrainment increases with the increase of the jet velocity and the jet length, but decreases as the jet diameter increases. They give a simple correlation (Table 5.1). Note that the correlation was obtained from highly scattered data.

Szekely (115) considered that the entrainment phenomenon in the pouring of a molten metal stream into a liquid metal pool is mainly due to volumetric influx of the air boundary layer associated with the jet surface. He derived a theoretical equation to calculate the entrainment rate due to the boundary layer for any jet length (Table 5.1).

Swiggett (114) found that for low velocity turbulent jet plunging into  $\text{CO}_2$  - water system, the rate of  $\text{CO}_2$  absorption is independent of the jet length.

Henderson et al. (48) studied the entrainment process in an air-water system. Nozzles of  $\frac{1}{10}$ ,  $\frac{1}{4}$  and  $\frac{1}{2}$  inch diameter having length to diameter ratio ( $l_n/d_n$ ) 0, 1 and 10 respectively were



used. The jet length was varied up to 100 nozzle diameters. They mainly studied the effect of jet length and nozzle design on the entrainment rate. For the jet velocities less than 15 m/s using  $\frac{1}{10}$  inch nozzle, he reports that over a significant range of the jet length (0 to 18 cm), the air entrainment is independent of the jet length. However, for jet velocities greater than 15 m/s the surface irregularities develop and the entrainment rate increases with the increase of either velocity or the length of the jet. With  $\frac{1}{10}$  inch nozzle having zero length the entrainment rate was zero. Moreover, an increase in the ratio ( $l_n/d_n$ ) considerably increased the entrainment rate. They finally correlated the entrainment ratio with a parameter based on surface roughness of the jet. The correlation is given in Table 5.1.

Ciborowski and Bin (25) in Poland measured the air entrainment rate by modifying the method employed by Ohyama et al. (80). They obtained the entrainment data in water as well as in 25 and 40% glycerol solutions. At low jet velocities their work is an extension to the work done by Lin and Donnelly. They report that the Weber number ( $We$ ) is approximately equal to 20 and constant for Reynolds number ( $Re$ ) within the range 3350 to 25000. The range exceeds that investigated by Lin and Donnelly. Both the  $Re$  and the  $We$  are calculated for the minimum entrainment velocity ( $V_e$ ) at the plunge point.

Ciborowski and Bin (25) correlated their data by a rather complicated correlation shown in Table 5.1. They report that a simple plot of the entrainment ratio ( $\frac{Q_a}{Q_1}$ ) against Reynolds number of the jet is not linear. The constant  $A$  in the correlation varies:

for water 0 to 1; for glycerol greater than 1. They have not mentioned the actual values of  $A$  from their experiments. They compared their data with that of Ohyama et al. (80), but found sheer disagreement with the data pertaining to small diameter jets and glycerol solution.

Recently (1972, 1973) Van De Sande and Smith (123, 124) have studied comprehensively the air entrainment rate by

the turbulent jets. They have characterized the jet velocity as being low or high. The jet velocities less than 5 m/s are considered as low jet velocities. The high jet velocities have no defined minimum value. Their minimum is given by  $We$  equal to 10. So, the jets having  $We$  greater than 10 are in the high velocity region. A transition region exists between the low and the high jet velocities.

They say that the impact phenomenon at low jet velocities is so complex that theoretical or even quasi-theoretical treatment of the problem is not possible.

At the low jet velocities ( $2 < V_j < 5$  m/s) for which the jets are not broken, they related the air entrainment rate with the kinetic energy of the jet. The correlation is given in Table 5.1. For the jets near or beyond the break up length, they give a different correlation; but, again, the air entrainment rate is related to the kinetic energy of the jet (Table 5.1).

For the high velocity jets ( $We > 10$ ), the entrainment rate for vertical jet is given by:

$$Q_a = Q_b + Q_c \quad 5.9$$

where  $Q_c$  is the volumetric rate of the air captured by the jet

surface and  $Q_b$  is the volumetric rate of the boundary layer air drawn below the liquid surface by the jet.  $Q_c$  is calculated by equation 5.10 in Table 5.1, and  $Q_b$  is obtained from Fig. 5.3. The value of  $d_j^*$  (envelope diameter of the plunging jet) is given by the empirical equation:

$$\frac{d_j^*}{d_n} = 0.085 (We \times Re_{1j})^{\frac{1}{6}} \quad 5.11$$

which is valid for  $We \cdot Re_{1j} > 7 \times 10^6$ .

In the equation 5.11:

$$Re_{1j} = \frac{v_j l_j \rho_a}{\eta_a} \quad 5.12$$

The boundary conditions for this correlation are:

$$(1) \quad We > 10$$

$$(2) \quad Re_{1j} < 5 \times 10^5.$$

Besides measuring the air entrainment rate Ciborowski and Bin, Van De Sande and Smith also measured the depth of penetration of bubbles.

Ciborowski and Bin (25) correlated the data for the maximum penetration depth of bubbles by the equation:

$$\frac{h}{d_n} = 1.15 + 3.17 \frac{v_j}{U} \quad 5.13$$

where  $h$  is the maximum penetration depth of the bubbles,  $d_n$  is the nozzle diameter, and  $U$  is the bubble velocity. They also noted that the velocity of the rising bubble at the maximum penetration depth was 0.3 m/s.



Van de Sande and Smith (122) obtained the penetration depth of the jet by measuring the distance the air bubbles could travel under water surface. They correlated their data to predict the penetration depth by:

$$h = 1.75 v_j^{0.85} d_j^{0.65} \quad 5.14.$$

for  $v_j$  less than 3 m/s  $h$  deviated from that predicted by the equation 5.14.

In a recent (1974) work, Van De Sande (121) also considered the air entrainment rate ( $Q_a$ ) in correlating the data for the depth of penetration. So now:

$$h = 0.42 \frac{v_j^{4/3} d_j}{Q_a^{0.25}} \quad 5.15$$

So far, all the known literature concerning the mechanism and quantitative estimation of the air entrainment rate by the plunging system has been reviewed. What remains is the review on mass transfer aspects, and this is presented in the following sections. From the mass transfer point of view the study of bubble formation, bubble coalescence, bubble retention time and bubble size distribution is important.



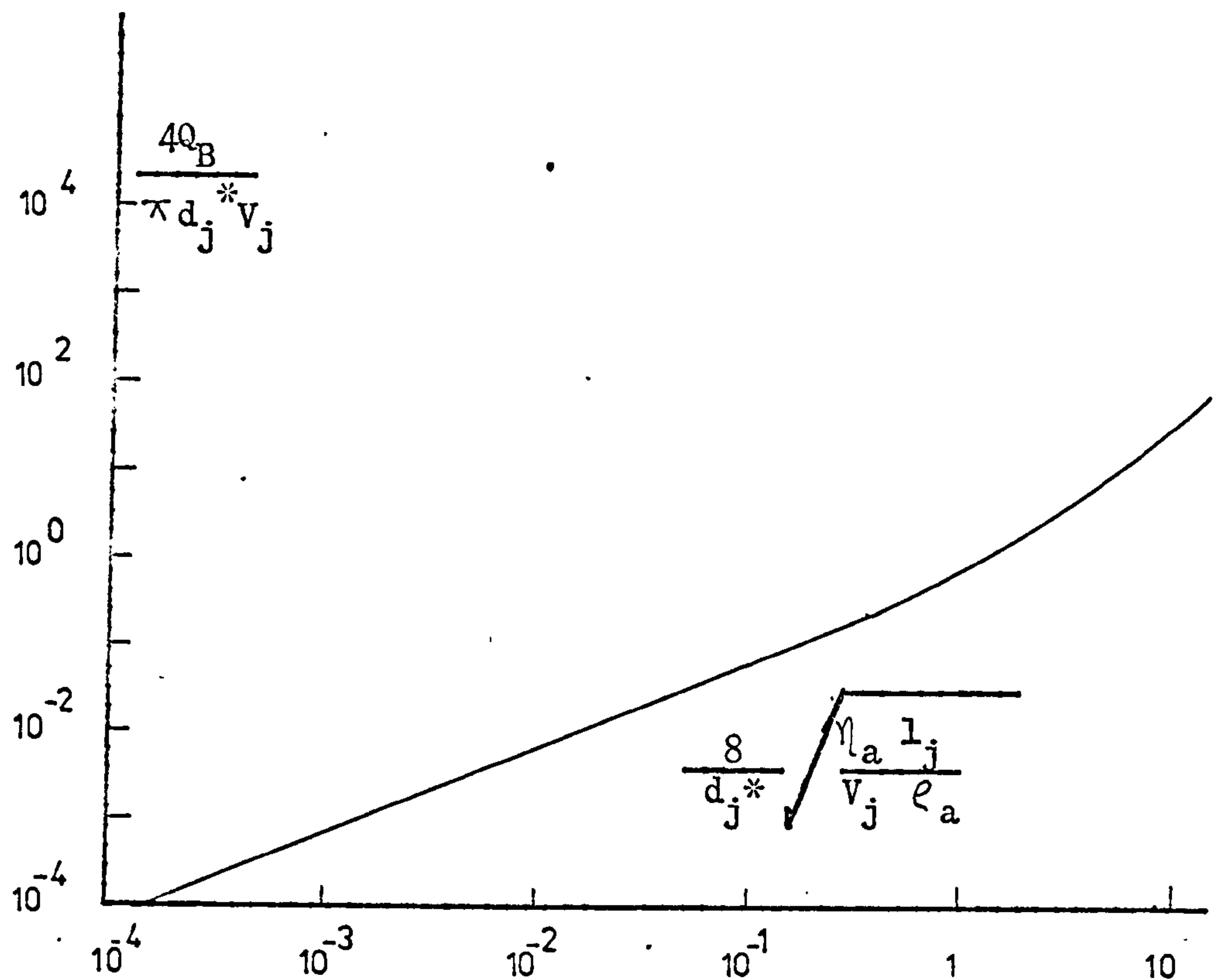


Fig. 5.3. Relationship for the air entrainment rate by the boundary layer around the jet (after Van de Sande and Smith (123)).

The results on the bubble size investigations reported by some authors are first described.

#### 5.4 BUBBLE SIZE DISTRIBUTION IN A PLUNGING JET SYSTEM

Ciborowski and Bin (25) and Hauxwell (47) measured the bubble sizes by taking photographs of the bubbles; however, Van de Sande measured by using the technique introduced recently (1971) by Todtenhaupt (117).

Ciborowski and Bin report that in the plunging jet system the average bubble diameter is within the range: 0.6 to 1.7 mm for

water; 1.3 to 3.6 in 40% glycerol. Moreover, the bubble size distribution is normal.

Hauxwell (47) observed that the bubble diameters in the bubble swarm are in the range: 1 to 4 mm for the air-water system. The bubbles at the periphery of the swarm are relatively smaller. However, this disagrees with the findings of Van de Sande (121) discussed below. Hauxwell observed that the bubble diameter decreases with the decrease in jet diameter.

Van de Sande found that the Sauter mean diameter of the bubble is 3.5 mm at the outer surfaces of the two phase cone. He reports that measurement of the bubble sizes inside the bubble swarm indicated that 95 % of the bubbles have a diameter less than 1.4 mm; however, he says that the measurements are doubtful because of high turbulence inside the two phase cone.

## 5.5 MASS TRANSFER IN A PLUNGING JET REACTOR

Mertes (73) studied the potential of the plunging jet system as a device for mixing and reacting gas and liquid phases. Later Burgess et al. (16) claimed that the plunging jet reactor is a more efficient contactor volumetrically than the typical stirred tank, packed column, or bubble plate gas-liquid contactors. They measured the interfacial areas in the plunging jet reactor by absorbing  $\text{CO}_2$  in NaOH solution, and found that the interfacial area is a function of the jet surface roughness, and the jet velocity.

De Frate and Rush (31) found that all the  $\text{CO}_2$  entrained in the plunging jet reactor was absorbed by sodium hydroxide solution.

Hauxwell (47) studied the effect of the jet parameters on the gas absorption rate in a plunging liquid jet reactor. He studied the absorption of  $\text{CO}_2$ ,  $\text{O}_2$  and  $\text{N}_2$  in degassed tap water. The diameter of jets varied from 1.4 to 6.8 mm. The jet Reynolds number was in the range of 4000 to 20,000. Hauxwell used the term "Transfer Factor" to define the product of overall mass transfer coefficient and specific interfacial area. Transfer factor is thus directly proportional to gas mass transfer. The results showed that the Transfer Factor is inversely proportional to the solubility of the gas in the liquid: from interface mass transfer theory the ratio of the gas film resistance to the mass transfer is directly proportional to the solubility. The "Transfer Factor" for  $\text{O}_2$  and  $\text{N}_2$  are not significantly different. The value of the Transfer Factor calculated for  $\text{CO}_2$  absorption is about one-third of that for  $\text{O}_2$  and  $\text{N}_2$ , indicating the effect of increased solubility. He plotted his results for oxygen transfer in terms of Transfer Factor versus  $(\text{Re}_j) \times (\text{We})$ ; and the Transfer Factor was found to vary with first power of  $(\text{Re}_j) \times (\text{We})$ . From this he inferred that the oxygen transfer rate would be directly proportional to kinetic energy of the jet, which coincides with the findings of Ahmed and Glover (1).

Van de Sande and Smith (122) also measured oxygen transfer rates in a partially deoxygenated pool of water. They report that the oxygen transfer coefficient increases with the increase of the jet velocity and/or the jet diameter. Also, as the jet velocity increases  $K/Q_a$  (ratio of the oxygen transfer coefficient to the air entrainment rate) increases; however, the jet diameter does not seem to have any significant effect on this ratio.



Moreover, the aeration efficiency decreases with the increase of power of jet.

Van de Sande (121) correlated the oxygen transfer coefficient with the equivalent air entrainment rate by the following equation:

$$K_L A = 6.2 \times 10^{-2} V_j^{1.33} d_j Q_a^{0.3} \quad 5.16$$

The above equation is semi-theoretical, since the constant of proportionality and the powers of  $V_j$  and  $Q_a$  are obtained by fitting the experimental data. In obtaining the above equation it was assumed that the two phase is saturated and the oxygen transfer takes place by the physical exchange of the saturated water through the two phase cone surfaces. This assumption is weakened by the fact that in aeration by diffuser units, despite the high turbulence and shear at the diffuser pores, the oxygen transfer from the bubbles is only 3% at zero diffuser submergence (Lamb (60)). Van de Sande showed that the above equation fitted well with the experimental results; however, one reason for good fit could be the right selection of the parameters in the equation. In contrast to the above relation, this author found that the oxygen transfer rate is directly proportional to air entrainment rate in biological system. This will be described later in detail. Because of complicated bubble dynamics in the liquid pool it seems dangerous to base any correlation on the above assumption. The best thing is to collect the facts on mass transfer aspects by intensive experimentation.



## 5.6 DISCUSSION

From the above review, it is clear that a good effort has been made during the past few years to explore various aspects of the plunging jet system. The mechanism of air entrainment is now understandable. Its knowledge is important for any theoretical analysis of the entrainment phenomenon.

The system has been investigated quantitatively by several authors. The amount of air entrainment was measured and several correlations have been produced for calculation of entrainment rate. Some correlations are simple and some are too complicated to use. Most of these correlations are derived from highly scattered data. In addition, there is lack of agreement between the results of various authors.

Possibly the above discrepancies could have been due to one or more of the following reasons:

- (a) Inaccurate measurement of the entrainment;
- (b) Use of inhomogeneous data (e.g. data of low jet velocities and high jet velocities processed combinedly);
- (c) Extrapolation of angular jet data to vertical jet data;
- (d) Variations in experimental apparatus.

From the above review, it is realized that an important thing is lacking; that is, the investigation on the plunging jet system as a "biological reactor" for its application in waste treatment and fermentation processes. This aspect of the plunging jet system as described earlier is the main objective of this work.

## Chapter 6

## 6. MEASUREMENT OF OXYGEN TRANSFER RATE IN AN AERATION PROCESS

For a rational design of an aeration plant, it is important to know the "ability" of an intended aeration unit to maintain an economic dissolved oxygen concentration in the aeration tank and to cope with the oxygen requirements of the micro-organisms. This ability is decided by the "oxygenation capacity" of the aeration unit, which is defined as the kilogram of oxygen transferred to a cubic meter of liquid maintained at zero dissolved oxygen concentration under the following standard conditions:

Temperature of liquid	20°C
Atmospheric pressure	760 mm Hg.
Dissolved oxygen concentration	0.0
Water purity	Clear.

The rate of oxygen transfer in a turbulent liquid is given by the equation:

$$\frac{dC_L}{dt} = K_L a (C^* - C_L) \quad 2.3$$

where  $\frac{dC_L}{dt}$  is rate of change of dissolved oxygen concentration in the liquid,

$K_L a$  is oxygen transfer coefficient,

$C^* - C_L$  is oxygen deficit in liquid.

Integration of equation 2.3 for the initial conditions  $t = 0$  and

$C_L = 0$  gives:

$$C_L = C^* (1 - e^{-K_L a t}) \quad 6.1$$

where  $C_L$  increases exponentially with  $t$ .

A record of dissolved oxygen concentration with time for aeration of deoxygenated water would be obtained as shown in Fig.6.1.

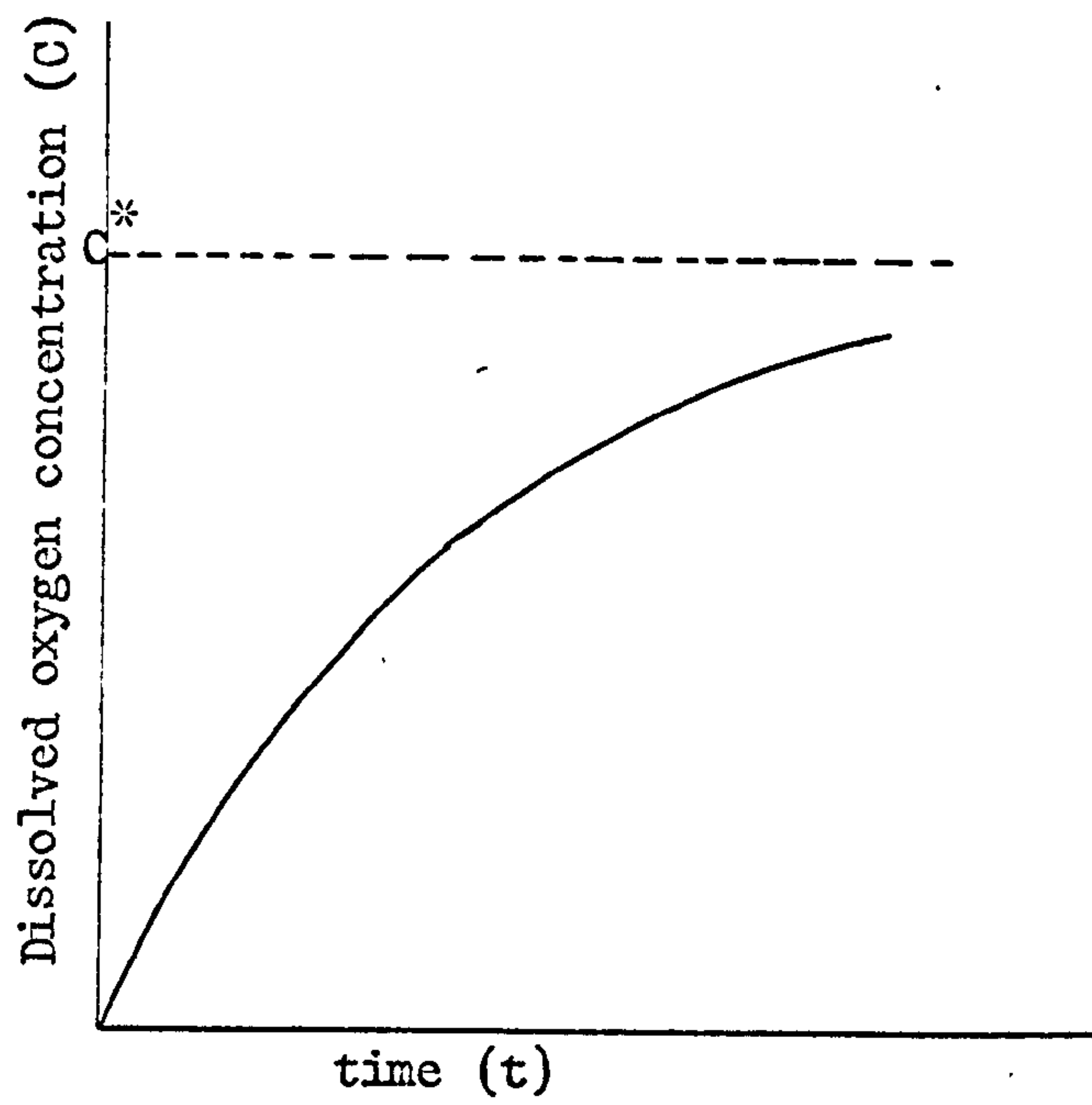


Figure 6.1. Variation of dissolved oxygen concentration with time during the course of aeration.



The time required to approach the saturation value will depend upon the oxygen transfer coefficient ( $K_L a$ ) of the aeration system.

Thus with the knowledge of  $K_L a$  the oxygenation capacity (OC) is calculated by:

$$OC = K_L a C^* \quad 6.2$$

where  $C^*$  is saturation concentration of oxygen.

Oxygenation capacity and aeration efficiency are usually expressed at standard conditions.

So, the  $K_L a$  determined at temperature  $T$  can be related to that at  $20^\circ\text{C}$  by the equation:

$$K_{L a_{20^\circ\text{C}}} = K_{L a_T} (\theta)^{(20-T)} \quad 2.8$$

where  $\theta = 1.024$ .

If the test liquid is other than water such as waste liquor, then  $K_L a$  is divided by the  $\alpha'$  factor of the waste ( $\alpha'$  factor is the ratio of  $K_L a$  in waste liquor to the  $K_L a$  in water). Both  $K_L a$  values are determined under identical aeration conditions.

Oxygen saturation value ( $C^*$ ) is affected by the barometric pressure, temperature, and the type of liquid (i.e. waste liquor). Adjustments for the influence of barometric pressure and the waste liquor in the value of  $C^*$  is made by the relation:

$$C^* = C^*_c \frac{P'}{760} \beta \quad 6.3$$

where  $P'$  is barometric pressure in mm,

$\beta$  is  $C^*_{\text{waste}}/C^*_{\text{water}}$  )

and  $C^*_c$  is  $C^*$  at standard conditions or any other conditions specified by  $c$ .

The influence of temperature on  $C^*$  is calculated from the proceedings paper: "Solubility of Atmospheric Oxygen in Water", American Society of Civil Engineers (111) as:

$$C^* = 14.652 - (0.4102)T + (0.0079)T^2 \quad 6.4$$

where  $C^*$  is in mg/lt. and  $T$  in  $^{\circ}\text{C}$ .

Oxygenation capacity can be stated at standard conditions or any other specified conditions signified by subscript  $c$  by the general equation:

$$(OC)_c = K_L a (C^*_c - C_{Lc}) (e^{20-T}) \left(\frac{1}{\alpha'}\right) \quad 6.5$$

#### 6.1 UNSTEADY-STATE AERATION OF DEOXYGENATED TAP WATER

Tap water is deoxygenated by adding sodium sulphite and  $\text{Co}^{++}$  catalyst. The deoxygenated water is aerated and the concentration of dissolved oxygen at equal time intervals are noted or recorded.

The values of oxygen deficit  $(C^* - C_L)$  are calculated. The slope of  $(C^* - C_L)$  against  $t$  on a semilog scale when multiplied by 2.3, gives  $K_L a$ .

#### 6.2 STEADY-STATE AERATION OF DEOXYGENATED TAP WATER

In this method deoxygenated water or low oxygen concentration water ( $C_i$ ) is fed at a constant flow rate ( $q$ ) to an aeration tank and a constant dissolved oxygen concentration ( $C_L$ ) in the tank is eventually obtained. The liquid volume in the tank is kept constant.

Oxygen mass balance on the system gives:

$$q(C_L - C_i) = V K_L a (C^* - C_L) \quad 6.6$$

from which  $K_L a$  can be calculated.

### 6.3 MEASUREMENT OF AERATION UNDER PROCESS CONDITIONS

The performance of an aerator can be evaluated under process conditions. When liquid containing active organisms is aerated, then the dissolved oxygen concentration rises to an "apparent saturation" value ( $C'$ )—less than  $C^*$ —which depends upon the respiration rate ( $r$ ) (Refer to Fig. 11.7). Equation 2.3 is modified to account for the oxygen utilization due to respiration as:

$$\frac{dC_L}{dt} = K_L a (C^* - C_L) - r \quad 6.7$$

Equation 6.7 can also be written as:

$$\frac{dC_L}{dt} = (K_L a C^* - r) - K_L a C_L \quad 6.8$$

At equilibrium:

$$\frac{dC_L}{dt} = 0 \text{ and } C_L = C' \text{ (apparent saturation value).}$$

Substitution of these values in equation 6.7 gives:

$$r = K_L a (C^* - C') \quad 6.9$$

Elimination of  $r$  from equations 6.7 and 6.9 gives:

$$\frac{dC_L}{dt} = K_L a (C' - C_L) \quad 6.10$$

In an unsteady-state procedure, mixed liquor is aerated for a while and then aeration is stopped. The level of dissolved oxygen built up during the aeration falls to zero by the respiration process. The rate of decrease of oxygen concentration determines the respiration rate. The aeration is restarted and increase in oxygen level is noted with time. According to equation (6.8),  $K_L a$  is determined directly from the slope of the plot  $\frac{dC_L}{dt}$  versus  $C_L$ .



Alternatively,  $K_L a$  can easily be determined without knowing the value of  $r$  by the method described in 6.1, by plotting  $(C' - C_L)$  versus  $t$  on semilog scale, or by the method described in 11.2.2

At equilibrium  $K_L a$  is given by the following equation which is obtained from equation 6.9:

$$K_L a = \frac{r}{(C^* - C')} \quad 6.11$$

Thus  $K_L a$  can be calculated from equation 6.11 if  $r$ ,  $C^*$  and  $C'$  are known. This implies that  $K_L a$  and  $r$  are constant during aeration.

Though  $C'$  is assumed to be constant in equation 6.11, in fact it does not remain constant in a continuous treatment plant. This is due to continuous changes in respiration, constituents concentration, and changes in species distribution. In addition, changes in surface tension suspended solids,  $\alpha'$  factor ( $K_L a_{\text{waste}}/K_L a_{\text{water}}$ ), affect the transfer capabilities of the system as suggested by Kayser (57).

From equation 6.11, it is obvious that large values of  $C'$  or small differences in  $C^* - C_L$  will induce large errors in  $K_L a$ . It is advisable, therefore, to use equation 6.11 only when  $C'$  is less than 5 mg/lt (57).



#### 6.4 SODIUM SULPHITE OXIDATION METHOD

The Sulphite method was used in the preliminary oxygen mass transfer studies in this work. The Sulphite method is a widely accepted method for the measurement of aeration performance and the method was first used by Cooper, Fernstorm and Miller (26). In this method, a solution of sodium sulphite catalysed with  $\text{Co}^{++}$  or  $\text{Cu}^{++}$  ions is aerated in the aeration tank. The rate of sulphite depletion as a result of oxidation gives the rate of oxygen transfer into the system.

Conflicting results and opinions are found in the literature as regards the merits of the sulphite method. For example: Morgan and Bewtra (77); Dreir (34); Carpini and Roxburg (23) reported that the oxygen transfer rate in the sulphite oxidation is higher than that obtained in treatment plants. On the other hand, authors: Schultz and Gaden (101); Phillips and Johnson (87); Miyamoto (74); Yoshida et al. (135) found that the transfer rate agrees well with that obtained in field tests and in aeration of tap water.

Hirose et al. (51) report that in a sparged agitated fermentor the oxygen transfer rates as well as the increase in oxygen transfer rates (due to increase in rpm) in the sulphite and a biological system were approximately the same in  $\text{Co}^{++}$  catalysed, but different in  $\text{Cu}^{++}$  catalysed sulphite solutions.

## Chapter 7

## 7. A LITERATURE SURVEY ON SULPHITE OXIDATION

A review of the literature on the oxidation of catalysed sodium sulphite solution shows that the kinetics of the reaction is not clearly understood, though the reaction was first studied in 1898 by Jorissen (56). The recent data on the kinetics of the reaction is given by Reith (94). He performed the experiments in a wetted wall column and found the kinetics as second order with respect to oxygen, zero order with respect to sulphite, and first order with respect to catalyst. This data was found at higher sulphite concentration (0.8 M) and higher cobaltous sulphate concentrations ( $3 \times 10^{-5}$  to  $5 \times 10^{-3}$  kmol/m<sup>3</sup>). Wesselingh and Van't Hoog (129), Onda et al. (81) and Astarita et al. (3) also report that the reaction is second order with respect to oxygen at higher sulphite and catalyst concentration; however, with increasing oxygen pressures, Wesselingh and Van't Hoog noted a decrease in reaction order, while Onda et al. found that the order changes from two to one. Linek and Mayrhoferova (67) observed that the reaction between oxygen and sulphite solution is first order for oxygen concentrations higher than approximately  $6 \times 10^{-4}$  kmol/m<sup>3</sup> at the interface and second order for lower oxygen concentrations. Linek (64) suggests that the change of order from two to one with increasing oxygen partial pressure is due to a decrease in pH at the interface. At higher absorption rates if the diffusion of sulphite to the interface is slow, then the concentration of sulphite at the interface would be less than that of the bulk; and so also the pH at interface would be reduced. Thus the decrease in pH results in decrease in



absorption rate and hence order of reaction decreases. From this hypothesis Linek warns that the rate constants determined at higher absorption rates might be somewhat lower than their correct value since they correspond to pH less than that of the bulk. Sawicki and Barron (100) studied the kinetics of sulphite oxidation in heterogeneous systems. They report that the heterogeneous oxidation of sulphite is a second order reaction with respect to oxygen concentration at the interface. Phillips and Johnson (87) also found that by agitating sulphite solution in an unsparged vessel from zero to higher rpm, the order of reaction with respect to oxygen changes from two to one. At zero rpm, the system is heterogeneous and the reaction order of two agrees with the finding of Sawicki and Barron (100). Barron and O'Hern (6) studied the influence of hydrodynamics of solution on reaction kinetics by passing a homogeneous solution of sodium sulphite (catalysed) and oxygen in a rapid mixer. This technique eliminates the effect of diffusional resistances on reaction mechanisms, when the oxygen is in the gas phase. By this method the rate of reaction is found to be zero order with respect to oxygen, and three-halves with respect to sulphite. At very low sulphite concentration ( $\leq 0.07 \text{ kmol/m}^3$ ) and catalyst concentration ( $\leq 6 \times 10^{-7} \text{ kmol/m}^3$ ) the results were found to be somewhat different; under these conditions, Yagi and Inoue (134) found the reaction as first order with respect to sulphite, oxygen and cobalt ions.

Conflicting results are also reported in the literature on whether the reaction is controlled by the gas film resistance



(Maxon and Johnson (70)) or the liquid film resistance (Bartholomew et al. (7), Bassett and Parker (4)). In many cases the gas film resistance is assumed to be negligible.

The effect of ions of heavy metals on sulphite oxidation mechanism has also been studied: Westerterp et al. (130); Phillips and Johnson (87); Roxburgh (99) found that ions of heavy metals like Cu, Fe and Co accelerate the rate of sulphite oxidation. Yagi and Inoue (134) report that the oxidation of sodium sulphite to sulphate follows a chain reaction of an unusual length in the presence of a catalyst. They observed the formation of cobalt complex by ultraviolet spectra.

The oxygen transfer in sulphite solution is found to be influenced by:

- (a) The design of the reaction vessel;
- (b) The method of agitation of liquid phase;
- (c) The metal used as a catalyst.

In an unsparged vessel, the oxygen transfer in cobalt catalysed solution is found to be five times that obtained in Cu catalysed solution. However, both Cu and Co catalysed solutions give the same oxygen transfer in a sparged vessel (87). In the case of iron, initially the transfer rate increases to a high value even higher than that with Co, but drops rapidly with time (99). On the other hand, De Waal and Okeson (32) report that dissolved iron has no influence on the reaction. Phillips and Johnson (87), and Roxburgh (99) say that the results obtained with Cu ions are not reproducible. Roxburgh studied the effect of Cu,

Fe, Co, and Ni ions on sulphite reaction in different gas-liquid contacting devices. These devices were: unbaffled stir jar; 3 and 5 litres sparged baffled fermentors fitted with turbine agitator; and shake flasks of Erlenmeyer pattern, agitated on a horizontal rotary shaker. Roxburgh found that with the increase of agitation the oxygen transfer coefficient,  $K_L a$ , increases with all metals in all devices, except in the case of Cu where it decreases only in unbaffled stir jar and in closed shake flask. Moreover,  $K_L a$  in Cu catalysed solution in horizontal rotating fermentor is not affected when the air pressure is varied from one to two atmospheres. These results are opposite to the results reported by Phillips and Johnson (87). They found that in unsparged vessel, the oxygen transfer increases as 1.5 power of oxygen partial pressure; however, oxygen transfer is directly proportional to the oxygen partial pressure in sparged vessel. According to Schultz and Gaden (101), low agitation either in liquid phase or in gas phase has no effect on  $K_L a$ , but high agitation of liquid phase decreases  $K_L a$ . Carpani (23) observed large variations in  $K_L a$  in water and sulphite solution in unsparged vessel under identical agitation. He also reported that agitation decreases  $K_L a$  of catalysed sulphite solution and increases  $K_L a$  of water. Moreover, in unstirred conditions  $K_L a$  of sulphite solution is 15 times that of water and with agitation (160 rpm), it decreases to half the value of water.

The reason for the high transfer coefficient  $K_L a$  in sulphite solution is interpreted by Yoshida et al. (135) as being due to relative increase in interfacial area. Formation of smaller



bubbles in sulphite solution cause an increase in interfacial area per unit volume of liquid. In addition, a double layer of ions develops around the small bubbles, because of the ionic effect. This layer retards the bubble coalescence of the smaller bubbles and as a result of this, bubbles remain in the liquid for a longer period of time, which consequently increases  $K_L a$  in the sulphite solution (135).

Recently (1972) Linek (65) has reported the existence of interfacial turbulence in stirred sulphite solutions. He showed that interfacial turbulence begins only when the oxygen absorption is sufficiently high enough to cause great local changes in the physical properties of the solution at the interface. In his opinion, it is probable that the chemical mass transfer coefficient is an over-estimation of the physical mass transfer coefficient because of the interfacial turbulence induced by chemisorption.

In the absence of catalysts, the rate of sulphite oxidation is independent of sulphite concentration (134). In the presence of a catalyst, the oxygen transfer increases with the increase of sulphite concentration and attains a constant value at higher sulphite concentrations according to De Waal and Okeson (32) and Linek (64). But, Wesselingh and Van't Hoog (129) reported that the absorption decreases when the sulphite concentration exceeds a value of about  $0.5 \text{ kmol/m}^3$ . However, Linek (64) explained that this decrease is, in fact, due to the effect of impurities.

With the increase of temperature, the rate of oxidation of catalysed sulphite solution increases (129, 32).

It is evident from the above review that the disagreement between some of the reported results can be interpreted as being due to varying experimental conditions employed by various investigators. Therefore, it can be concluded that in many cases the observed reaction kinetics depend on the basic design of reaction vessel and the method of agitation of the gas-liquid interface. For this reason, the oxidation of sulphite solution was studied with reference to the experimental set up adopted in this work.



## Chapter 8

8. • OXIDATION OF CATALYSED SODIUM SULPHITE SOLUTION  
IN 100 LITRES QVF VESSEL

For the study of oxidation of sulphite solution the experiments were planned to investigate the effect of the following parameters on oxygen transfer:

- (a) pH of the solution;
- (b) concentration of  $\text{Co}^{++}$  ions in both agitated and unagitated liquids;
- (c) concentration of sodium sulphite;
- (d) oxygen pressure in the gas phase;
- (e) stirrer rpm.

Experiments were performed under the following standard conditions, saving the condition which was in itself a variable to be investigated.

The standard conditions were:-

- |  |  |
|--|--|
| (a) volume of liquid in the reactor                | $4.4 \times 10^{-2} \text{ m}^3$                             |
| (b) liquid feed rate (continuous experiments)      | $1.66 \text{ and } 2.33 \times 10^{-5} \text{ m}^3/\text{s}$ |
| (c) stirrer rpm                                    | 3100 and 3300  |
| (d) cobaltous sulphate concentration in the liquid | $4 \times 10^{-6} \text{ kmol /m}^3$                         |
| (e) pH of solution                                 | 8.5  |
| (f) Gas phase                                      | air (1 atm.)   |

## 8.1 EXPERIMENTAL

The apparatuses used for the study of sulphite oxidation in batch and continuous reactor as well as with pure oxygen are described in the following.

### 8.1.1 Apparatus for Continuous and Batch Experiments

The sulphite oxidations were studied in a 100 lt. QVF vessel equipped with the mixing unit as shown in Plate I. This apparatus was used because it was available. The mixing unit comprised of a 12.7 cm diameter glass tube with an open lower end and a glass stirrer inside the tube. At 25 cm from the lower end, the tube had 6 orifices 2.54 cm in diameter. A variable speed geared motor rotated the stirrer inside the tube. A small exhaust fan extracted the air from the vessel at a rate of  $1.33 \times 10^{-4} \text{ m}^3/\text{s}$ . For liquid levels below the orifice the rotating impeller pumped the liquid through the orifices in the form of jets and imparted mixing by circulating the liquid contents. The jets impacted on the liquid surface and entrained the surrounding air in the form of bubbles.

The samples for analysis were directly siphoned from the vessel.

The apparatus described above was employed as a batch reactor.

For continuous experiments, the reaction vessel was connected with inlet and outlet feed arrangements (Fig. 8.1). The liquid was fed to the reaction vessel from a reservoir by gravity. The liquid feed rate was measured by a rotameter and controlled and

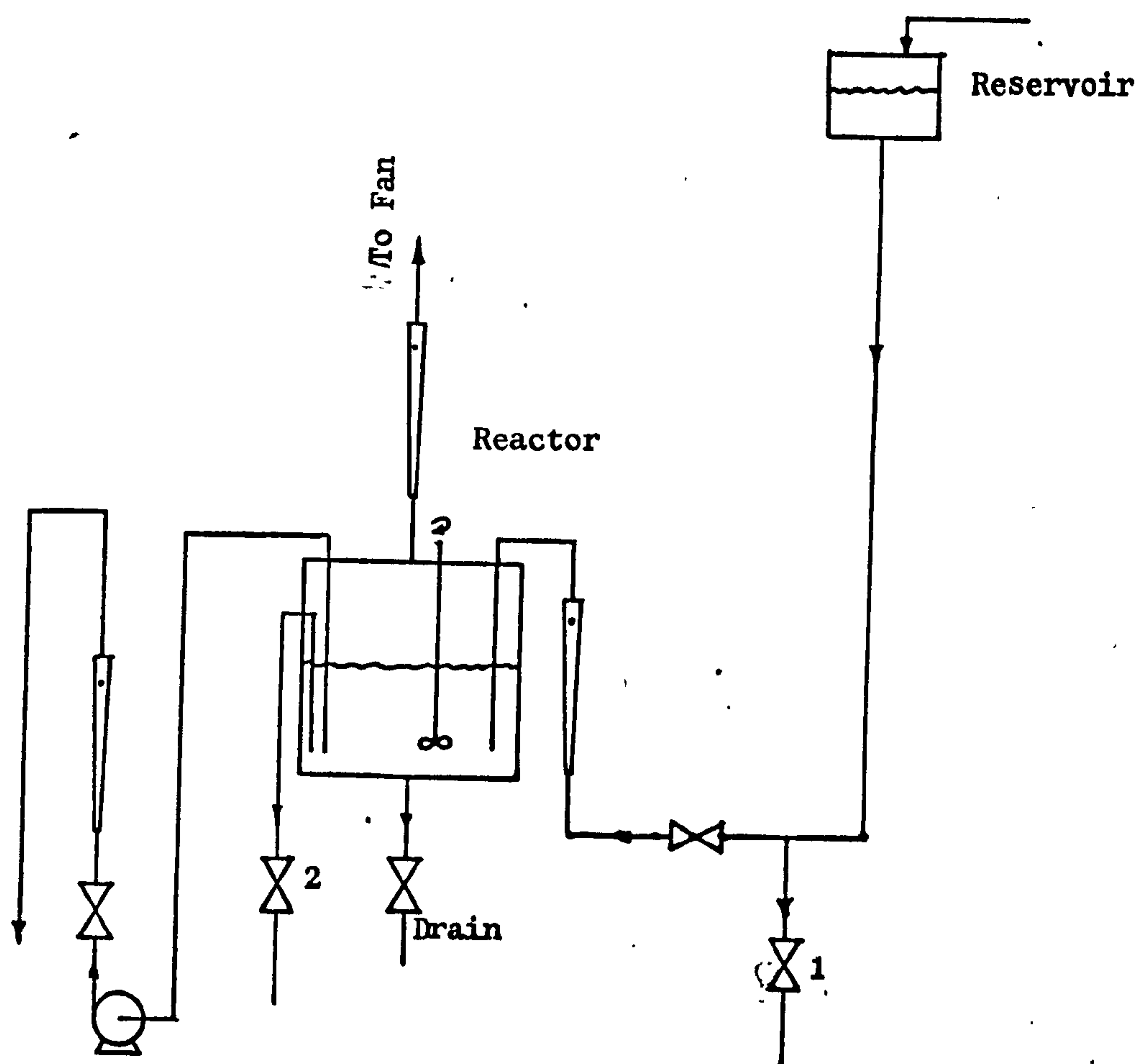


Figure 8.1. Flow diagram for continuous experiments.



kept constant by a manual valve. A small pump and valve at its outlet removed the reaction products at a rate equal to the feed rate and thus kept the volume of the liquid in the reactor constant. Feed samples were taken from valve 1 and the product samples were siphoned through valve 2.

#### 8.1.2 Apparatus for Experiments with Pure Oxygen

The experiments using pure oxygen were performed in the apparatus shown in Plate I. The reaction vessel was sealed as well as possible, but because of the large number of connections on the vessel, a complete prevention of leakage was not possible. Hence, it was not possible to maintain a reduced pressure less than  $50 \text{ kN/m}^2$  within the vessel. However, for pressures greater than  $50 \text{ kN/m}^2$  no leakage into the vessel was observed.

Oxygen from a cylinder was supplied to the vessel through the tube A as shown in Plate I. A vacuum pump was connected to a vessel port by tube C and a valve. When the desired vacuum was obtained the valve was closed. A vacuum gauge and a mercury manometer were connected through a valve to a vessel port.

A 25.4 mm diameter polyethylene tube D (Plate I), with its free end below the liquid level, was used for filling the solution in the vessel. The advantage of this tube in filling operation will be discussed later. A 6.35 mm sampling tube E was inserted through the tube D. The end of tube E was kept well below the liquid level so that a true sample of the liquid could be collected.

It is obvious that the samples from the vessel cannot be siphoned in the usual way when there is a reduced pressure inside the vessel. This difficulty was overcome by using a sampling device shown in Fig. 8.2. This device was simply a glass bottle. At the top it was connected through a two-way valve to a vacuum pump and  $N_2$  supply. The bottom of the bottle was connected through a valve to the sampling tube coming from the vessel and to the sample outlet valve.

## 8.2 EXPERIMENTAL PROCEDURE

The following steps were performed in all experiments:-

1. Sodium sulphite and cobaltous sulphate solutions were made in tap water.
2. The pH of the sulphite solution was measured by a direct reading pH meter. The pH was varied by adding sulphuric acid or sodium hydroxide to the solution.
3. The cooling water was supplied to the QVF seal fitted to stirring unit.
4. The speed of the stirrer was measured by a stroboscope whenever this measurement was necessary.
5. The temperature of solution was kept at  $20 \pm 1^\circ C$  by adding ice.
6. During a run the samples were taken from the reaction vessel at equal intervals of time. The intervals ranged from 3 to 10 minutes. These samples were analysed by standard iodometric titration to determine

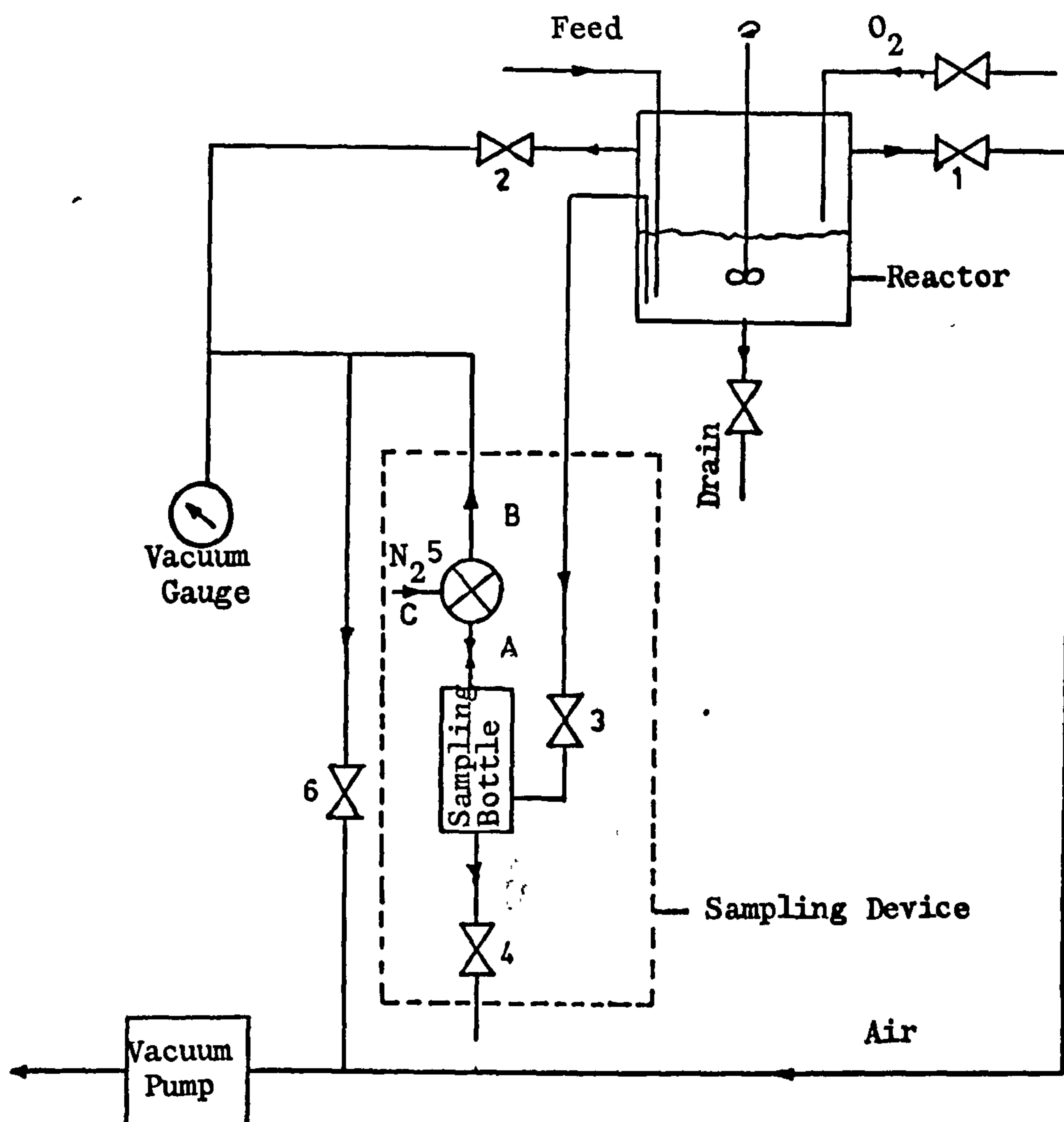


Figure 8.2. Flow diagram for experiments with Oxygen below Atmospheric Pressure



the rate of sodium sulphite depletion which is equivalent to the oxygen transfer rate (refer to Appendix I).

### 8.2.1 Procedure for Continuous Experiments

At the start of this investigation a few batch experiments were performed at very low sulphite concentrations ( $< 0.06 \text{ kmol/m}^3$ ). From the results of these experiments, it was found that the rate of sulphite depletion varied with the time and hence the rate of oxygen transfer was not constant. Because of this non-linearity, continuous experiments were planned.

In continuous experiments, the sulphite solution at constant concentration was fed into the reactor at constant feed rate and simultaneously the liquid from the vessel was removed at a rate equal to the feed rate. The concentration of sulphite in the vessel attained an equilibrium value under steady-state conditions. When the steady conditions were obtained, the oxygen transfer was calculated by the equation,

$$J^* = \frac{8}{S} \frac{q y}{S} (W - W_o) \quad (\text{Refer Appendix I})$$

where  $J^*$  is oxygen transfer rate in kg/s,

$q$  is feed rate in  $\text{m}^3/\text{s}$ ,

$y$  is normality of thiosulphate

$S$  is liquid sample in ml,

$W_o$  is mean of thio sulphate,

titrations on feed samples in ml,

and  $W$  is mean of thiosulphate titrations on product samples at steady state, in ml.



If an experiment is started with initially tap water in the vessel, the sulphite concentration in the vessel would increase from zero to a steady value. The time to reach steady value would depend obviously on concentration of sulphite in feed and the rate of oxygen transfer for a given reactor volume. A longer run time would mean a larger reservoir and large quantities of sulphite if the exit product sulphite solution is not re-used. Economies of material and time were reached by starting the experiment with a sulphite solution of an arbitrary concentration in the reactor itself. The concentration of sulphite in the reactor was chosen to be little less than that in the reservoir. The concentration of the catalyst was the same in the reservoir and in the reaction vessel. With this modification, the steady conditions were reached in relatively short time periods.

To perform a continuous experiment, a known amount of sodium sulphite was added to the reaction vessel in the form of a concentrated solution. The solution in the vessel was made up to 44 lts., by adding tap water. A known amount of cobaltous sulphate solution was also added to the reactor. The steps 2 to 5 as mentioned previously were performed prior to an experiment or first experiment in a series of experiments. Then the stirrer and the pump were switched on. At the same time, liquid was fed to the vessel from the reservoir by opening the valve in the feed line. The flow rate of feed and product were kept constant by regulating the flow by the respective valves in the feed and product lines. The air inside the vessel was continuously extracted by a small exhaust fan. The oxidation of solution in

the reservoir by atmospheric air was avoided by continuous bubbling of  $N_2$  gas through the reservoir solution. The reservoir was flushed with  $N_2$  before it was filled up with sulphite solution. In all experiments the stirrer speed was either 3300 or 3100 rpm. At this speed, it could be safely assumed that the contents of the reaction vessel are homogeneous.

Fig. 8.3 shows a plot of sulphite concentration in the feed and product obtained from a steady state experiment. By chance in this particular experiment the initial concentration of sulphite in the reactor corresponds to the steady-state concentration.

The detailed results of the continuous flow experiments are given in Appendix V.

#### 8.2.2 Procedure for Batch Experiments

From the results of steady state runs it was found that at higher sulphite concentration ( $> 0.06 \text{ kmol/m}^3$ ) the oxygen transfer rate is independent of sulphite concentration. This suggested that the sulphite concentration would deplete linearly with time in a batch reactor for a constant oxygen transfer rate at a higher sulphite concentration. This finding made it possible to perform batch experiments in order to determine the oxygen transfer rates.

In a batch experiment a catalysed sulphite solution of concentration greater than  $0.06 \text{ kmol/m}^3$  was aerated and the samples from the reactor were siphoned at equal time intervals, ranging from 5 to 10 minutes. The samples were analysed by

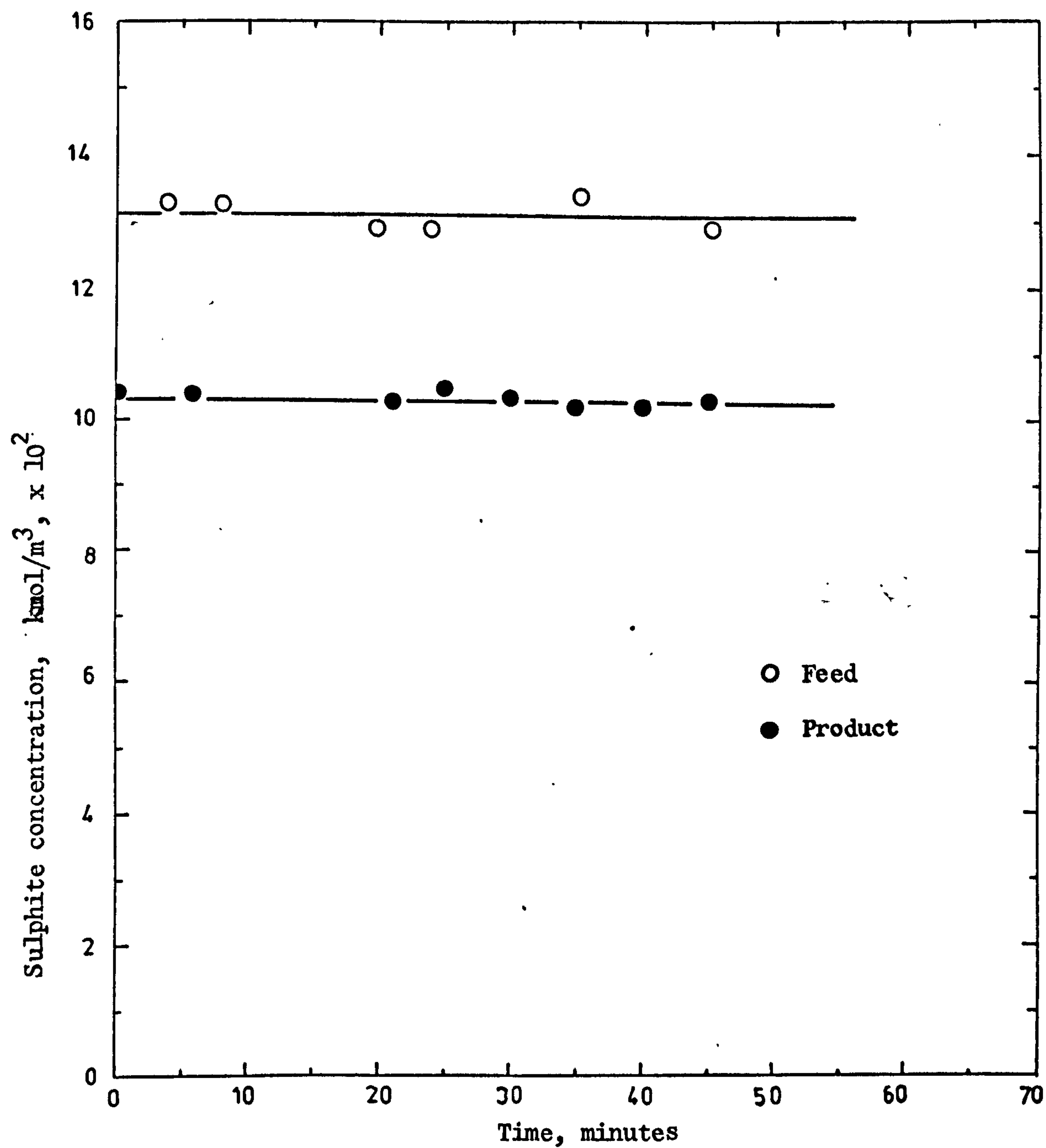


Figure 8.3. Typical result of a continuous experiment for sulphite oxidation ( $C_0^{++} = 4 \times 10^{-4}$  kmol/m<sup>3</sup>).



iodometric titration. Thiosulphate titrations in ml were plotted against time and the slope was determined by regression analysis. Oxygen transfer was then determined by the equation,

$$J^* = \frac{8 V y}{S} \left( \frac{dW}{dt} \right) \quad (\text{Refer to Appendix I})$$

where  $J^*$  is oxygen transfer in kg/s,

$V$  is volume of liquid in the reactor in  $m^3$ ,

$y$  is normality of thio sulphate,

$S$  is volume of sample in ml and

$\left( \frac{dW}{dt} \right)$  is rate of increase of thiosulphate volume in titrations (slope by regression analysis) in ml/s.

Fig. 8.4 shows the increase of thiosulphate titration volume due to corresponding decrease in sulphite concentration with time.

In batch experiments the sulphite consumption and the run time was considerably reduced as compared to continuous experiments. In addition, results obtained by batch experiments are more reliable than those obtained in continuous experiments, since in continuous experiments feed and product flow rates are subject to some error. Because of these reasons, it was decided to determine oxygen transfer rates by batch experiments at higher sulphite concentrations. The detailed results of all batch experiments are given in Appendix V.



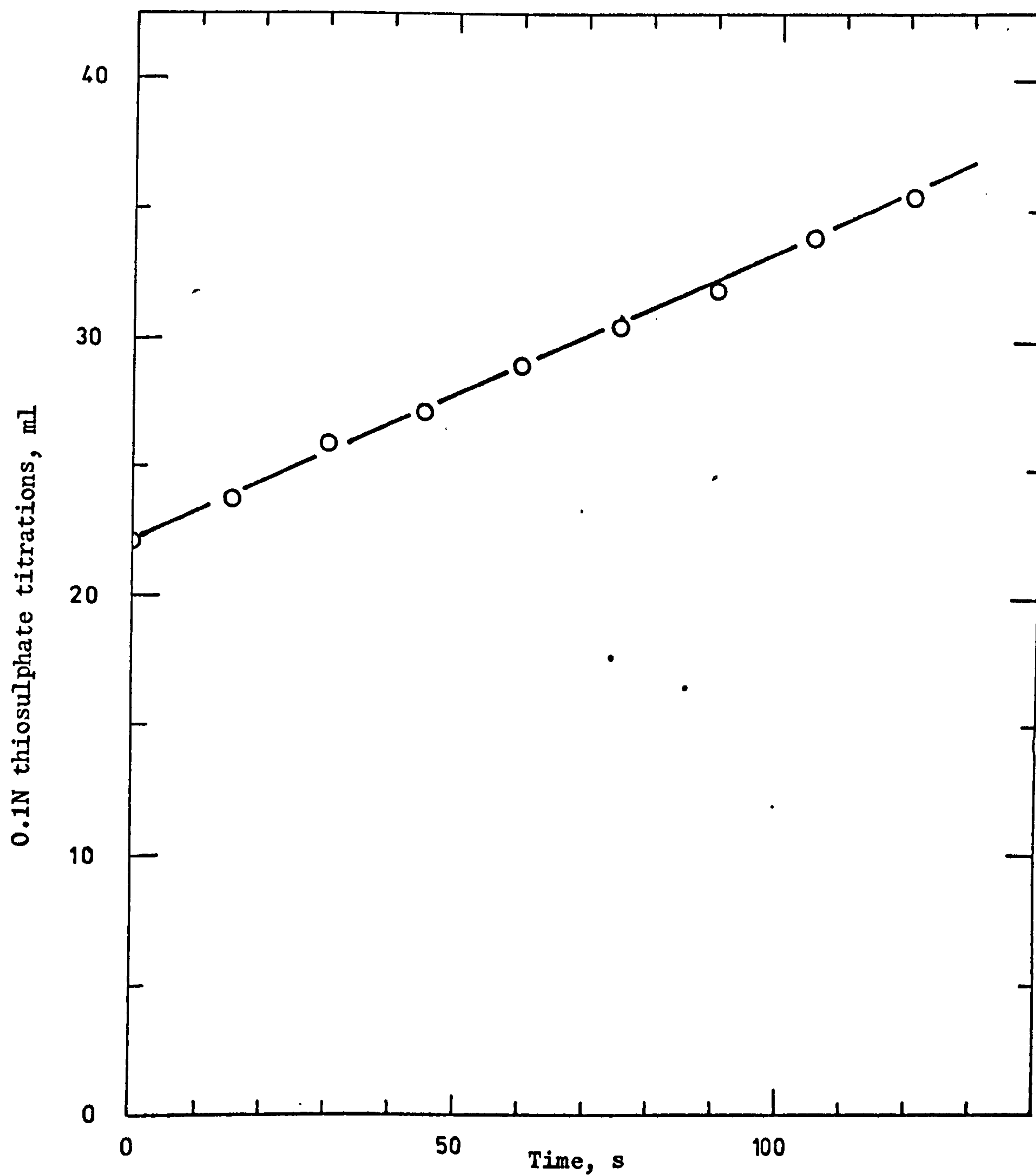


Figure 8.4. Linear increase in thiosulphate titrations due to linear decrease in sulphite concentration of samples from batch reactor

### 8.2.3 Procedure for Experiments with Pure Oxygen

To perform an experiment with pure oxygen it was essential to replace the air inside the vessel by oxygen. This was achieved by first filling the vessel with water. It was not possible to fill up the vessel completely as it is obvious from the shape of the upper part of the vessel. Moreover oxygen pressure in the vessel was varied from a value less than atmospheric pressure to a value above atmospheric pressure. Thus the experimental technique when the vessel was under less than atmospheric pressure was different from that when it was above atmospheric pressure.

#### Oxygen pressure above atmospheric pressure

When the oxygen pressure in the vessel was equal to or greater than the atmospheric pressure, the procedure was as follows. The symbols used in this description refer to Fig. 8.5 and Plate I. The vessel was filled with water and during the filling operation valve 1 was kept open to let the air being displaced escape out of the vessel. The small amount of air left in the upper part of the vessel was flushed with oxygen. Valves 1 and 2 were now closed. The vessel was filled with oxygen by draining the water out of the vessel and simultaneously supplying the oxygen to fill the space of the outflowing water. The supply of oxygen was so regulated that the pressure within the vessel was a bit higher than the atmospheric pressure. This prevented the air from leaking into the vessel. The water was drained out until its level was just above the lower end of the feed pipe D, (Plate I). By keeping the water level above the

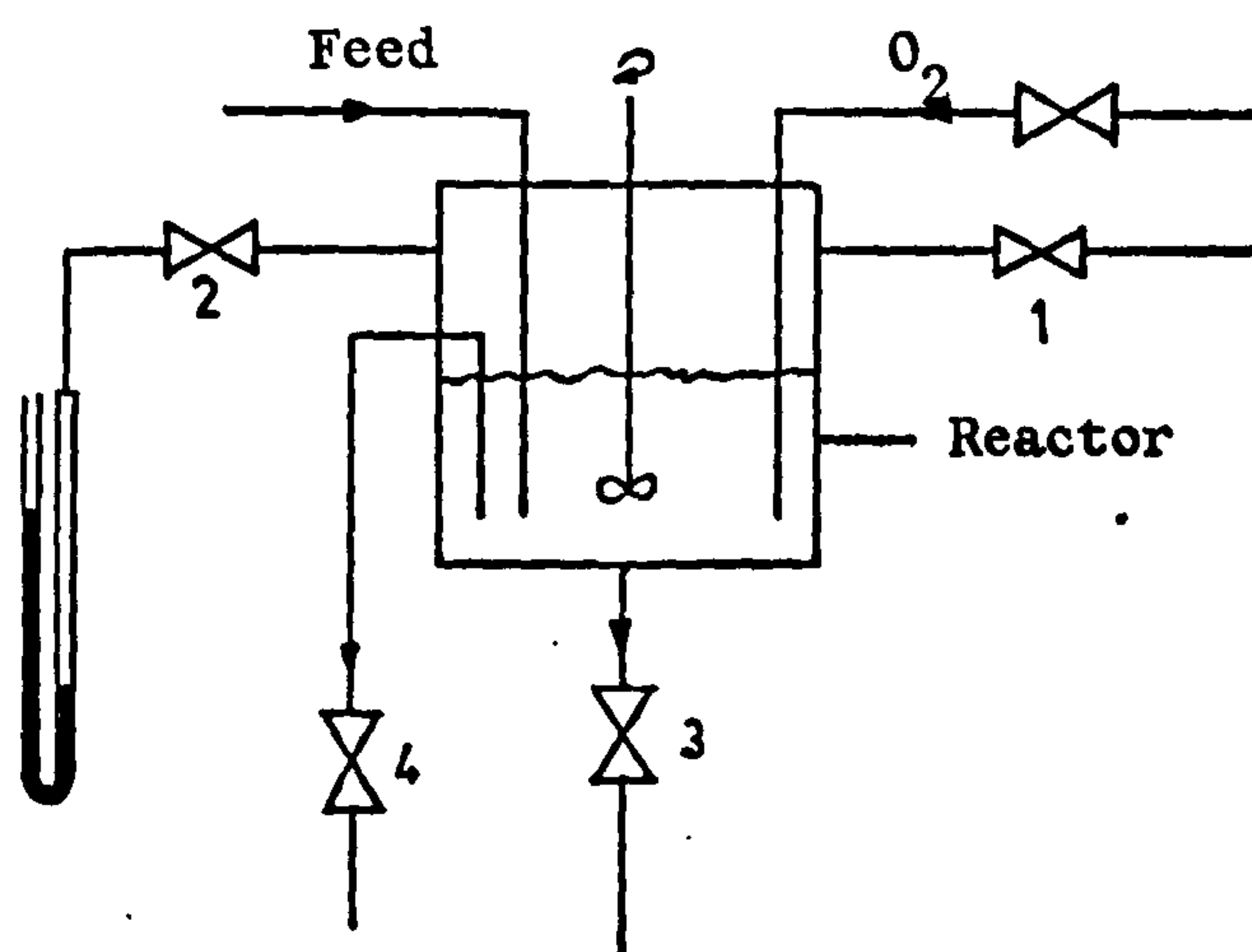


Figure 8.5. Flow diagram for Experiments with Oxygen  
above Atmospheric Pressure

outlet of the feed pipe, the oxygen in the vessel was, in fact, sealed from the outside air although the feed pipe was open to atmosphere. The volume of water at this level was about 32 lts. and therefore 12 lts. of concentrated sulphite solution was added to vessel to obtain 44 lt. of solution (standard volume).

The feed pipe arrangement had the great advantage in the sense that solution was added and the samples were taken without letting outside air leak into the vessel. Access to the inlet of the feed pipe was made by disconnecting the QVF flange F (Plate I), and taking off the 'sampling assembly'. A funnel was inserted into the feed pipe and the concentrated sulphite solution was added gently. When the solution was being added the oxygen pressure increased and consequently the column of liquid in the feed pipe also increased. Obviously, if the solution were added non-stop, the oxygen pressure would continue to rise and the liquid column in the feed pipe would also rise up to the point of feed entrance and then no more solution could be fed. The addition of solution was therefore facilitated by releasing the build up pressure in the vessel by opening the valve 1. Valve 1 was closed as soon as the column in the feed pipe was about 25 mm. After the addition of sulphite solution cobaltous sulphate solution was added and the volume of the solution was made up exactly equal to 44 lt., by adding tap water. The sampling assembly was then fitted to the vessel. The pH of the solution was brought to 8.5 by adding sulphuric acid.

The run was started by closing the valve 1 and switching on the stirrer. Valve 2 was opened and the manometer indicated the



pressure of oxygen in the vessel. As the oxygen was consumed by oxidation, the oxygen pressure also decreased. By a continuous, regulated supply of oxygen to the vessel the pressure was maintained at a constant level.

#### Oxygen pressure below atmospheric pressure

The flow diagram for the apparatus used with oxygen below atmospheric pressure is shown in Fig. 8.2. The experiments in this case differed from the experiments with oxygen above atmospheric pressure only in the method of sampling. The methods for flushing the vessel with oxygen and feeding the solution to the vessel were the same as mentioned above.

At the beginning of the experiment all the valves were closed. To obtain a desired reduced pressure inside the vessel, valve 1 was opened and the vacuum pump was started. When valve 2 was opened the vacuum gauge showed the pressure inside the vessel. The vacuum pump was stopped when the desired vacuum was achieved, the valve 1 was closed and the stirrer was switched on.

As the solution in the vessel oxidized the oxygen was consumed and the pressure fell. The reacted oxygen was replaced by supplying the oxygen from an oxygen cylinder and regulated so as to keep the pressure constant. Down to a pressure of 570 mm Hg no variations in the pressure were observed due to leakage. But at lower pressures of 380 mm of Hg, the pressure increased gradually with time. The pressure was allowed to increase by an amount of 12.7 mm Hg. When this limit was reached the vacuum was corrected by opening the valve 1 and starting the vacuum pump.

In experiments at higher reduced pressure the pressure was reduced more than the desired value so that the variation was  $\pm 12.7$  mm Hg about the desired value. It was estimated that the air which leaks because of pressure variations is only 6% of total oxygen in the vessel. The samples were taken from the sampling device after equal time periods. The sampling method was as follows.

Nearly 30 seconds before the sampling time, valve 2 was closed and valve 6 was opened. Valves 3 and 4 were also closed. The two-way valve 5 was opened in such a way that it connected the flow between tubes A and B, and disconnected the flow between tubes A and C. This operation, in fact, disconnected the vacuum pump and the vacuum gauge from the reaction vessel and connected them with the sampling device. The vacuum pump was started and soon a high vacuum was created in the sampling bottle. The valve 6 and the two-way valve 5 were now closed. As the next step valve 3 was opened and the liquid from the vessel rushed into the sampling bottle through the sampling tube, because of the relatively higher vacuum in the bottle. When about 50 ml of the liquid was collected, valve 3 was closed. Two-way valve 5 was opened to connect only tubes A and C. The  $N_2$  filled the vacuum and the liquid in the bottle was drained out by opening the valve 4. This completed the flushing operation of the sampling line. By this time the actual sampling time was reached and by repeating the above steps 50 ml of the sample was collected. The sample was drained out slowly by opening the valve 4 slightly. While the liquid was draining out, a 10.6 ml sample was taken by 10 ml syringe (by calibration it was found that 10 ml sample actually collected 10.6 ml of liquid).



### 8.3 RESULTS AND DISCUSSION

#### 8.3.1 Effect of Sulphite Concentration on Oxygen Transfer Rate

Fig. 8.6 shows the effect of sulphite concentration on oxygen transfer rate in continuous reactor at a catalyst concentration of  $4 \times 10^{-6}$  kmol/m<sup>3</sup>. It is obvious that at very low sulphite concentrations (  $< 0.06$  kmol/m<sup>3</sup> ) the oxygen transfer rate increases nonlinearly with the increase of sulphite concentration.

However, at higher sulphite concentrations (  $> 0.06$  kmol/m<sup>3</sup> ) the oxygen transfer rate attains a maximum value and is independent of sulphite concentration. Wesselingh and Van'T Hoog (129) found that the oxygen transfer rate decreases when sulphite concentration exceeds 0.5 kmol/m<sup>3</sup>. Similarly, oxygen transfer rate decreased when ionic strength of solution was increased by adding sodium sulphate to the solution. But according to Linek (64) in either case the decrease in oxygen transfer rate is due to the increase in inhibiting impurities.

#### 8.3.2 Effect of Impurities in Tap Water on Oxygen Transfer Rate

The results of two batch experiments with sulphite solution in tap water and in distilled water showed that the impurities in tap water increase the oxygen transfer rate by 22.4%, the experimental error being 10%. This could have been due to residual surface active agents present in tap water. Levich (61) reports that the bubble rise velocity in distilled water was found to be significantly higher than that in tap water. Thus longer retention time of bubbles in tap water would increase the oxygen transfer rate.

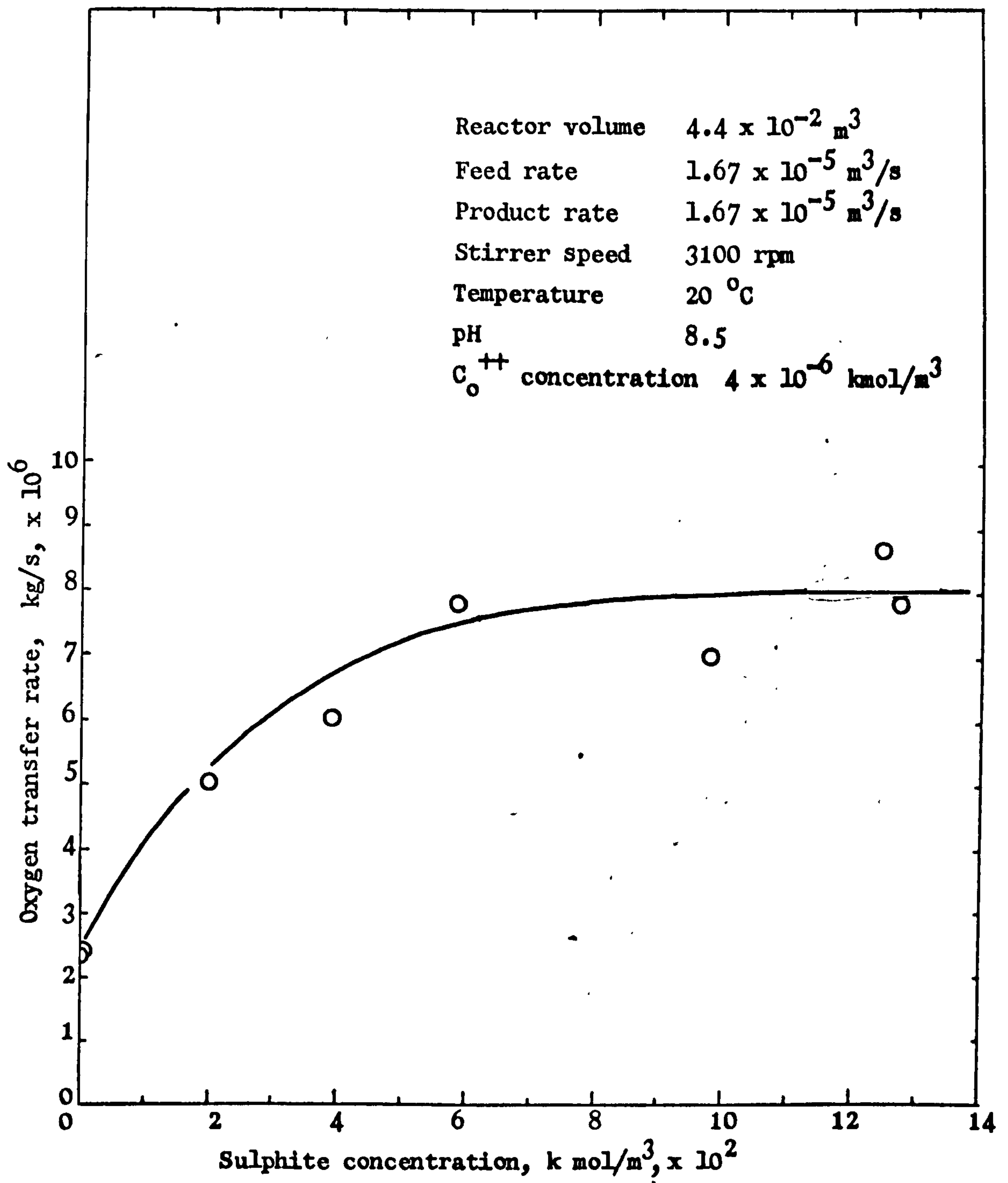


Figure 8.6. Effect of sulphite concentration on oxygen transfer rate.



### 8.3.3 Effect of the Presence of Sodium Sulphate on Oxygen Transfer Rate in Sulphite Solutions

In one steady state experiment, the effect of the presence of sodium sulphate on the rate of oxygen transfer was investigated. The feed contained  $0.2 \text{ kmol/m}^3$  sodium sulphite and  $0.2 \text{ kmol/m}^3$  sodium sulphate. The oxygen transfer rate was decreased by 12.6% due to the addition of large concentrations of sodium sulphate in the feed. Hence, it follows that small amount of sodium sulphate formed during the oxidation will not have a significant effect on oxygen transfer rates.

### 8.3.4 Effect of pH on Oxygen Transfer Rate

The rate of oxygen transfer increases linearly with the increase of pH of the sulphite solution, as shown in Fig. 8.7. The same effect of pH was also observed by Wesselingh and Van't Hoog (129).

### 8.3.5 Effect of Catalyst Concentration on Oxygen Transfer Rate

The effect of cobaltous sulphate (catalyst) concentration on oxygen transfer was investigated in agitated sulphite solutions. Fig. 8.8 shows the effect of cobaltous sulphite concentration on oxygen transfer rate at low sulphite concentrations ( $0.015 \text{ kmol/m}^3$ ). This sulphite concentration is in the region where oxygen transfer rate is a function of sulphite concentration. For the range of cobaltous sulphate concentration investigated the oxygen transfer rate was found to increase towards some maximum value.

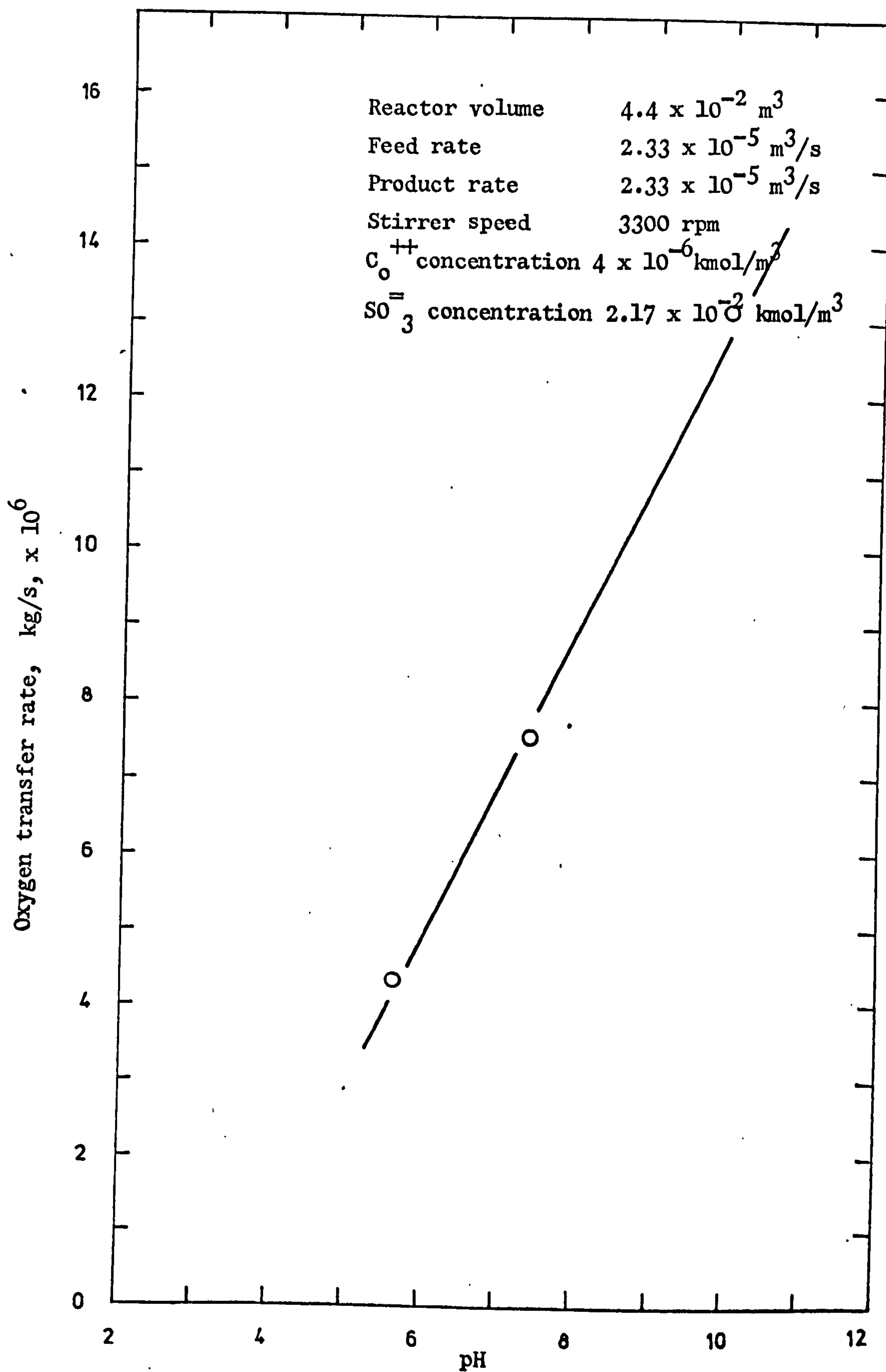


Figure 8.7. Effect of pH on oxygen transfer rate

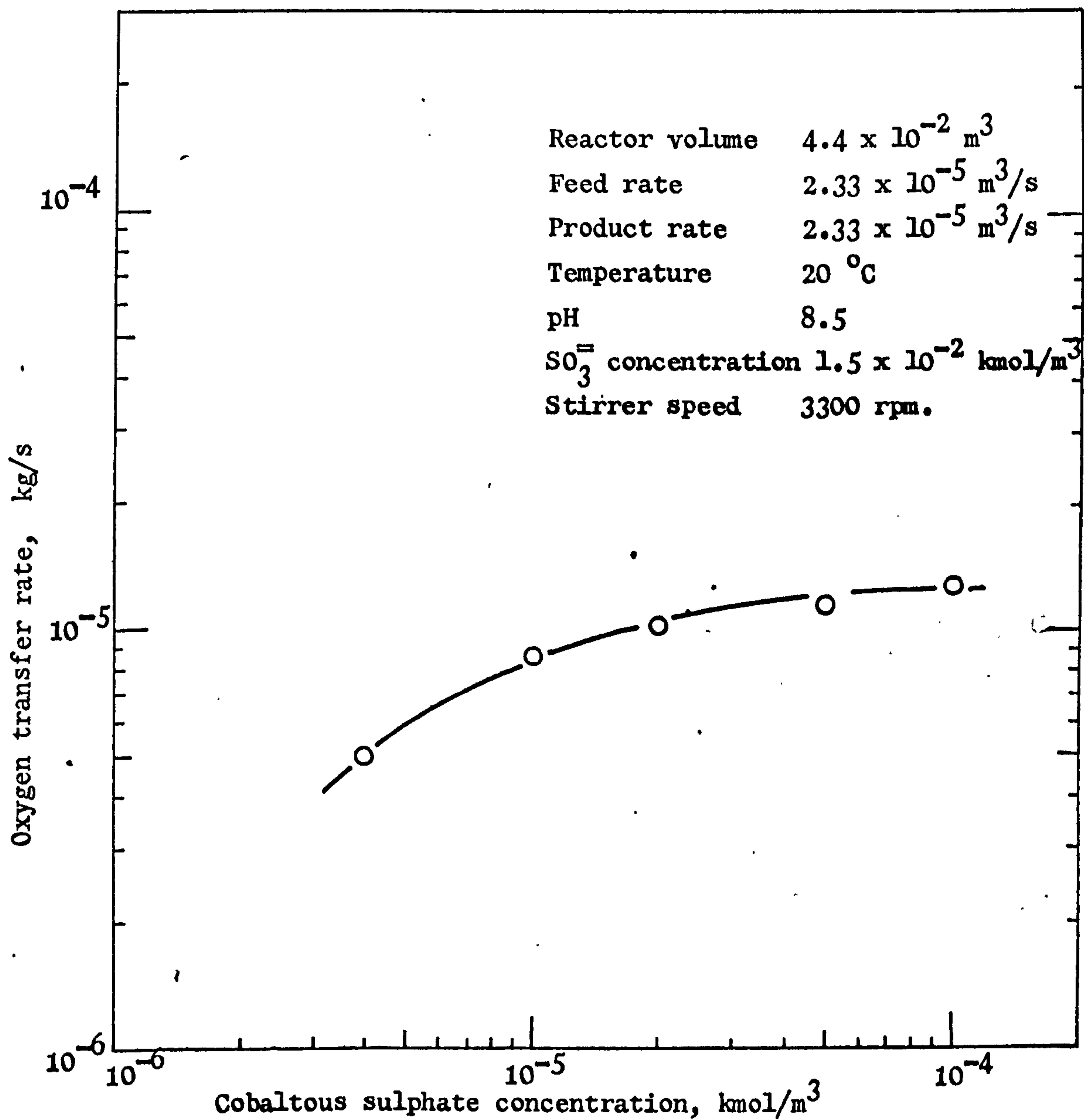


Figure 8.8. Effect of catalyst concentration, on oxygen transfer rate in stirred reactor at steady sulphite concentration ( $0.015 \text{ kmol/m}^3$ )

The effect of cobaltous sulphate concentration on oxygen transfer rate in agitated liquid containing sodium sulphite solution in the range 0.06 to 0.32 kmol/m<sup>3</sup> is shown in Fig. 8.9. The sulphite concentration is in the region where the oxygen transfer rate is independent of sulphite concentration. The oxygen transfer rate was found to be nearly constant and not affected by the cobaltous sulphate concentration except in one case where high oxygen transfer was obtained at a catalyst concentration of  $3 \times 10^{-4}$  kmol/m<sup>3</sup>. At this catalyst concentration scums were observed; however, there is evidence that higher catalyst concentration increases  $K_L a$  (Hirose et al.(51)).

#### 8.3.6 Effect of Oxygen Pressure on Oxygen Transfer Rate

The effect of oxygen pressure on oxygen transfer rate in catalysed sulphite solution is shown in Fig. 8.10. Concentration of cobaltous sulphate and sodium sulphite are in the range where the oxygen transfer is independent of the sulphite and catalyst concentration. Only six data points were obtained and there is some scatter in the results. The oxygen transfer rate at 21 kN/m<sup>2</sup> (0.2 atm.) corresponds to the value obtained with air and agrees with the results obtained with pure oxygen. The relationship between the oxygen transfer rate and the oxygen pressure is linear at 5% probability and hence it can be concluded that the oxygen transfer rate is directly proportional to the oxygen pressure in the gas phase.



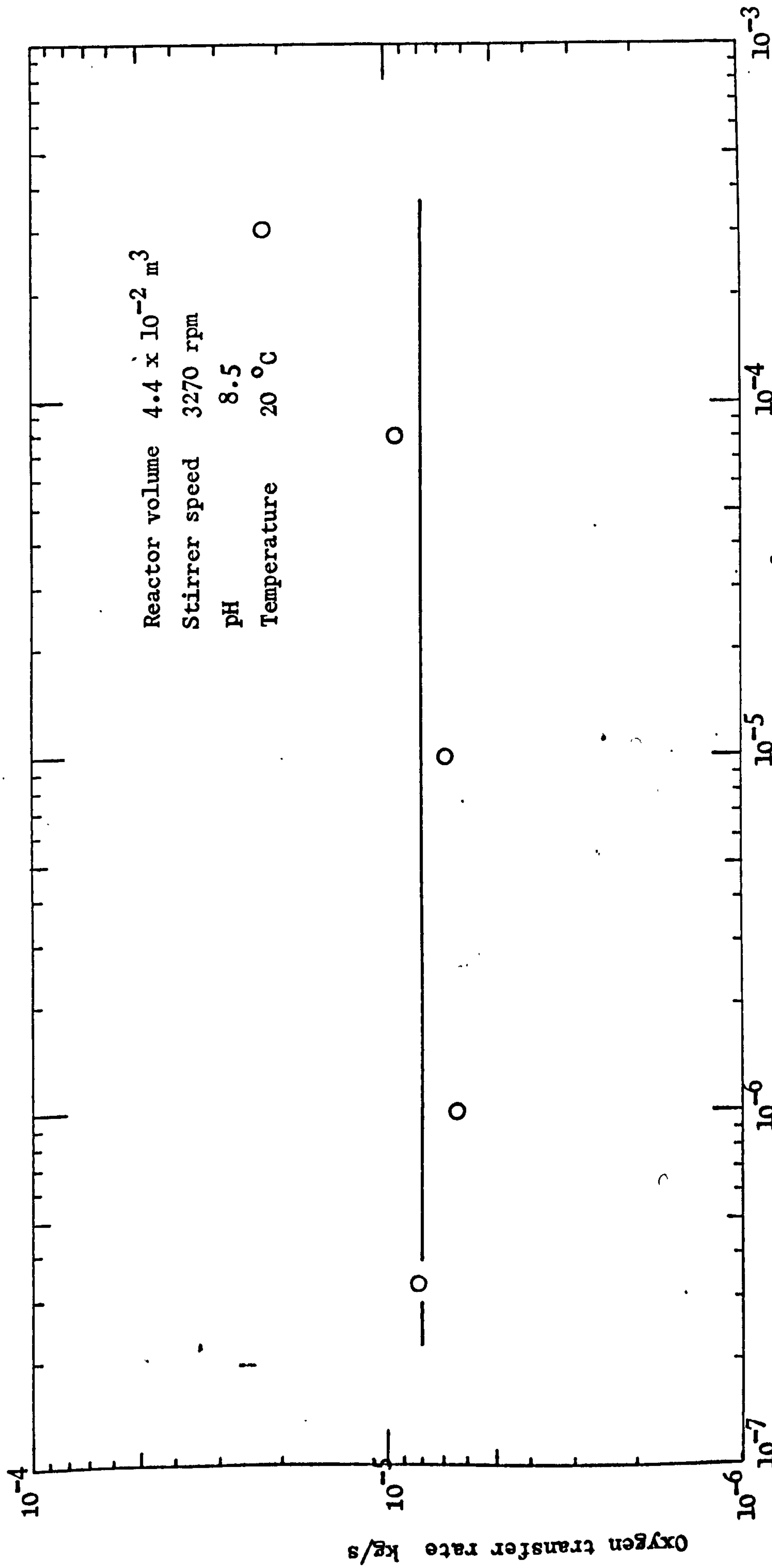


Figure 8.9. Effect of catalyst concentration on oxygen transfer rate in stirred reactor at sulphite concentration greater than  $0.06 \text{ kmol/m}^3$ .

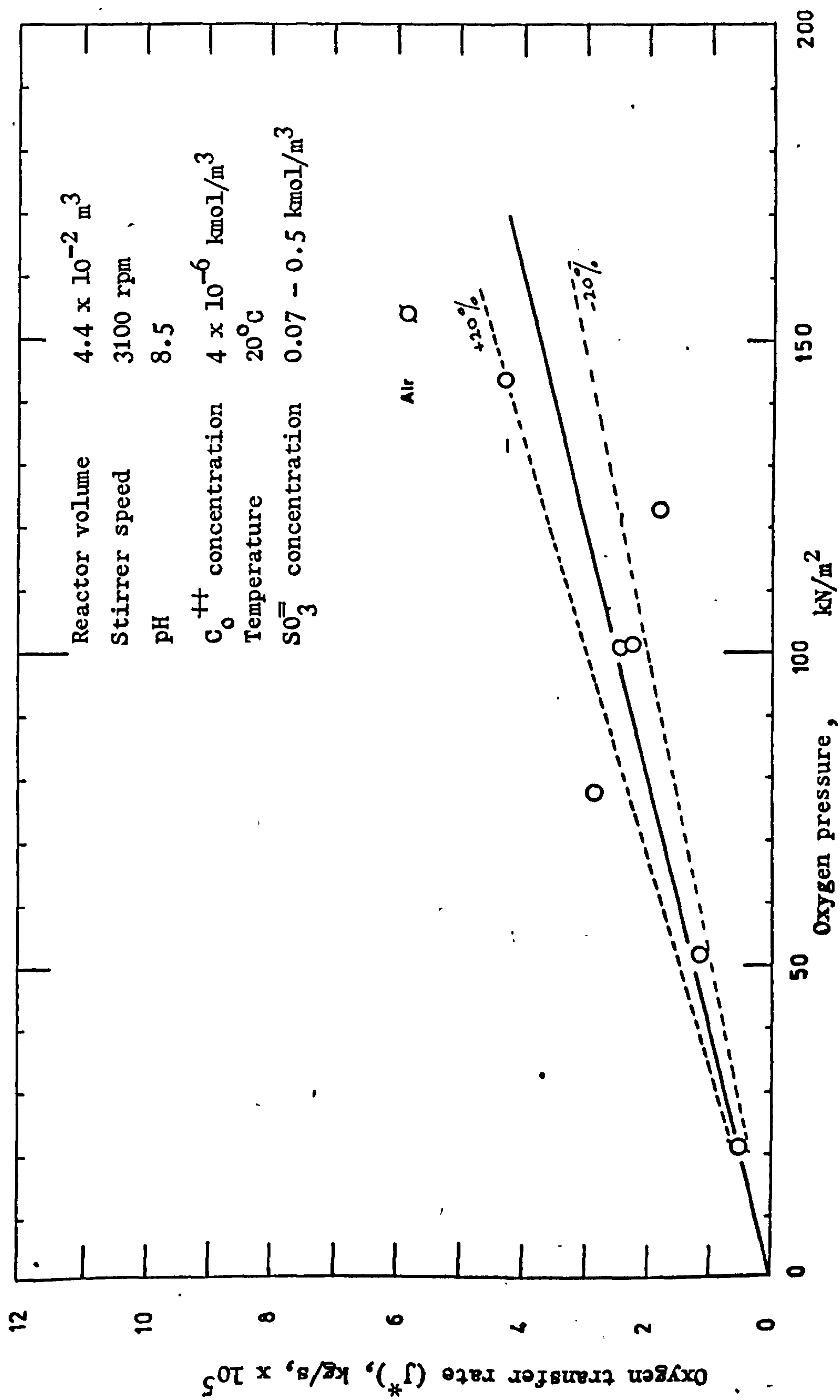


Figure 8.10. Effect of oxygen pressure on oxygen transfer rate.

### 8.3.7 Effect of Stirrer Speed on Oxygen Transfer Rate

The oxygen transfer rate increases linearly with the increase in stirrer speed, as shown in Fig. 8.11. This is probably due to a linear increase in interfacial area with stirrer speed.

### 8.3.8 Mechanism of Oxygen Transfer

The results reported in Figs. 8.6, 8.8, 8.9 and 8.10, in fact, help in formulating the mechanism of oxygen transfer in stirred sulphite solutions.

Oxygen transfer rate is a function of both the catalyst and sulphite concentrations when their concentrations are very low. This is shown in Figs. 8.6 and 8.8. In fact, in the region where the oxygen transfer increases with the increase of sulphite and/or catalyst concentration, the oxygen transfer will depend upon the overall mass transfer coefficient and the reaction rate depending whether the reaction is slow or fast.

The maximum and constant rate of sulphite oxidation in Figs. 8.6, 8.9 and 8.10 indicates that at higher concentrations of either sulphite or catalyst the reaction eventually becomes virtually instantaneous at the interface. Under these conditions the oxygen concentration at the interface is zero (therefore no reaction kinetics is involved) and the maximum oxygen transfer rate controlled by gas film will take place according to the equation:

$$\bar{J} = K_g P \quad 3.21$$

where  $P$  is the partial pressure of oxygen in the gas phase and  $K_g$  is gas-film mass transfer coefficient.

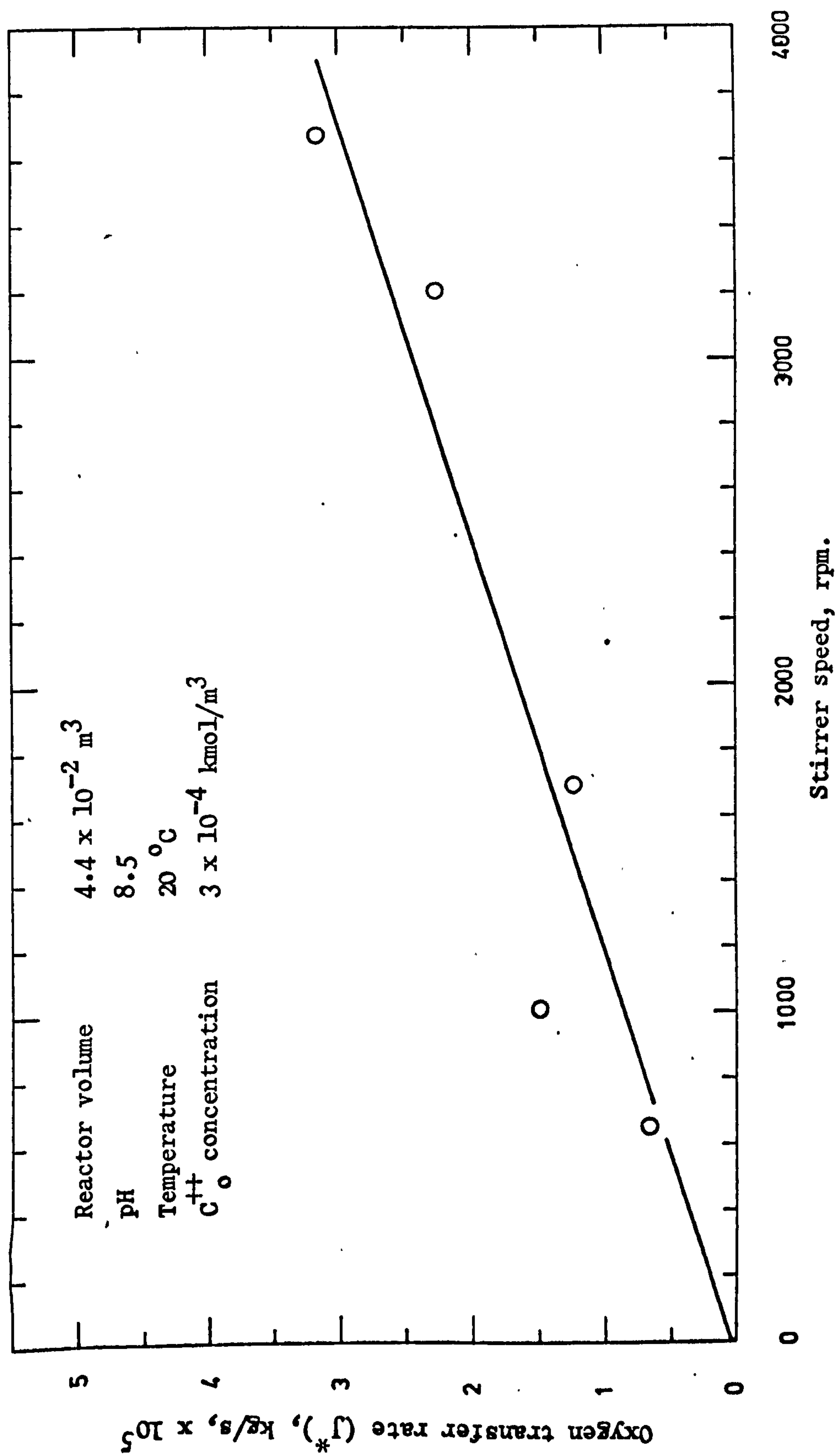


Figure 8.11. Effect of stirrer speed on oxygen transfer rate.



The experiments in which the oxygen pressure was varied show that the oxygen transfer rate is directly proportional to the pressure of oxygen in the gas phase, thus confirming equation 3.21.

It is clear from the above discussion that the maximum amount of oxygen which could be available to micro-organisms in an aeration process can be measured by the sulphite method. In addition, the measurement of interfacial areas or oxygen transfer coefficients are more accurate when only the gas film is controlling the mass transfer than when both the gas and liquid film are controlling. This is because the liquid film resistance  $K_L$  varies with the hydrodynamics and physical conditions of the liquid whereas  $K_g$  does not. Measurement of interfacial areas by the sulphite method makes a better comparison of the performance of different aeration devices possible.

#### 8.3.9 The Valid Conditions for Sulphite Method for Measurement of Aeration

From the results and discussion in the preceding sections, it follows that the conditions under which oxidation of sulphite is independent of chemical kinetics and the oxygen transfer rate is maximum from gas phase to the oxygen free solution would be the valid conditions for evaluating the performance of an aerator. For instance, these conditions are obtained at sulphite concentrations greater than  $0.06 \text{ kmol/m}^3$  and catalyst concentration less than  $5 \times 10^{-5} \text{ kmol/m}^3$ .

#### 8.4 100 LITRES QVF VESSEL AS A JET-VORTEX AERATOR

The 100 lt. QVF vessel with the mixing unit described earlier acted as a jet-vortex aerator, because apart from the jets through the orifices a vortex was formed in the draft tube and a cluster of bubbles surrounding the vortex was observed. Thus the aeration in the vessel was the sum of the aeration due to plunging jets and the vortex aeration.

In order to study the aeration by the plunging jet alone a separate apparatus was used as described in the following section.

## Chapter 9

## 9. AIR ENTRAINMENT BY A PLUNGING LIQUID JET

This chapter deals with the quantitative study of air entrainment in a plunging jet system. A new experimental technique for measurement of entrainment rates is described. Data on entrainment for both cylindrical and annular jet nozzles are presented. The annular jet nozzles were designed in the hope that the annular jets would entrain more air than cylindrical jets, since the entrainment through the inner tube of the annular nozzle would be additional entrainment. Entrainment phenomenon is studied in relation to nozzle and jet parameters. Finally, the entrainment data is correlated by a dimensionless equation.

### 9.1 EXPERIMENTAL

Plate II shows the basic experimental set-up employed for the study of air entrainment and aeration by a plunging jet. In future, to avoid repetition, only the additions and/or modifications to this set-up will be mentioned. The apparatus mainly comprises of:

- (a) A PVC (250 gallons) circular liquid holding tank;
- (b) Centrifugal pump to recirculate the liquid from the tank through a nozzle;
- (c) Nozzles to produce liquid jets;
- (d) Framework over the tank for adjustment and positioning of the nozzles;
- (e) Rotameter or orifice plate to measure the liquid flow rate.

A two-inch heavy duty centrifugal pump (95 feet head and 10,000 gallons/hour flow rate) was bought from British Labour Pump



Co. Ltd., Wellingborough, England. The pump inlet port was connected to an outlet at the tank base and the outlet port was connected to an L shaped 2 inch steel piping (Plate II). A bend connected to the free end of this piping directed the liquid flow downwards. A 2 x  $1\frac{1}{2}$  inch reducing socket was connected to this bend, so that  $1\frac{1}{2}$  inch polythene tube could be used to connect the steel piping with the inlet of the nozzle. The use of a flexible tube for connecting the nozzle to the steel piping greatly helped in adjustment and positioning of the nozzle especially when angular jets were required. All temporary connections of flexible pipings were secured by jubilee clips.

The liquid flow rate was controlled by a two-inch pneumatic or manually operated diaphragm valve (Plate II). The pneumatic valve was used only with sulphite system; otherwise a manually operated Saumer's two-inch diaphragm valve was used. This was because the work on the sulphite system was done at the university where a supply of compressed air was available, and the work on air entrainment and aeration of biological systems was done at the National Institute of Agricultural Engineering, Silsoe, where the supply of compressed air was not available.

A 35 mm ( $1\frac{3}{8}$  inch) circular hole and 3.2 mm thick stainless steel orifice plate was used to measure the liquid flow rate of the jet. The orifice plate along with gaskets on either face were placed between the flanges of 2 inch piping. The circular hole of the orifice plate was made concentric with the piping. Two metres length of straight pipe between the orifice plate and the diaphragm valve was chosen to get a streamlined flow at the

upstream region of the orifice plate. A mercury manometer was used to measure the pressure differential between a pair of radius taps ( $\frac{3}{8}$  inch diameter) located at one pipe diameter upstream and half pipe diameter downstream from the orifice plate (Perry (86)). Fig. 9.1 shows the calibration curve for the orifice plate. When the orifice plate was used, most of the experiments were performed for flow rates greater than  $1.14 \times 10^{-3} \text{ m}^3/\text{s}$  (900 gallons/hour). The orifice plate was also calibrated for viscous slurry containing varying concentrations of suspended solids. It is seen from Fig. 9.1 that the calibration curve is the same for water and the viscous slurry used in this work.

Cylindrical nozzles of diameters 9.5 mm ( $\frac{3}{8}$  inch), 12.7 mm ( $\frac{1}{2}$  inch), 22.2 mm ( $\frac{7}{8}$  inch), 28.6 mm ( $1\frac{1}{8}$  inch) and 38.1 mm ( $1\frac{1}{2}$  inch) were used to produce cylindrical jets. These are shown in Fig. 9.2 and Plate III. The nozzles were made of perspex. The effective length of nozzle ( $l_n$ ) is the length of the nozzle after convergence of the flow. The nozzle aspect ratio ( $l_n/d_n$ ) is not constant for all nozzles. The frictional losses in the nozzle due to sudden contraction of flow were minimized by tapering the flow through the nozzle.

Fig. 9.3 shows the annular nozzle. The design of this nozzle was invented by the author and his principal supervisor. The jet produced by this nozzle is termed an annular jet because it is produced by the liquid flowing through an annulus. Basically, it comprises of two concentric tubes of 15.9 mm ( $\frac{5}{8}$  inch) diameter and 19 mm ( $\frac{3}{4}$  inch) diameter. The upper end of the outer tube is bent at an angle of 50 degrees while the inner tube passes through the

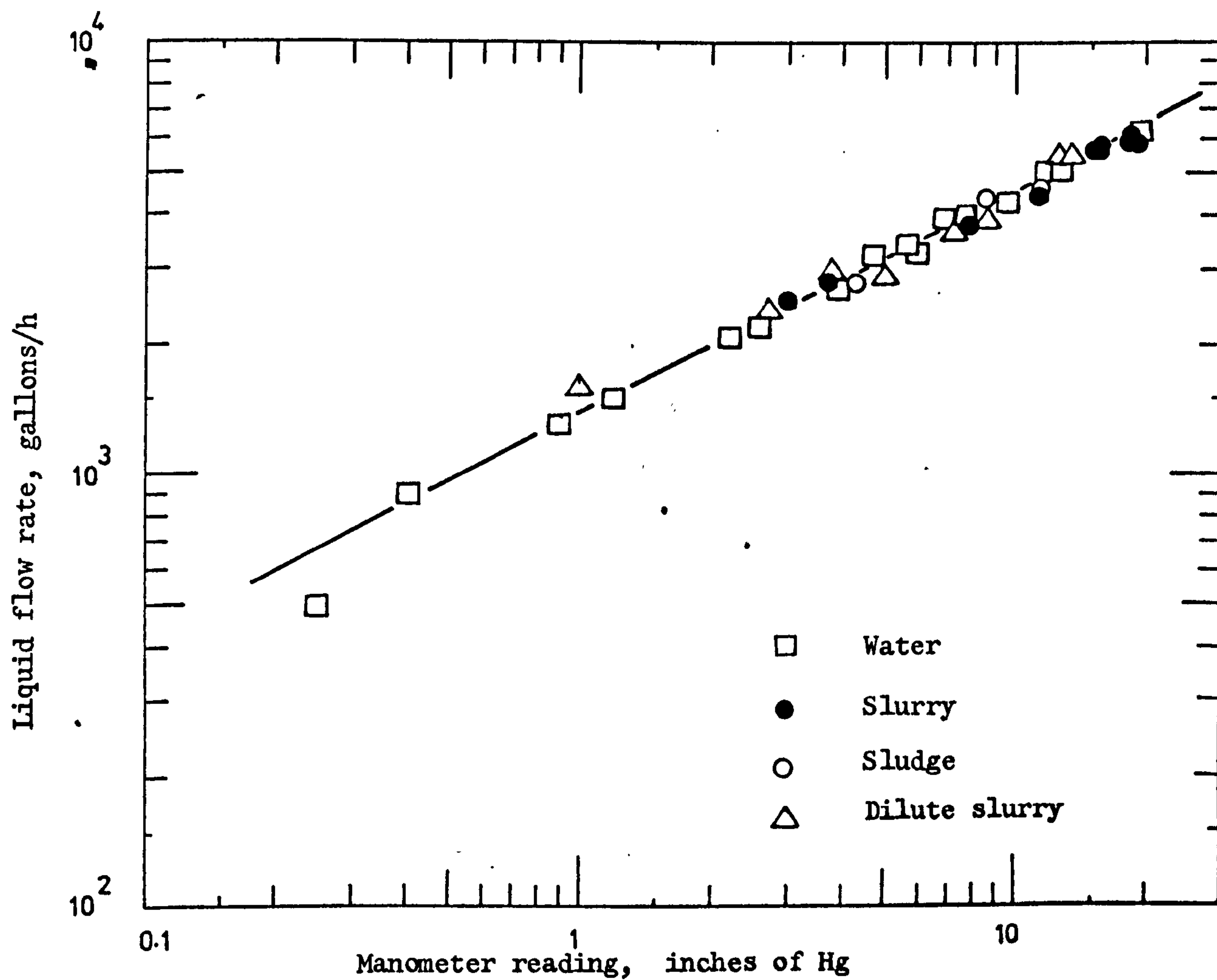
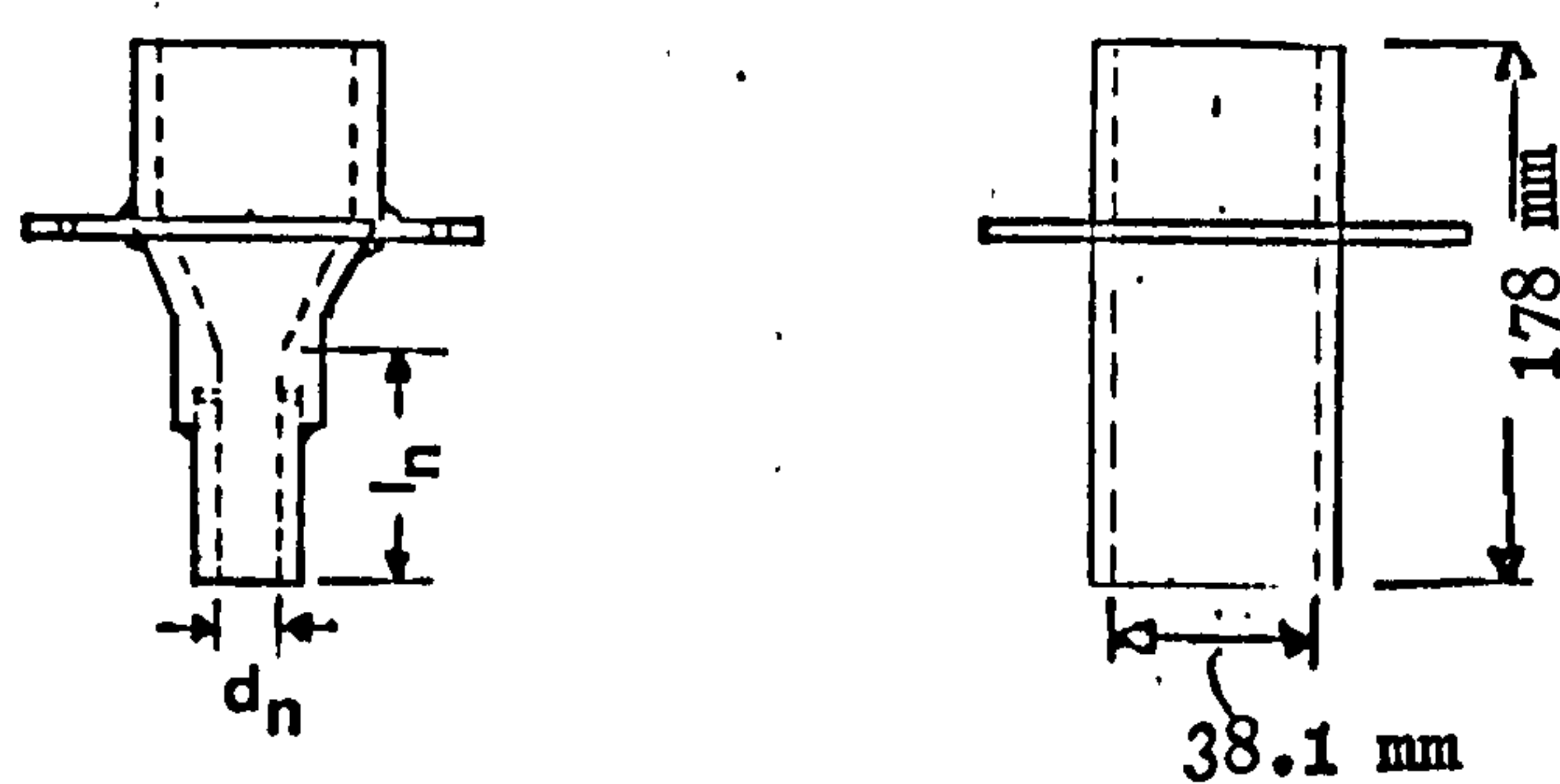


Figure 9.1. Calibration curve for orifice plate



Nozzle	$d_n$ (mm)	$l_n$ (mm)	$l_n/d_n$
1	9.5	79.3	8.3
2	12.7	87	6.9
3	22.2	89	4
4	28.6	98.4	3.5
5	38.1	178	4.7

Figure 9.2. Cylindrical nozzles.



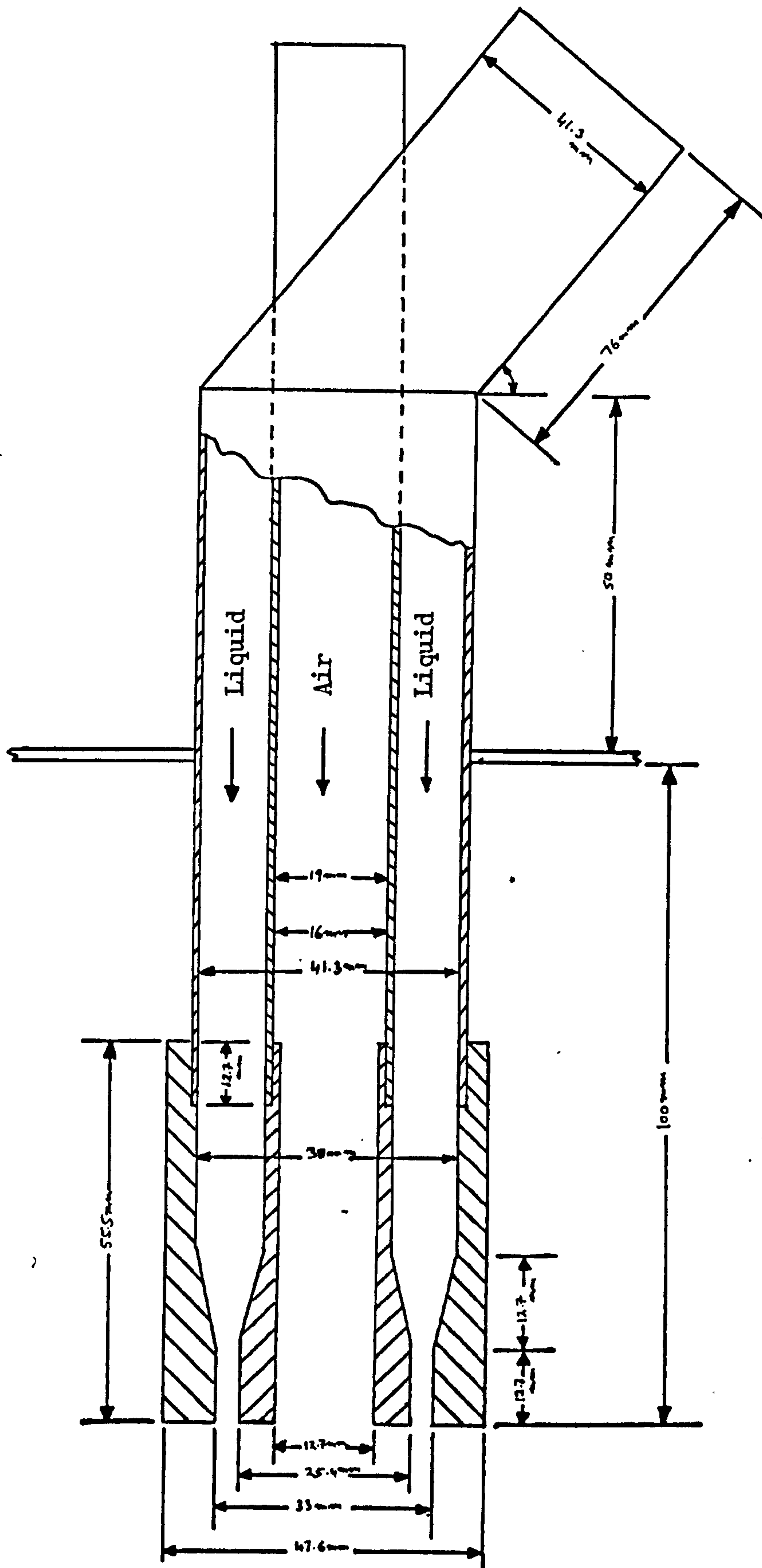


Figure 9.3. Annular nozzle

wall of the outer tube. The liquid entering into the outer tube flows towards the annulus with a small deviation in its direction of flow due to a 50 degrees bend. This would induce less distortion in the flow as compared to that induced by a 90 degrees bend. Moreover, the annular section was made long to streamline the flow before it undergoes contraction to enter into the smaller annulus.

Several interchangeable nozzle end pieces shown in Fig. 9.4 were made. The ends of the concentric tubes were threaded to accommodate these end pieces. A pair of nozzle end pieces when joined to the concentric tube accomplished an annular nozzle. The inside and outside diameter of the nozzle end will depend upon the dimensions of the selected pair of nozzle end pieces. In this work, experiments were performed with four annular nozzles having inside ( $d_{ni}$ ) and outside diameter ( $d_{no}$ ), as follows:

Nozzle	$d_{ni}$ (mm)	$d_{no}$ (mm)
1	25.4	38.1
2	25.4	33.
3	25.4	29.2
4	15.9	19.7

The problem of nozzle adjustment over the tank liquid surface was solved by the framework made of  $1\frac{1}{2}$ " x  $1\frac{1}{2}$ " Dexion (Plate II). A frame similar to a portal frame was constructed by erecting two equal supports on top of the tank and diametrically opposing each other. A nozzle holder was made of two vertical lengths of Dexion whose lower ends were bolted to the corners of one side of a rectangular and horizontal platform - 18 mm x 25 mm (Plate IV). Finally, the vertical lengths of nozzle holder were bolted to the horizontal

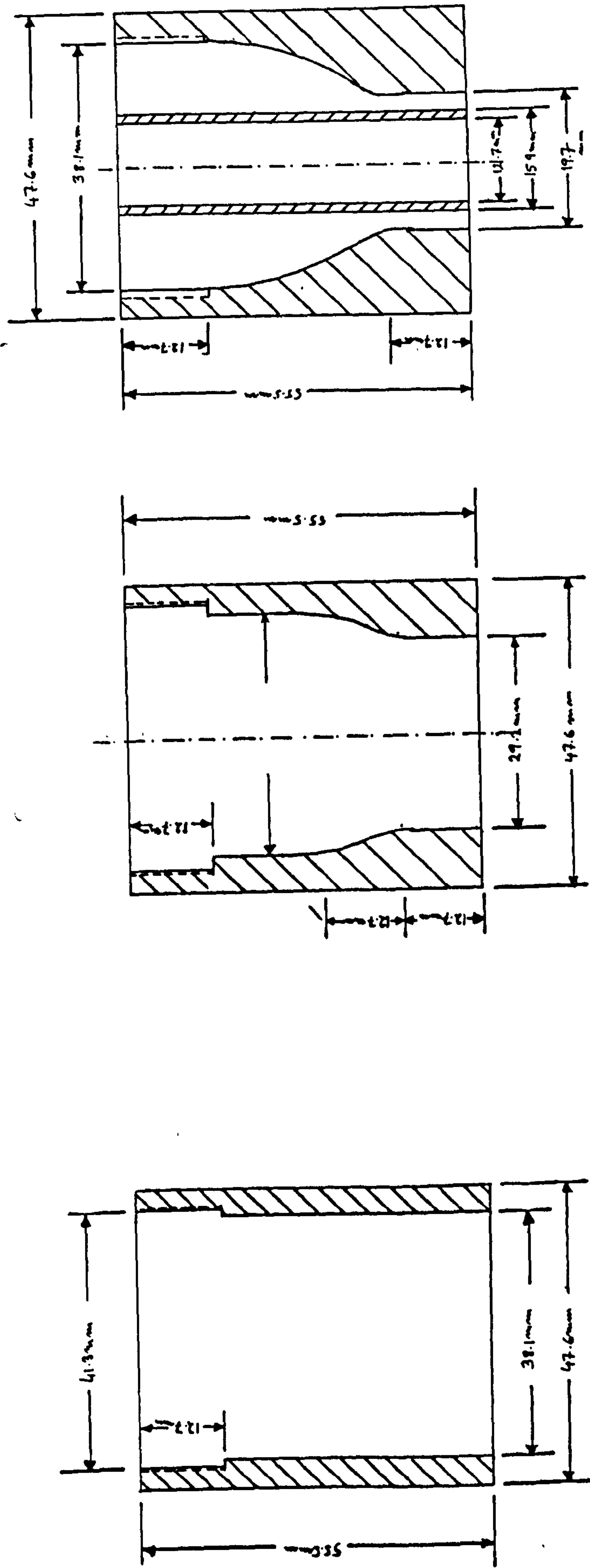


Figure 9.4. End pieces for annular nozzles.

beam of the frame so that the axis of the nozzle fixed to the platform is vertical to the liquid surface in the tank. The length of the jet could be adjusted by just raising or lowering the nozzle holder. By the time experiments on air entrainment were to be performed a second nozzle holder, shown through Figs. 9.5a to 9.5d, was designed and made. With this holder the adjustment of nozzle for angular jets was easy, and straightforward. The holder was made in two parts, A and B. Figs. 5a, 5b, and 5c show the front, side and plan views of the part A. The part A provides a platform D, whereupon the nozzle flange can be seated and bolted; moreover, the platform can be rotated through about 80 degrees around the pivot P, and its position can be locked by tightening the nut on pin E. The holes in the back plate F are aligned to the slots in Part B, and then bolted. The long slots permit the horizontal movement of the nozzle. The vertical Dexion legs are bolted to the main framework.

The volume of air being entrained by the jet was measured by a concealed jet technique in which the jet was concealed by bolting the nozzle flange to both the horizontal plate of the nozzle holder and the flange of the reducing socket D (Fig. 9.6). Rubber gaskets were placed between the flanges to avoid air leakage. The tube concealing the jet was perforated at its lower end and the perforated part of the tube was always kept well under the water surface. The liquid displaced by the jet inside the tube was replaced by liquid flowing through these perforations.

The air being entrained by the jet was drawn from the atmosphere through the flexible air duct. At the free end of this duct, a



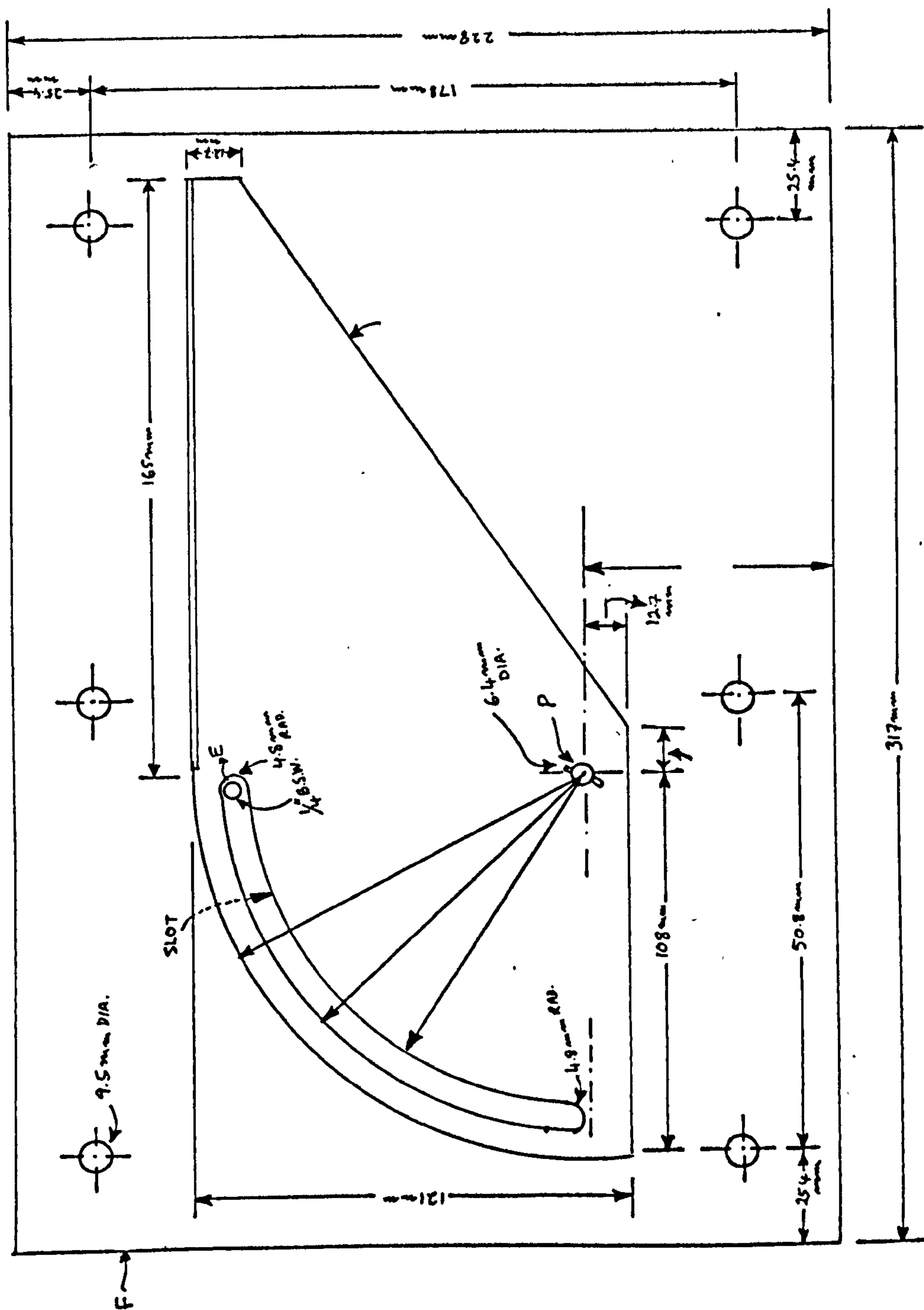


**Figure 9.5a. Nozzle holder - part A - front view**

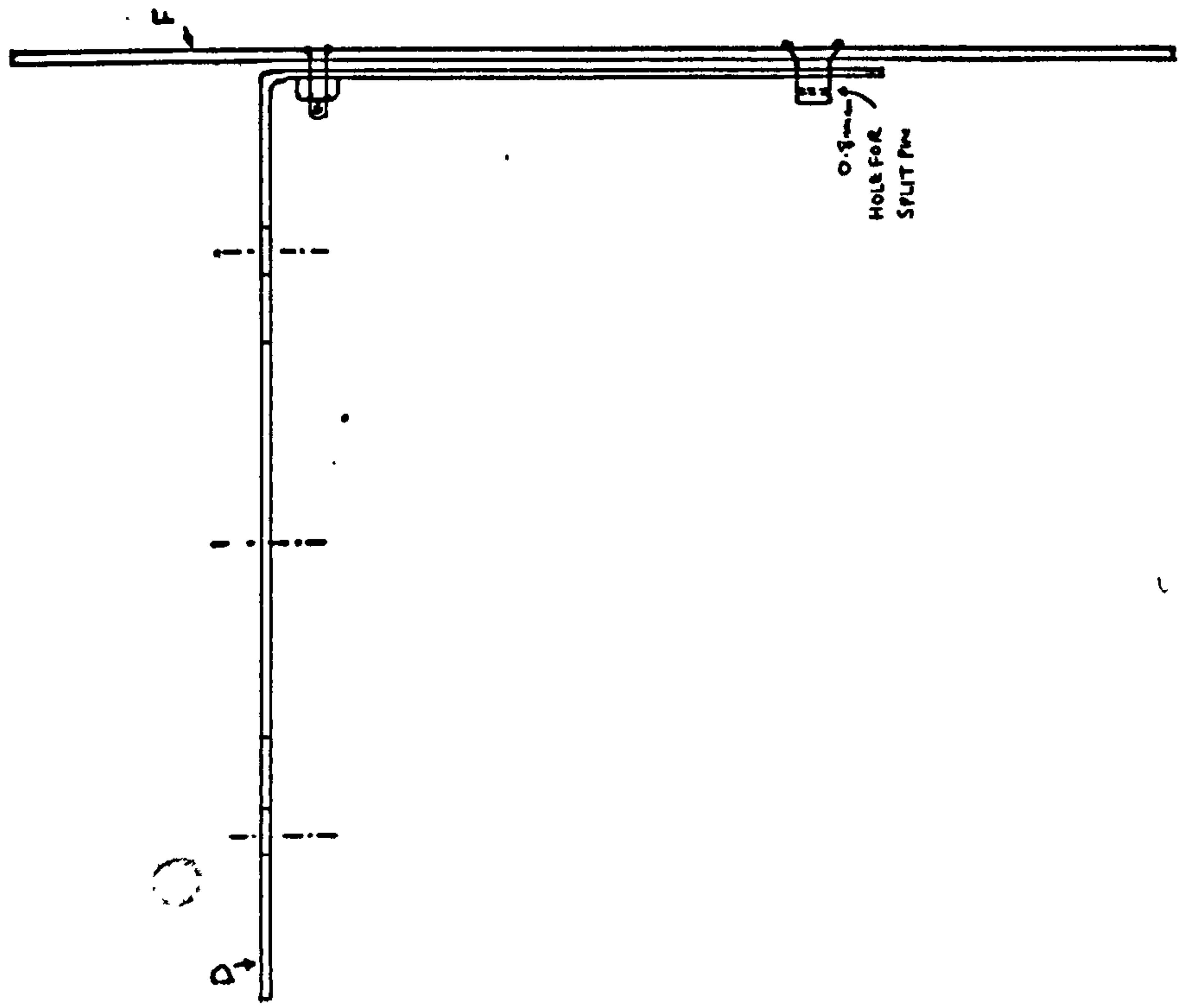


Figure 9.5 b. Nozzle holder - part A - side view.

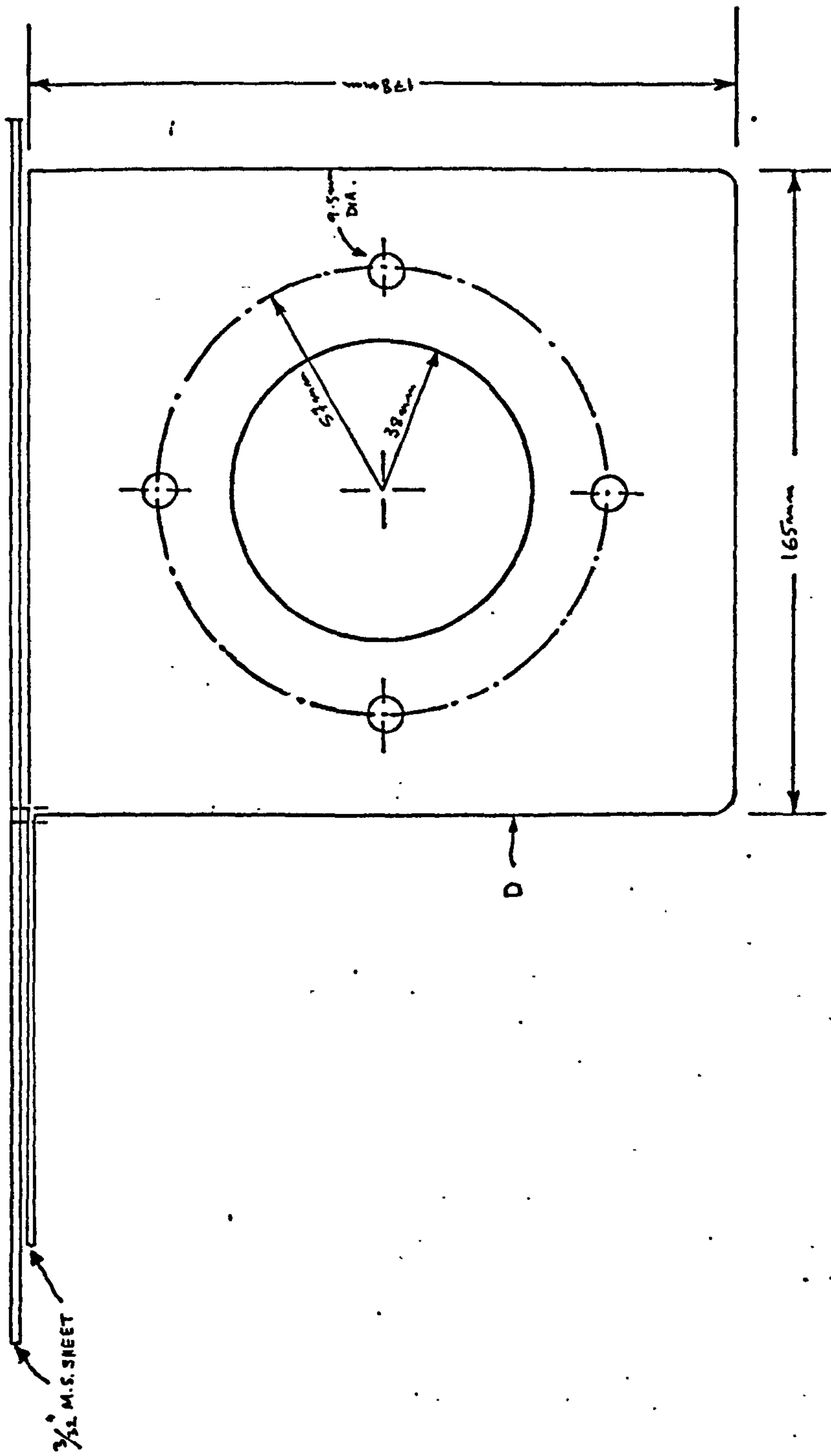
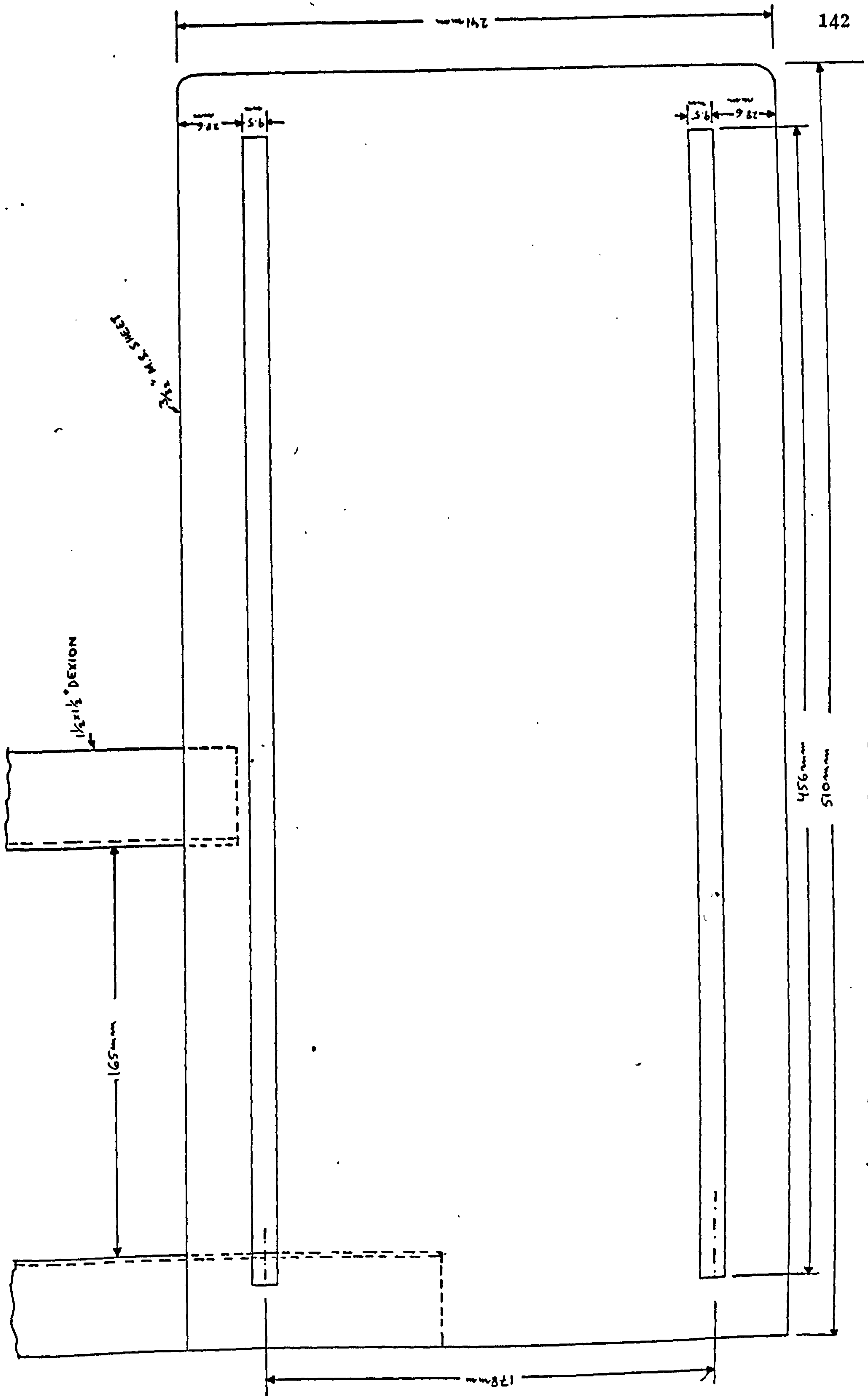


Figure 9.5 c. Nozzle holder - part A - plan.



Nozzle holder -- part B.

Figure 9.5 d.



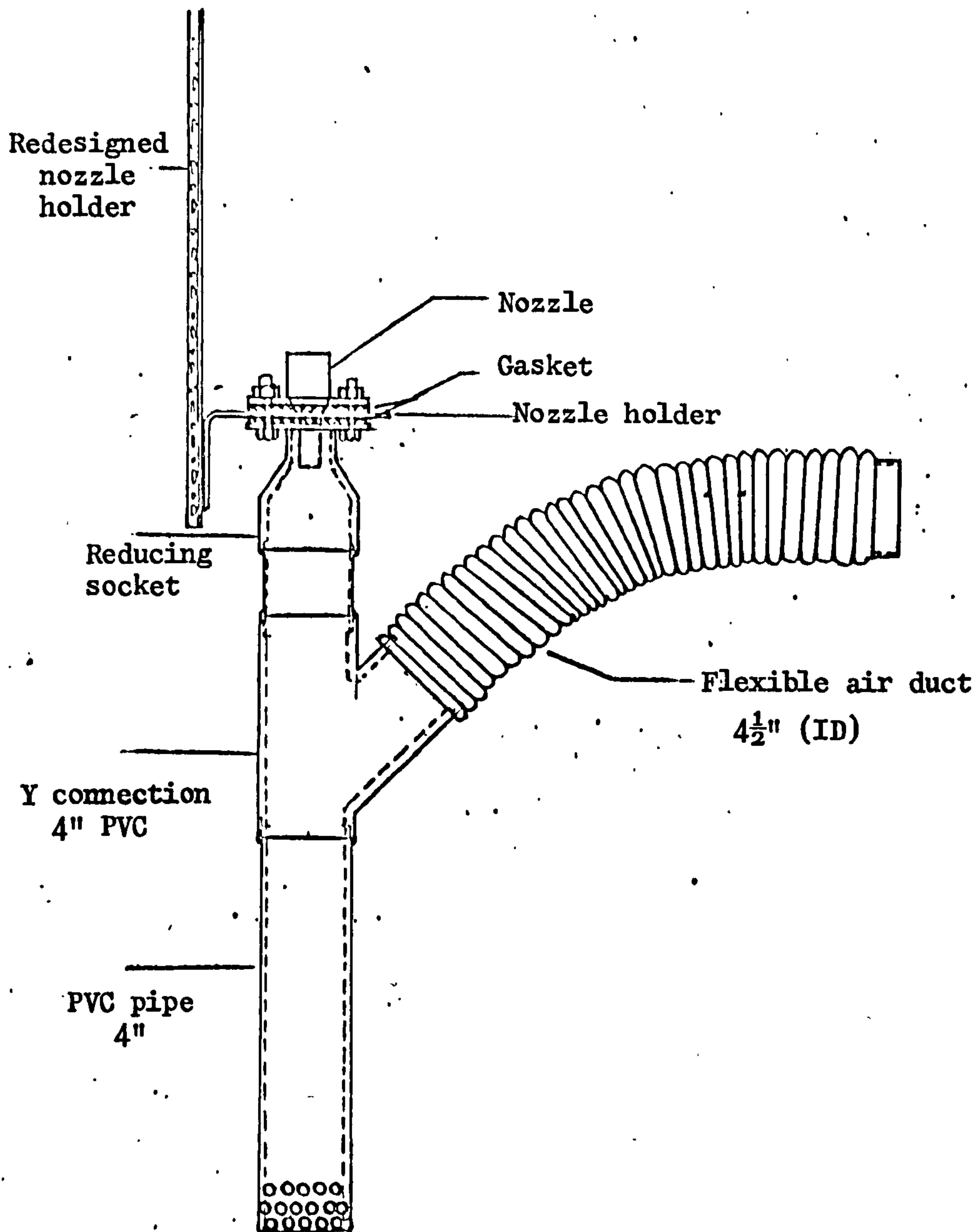


Figure 9.6. Concealed jet for measurement of air entrainment rate

small piece of 4 inch PVC pipe was connected. All air duct joints were made leakage proof. The velocity of air flowing in the air duct was measured by placing a 4 inch vane type electronic anemometer (Air Flow Developments Ltd., Lancaster Road, High Wycombe, Bucks., England) at the inlet of the air duct. The anemometer was accurate for air velocities in the range 0.12 to 25 m/s.

At high jet velocities small fluctuations in jet flow rate were observed, and they caused corresponding fluctuations in the air entrainment as well. In this case, the mean of the high and low readings of the anemometer was taken.

Air entrainment data were obtained only with vertical jets and the air-water and air-biological (few experiments) system.

For annular jets the combined entrainment by the outside and inside jet periphery was measured by connecting the inner tube of annular nozzle with the main duct via a branched tube from the main duct — the anemometer being located at the inlet of the main duct. In some cases, the air entrainment only through the inner tube was measured separately, using a gas meter.

## 9.2 RESULTS AND DISCUSSION

The effect of jet parameters on entrainment rate was investigated. The results were obtained for cylindrical and annular nozzle diameters described earlier in 9.1. Entrainment rates at various jet velocities including the maximum and minimum practical jet velocity were obtained. The minimum practical limit of jet velocity is defined by the minimum measurable entrainment rate. The maximum practical limit of jet velocity is governed by the pump capacity.

The ranges of jet velocities ( $V_j$ ) at the nozzle end for various nozzles were as follows:-

Cylindrical nozzles:

$d_n$ (mm)	$V_j$ (m/s)
9.5	15.52 - 20.7
12.7	16.5 - 28.5
22.2	4.3 - 13
28.6	2.9 - 8.0
38.1	1.85 - 4.5

Annular nozzles:

$d_{no}$ (mm)	$d_{ni}$ (mm)	$V_j$ (m/s)
19.7	15.9	10.3 - 21.2
29.2	25.4	9 - 19
33.	25.4	4.1 - 12.5
38.1	25.4	3.5 - 7.2

Thus, generally speaking, the jet velocities were in the range 1.85 to 28.5 m/s.

The entrainment data for cylindrical jets were obtained at jet lengths of 0.41, 0.66, and 1.05m jets, whereas the data for annular jets were taken at jet lengths of 0.66 and 0.98 m.

### 9.2.1 Effect of Jet Velocity on Air Entrainment Rate

Fig. 9.7 shows the effect of jet velocity on air entrainment rate for various cylindrical and annular nozzle diameters. The jet velocity corresponds to the velocity of the jet at nozzle, and where the jet diameter is approximately equal to nozzle diameter. It is obvious from Fig. 9.7 that entrainment rate increases with the increase of jet velocity for both cylindrical and annular jets.

### 9.2.2 Effect of Nozzle Diameter on Entrainment Rate

Entrainment rate increases with the increase of nozzle diameter for both cylindrical and annular nozzles as shown in Fig. 9.7.

### 9.2.3 Effect of Jet Length on Entrainment Rate

Fig. 9.8 shows the entrainment rate - plotted against jet velocity - at different jet lengths with cylindrical and annular nozzles. It is obvious that the entrainment rate increases with the increase of jet length for both cylindrical and annular jets. But, for the cylindrical jets, entrainment rates at 0.66 m and 1.05 m jet length are approximately the same. It follows that in the case of cylindrical jets the entrainment rate is not affected when jet length exceeds 0.66 m.



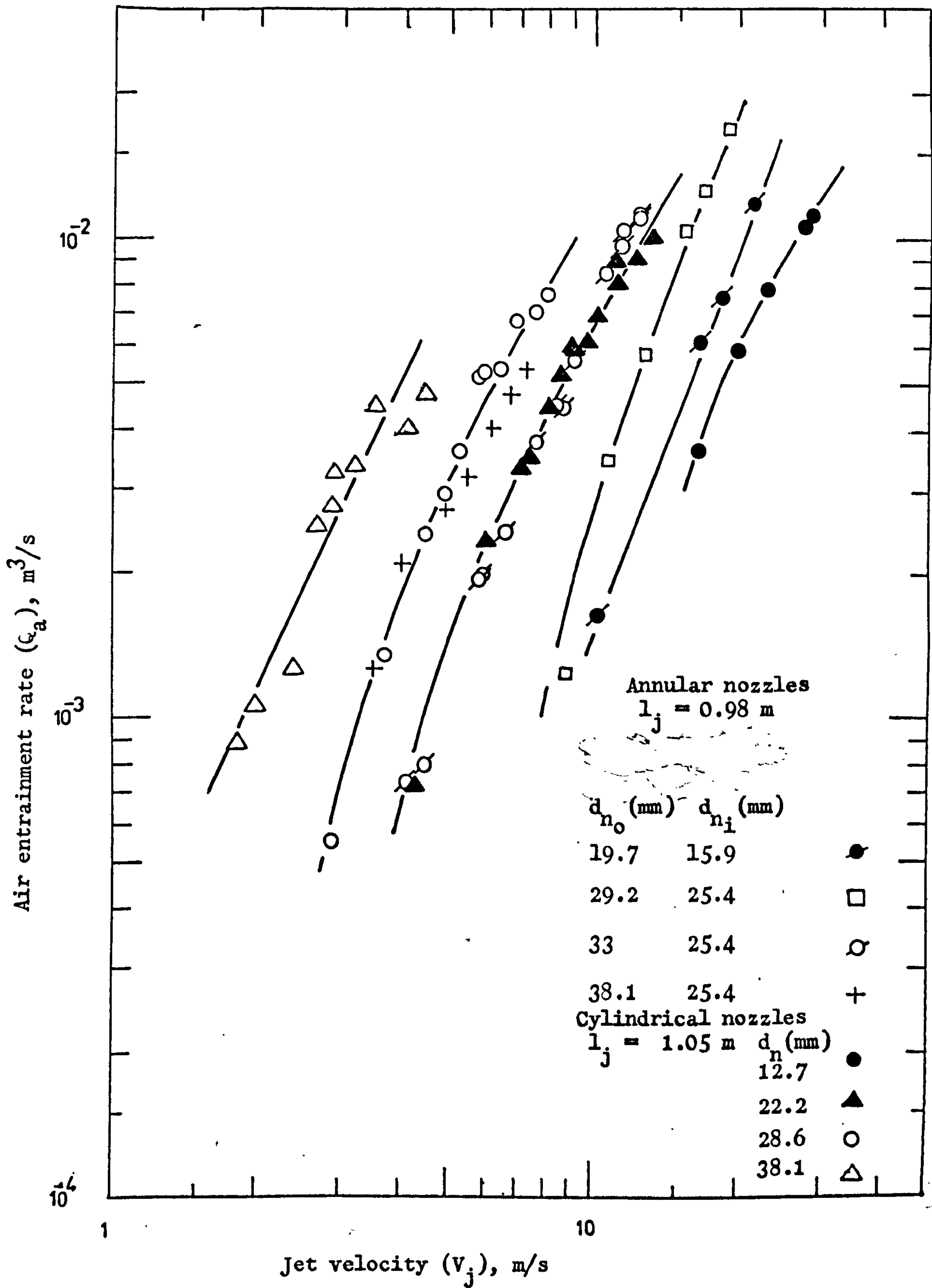


Figure 9.7. Relation of air entrainment rate with jet velocity for cylindrical and annular jets

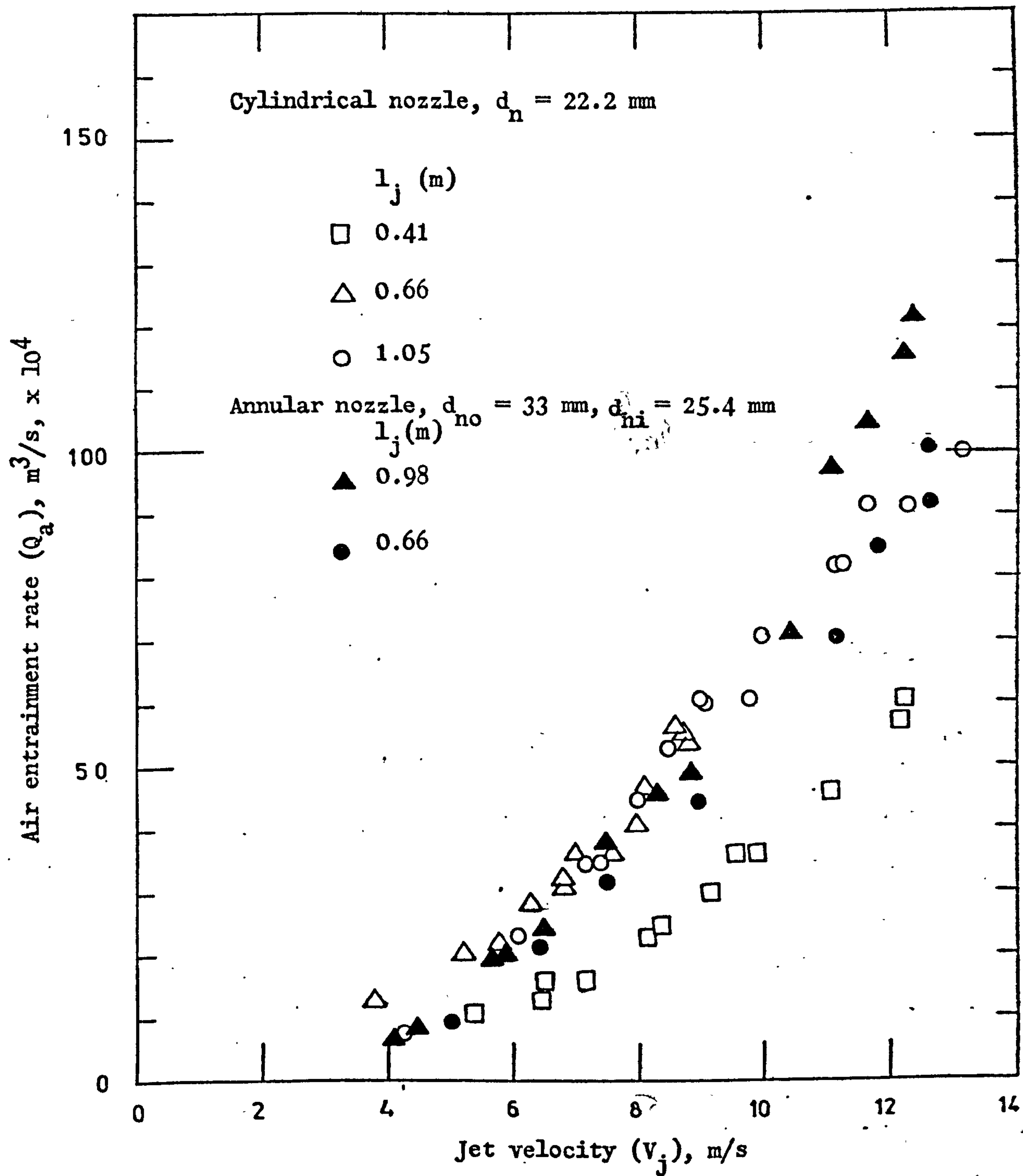


Figure 9.8. Effect of jet velocity on air entrainment rate at different jet lengths (cylindrical and annular jets)

#### 9.2.4 Air Flow Through Inner Tube of Annular Nozzle

Since in an annular jet additional air is entrained by the inside periphery of annular jet, therefore, as a point of interest, the air flow through the inner tube of the annular nozzle was measured separately at different jet lengths and at different jet velocities. Fig. 9.9 shows the results obtained with annular nozzle ( $d_{no} = 33$  mm,  $d_{ni} = 25.4$  mm). These results indicate that air flow through the inner tube increases with the increase of jet velocities and decreases with the increase of jet length.

The decrease was rapid up to 7.6 cm of jet length but with further increase of length no significant decrease in entrainment was observed at higher jet velocities. The rate of increase of air flow diminishes with the increase of jet velocity.

From these results, it is estimated that the air flow through the annulus is about 10% of the total air entrainment at a jet length of 0.66 m. This ratio of air flow rate through the annulus to the total entrainment will diminish with the increase of jet length as is obvious from Fig. 9.9.

#### 9.2.5 Correlation of Air Entrainment with Power of Jet

The ratio of entrainment rate to nozzle diameter ( $\frac{Q_a}{d_n}$ ) is correlated with power of jet in Fig. 9.10 for the jet lengths where entrainment rate is independent of the jet length. Also, a few data points for the entrainment rate in a biological system described in Chapter 11 are also shown in Fig. 9.10 and agree with the results obtained with tap water. The scatter at low jet power ( $< 0.02$  kW) is considerably reduced at high jet powers ( $> 0.02$  kW).

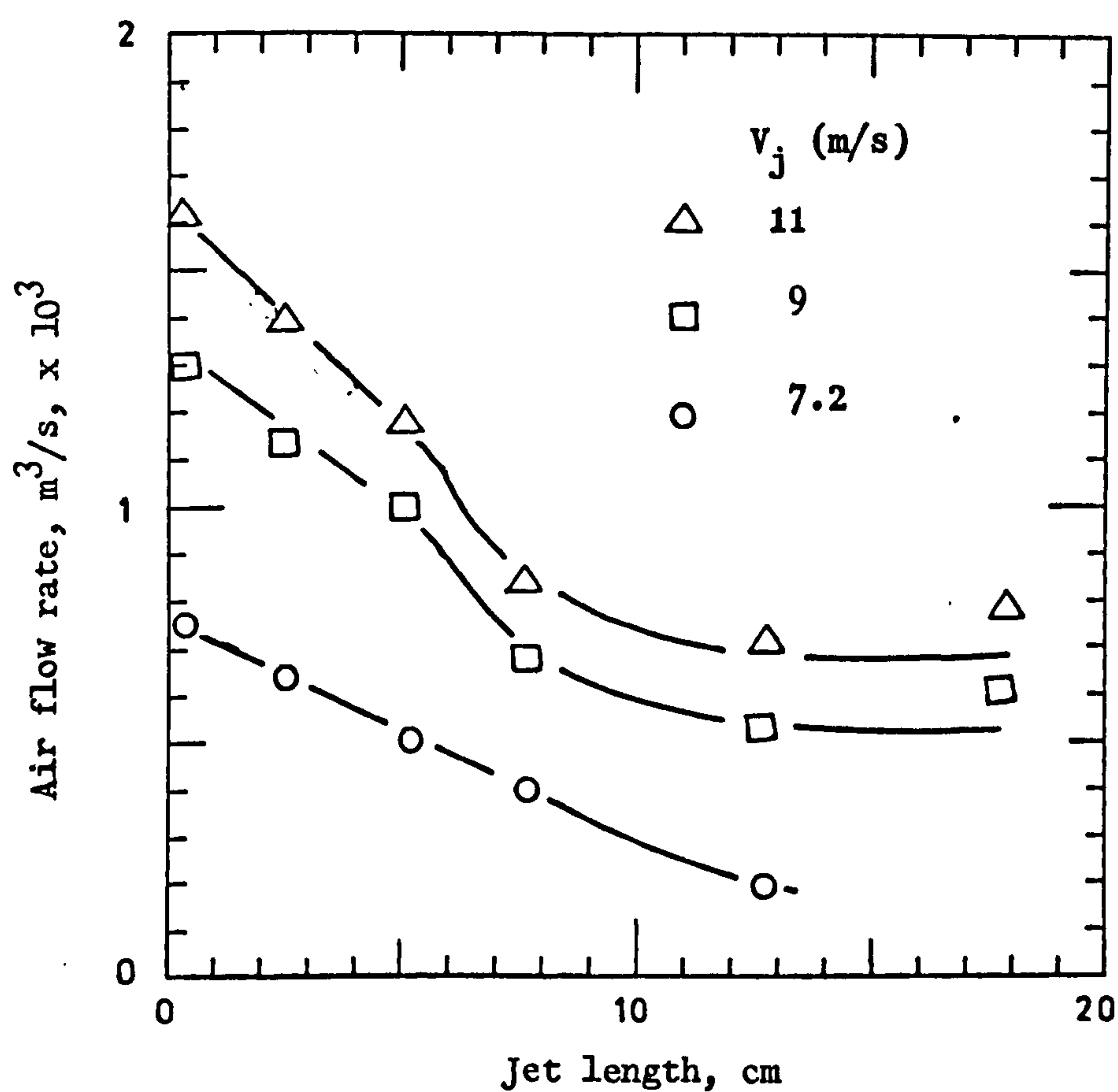


Figure 9.9. Effect of jet length on air entrainment rate through the inner tube of annular nozzle at different jet velocities (annular nozzle  $d_{no} = 33$  mm,  $d_{ni} = 25.4$  mm)



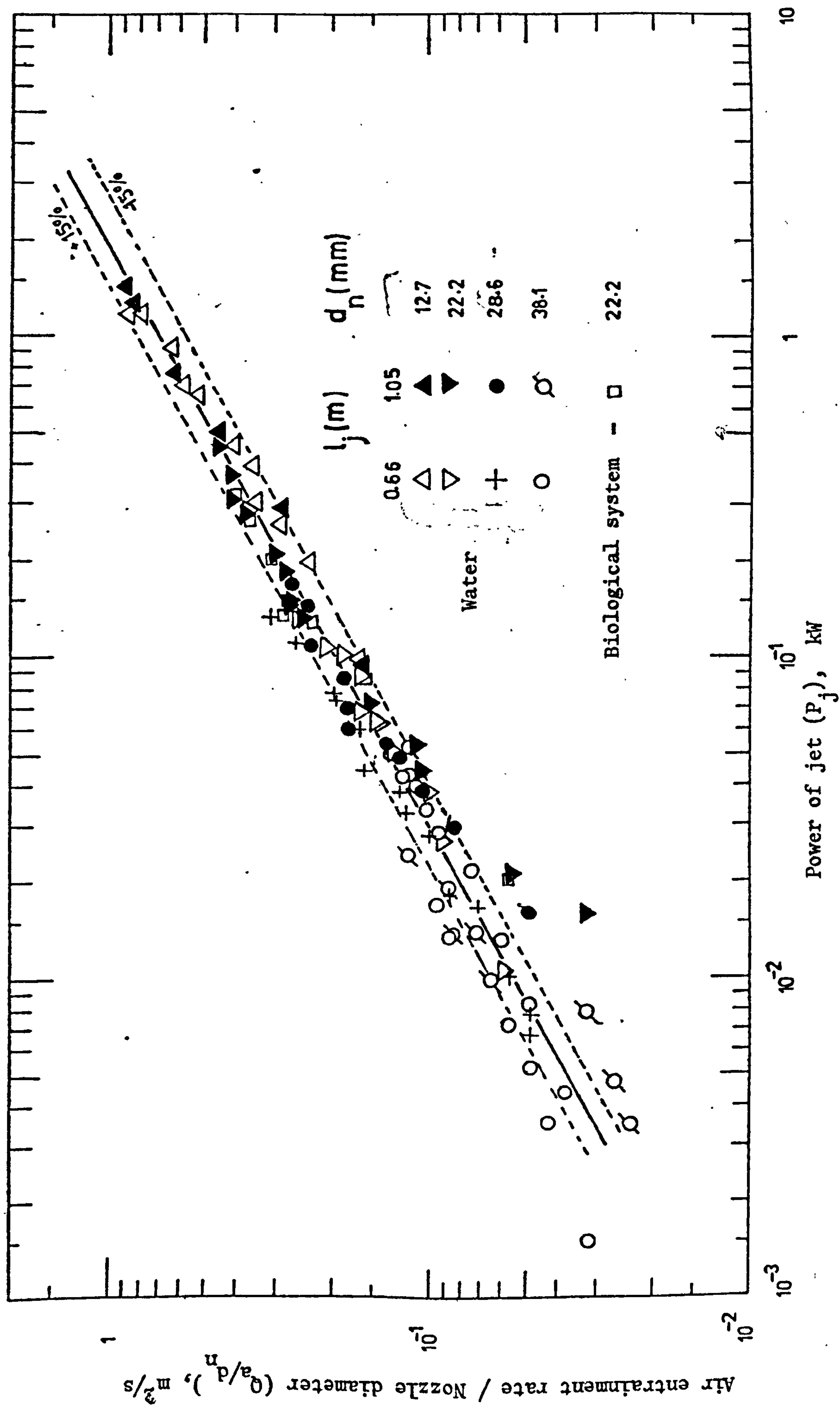


Figure 9.10. Correlation of air entrainment with power of jet.

The data in Fig. 9.10 is correlated by the equation:

$$\frac{Q_a}{d_n} = 0.855 P_j^{0.673} \quad 9.1$$

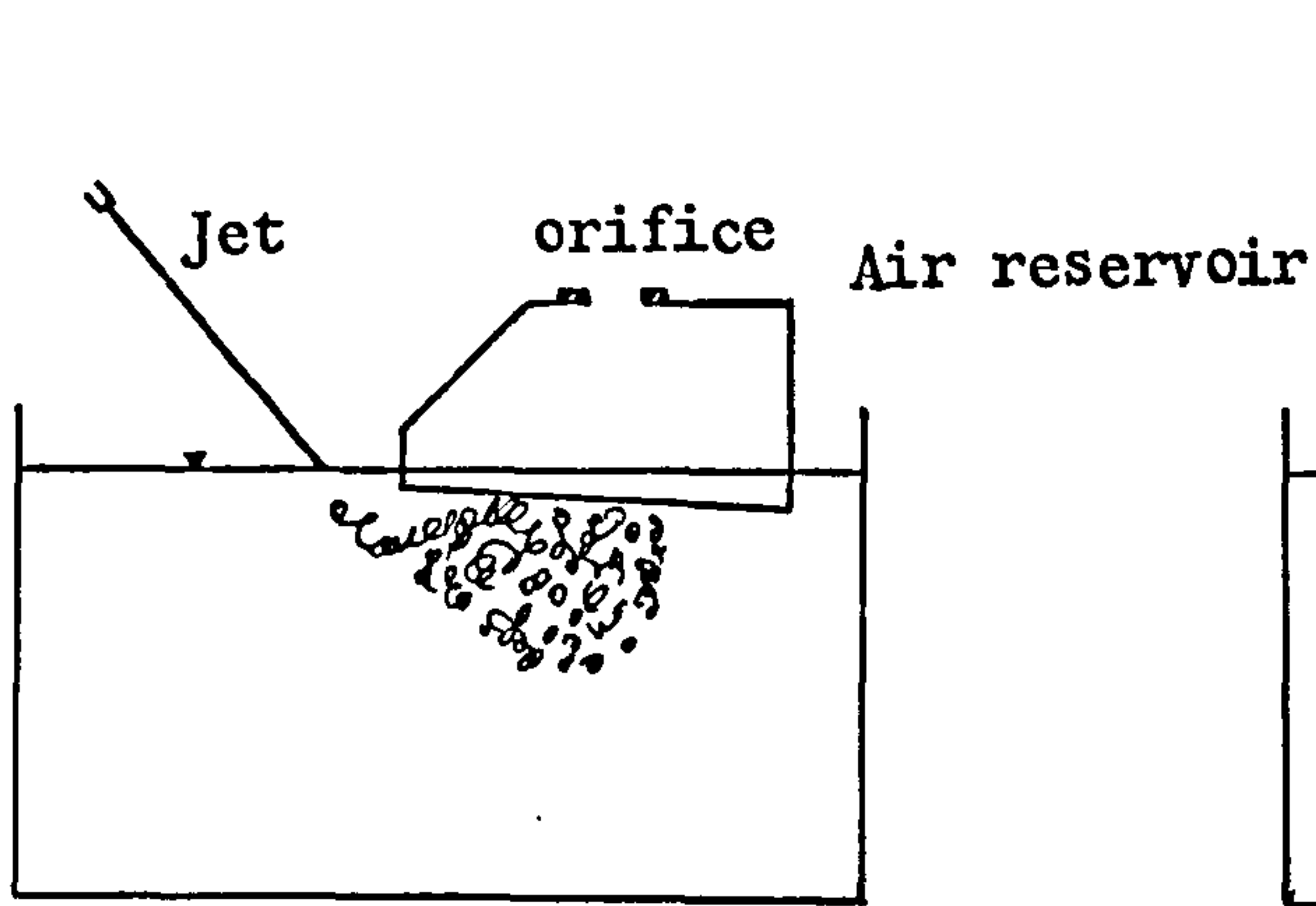
which is accurate within  $\pm 15\%$  especially at jet power greater than 0.02 kW. In equation 9.1  $Q_a$  is air entrainment rate in  $m^3/s$ ,  $d_n$  is cylindrical nozzle diameter in m, and  $P_j$  is power of jet in kW.

#### 9.2.6 Comparison of Results with the Data of Other Workers

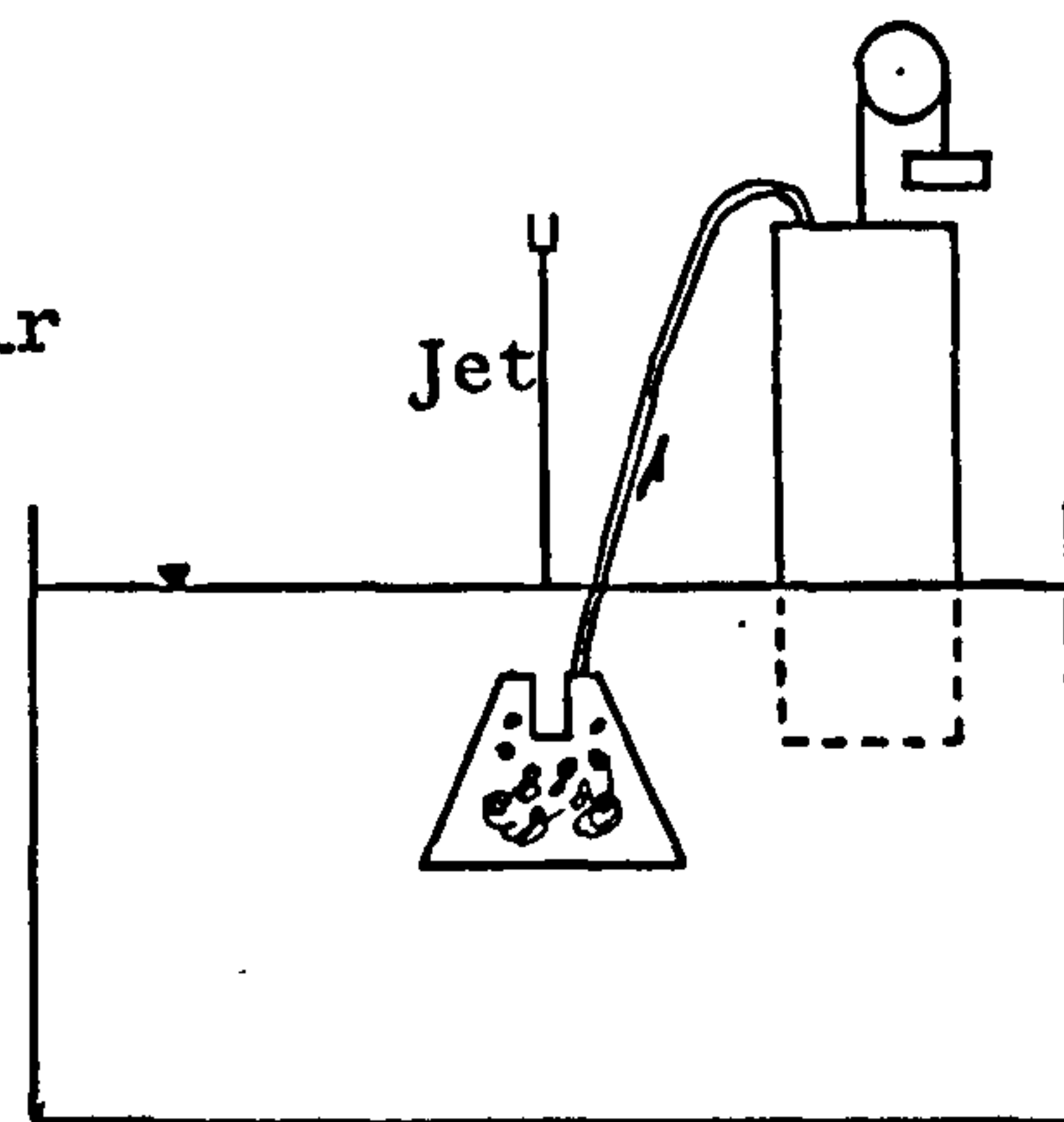
As pointed out earlier, the data on entrainment so far obtained by various authors are not compatible. This incompatibility could be attributed to different experimental designs used for measurement of entrainment rate.

It seems appropriate here to examine the different experimental methods employed in the past to measure entrainment rate. Fig. 9.11 shows these methods along with the design developed in this work. Shirley (107); De Frate and Rush (31); Van de Sande and Smith (123) used inclined jets, whereas Ohyama et al. (80), Henderson et al. (48), Ciborowski and Bin (25), and this author used vertical jets.

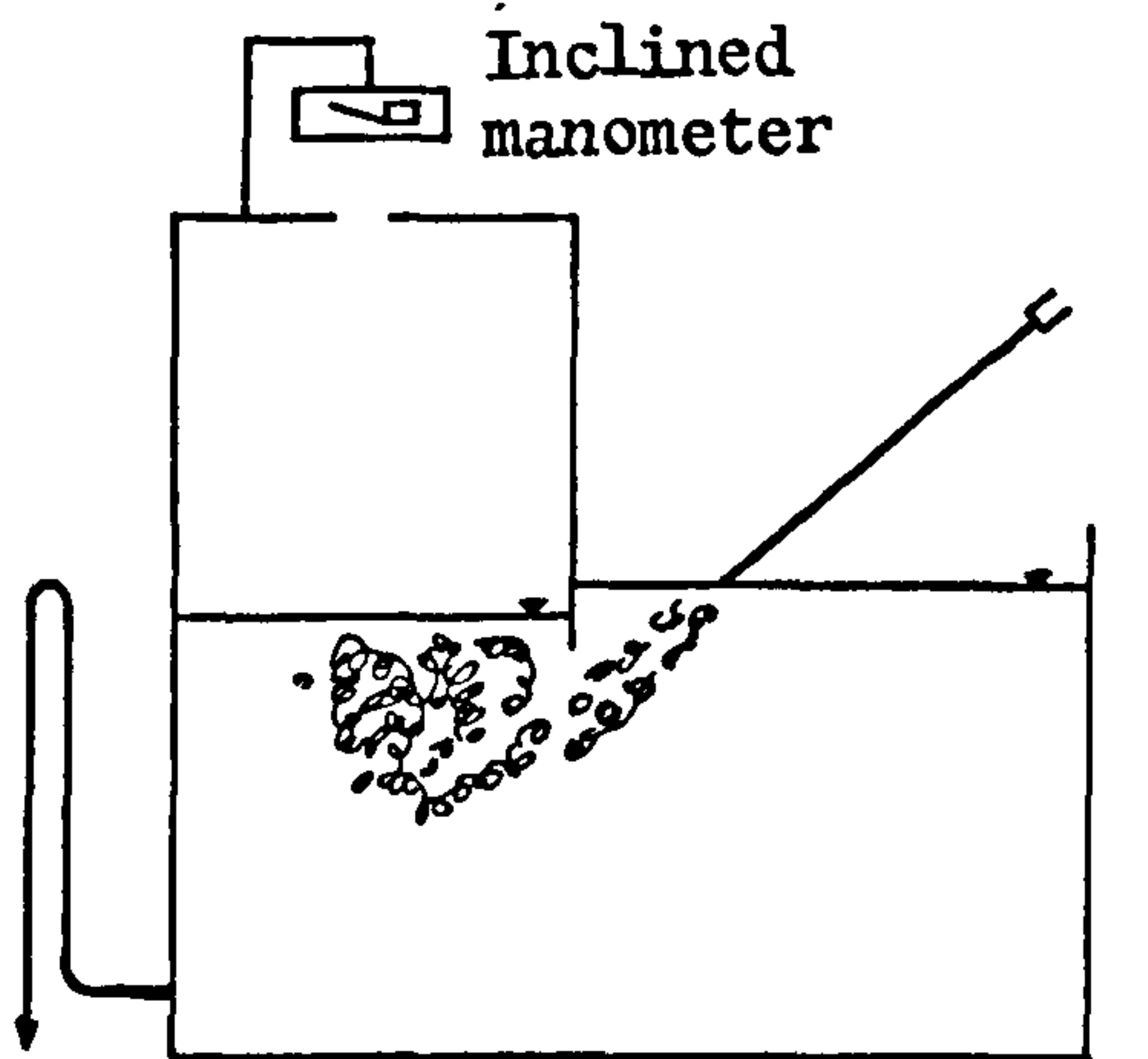
The apparatuses of Shirley, De Frate and Rush, Van de Sande and Smith are the same in principle. They differ only in the method of measurement of air entrainment rate. The measurement of small air flow through the orifice plate by measuring the slight pressure differential in the air reservoir does not seem to be an accurate method. The range of pressure differential across the orifice reported by Shirley in his experiments was 0.0025 inch to 1 inch of water, whereas in experiments of De Frate and Rush, the range of manometer reading was 0.3 to 1.5 inch of water.



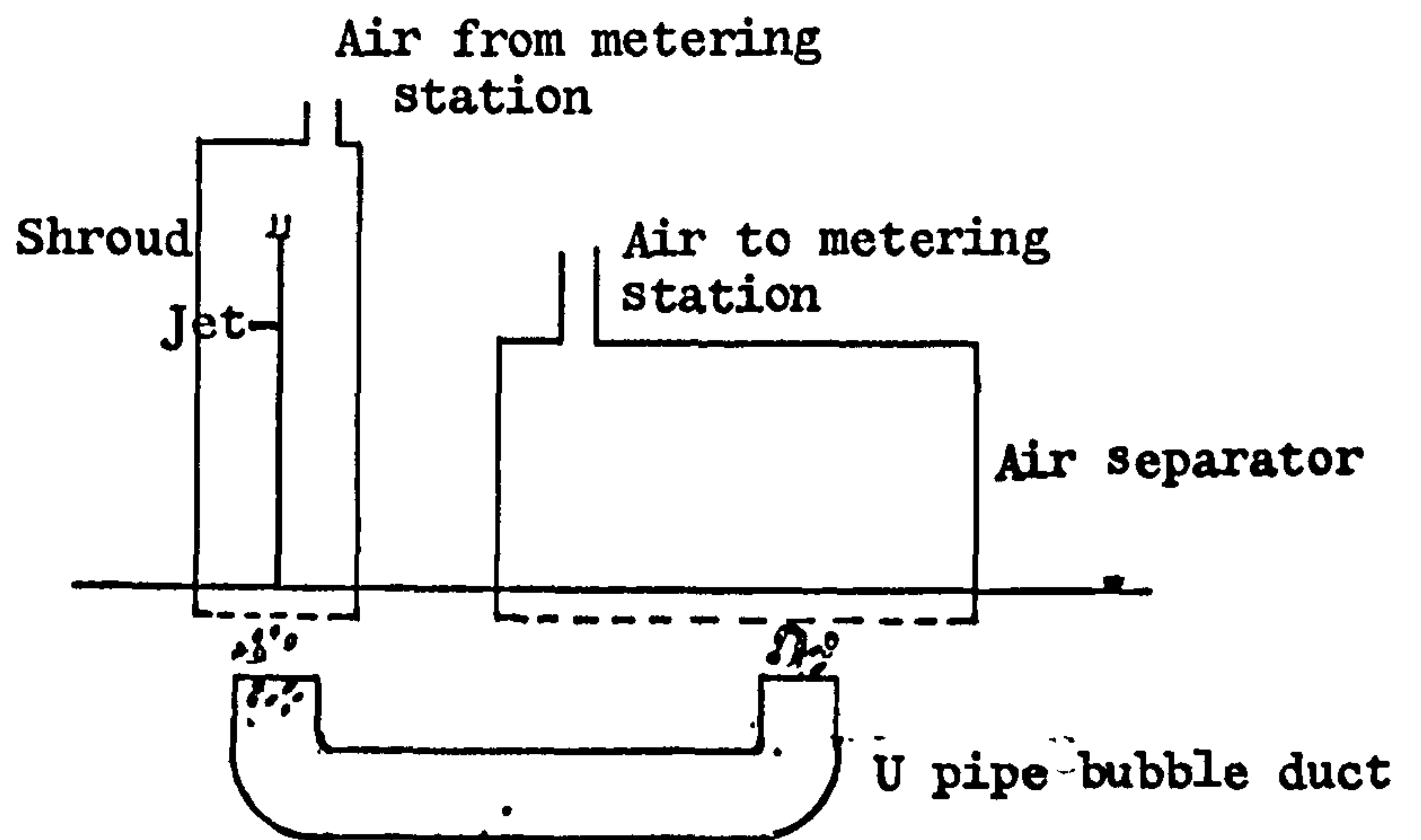
SHIRLEY (1950)



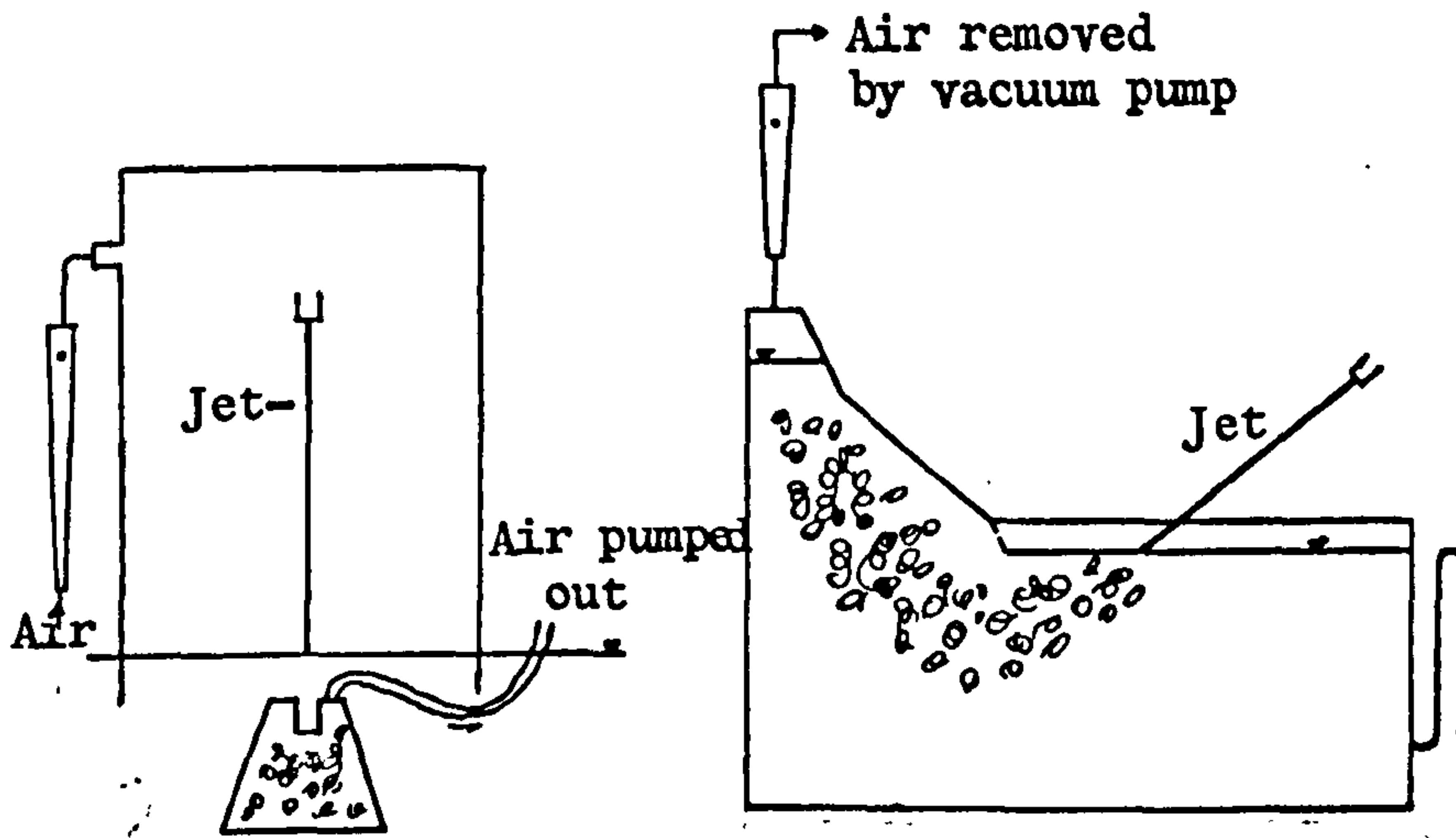
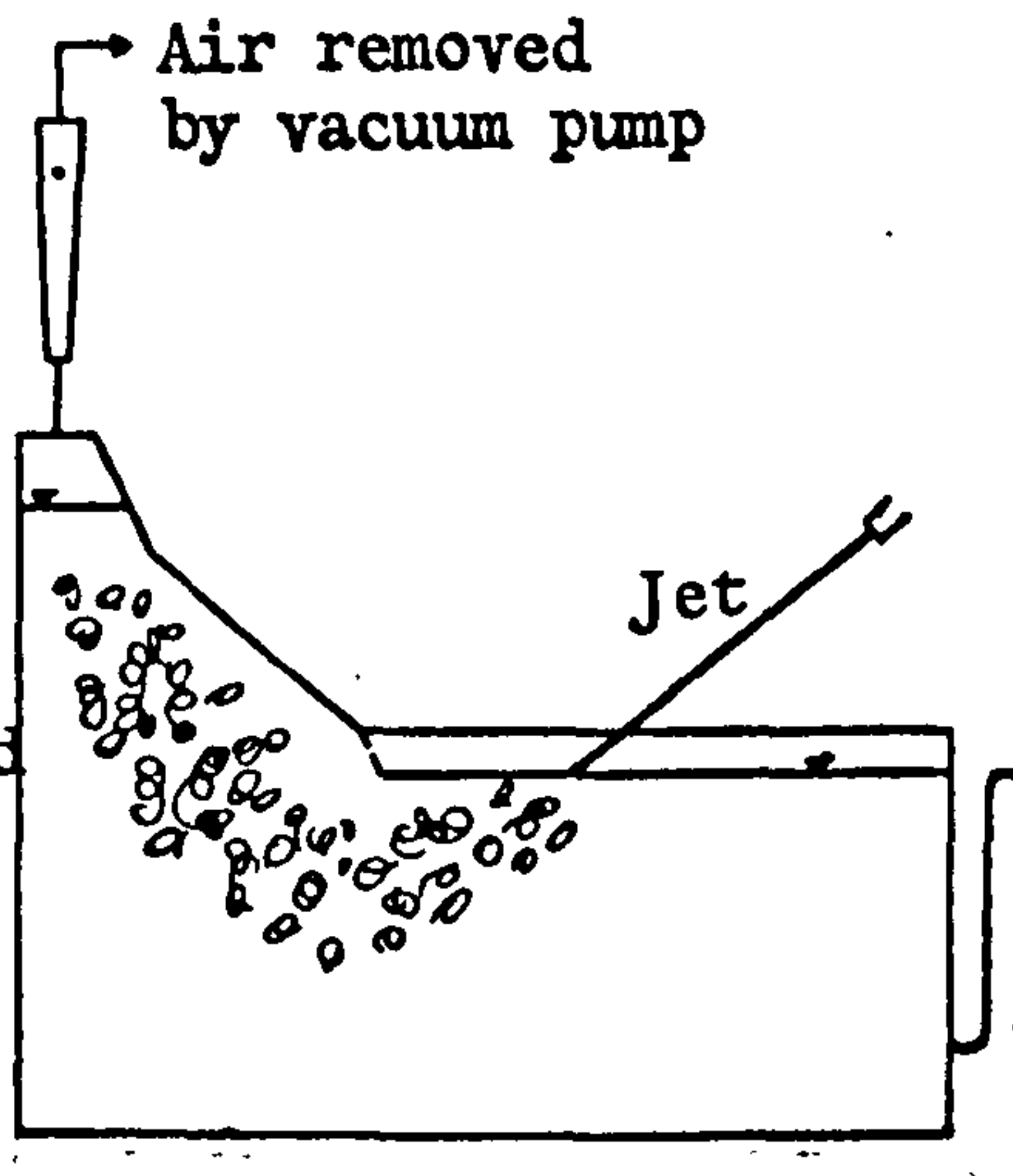
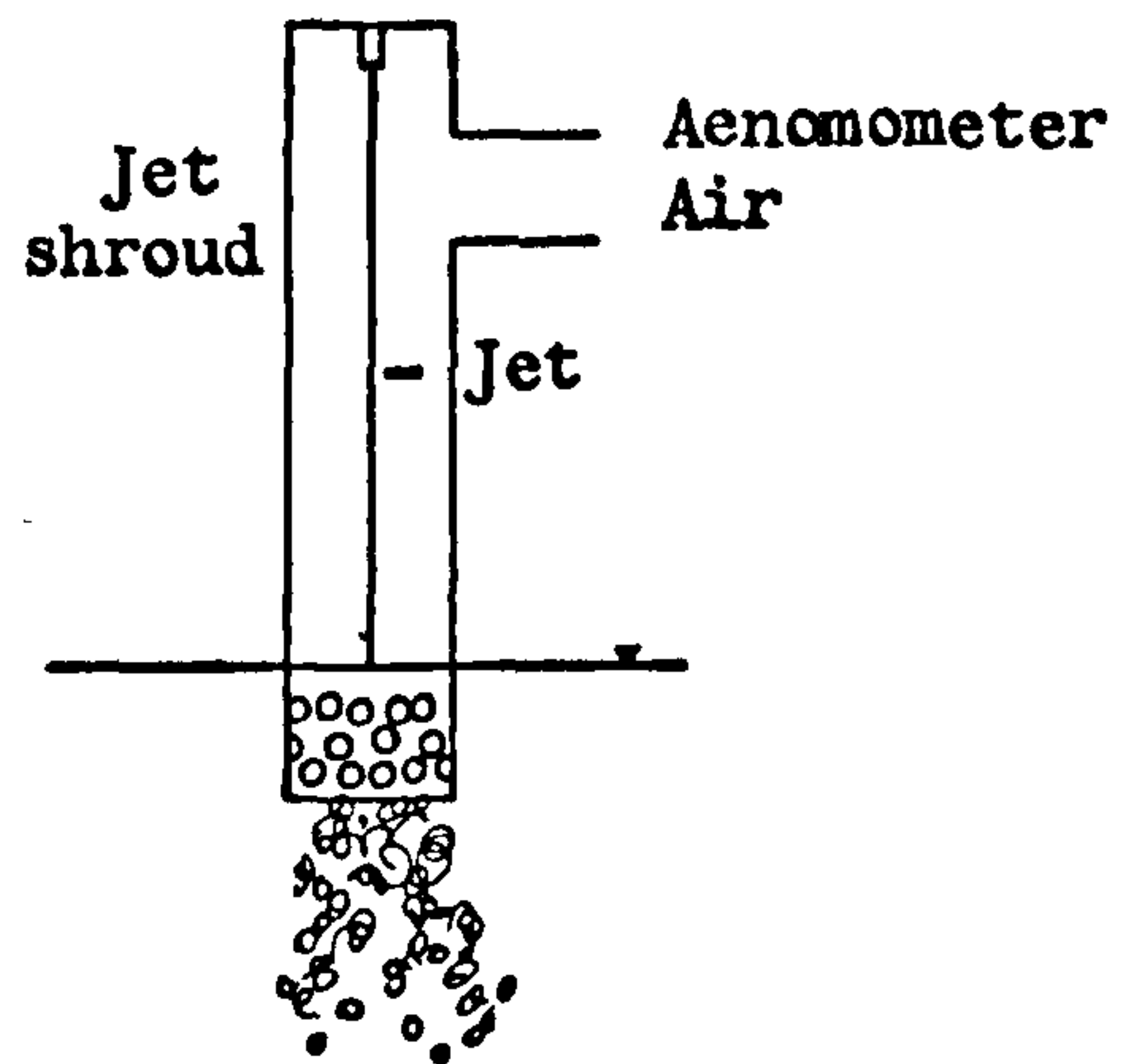
OHYAMA et al. (1953)



De FRATE and RUSH (1969)



HENDERSON et al. (1970)

CIBOROWSKI and BIN  
(1972)VAN DE SANDE and  
SMITH (1973)

PRESENT WORK (1974)

Figure 9.11. Experimental designs for measurement of air entrainment rates by plunging liquid jets.



The apparatus of Ciborowski and Bin (25) is, in fact, a modification of the apparatus designed by Ohyama et al. (80). Both employ a trap to capture the entrained air. The volume of the trap is small and is insufficient to confine larger volumes of air entrained at high jet velocities. Also, the lateral motion of the water inside the trap is hampered by the presence of solid walls of the trap.

The apparatus of Henderson et al. (48) is suitable only for high jet velocities because the entrained air has to be carried through the pipe to the measuring site.

In the apparatuses of Shirley, De Frate and Rush, Van de Sande and Smith, at a certain jet velocity the entrained air bubbles would hit the bottom of the tank and would disperse in the liquid randomly. Under these conditions some bubbles may escape to the atmosphere through the free liquid surface. In fact, maximum jet velocity is limited by the depth of liquid column.

The method developed in this work is simple and free from the various drawbacks mentioned above. In particular, the method is good at higher jet velocities. The jet velocity is not limited by the geometry or the turbulence of the tank. There is no obstruction to motion of water at plunge point due to the presence of numerous holes in the shroud. Also, the data for vertical jets are directly obtained.

In addition to the above differences in experimental technique, there are other factors which hamper the direct comparison of the data obtained by various authors. For instance, most of the reported data was obtained with low jet velocities using varying



nozzle designs, nozzle diameters and jet length. All these factors make it difficult to compare the results as well as compare the experimental methods. Despite these difficulties, the data can be utilized for a rough comparison.

Hence, Fig. 9.12 shows the data of Shirley, Van de Sande and Smith, along with the data of the present author. The two parameters of air entrainment rate,  $Q_a$ , and jet liquid flow rate,  $Q_l$ , were chosen for the comparison of the data. Although at first sight the three sets of data do not agree well, there are some common points which will be described in due course.

Before proceeding further, it should be noted that Shirley (107), Van De Sande and Smith (123) measured air entrainment rates by angular jets. They obtained entrainment rates for vertical jets by extrapolation of the angular jet data. Now the effect of jet angle on air entrainment rate is controversial. By varying the jet angle from 40 to 70 degrees, Shirley observed a decrease in entrainment rate. He thought that minimum entrainment would occur when the jet is vertical. Therefore he drew smooth curves through the experimental points of angular jets and extended this curve up to an arbitrary minimum at 90 degrees. In contrast, Van De Sande and Smith (128) report that though the air entrainment decreased with the increase of jet angle, the decrease is not significant when jet angle varies from 60 to 75 degrees. Hence, the entrainment data for jet angle greater than 60 degrees represents approximately the data for vertical jets.

So, if Shirley's data are replotted for entrainment rates at 70 degrees, they will be displaced slightly upwards. Furthermore, the curves probably refer to entrainment at low jet lengths, as

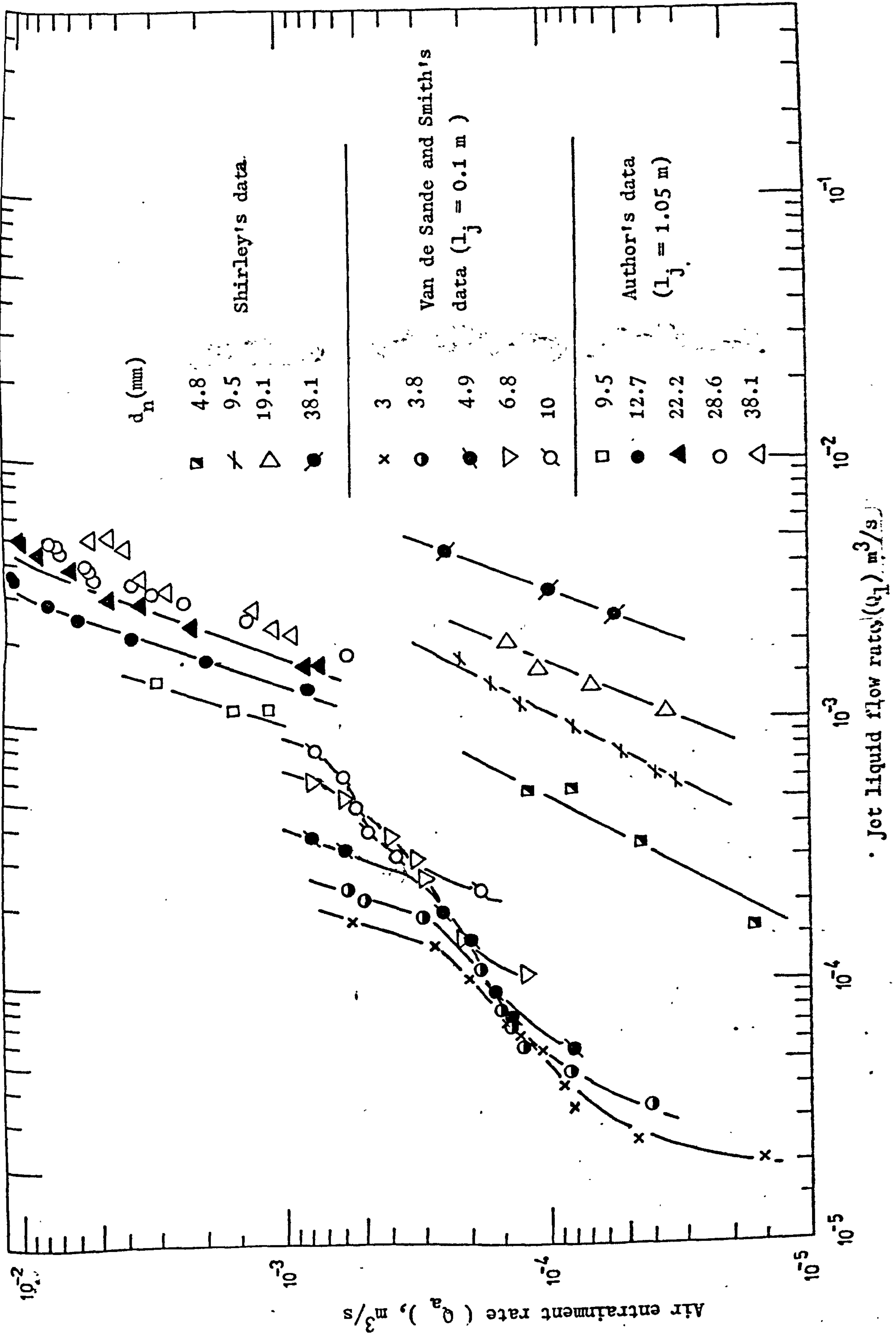


Figure 9.12. Relation of air entrainment rate with jet liquid flow rate.

suggested by his diagram of experimental apparatus (Shirley did not mention jet length in his experiments). The entrainment for long jet lengths such as 1.05 m, will be increased significantly. This means that adjustment of Shirley's data for 1.05 m long vertical jets would displace upwards the curves drawn in Fig. 9.12 and possibly the displaced curves might agree with this author's data.

Van De Sande and Smith (123) worked with nozzles having smaller diameters. So the author's results cannot be directly compared with their results. However, a few common points stem from the plot in Fig. 9.12.

From the plot of Van De Sande and Smith's data, one notices that for small jets with the increase of jet liquid flow rate there is an initial rapid increase in the entrainment rate, then a lower rate of increase for a particular range of liquid flow rate (transition region). Beyond this range of liquid flow, the entrainment rate again increases at a higher rate (high velocity region:  $We > 10$ ). In this region it is evident from Fig. 9.12 that the rate of increase of entrainment with jet liquid flow rate seems to be of the same order as indicated by this author's data.

Another point worth noticing is that the length of the transition region with respect to jet liquid flow rate is gradually shortening with the increase of jet diameter. It seems likely that this transition region would be negligible for jet diameters greater than 10 mm. In Fig. 9.8, the air entrainment increases almost linearly with the increase of jet velocity even if the velocity is in the lower region ( $We < 10$ ). No distinctive transition region



is observed at low jet velocities. Hence, from Fig. 9.12, it seems that the establishment of a transition region is a characteristic of smaller diameter jets.

In Figs. 9.13, 9.14 and 9.15, the air entrainment rates are plotted against jet liquid flow rate for various nozzle diameters and jet lengths. The solid lines represent the air entrainment rates predicted by the theory developed by Van De Sande and Smith (123) for high velocity jets. The data points of the 38.1 mm diameter nozzle have a Weber number less than 10, therefore, the theory should not be applied to them. It is obvious that for cylindrical nozzle diameters 9.5 mm, 12.7 mm and 22.2 mm, the results agree well with the theory, although, in some cases, a systematic discrepancy exists.

This sort of disagreement is, in fact, expected with the type of nozzles employed in the present work. The nozzle aspect ratio  $(\frac{l_n}{d_n})$  is much less than 50 and varies from 3.45 to 8.33 as shown in Fig. 9.2. Hence the turbulence induced by the pump in the flow makes the jet shape more irregular.

For 28.6 mm and 38.1 mm diameter nozzles, the jet shape was very ill-defined. One-seven-hundredth of a second exposure photographs were taken of all jets at low and high jet velocities. A few typical photographs are shown in Plates V, VI, VII, VIII and IX. The plate V shows a jet from 28.6 mm diameter nozzle having a velocity at the nozzle end equal to 3.13 m/s. The jet surface is smooth for 7 cm from the nozzle end, but soon variations develop along the jet length. The surface of the jet from 38.1 mm diameter nozzle is very ill-defined as is evident from Plate VI. The



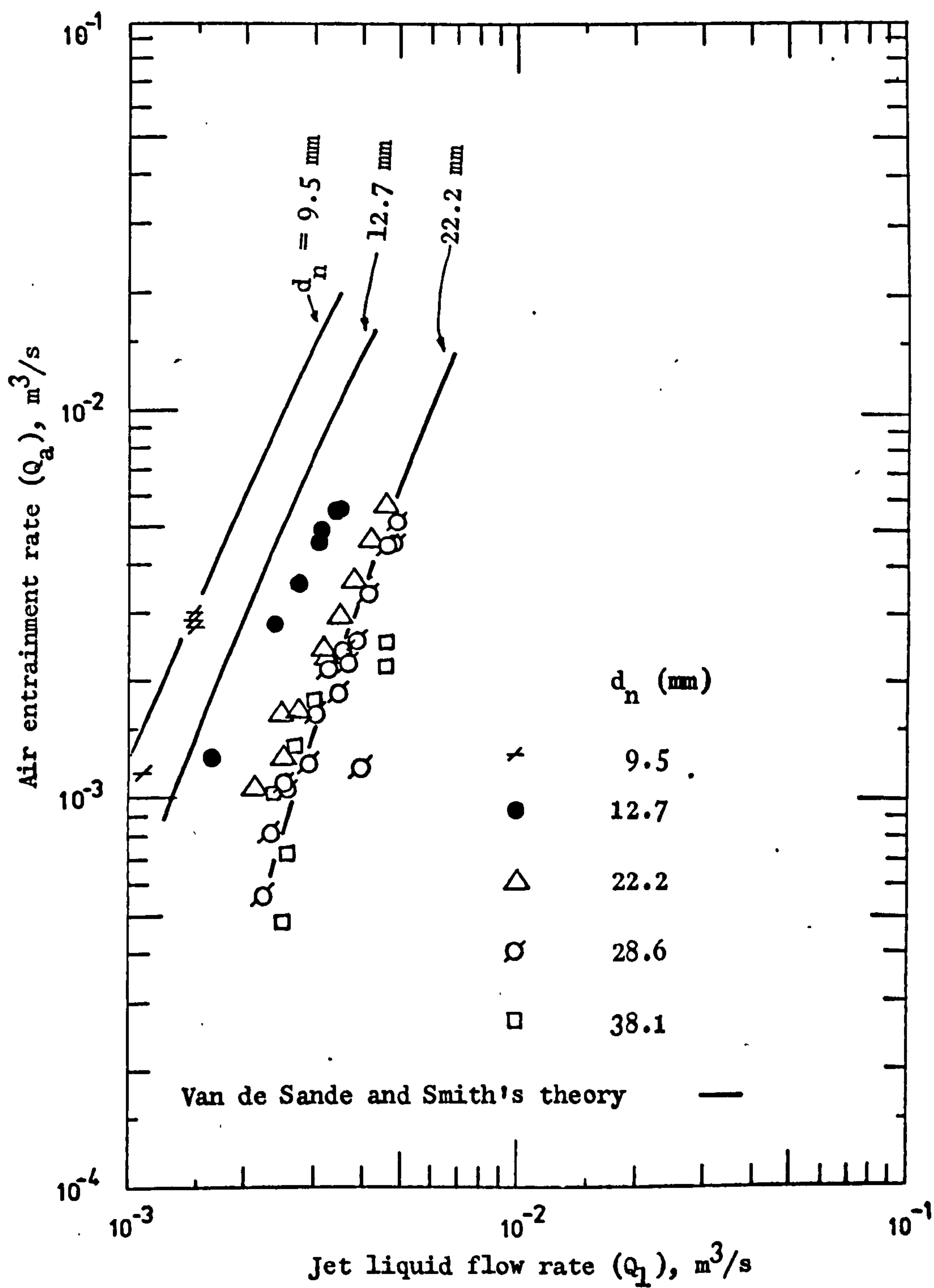


Figure 9.13. Relation of air entrainment with jet liquid flow rate for different cylindrical nozzles at 0.41 m jet length.

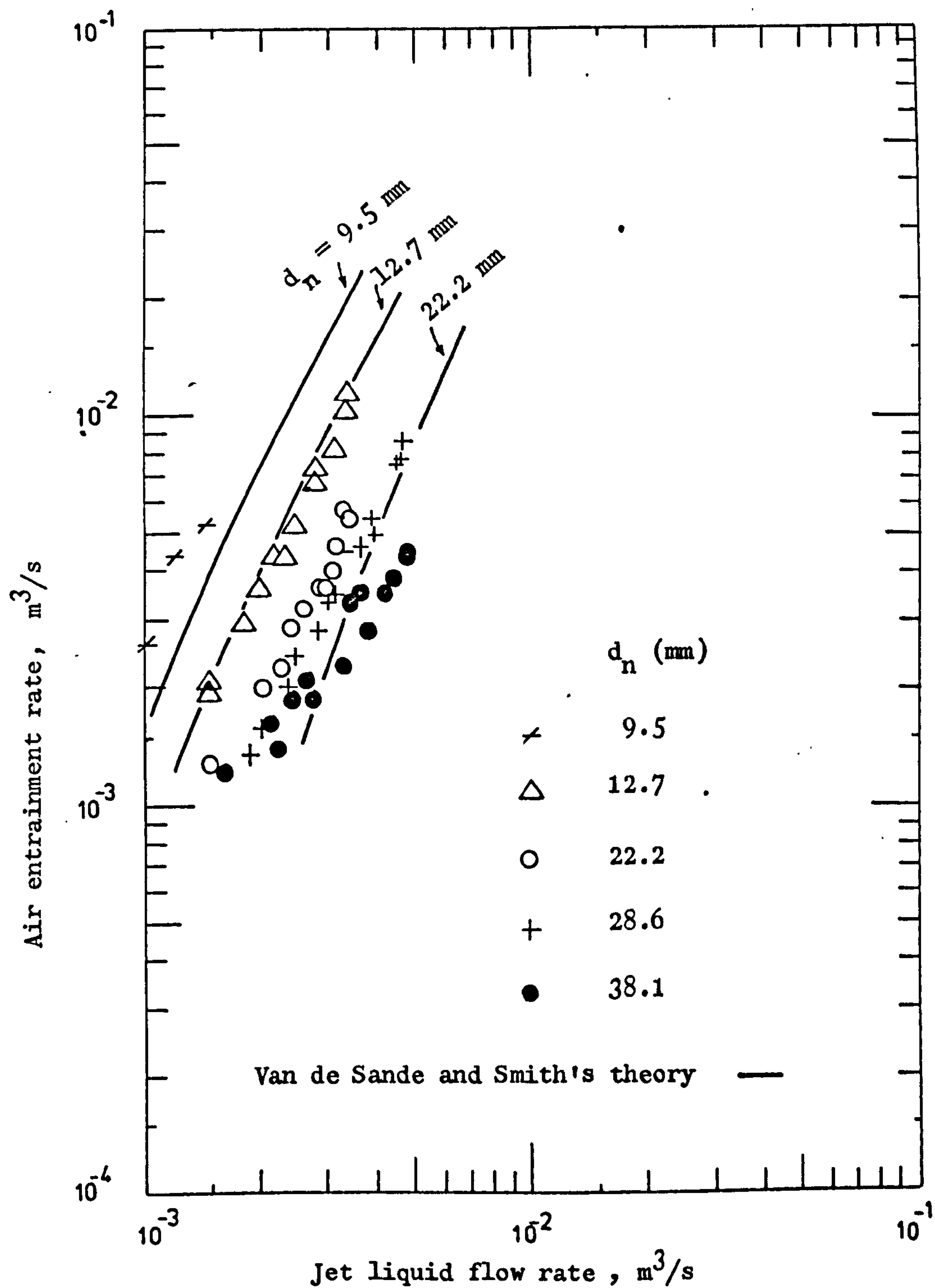


Figure 9.14. Relation of air entrainment rate with jet liquid flow rate for different cylindrical nozzles at 0.66 m jet length

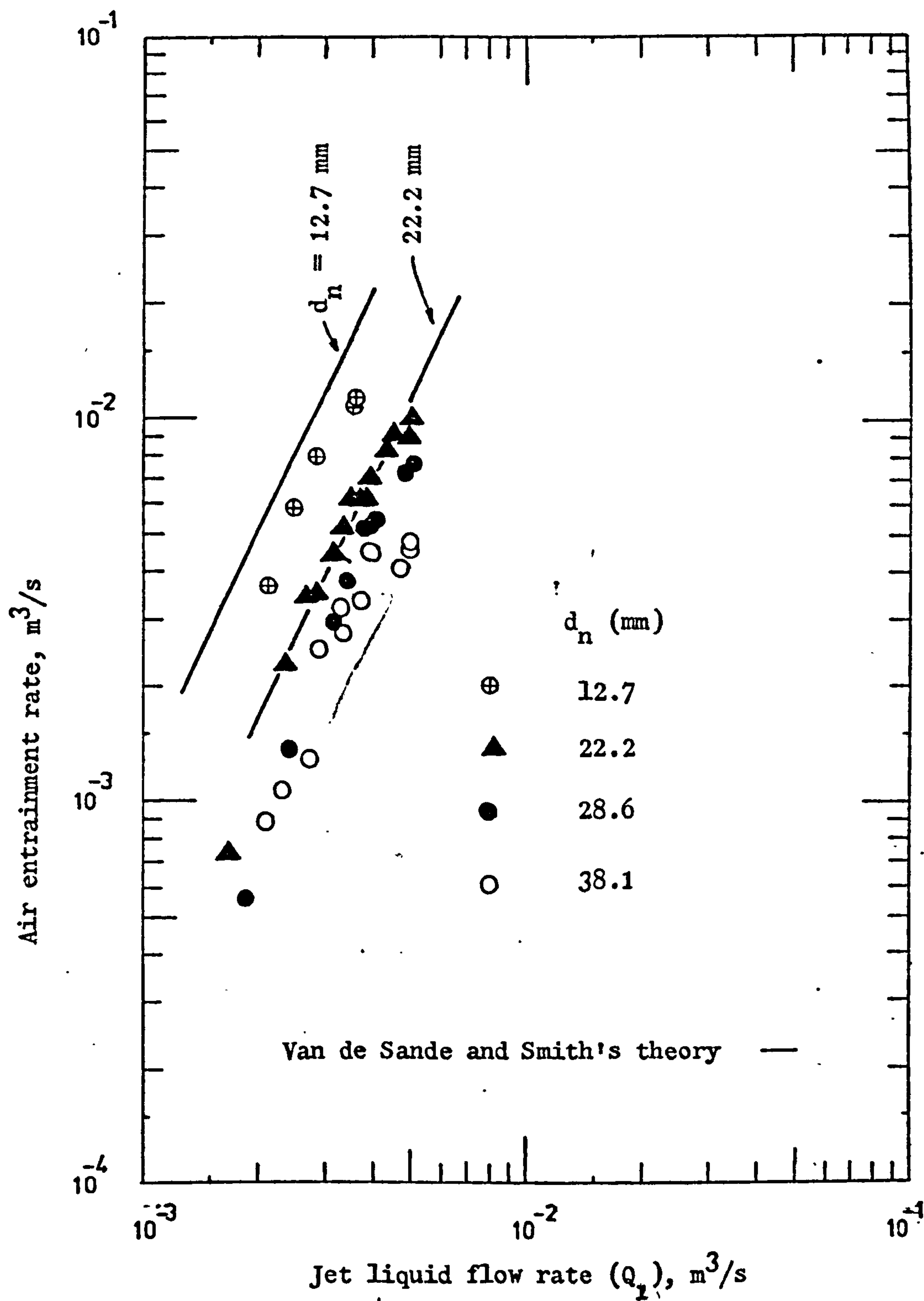


Figure 9.15. Relation of air entrainment rate with jet liquid flow rate for different cylindrical nozzles at 1.05 m jet length.

expansion of the jets from the 9.5 mm, 12.7 mm and 22.2 mm diameter nozzles is to some extent uniform. The photograph of the jet from 9.5 mm diameter nozzle has been included to show the persistence of the central core of the jet. In a long time exposure photograph the outer envelope will hide this central core of the jet. This photograph, in fact, substantiates the theory that the air is captured between the outer envelope and the inner core of the jet.

The surfaces of the jets from 28.6 mm and 38.1 mm diameter nozzles are so ill-defined that it is not realistic to measure envelope diameter at plunge point ( $d_j^*$ ) from the photograph shown. However,  $d_j^*$  is measured for the jets from 12.7 mm and 22.2 mm diameter nozzles at different lengths. Following Van De Sande and Smith (123)  $d_j^*$  is plotted against  $We \times Re_{1j}$  in Fig. 9.16. The results are uniformly scattered around Van De Sande and Smith's empirical equation:

$$\frac{d_j^*}{d_n} = 0.085 (Re_{1j} \times We)^{\frac{1}{6}} \quad 9.2$$

Hence, theoretical curves in Fig. 9.13, 9.14 and 9.15 are calculated by using equation 9.2.

The results indicate that there is definite disagreement between the theory and the entrainment by large diameter nozzles ( $d_n > 22.2$  mm). It is difficult to give any physical explanation for this disagreement; however, from the study of the jet photographs, it seems likely that the jets are adversely affected by induced turbulence. The entrainment rate is enhanced due to increased turbulence (the theory predicts much lower rates).

Since the equation 9.2 does not fit to jets from nozzle diameters greater than 22.2 mm, hence the Van De Sande and Smith's theory is applicable to nozzle diameters less than 22.2 mm. For



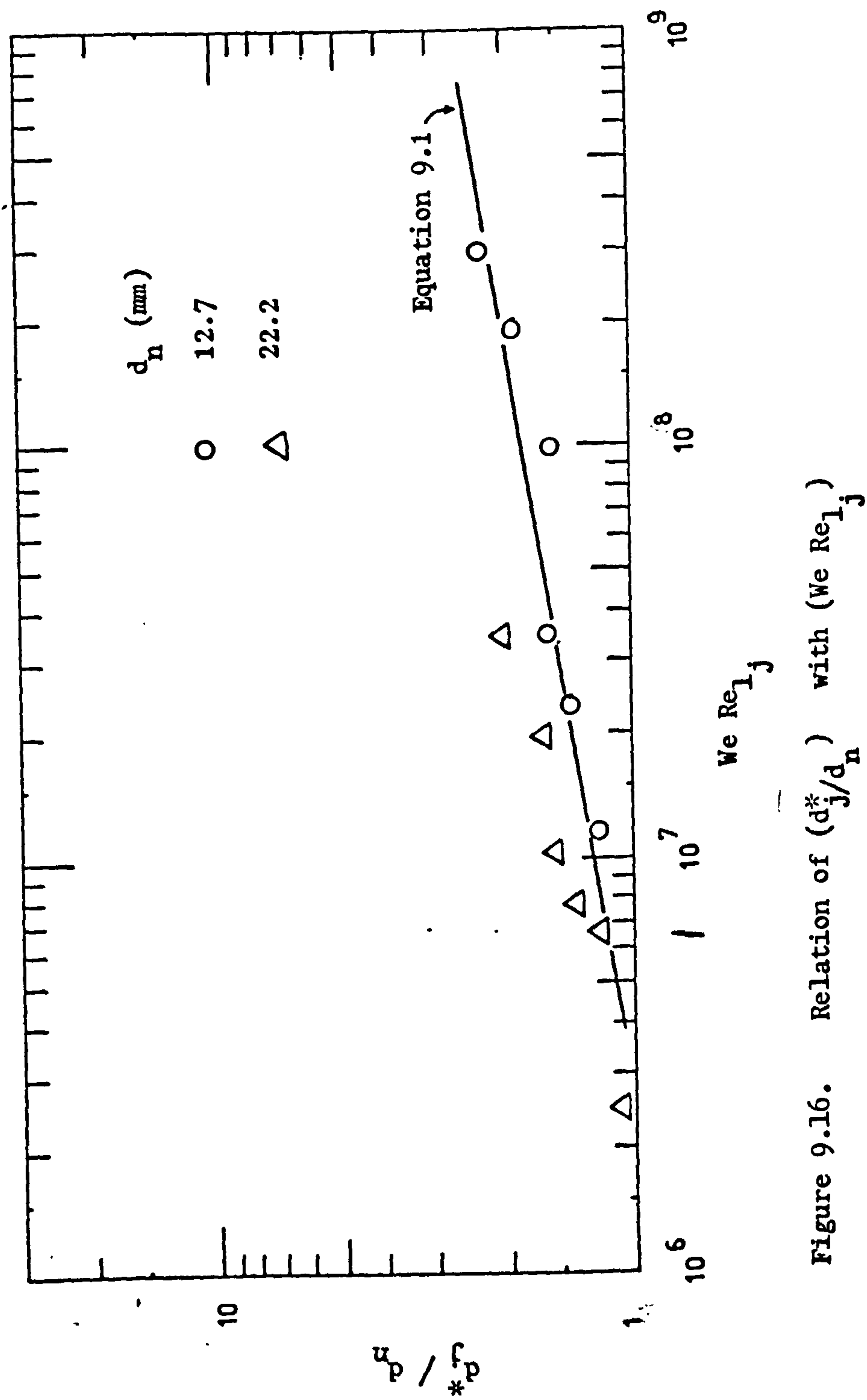


Figure 9.16. Relation of  $(d_j^* / d_n)$  with  $(We Re_{1j})$

some of the results plotted in Figs. 9.13, 9.14 and 9.15,  $Re_{1j}$  is greater than  $10^5$  which shows that the theory can also be satisfactorily applied when  $Re_{1j}$  is less than  $2 \times 10^6$ .

It should be noted that the theory depends upon the value of  $d_j^*$  which is given by an empirical equation. It is obvious that  $d_j^*$  is affected by the level of turbulence induced into the jet stream, unless the nozzle is designed to minimize the propagation of turbulence into the jet stream.

In view of the divergence observed between theory and experiment, particularly for the large diameter nozzles, an attempt has been made to develop an empirical correlation for entrainment by means of dimensionless analysis as described in the following section.

#### 9.2.7 Dimensionless Equation for Air Entrainment

Air entrainment in a plunging jet system is a physical phenomenon. Hence, the method of dimensional analysis can be applied to air entrainment phenomenon as it has been applied to many other physical problems: for instance, fluid flow through pipes.

Dimensional analysis applied to air entrainment phenomenon is presented in Appendix II, where a dimensionless correlation has been obtained by using the entrainment data of cylindrical nozzles (12.7 mm, 22.2 and 28.6 mm diameter) at jet lengths of 0.66 and 1.05 m. The correlation is given by the equation

$$En = 8.7 \times 10^{-5} (Re_j)^{0.77} (We)^{0.15} \quad \text{II.41}$$

and shown in Fig. 9.17. The correlation is applicable to cylindrical jets with lengths greater than 0.66 m, and is accurate within  $\pm 10\%$  for  $(Re_j)^{0.77} \times (We)^{.15}$  greater than  $10^4$ . Note that in the lower region the correlation is poor; however, it improves considerably in the higher region (Fig. 9.17). In addition, the entrainment data of 38.1 mm diameter nozzle is also shown in Fig. 9.17 and has considerable scatter in the lower region.

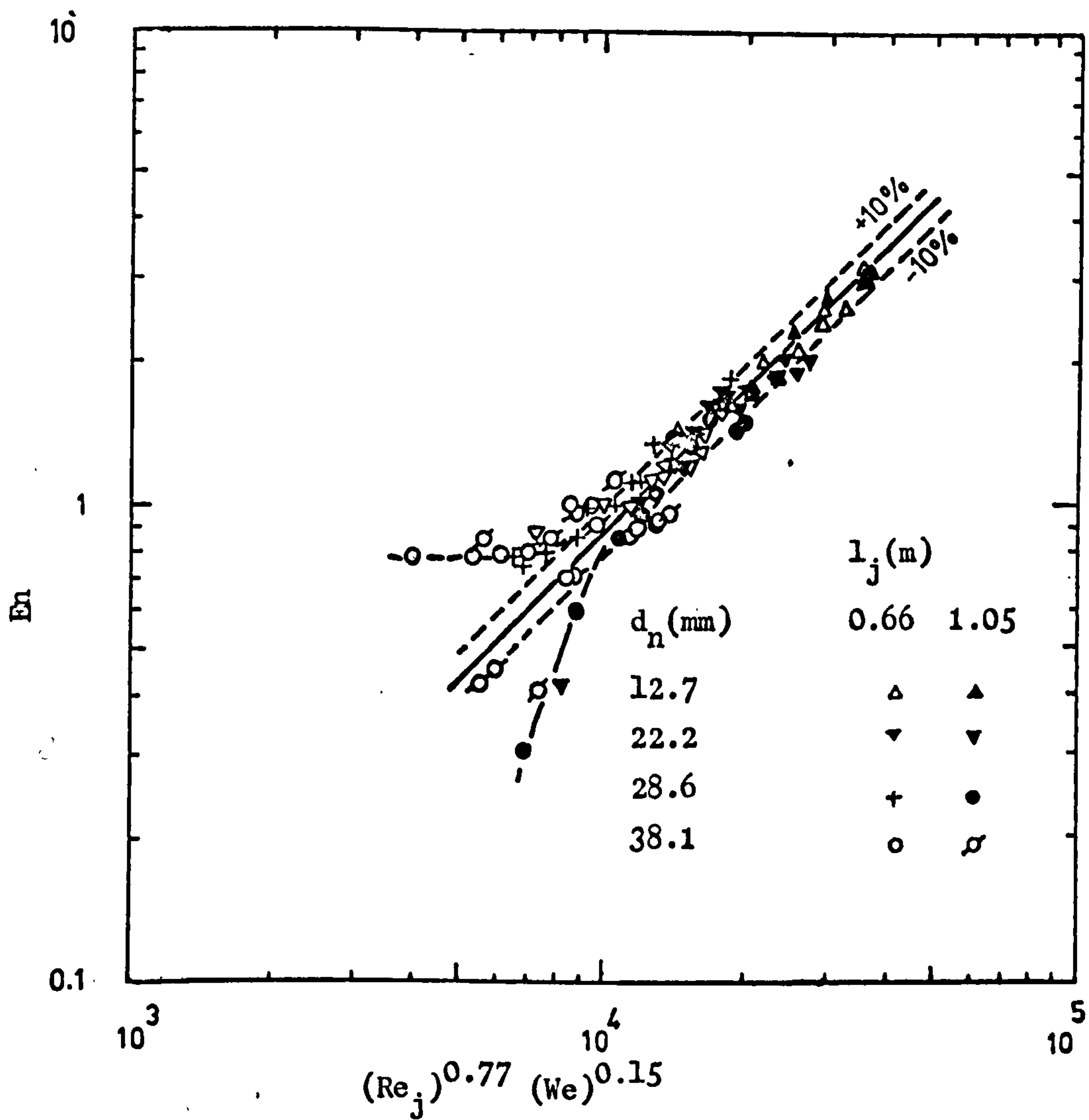


Figure 9.17. Dimensionless correlation for air entrainment by plunging jet.



## Chapter 10

## 10. PLUNGING LIQUID JET REACTOR

Burgess et al. (16) have defined a plunging liquid jet reactor as the flow geometry formed by a coherent liquid jet plunging through an ambient reactive atmosphere into a bath of same liquid.

In this chapter, oxygen transfer aspects of the plunging jet reactor in terms of jet parameters are presented. Oxygen transfer is measured by the sulphite method discussed in Chapter 8.

Mixing and circulation patterns in the tank are dealt with in the beginning of the chapter. It is important to note that the mixing and circulation pattern in the tank liquid are studied purely qualitatively. Particularly the circulation patterns are conceived from the visual observation of flow behaviour of the liquid at the surface. These patterns need further confirmation by visual observation in a transparent tank.

After a brief description of mixing and circulation pattern in liquid, the results on mass transfer aspects are presented and discussed. Correlations are derived for oxygen transfer rate which are of great practical value.

Finally, an attempt is made to calculate the average bubble diameter. The calculation is based on some assumptions. However, the results obtained are of the same order of magnitude as reported in the literature.

## 10.1 EXPERIMENTAL

The same experimental set up was employed as described in 9.1, except that the jet was not concealed. The experimental set up photographed in Plate II was the actual set up used for the study of aeration of the sulphite system. The small pump was later replaced by another pump and the rotameter by an orifice plate (9.1). Both these pumps were old and their specifications were missing. The pump discussed in 9.1 was the third pump and was bought because the previous pump failed to work with slurry.

The static head at pump inlet and outlet was measured by the two mercury manometers connected to the tappings at inlet and outlet piping of the pump. To find the head at pump outlet without considering the frictional losses of valve and orifice plate, the pressure head was measured at a point after the orifice plate. As the frictional losses in the straight pipe up to the point of measurement were small, the head at pump outlet would be the measured head in metres of water plus the height of the point of measurement above datum.

The photographs shown in plates X, XI and XII show the arrangement for centred, off-centred and angular jets.

## 10.2 MIXING IN THE REACTOR

The mixing in the aeration tank was studied qualitatively by tracer response tests. The concentration of tracer in the aeration tank was measured in terms of its conductivity, using a conductivity meter. Since conductivity of a solution has a linear relationship with the concentration of the solute, the concentration of tracer

in the aeration tank could be seen by the corresponding variations in its conductivity.

In a sulphite oxidation experiment the oxygen reacts practically at a constant rate with the sulphite solution. The reaction will take place in the vicinity of air bubbles and will not take place in the regions remote from air bubbles. One would expect a situation at any instant in which small pockets of liquid depleted in sulphite are distributed in the sulphite solution. This would result in numerous concentration gradients in the bulk liquid. A good mixing condition would tend to destroy the concentration gradients and would keep the sulphite concentration homogeneous at every instant. In this case, the mixing phenomenon was studied by approximately simulating these conditions as described in the following section.

#### 10.2.1 Experimental Procedure

One end of a conductivity cell was connected to the sampling valve and the other end to a 6.40 mm diameter polythene tube. The liquid flowing through the cell was fed back to the tank. The terminals of the conductivity cell were connected to a universal bridge set up for the measurement of conductivity. The response of the tracer was recorded by the pen chart recorder. To perform a mixing experiment, the conductivity cell was connected to the bridge. The bridge was switched on and was set ready for measurement. The tank was filled with 200 gallons of tap water. A 22.2 mm diameter cylindrical nozzle was mounted vertically. The liquid circulating pump was started and liquid flow was regulated by the pneumatic valve.



In a pulse tracer response test, two normal potassium chloride solution was used as a tracer. A 100 ml of potassium chloride solution was taken in a beaker and was injected quickly in the tank. The response of the tracer concentration was recorded on the chart recorder.

In addition, the degree to which mixing would nullify the local concentration gradients of sulphite was studied by simulating these conditions by continuously adding potassium chloride solution to tap water at a rate equal to the oxygen transfer rate in sulphite solution. The concentration of potassium chloride in terms of its conductivity was then recorded.

#### 10.2.2 Results and Discussion

For the sake of interest, the tracer was injected at three different regions: plunge point of the jet, bubbling zone (the liquid surface where the entrained bubbles emerged), and about 8 cm away from the plunge point. The results obtained from these tests (Fig. 10.1) show that the response to the tracer concentration was not the same when the tracer was injected at different regions. The tracer concentration reached approximately uniform value in 0.46 second with tracer injected at jet plunge point, 0.18 second with tracer injected at bubbling region and 0.55 second with tracer injected at 8 cm away from plunge point. This shows that mixing is different in different regions of the tank. However, in all cases a uniform concentration was reached in less than a second. The above results were obtained at 4.15 m/s jet velocity.

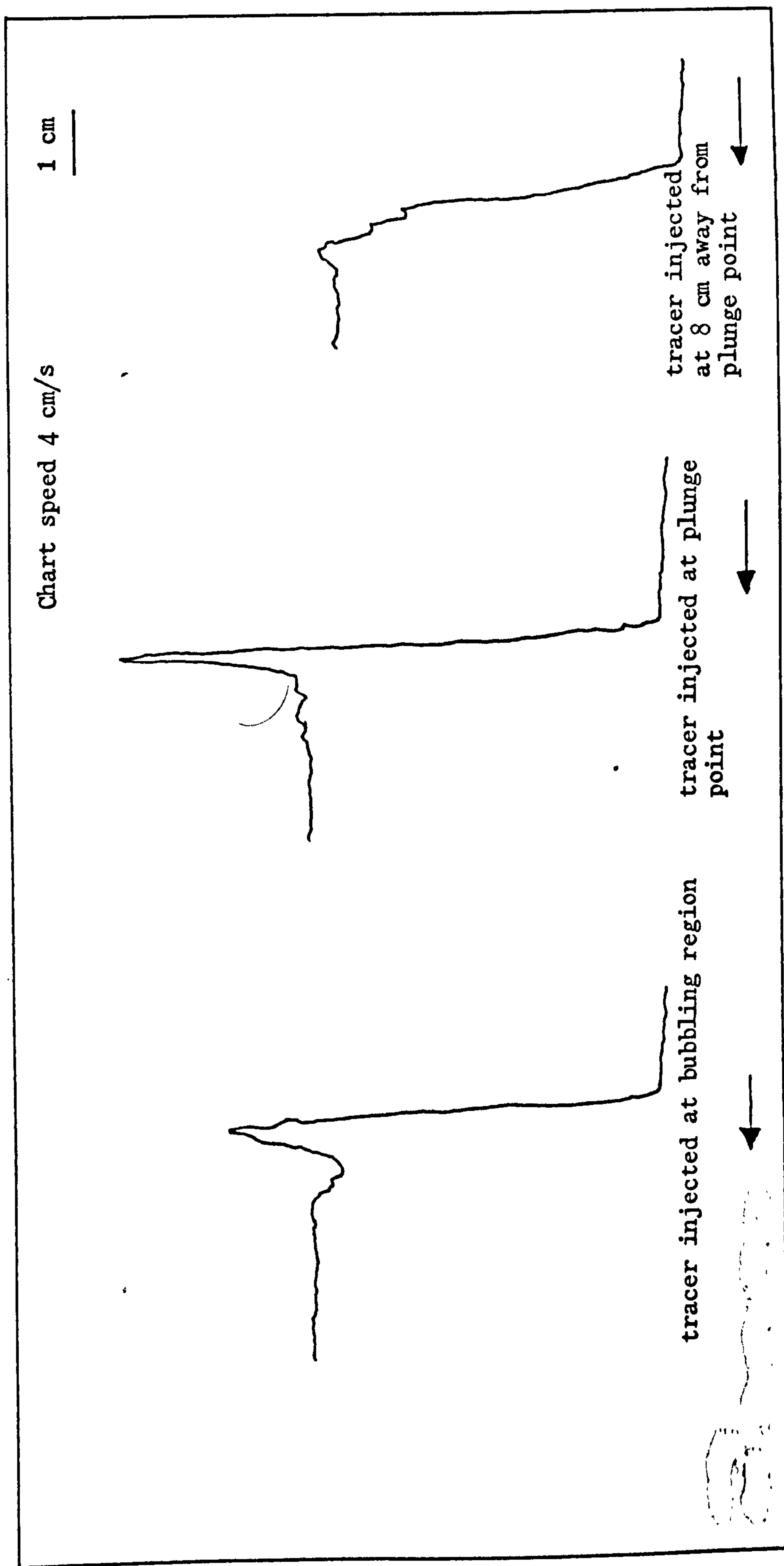


Figure 10.1. Pulse tracer response test in plunging jet system.

Figs. 10.2 and 10.3 show the tracer concentration at low (1.95 m/s) and high (7.2 m/s) jet velocities respectively, for the experiments in which potassium chloride solution was added continuously at a rate equal to oxygen transfer rate in sulphite solution. The results show that during the addition of potassium chloride solution its concentration does not increase uniformly and shows non-homogeneity. The variations in the tracer concentration at low jet velocity are higher than those at higher jet velocity as a result of poor mixing. Qualitatively, due to small variations in tracer concentration at high jet velocity, it can be assumed that with high velocity jet mixing is homogeneous during sulphite oxidation.

Van De Sande (121) also studied the mixing in a plunging jet aeration system. He measured the colouration of the liquid after injecting a pulse of bromothymol blue in slightly alkaline liquid. He concluded from his measurements that the flow patterns in the tank influence the mixing performance. Furthermore, the mixing times in his experiments were always considerably less than a minute, and thus his results agree with the present author in assuming that the contents of the aeration tank are homogeneously mixed.

### 10.3 LIQUID FLOW PATTERNS IN THE AERATION TANK FOR DIFFERENT JET POSITIONS

In the following sections, the different liquid flow patterns obtained by the plunging jets produced by nozzles in different positions are described.

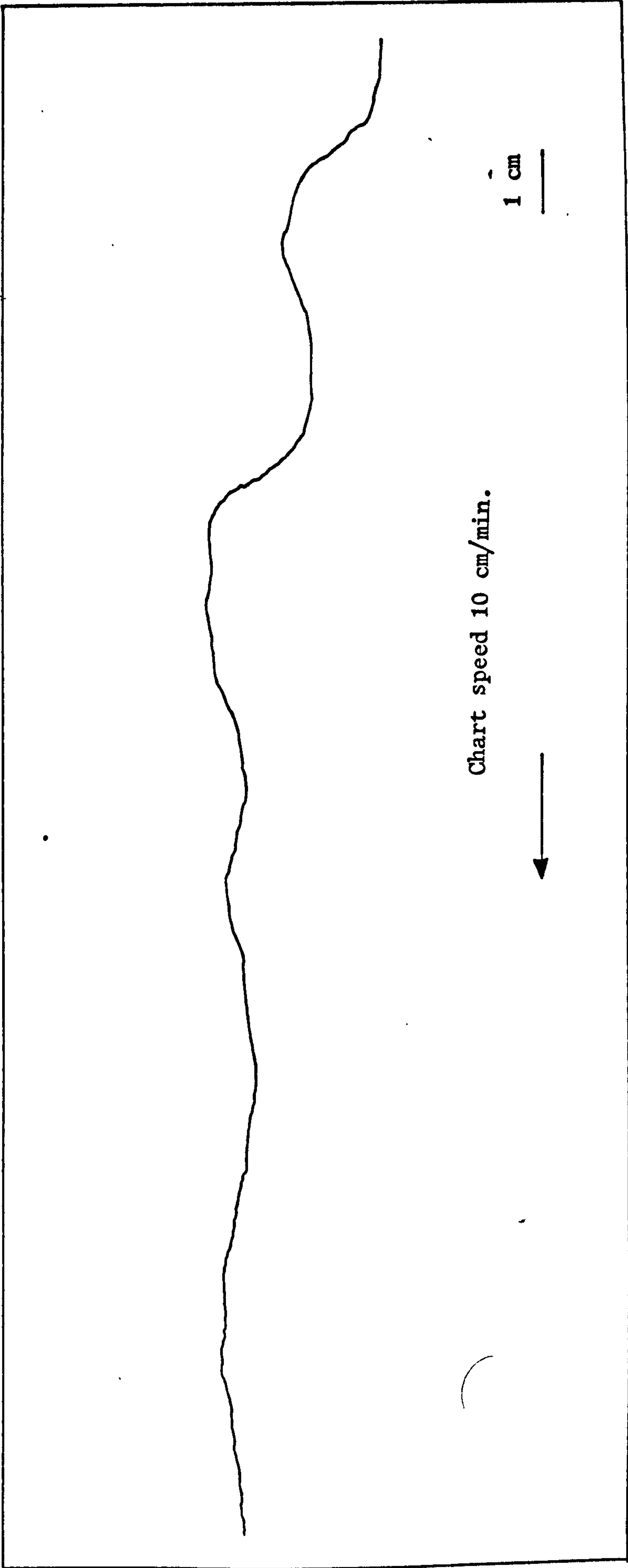


Figure 10.2. Variations in tracer concentration during continuous addition of tracer in the plunging jet system at low jet velocity (1.95 m/s)



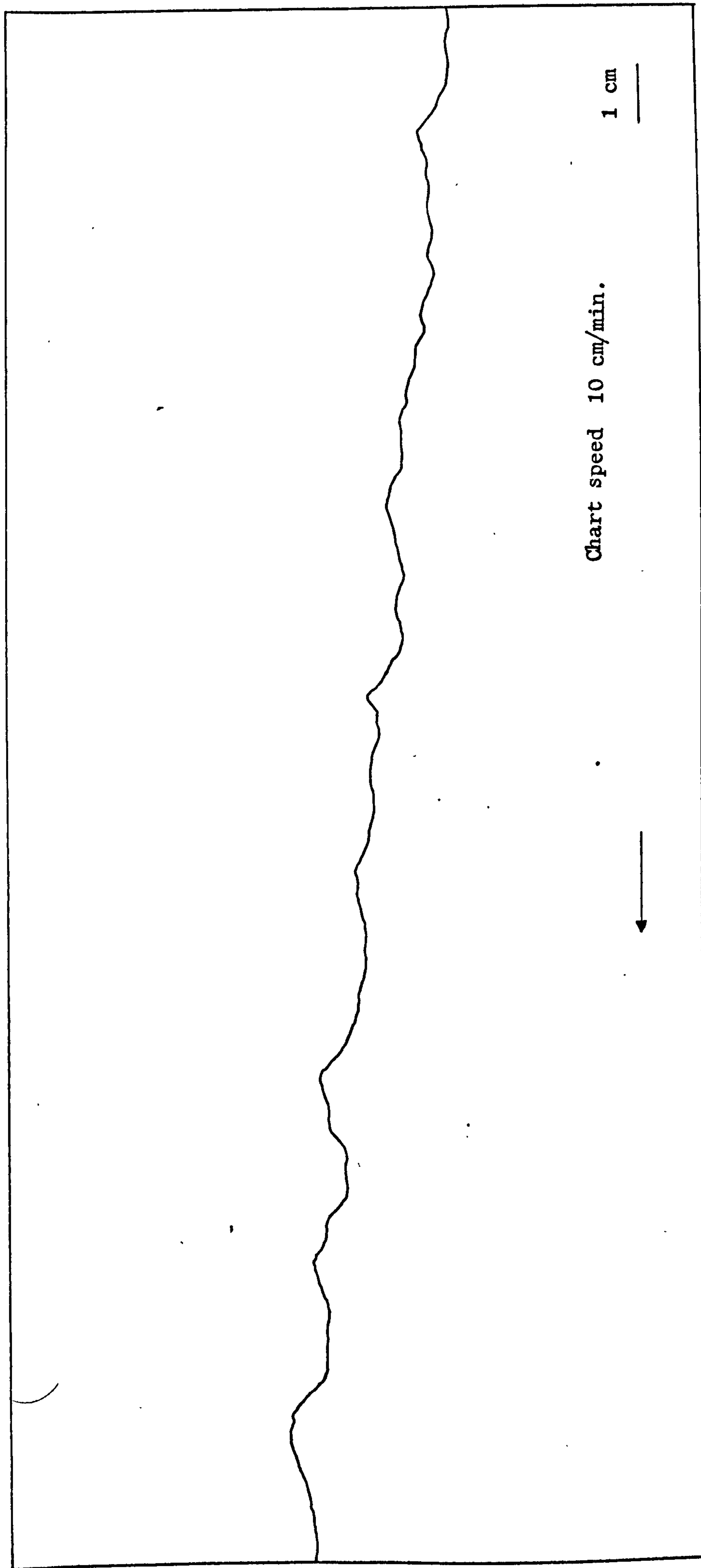


Figure 10.3. Variations in tracer concentration during continuous addition of tracer in the plunging jet system at high jet velocity (7.2 m/s).

### 10.3.1 Flow Pattern due to Plunging Central and Vertical Jet

Fig. 10.4a shows the flow pattern produced by a plunging vertical free jet. The air is entrained up to maximum depth of penetration, where it forms a cluster of bubbles. These bubbles were found to emerge at the liquid surface as a bubble swarm and thus form a confined bubbling zone at the liquid surface. The bubbling zone changed its location from time to time. Sometimes it was just at the plunge point and often a short distance away from the plunge point.

The bubble swarm conforming an air-water mixture rises towards the water surface due to buoyancy effects. Van De Sande (121) has shown by rough estimation that soon even at low jet velocities the buoyancy forces of bubble swarm override the impact force of the jet. After reaching the surface, the water in the air-water mixture spreads outwards. In effect, the action of the rising air-water mixture is to drag up the water which it contains to the surface and this results in continuous flow of water towards the rising cluster of bubbles.

### 10.3.2 Flow Pattern due to Plunging Angular and Central Jet

The flow pattern obtained in the tank with angular jet is shown in Fig. 10.4b. The bubbling zone was formed ahead of the plunge point of the jet. In this case the bubbling zone spread on a large portion of the surface. The level of liquid in front of the jet was higher than that behind the jet. The mechanism of pumping the water to the surface by the bubbling zone was the same as discussed in 10.3.1. As an addition to the phenomenon discussed

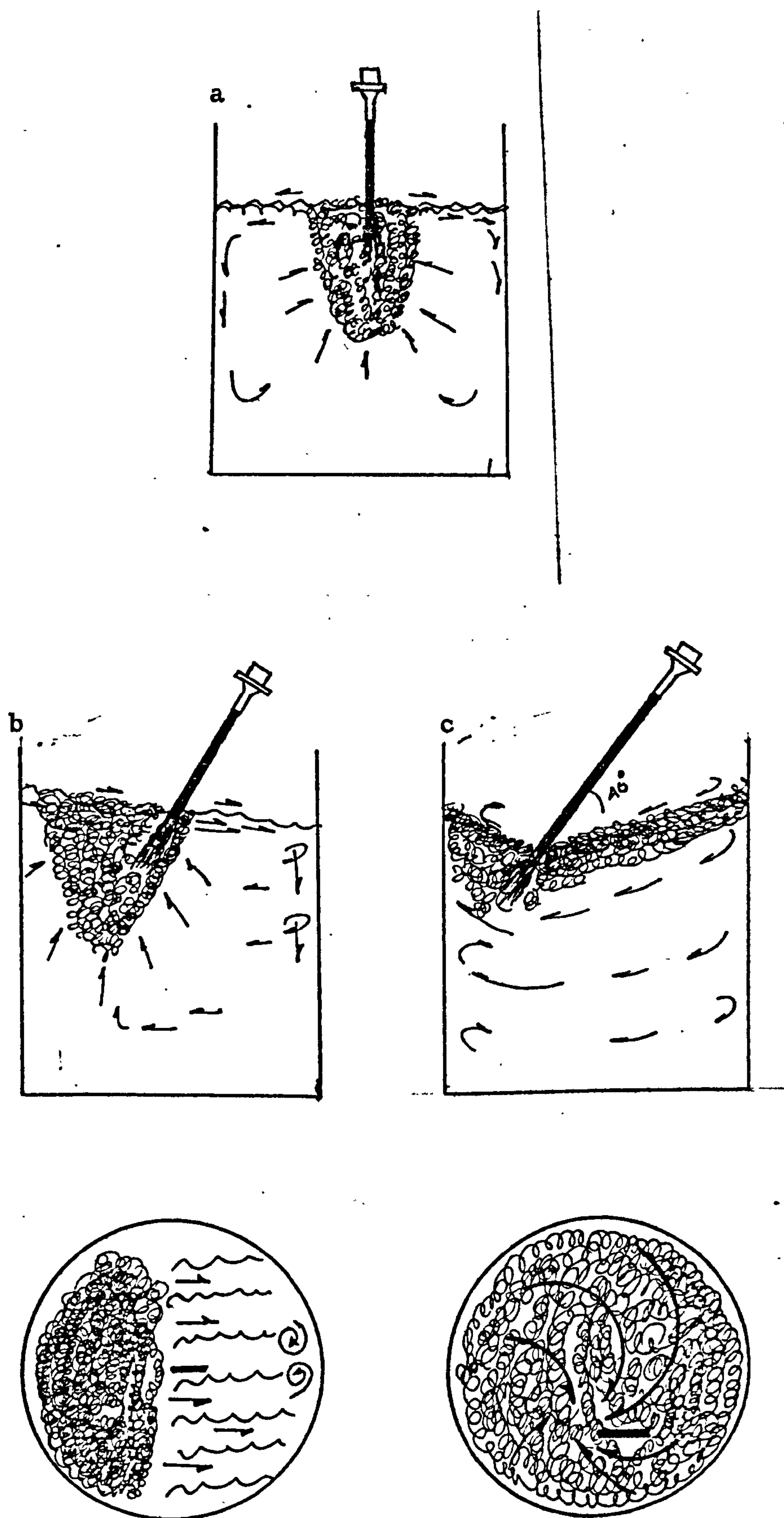


Figure 10.4. Flow pattern in aeration tank.

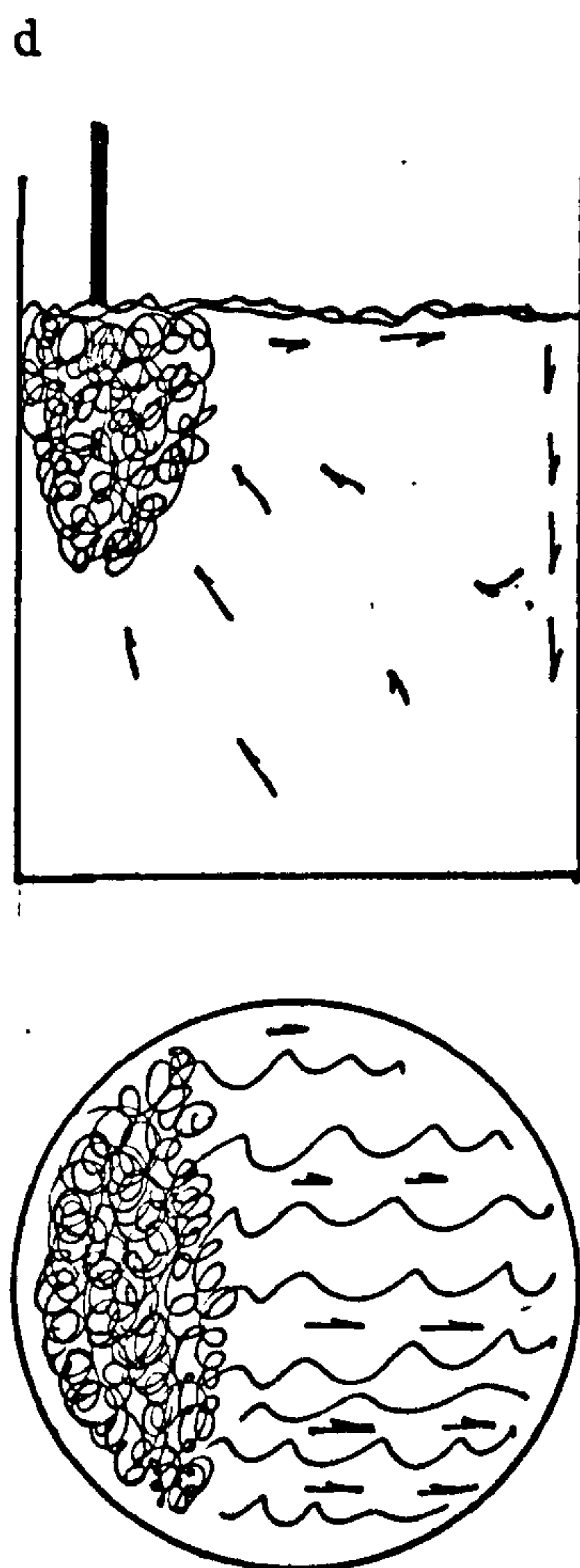


Figure 10.4 (continued)



in 10.3.1, the water flowed towards the lower level in the form of large surface waves. Behind the jet two vortices were formed as shown in Fig. 10.4b. The vortices dragged the water into the bulk. The water from the bulk flowed towards the bubbling region to supply the water which was being pumped to the surface by air-water mixture.

### 10.3.3 Flow Pattern due to Plunging Angular and Off-Centred Jet

Angular jets of 60 and 80 degrees with 20 cm off-centre gave more or less the same flow pattern as an angular and central jets. However, an off-centred jet with an angle of 40 degrees gave a different pattern (Fig. 10.4c). The jet rotated the liquid in the tank and this resulted in a vortex of the bulk liquid. The bubbling region was not similar to that observed in other cases. The entrained air dispersed in the liquid and rotated with the liquid.

The whole liquid surface became an air-water mixture and at very high jet velocities (9 m/s) the large portion of the surface was covered with foam.

### 10.3.4 Flow Pattern due to Plunging Vertical Off-Centred Jet

The flow pattern obtained by an off-centred vertical jet is shown in Fig. 10.4d. The flow pattern was similar to that obtained with angular and central jets, except that the vortices were not formed. The water pumped to the surface by the bubbling zone flowed towards the remote wall in the form of waves. At the wall the flow was diverted downwards. The liquid in the bulk flowed towards the bubbling region.

The foam formed in this case was persistent and covered large portions of the surface.

#### 10.4 OXYGEN MASS TRANSFER IN PLUNGING LIQUID JET REACTOR

##### 10.4.1 Experimental Procedure

One thousand kilograms of anhydrous sodium sulphite (97% purity) was bought from one manufacturer. The sulphite was found to dissolve slowly and when added to water at room temperature, it clumped together. For this reason, the sulphite was not added directly to the aeration tank, but a concentrated sulphite solution was made in hot tap water (30 to 40 °C) in a separate mixing unit. The solution was then pumped to the aeration tank and made up to 0.9 m<sup>3</sup> (200 gallons) by tap water. The final sulphite concentration was in the range 0.1 to 0.25 kmol/m<sup>3</sup>. Cobaltous sulphate in the form of a solution was added to the tank liquid and its concentration in the sulphite solution was  $4 \times 10^{-6}$  kmol/m<sup>3</sup>. The concentration of both the sodium sulphite and the catalyst corresponded to the valid conditions discussed in 8.3.9. The pH of the solution was 8.5. Except for a few experiments, the liquid temperature was  $22 \pm 2$  °C. In winter the temperature decreased significantly and therefore an electric immersion heater was used to keep a constant temperature. The sulphite oxidation reaction is exothermic. For oxygen transfer rates less than 1 kg/h, no noticeable increase in temperature was observed and the temperature remained fairly constant. Probably any increase in temperature was compensated by the decrease in temperature due to evaporative cooling. However, for oxygen transfer rates greater than 1 kg/h, the temperature

started increasing. In this case the temperature was kept constant by the cooling tubes (Fig. 10.5) through which cold water ( $10^{\circ}\text{C}$ ) was flowing.

Several runs were performed with one batch of solution till the concentration of sulphite reduced to a value of  $0.06 \text{ kmol/m}^3$ . Often the same solution was used for two or three days. In fact, when the solution was left open and not stirred for one or two days, it was observed that there was not an appreciable decrease in sulphite concentration.

To perform a run, a nozzle was fitted to the nozzle holder and nozzle was adjusted to the desired position. The compressed air supply for the control valve was switched on. The pump was started and the liquid flow was regulated by the control valve.

Liquid samples were taken by a 10 ml nominal syringe from the sampling valve and were analysed iodometrically (Appendix I) and the oxygen transfer rate was described by the equation:

$$J^* = \frac{8 V y}{S} \left( \frac{dW}{dt} \right) \quad (\text{Refer Appendix I}).$$

where  $J^*$  is oxygen transfer rate in  $\text{kg/s}$ ,

$V$  is volume of liquid in the reactor in  $\text{m}^3$ ,

$y$  is normality of thiosulphate,

$S$  is volume of sample in  $\text{ml}$ , and

$\left( \frac{dW}{dt} \right)$  is rate of increase of thiosulphate volume on titrations (slope by regression analysis) in  $\text{ml/s}$ .

All the experimental results are tabulated in Appendix V.

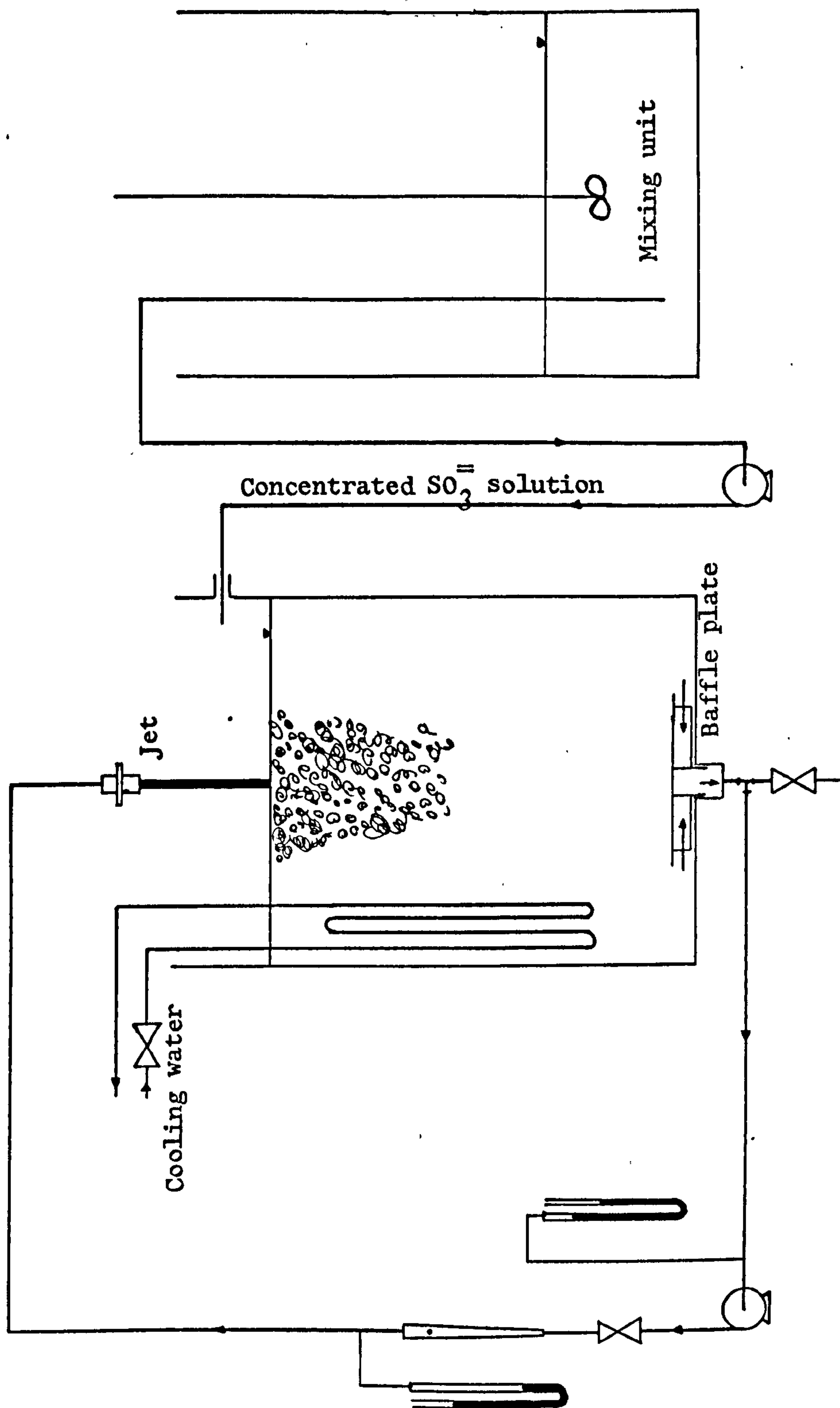


Figure 10. 5. Flow diagram of plunging liquid jet reactor.



At high jet velocities the air was entrained down to the bottom of the tank. In this case, some of the entrained air was drawn in the suction of the pump and thus an air-water mixture started flowing through the pump. This resulted in tremendous fluctuation in the readings of the rotameter and it was difficult to measure the actual flow rate.

This flow of air through the pump was prevented by a baffle plate fixed from the inside to the tank outlet (Plate IV). This plate was also used in experiments on air entrainment and aeration of the biological system. The baffle plate was made of perspex. The air being entrained hit the surface of the plate and thus was prevented from being drawn into the pump suction. It was observed that extremely fine bubbles were still being circulated through the pump and it was practically impossible to prevent their entrainment through the pump.

#### 10.4.2 Oxygen Transfer by Entrainment

The oxygen transfer rate measured by the sulphite depletion rate was, in fact, the sum of the transfer rates taking place through:

- (a) Entrained air bubble surfaces;
- (b) Liquid pool surface exposed to the air;
- (c) Jet surface exposed to the air.

Oxygen transfer rates through (b) and (c) can be varied independently and are not related to transfer rates through the entrained bubbles; therefore, only oxygen transfer rates due to entrainment are considered in this study and are calculated by the equation:

$$J = J^* - K_g (A_{\text{tank}} + A_{\text{jet}}) \hat{C} \quad 10.1$$

where

$J$  is oxygen transfer rate due to entrainment, in kg/s,

$J^*$  is total measured oxygen transfer rate in kg/s,

$K_g$  is gas-film mass transfer coefficient, in m/s,

$A_{\text{tank}}$  liquid pool surface area, in  $\text{m}^2$ ,

$A_{\text{jet}}$  jet surface area exposed to air in  $\text{m}^2$

$\hat{C}$  oxygen concentration in air,  $\text{kg}/\text{m}^3$ .

Glover and Thorley (Mrs.) (44) measured gas-film mass transfer coefficient as equal to  $1.458 \times 10^{-5}$  m/s by Dackwerts trough method (28), and this value was used in the above equation.

### 10.4.3 Results and Discussion

#### 10.4.3.1 Effect of jet length on oxygen transfer rate

Experiments were performed to determine the effect of jet length on oxygen transfer rate for cylindrical and annular jets. 22.2 mm diameter cylindrical nozzle and 33 mm outside, 25.4 mm inside diameter annular nozzle, were chosen, since they had approximately equal cross-sectional areas. For annular jets, the jet length was varied from 0.025 m to 0.41 m, and for cylindrical jets the jet length was varied from 0.045 m to 0.69 m. The velocity of the jet at the nozzle end was kept approximately equal to 11 m/s in all experiments. In Fig. 10.6 and Fig. 10.7 the oxygen transfer rates are plotted against vertical lengths of cylindrical and annular jets. The results show that eventually the oxygen transfer rates obtained with jets from two different

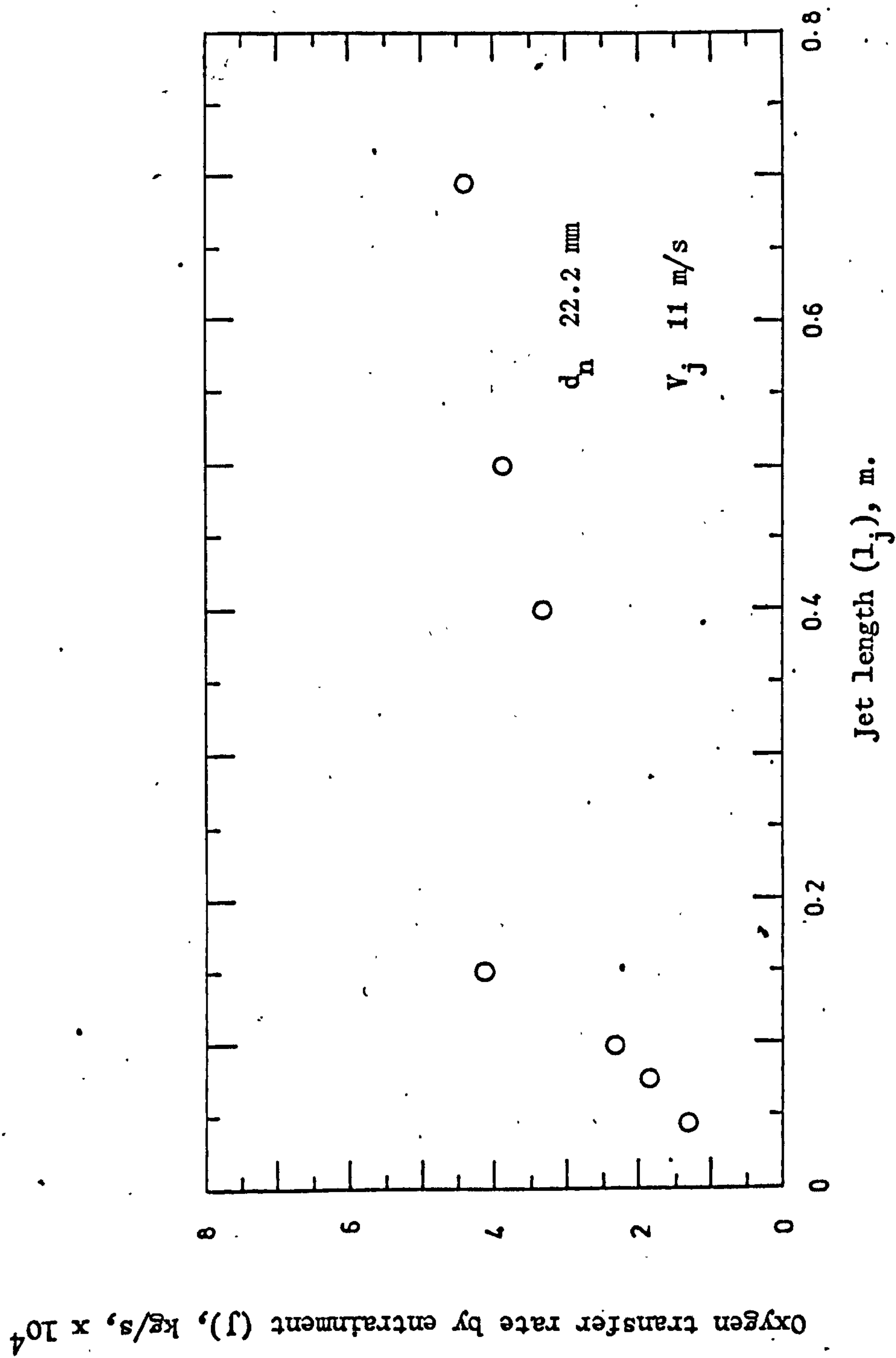


Figure 10.6. Effect of cylindrical jet length on oxygen transfer rate.

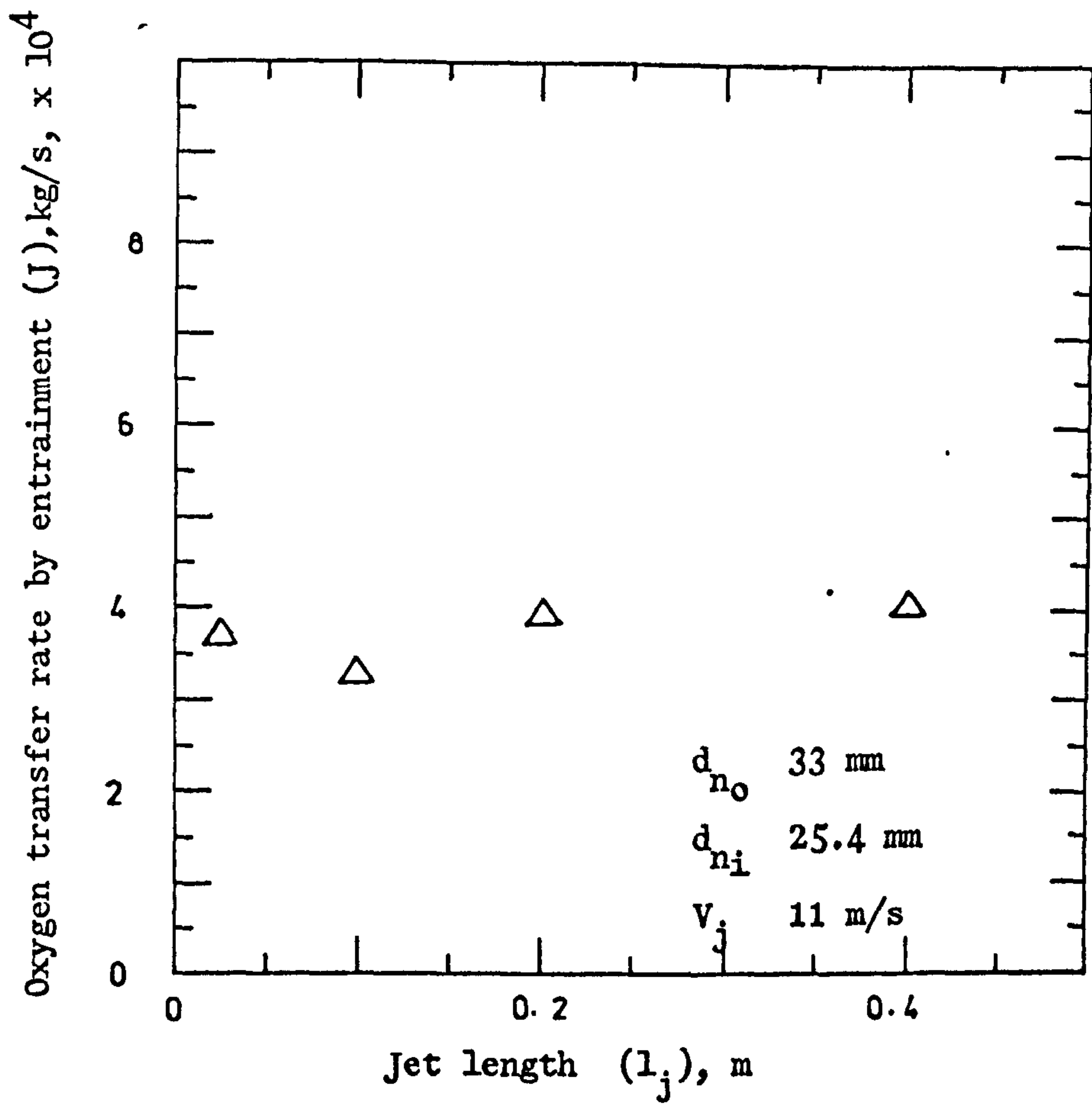


Figure 10.7. Effect of annular jet length on oxygen transfer.



nozzles are surprisingly equal and independent of jet length.

For the annular nozzle the oxygen transfer rate is approximately constant for the range of jet length investigated; however, for the cylindrical nozzle as the jet length is increased from 4.5 cm the oxygen transfer rate increases to a maximum value equal to the oxygen transfer rate for the annular nozzle. At low jet length differing behaviour of the two jets could be possibly attributed to the fact that because of the film-like thickness of the annular jet surface, the eddy disturbances grow in very short length of the jet ( few mm), whereas the diffusion of eddy disturbance to the jet surface on cylindrical jet is slow and hence at small lengths the jet is relatively smooth which results in low oxygen transfer rates.

The experimental results obtained by Van De Sande (121) with 3.9 mm and 5.8 mm diameter jets also show that the oxygen transfer rate increases gradually with the increase of jet length and then attains a steady value and so agree with the results presented here. However, the effect of cylindrical jet length on the oxygen transfer rate presented in this work disagrees with the results of Burgess et al. (16) who found with 2.54 mm diameter nozzle that the interfacial area per unit volume decreases initially with the increase of jet length and then attains a steady value.

#### 10.4.3.2 Effect of jet positions on oxygen transfer rate

With the aid of the framework and the nozzle holder (9.1), a 22.2 mm diameter cylindrical nozzle was adjusted to give different jet positions in relation to surface of the liquid in the tank.

The effect of following jet positions on oxygen transfer rate was investigated:

- (a) Centred and off-centred vertical jets;
- (b) Centred angular jets;
- (c) Off-centred angular jets.

When the jet impacts the geometrical centre of a tank liquid surface the jet is centred, otherwise off-centred: the distance between the jet plunge point and the geometrical centre is off-centricity of the jet.

10.4.3.2.1 Effect of centred and off-centred vertical jet on the oxygen transfer rate: Fig. 10.8 shows the results of 0.0, 0.2 m, and 0.41 m off-centred vertical jets and from this figure it is clear that the off-centricity of a vertical jet is immaterial as far as the rate of oxygen transfer is concerned.

10.4.3.2.2 Effect of centred - angular jets on the oxygen transfer rate:

The oxygen transfer rate was determined at different jet velocities for jet angles of 40, 60 and 80 degrees. The results of the angular jets are plotted along with the results of vertical jets in Fig. 10.9. From the plot it is obvious that the oxygen transfer rates at the different jet angles are not significantly different from each other, and also from the oxygen transfer rates of the vertical jets.

10.4.3.2.3 Effect of off-centred and angular jets on oxygen transfer rate:

Oxygen transfer rates were again determined for the angular jets described above, but now with 0.2 m off-centre. The results are

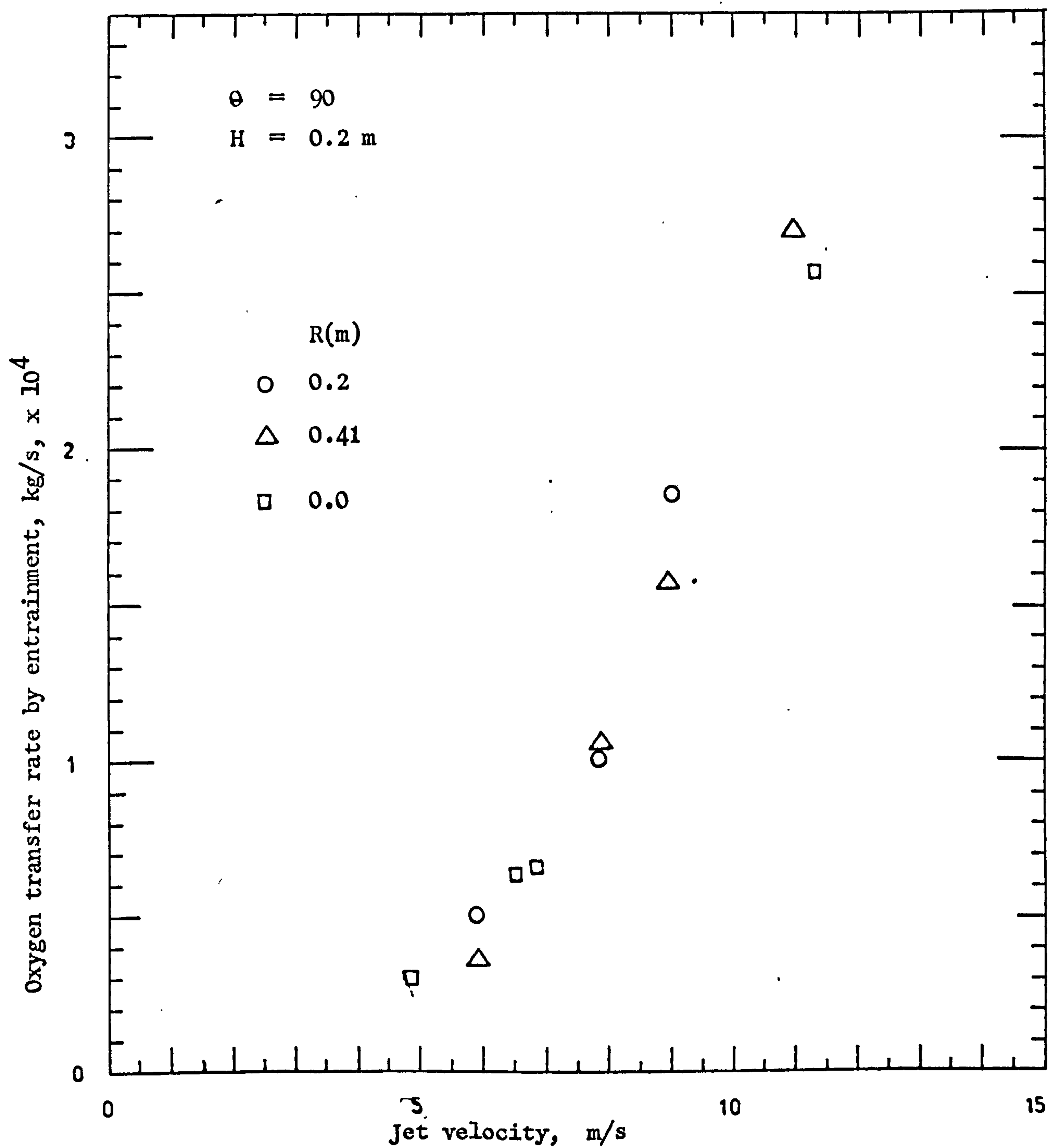


Figure 10.8. Effect of off-centre vertical jet on oxygen transfer rate.

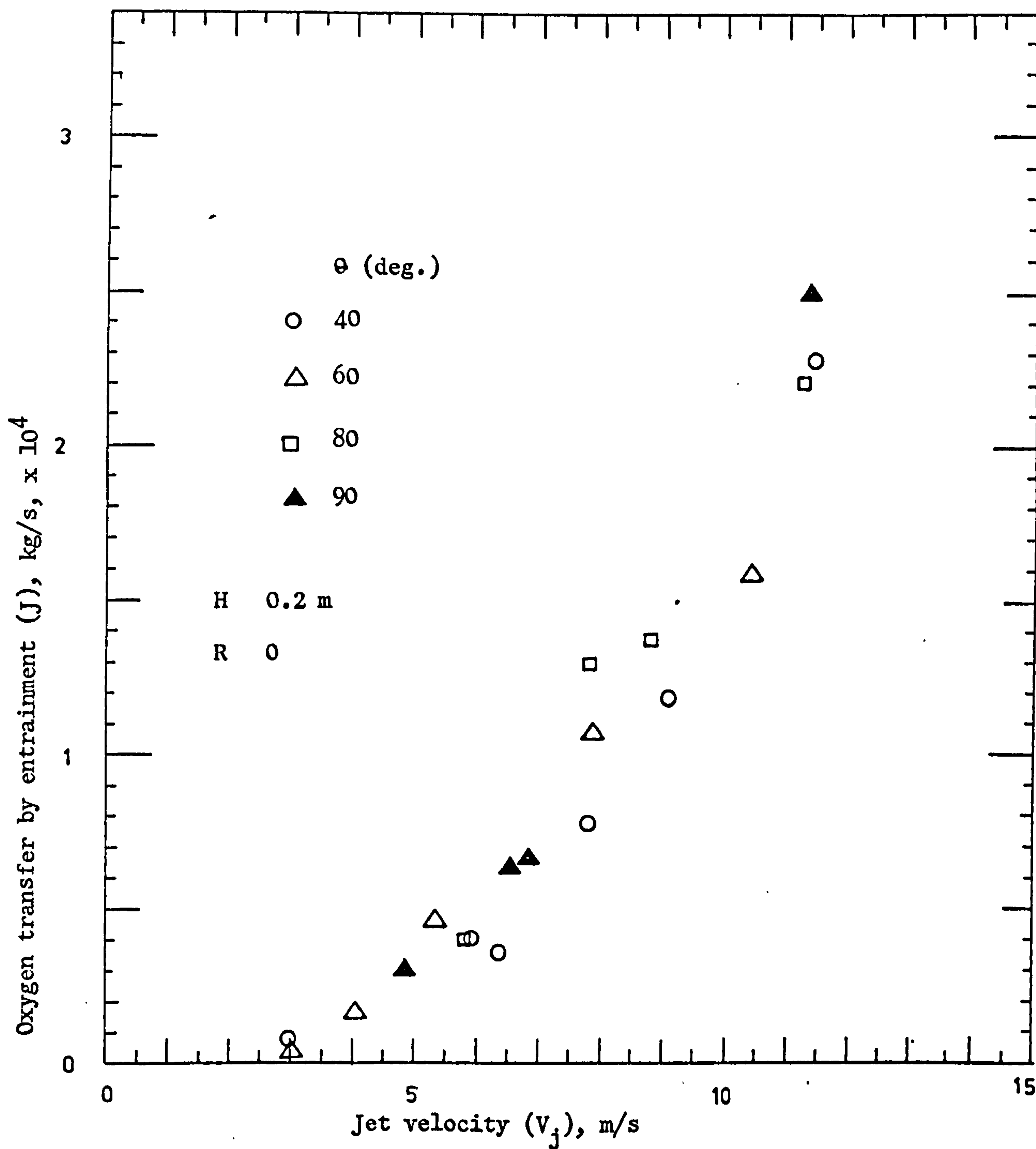


Figure 10.9. Effect of jet angle on oxygen transfer rate.

3



plotted in Fig. 10.10, together with 0.2 m off-centred vertical jet for the sake of comparison. The scatter is high in these results and is mainly caused by 40 degrees angular jet, but still the effect of jet angles on oxygen transfer rate cannot be significantly distinguished. Hence, it can be concluded that off-centred angular jets do not affect the oxygen transfer obtained by vertical jets significantly.

10.4.3.2.4 Discussion on 10.4.3.2 The reason of this investigation was that by changing the jet position the liquid circulation pattern could be changed and would affect the bubble motion or in other words, the bubble retention time. Hence, if a certain jet position affects the bubble dynamics so that a significantly higher oxygen transfer rate is obtained, then that position is of practical value. But from the results presented in the preceding (10.4.3.2), it is apparent that the oxygen transfer rates obtained at various jet positions were not significantly different from those obtained for vertical jets. This aspect will be considered later statistically.

#### 10.4.3.3 Effect of velocity and diameter of the jet on the oxygen transfer rate

Fig. 10.11 shows the effect of jet velocity and the diameter of cylindrical nozzle on the oxygen transfer rate. The oxygen transfer rate increases with the increase of jet velocity and is a power function of jet velocity. Also, at the same jet velocity, the increase in cylindrical nozzle diameter increases the oxygen transfer rate. The cylindrical nozzle diameter and jet velocity

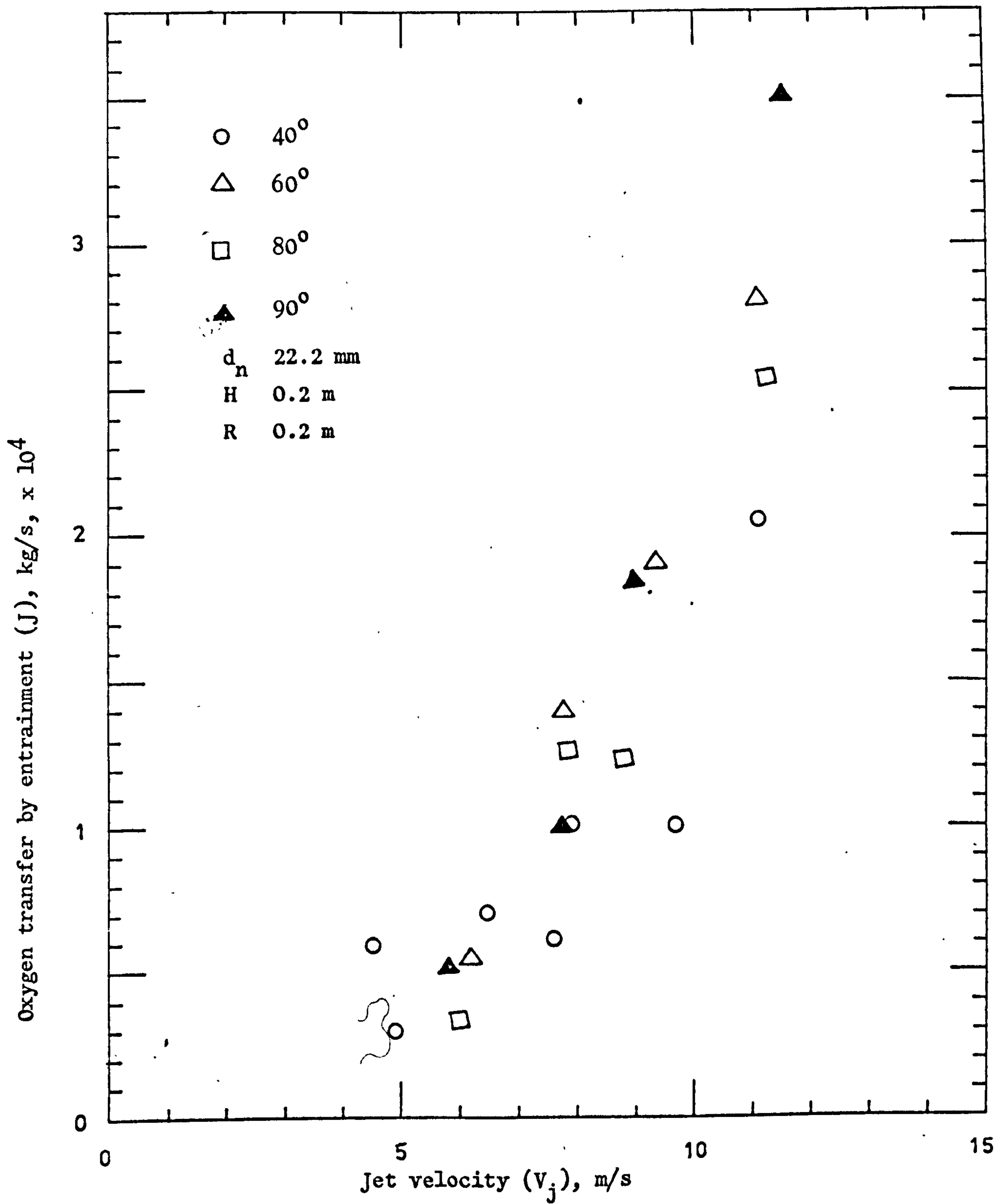


Figure 10.10. Effect of off centre angular jets on oxygen transfer rate.

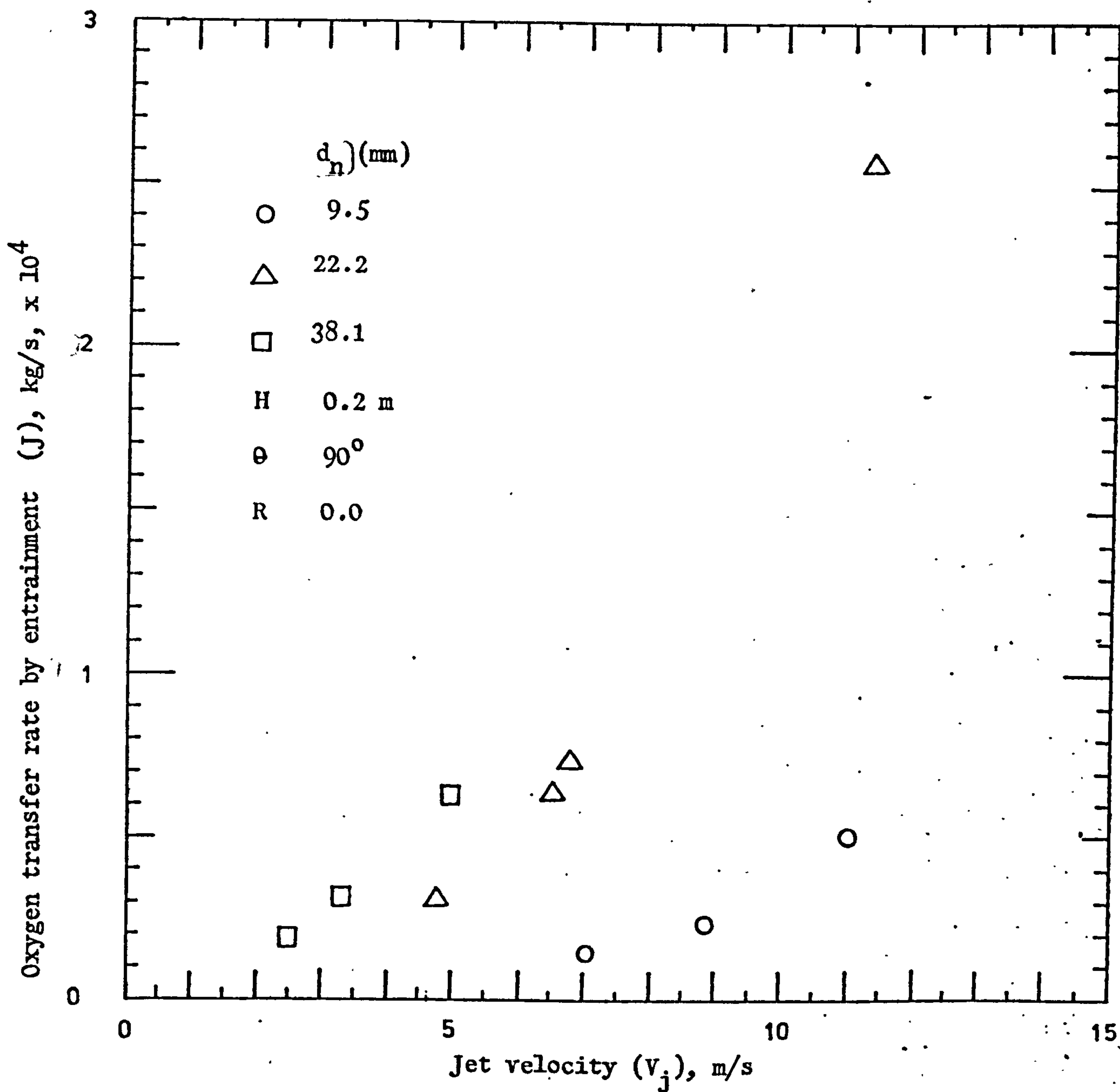


Figure 10.11. Relation of oxygen transfer rate by entrainment with velocity of jet and nozzle diameter.

are related quantitatively to oxygen transfer rates below.

#### 10.4.4 Correlation of Oxygen Transfer Rate with Jet Velocity and Nozzle Diameter

Above it was found that the oxygen transfer rate increases with the increase of both nozzle diameter and jet velocity. This, in fact, suggests that the oxygen transfer rate is related to jet Reynolds number ( $= \frac{V_j d_n \rho_1}{\eta_1}$ ) and is confirmed in Fig. 10.12, which shows that the oxygen transfer rate increases as the cube of Reynolds number; however, there is a diameter dependency: a smaller diameter nozzle gives a higher oxygen transfer rate. To investigate how the oxygen transfer rate is related to nozzle diameter in Fig. 10.12,  $J/Re_j^3$  is plotted against  $1/d_n$  in Fig. 10.13 for the three nozzle diameters; the correlation coefficient of the data in Fig. 10.13 is 0.99, and the slope is 1 by regression analysis, which means that the correlation is of the type - J proportional to  $Re_j^3/d_n$ . Hence, finally  $(J \times d_n)$  are plotted against  $Re_j^3$  for all the data in Fig. 10.14, which shows a good fit in the data. The correlation coefficient is 0.99, the slope of the line is 3, and the correlation equation is given by:

$$J = 4.7 \times 10^{-22} \left( \frac{Re_j^3}{d_n} \right) \quad 10.2$$

where J is oxygen transfer rate due to entrainment in kg/s,  $Re_j$  is jet Reynolds number based on jet diameter at nozzle end ( $= d_n$ ) and  $d_n$  is cylindrical nozzle diameter in m.



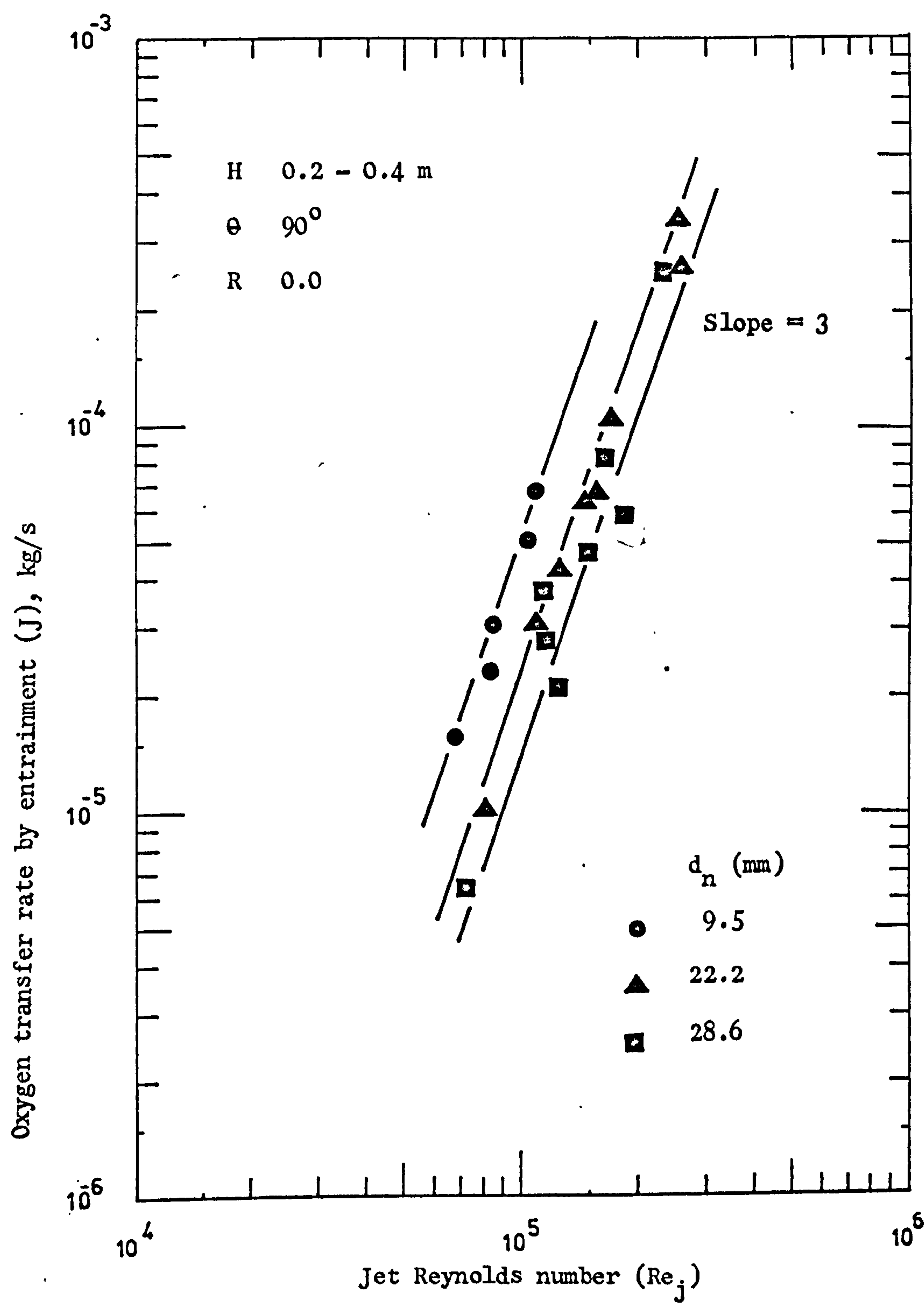


Figure 10.12. Relation of oxygen transfer rate with jet Reynolds number.

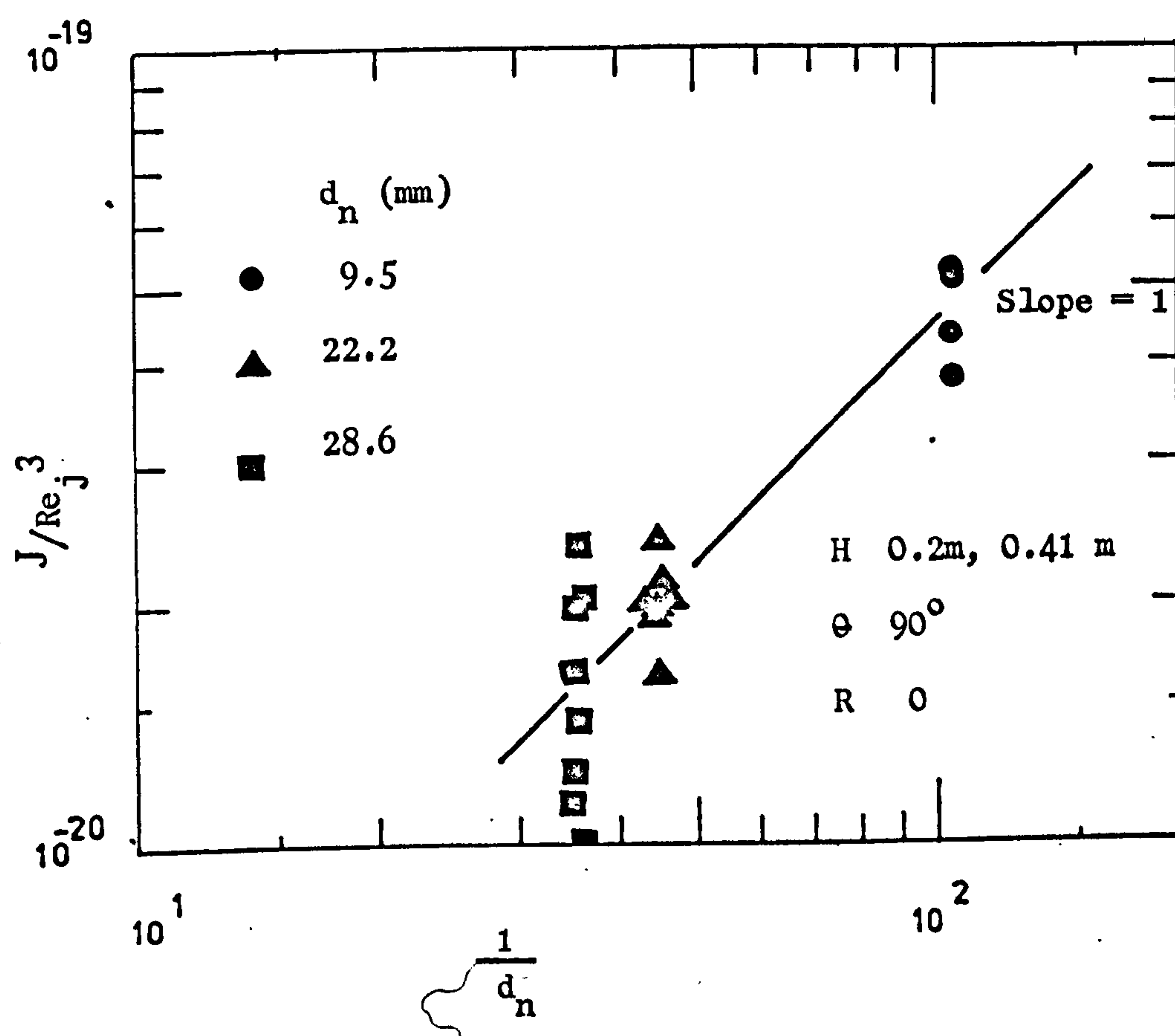


Figure 10.13. Relation of  $J/Re_j^3$  with  $\frac{1}{d_n}$

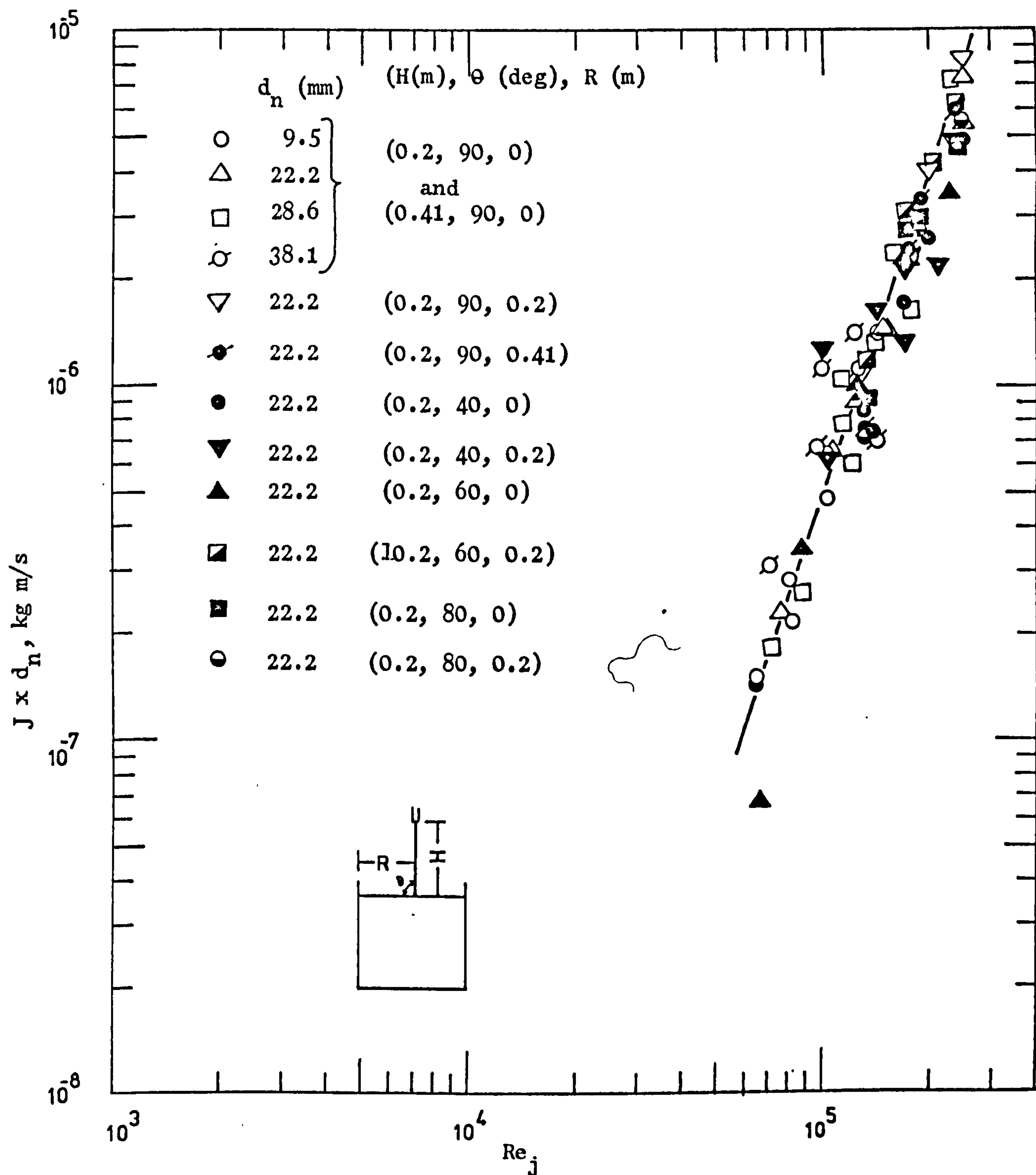


Figure 10.14. Correlation of oxygen transfer data with jet Reynolds number.

#### 10.4.5 Correlation of Oxygen Transfer Rate with Power of Jet

In the analysis below the liquid properties are considered constant. The power of jet is given by

$$P_j = W_1 \left( \frac{V_j^2}{2} \right) \times 10^{-3} \text{ kW} \quad 10.3$$

where  $W_1$  is the jet liquid mass flow rate in kg/s.

From 10.3,

$$P_j \propto (d_j^2 V_j) V_j^2 \quad 10.4$$

where  $d_j = d_n$

Since:

$$Re_j \propto (V_j d_j) \quad 10.5$$

therefore from equations 10.4 and 10.5:

$$P_j \propto \frac{(Re_j)^3}{d_j} \quad 10.6$$

From correlation 10.2 and the equation 10.6, it follows that:

$$J = K' P_j \quad 10.7$$

where  $K'$  is constant of proportionality and is independent of the jet diameter, jet length and jet positions.

The equation 10.7 is, in fact, a simple equation for oxygen transfer rate in plunging jet system.

The oxygen transfer rates for all jets with all jet positions are plotted against power of jets in Fig. 10.15. The statistical analysis of the data showed that the individual curves of each set of data can be regarded as parallel at 5% probability level. Also the individual curves are not significantly displaced from each other at 5% probability level. Hence, all the data plotted in Fig. 10.15 can be correlated by a common regression line at 5% probability level.



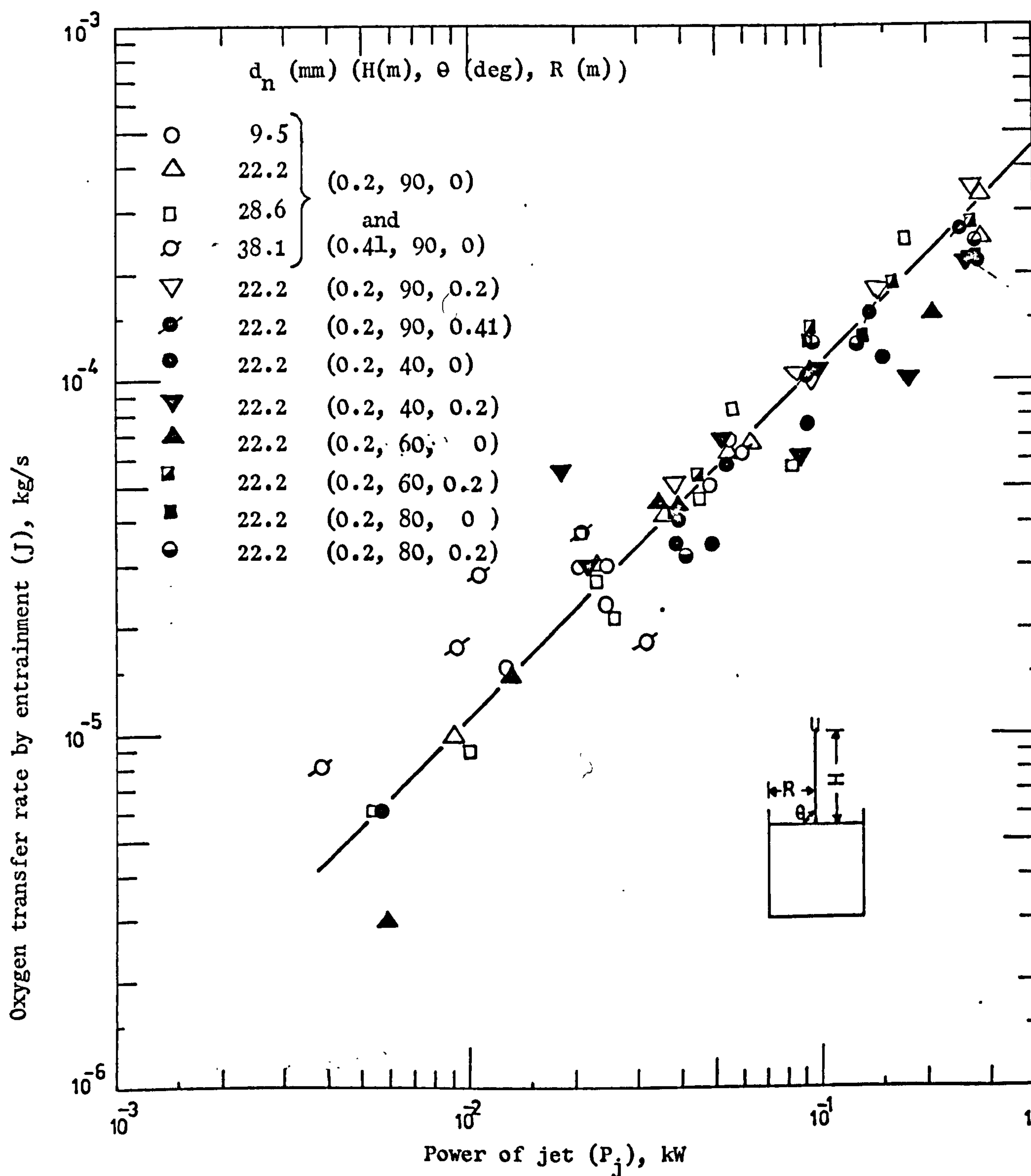


Figure 10.15. Correlation of oxygen transfer rate with power of cylindrical jet.

The slope of the common regression line is 0.904. This value of slope is not significantly different from 1 at the 5% probability level.

Hence from the statistical analysis of the data it is concluded that correlation

$$J = K' P_j \quad 10.7$$

is statistically true at 5% level. In addition, the position of jet is immaterial.

Since:

$$K' = \frac{J}{P_j} \quad 10.8$$

therefore,  $K'$  is the oxygen transfer efficiency or as commonly known the aeration efficiency of the system.

All the data is correlated by the equation

$$J = 4 P_j \quad 10.9$$

where  $J$  is in  $\text{kgO}_2/\text{h}$ , and  $P_j$  is in kW.

Therefore aeration efficiency,

$$K' = 4 \text{ kgO}_2/\text{kW h.}$$

In Fig. 10.16 aeration efficiency is plotted against power of jet,  $P_j$ . The plot shows a slight decreasing trend in aeration efficiency with the increase of power of jet. This decreasing trend is because the slope of the plot  $J$  versus  $P_j$  is 0.904.

Van De Sande (121) measured aeration efficiency by reaeration of deoxygenated tap water for nozzle diameters ranging from 3.9 mm to 12 mm. He noted higher values of aeration efficiency at lower jet velocities. The aeration efficiency decreased with the increase of jet velocity and the rate of decrease diminished with the increase of jet velocity. Moreover, his results

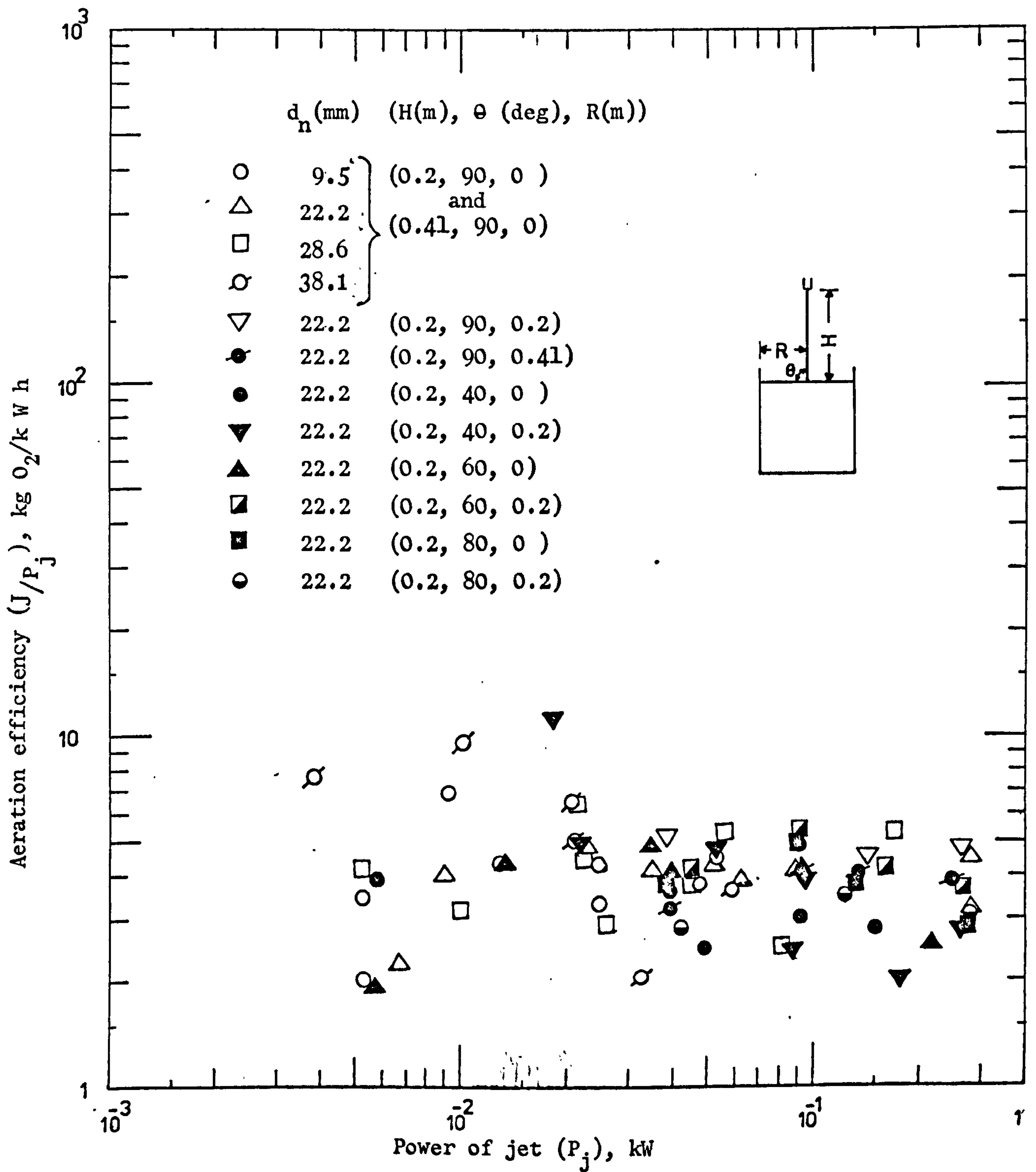


Figure 10.16. Effect of power of cylindrical jet on aeration efficiency.

show the diameter dependency of the aeration efficiency in the lower region of jet velocities - smaller jets giving higher aeration efficiency. However, this diameter dependency seems to disappear at high jet velocities as observed from his results.

The differing experimental conditions and the measurement method in the present work and the work of Van De Sande (121) do not justify the direct comparison of the results on aeration efficiency. However, there is an indication of agreement on some points. For instance, the results of two larger nozzle diameters, viz, 10 mm and 12 mm, indicate the independency of the jet diameter on the aeration efficiency. This agrees with the results presented in this work for nozzle diameters greater than 9.5 mm. In addition, after a rapid decrease of aeration efficiency for larger nozzle diameters (10 mm and 12 mm) at very low jet velocities, the trend in further decrease of aeration efficiency is slight. This also agrees, more or less, with the results presented here. However, the aeration efficiency is about  $1.5 \text{ kgO}_2/\text{kW h}$  at jet power of about 0.01 kW much less than the aeration efficiency ( $3 - 9 \text{ kg O}_2/\text{kW h}$ ) obtained at the same power of jet in this work. This difference is because the sulphite method gives the maximum oxygen transfer rate in the system (8.3.8). Therefore, higher aeration efficiencies are obtained as compared to tap water experiments.

The data of annular nozzles are also dealt with in the same way as the data of cylindrical nozzles. Thus, the oxygen transfer rate due to entrainment is plotted against the power of jet in Fig. 10.17 for four annular nozzles. The best line of fit is



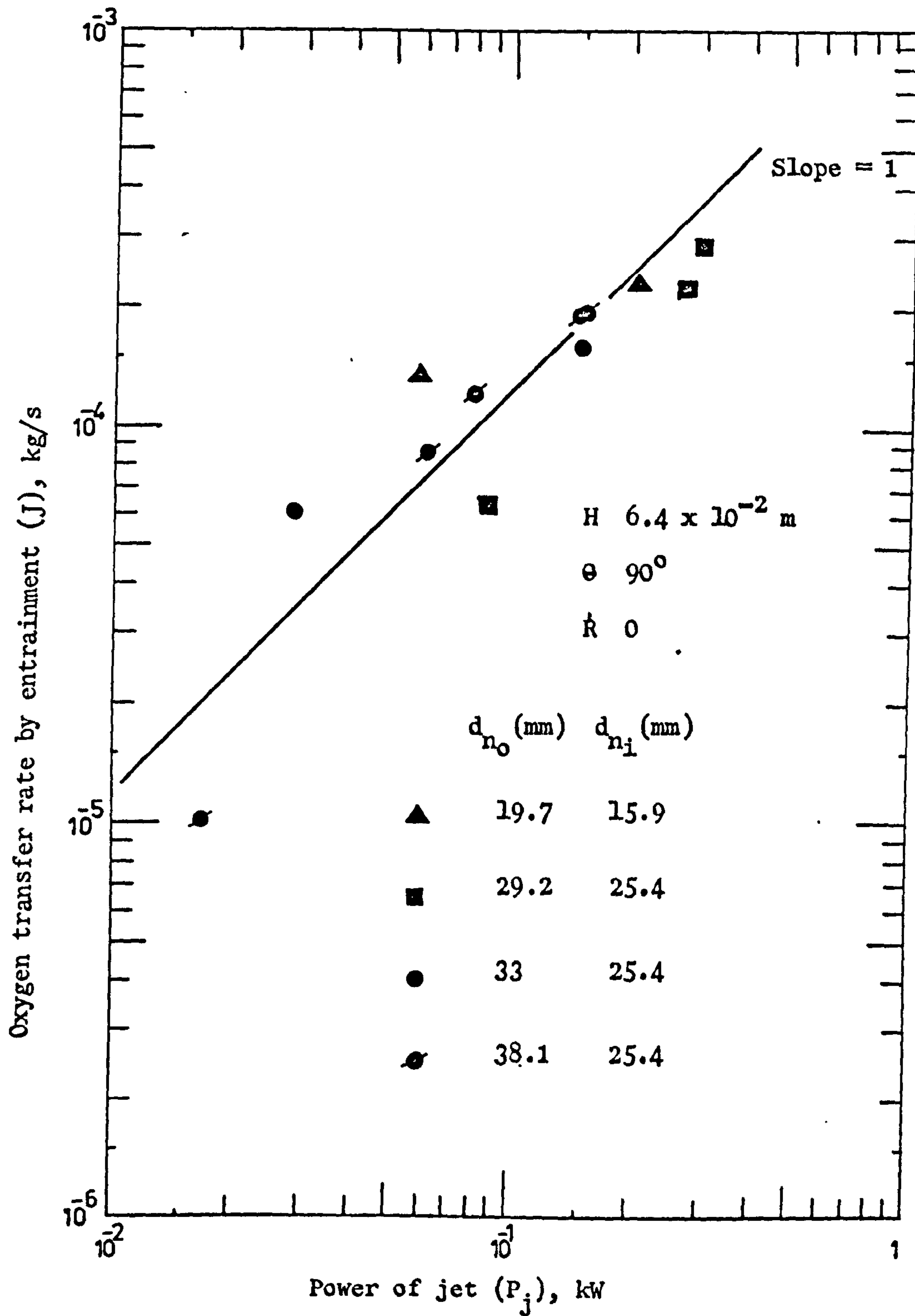


Figure 10.17. Relation of oxygen transfer rate with power of jet for annular jets.

drawn through the data by regression analysis. This line exactly coincides with the relation

$$J = 4 P_j$$

for cylindrical jets. This coincidence is remarkable. This shows that the above correlation is true at 5% probability whether the jet is cylindrical or annular.

For annular nozzles, the aeration efficiency is plotted against power of jet in Fig. 10.18. The results are highly scattered at low power of jet, but this scatter diminishes at high power of jets. When Fig. 10.18 is compared with Fig. 10.16, the variations in aeration efficiency lie in the same region as for the cylindrical jets. Hence, the performance of annular jets is not significantly different from that of cylindrical jets.

#### 10.4.6 Determination of Average Bubble Diameter

In this section a rough approach is made to calculate the average bubble diameter from the experimental data obtained on oxygen transfer rate and entrainment rate. The following assumptions are made to simplify the analysis:

- (a) Gas-film mass transfer coefficient ( $K_g$ ) is the same for all bubbles in all parts of the reactor. The assumption is reasonable, since the gas-film resistance is nearly independent of the hydrodynamics of the liquid phase.
- (b) The average retention time of bubbles is given by the time the average bubble would reach the surface vertically, from the maximum depth of penetration.

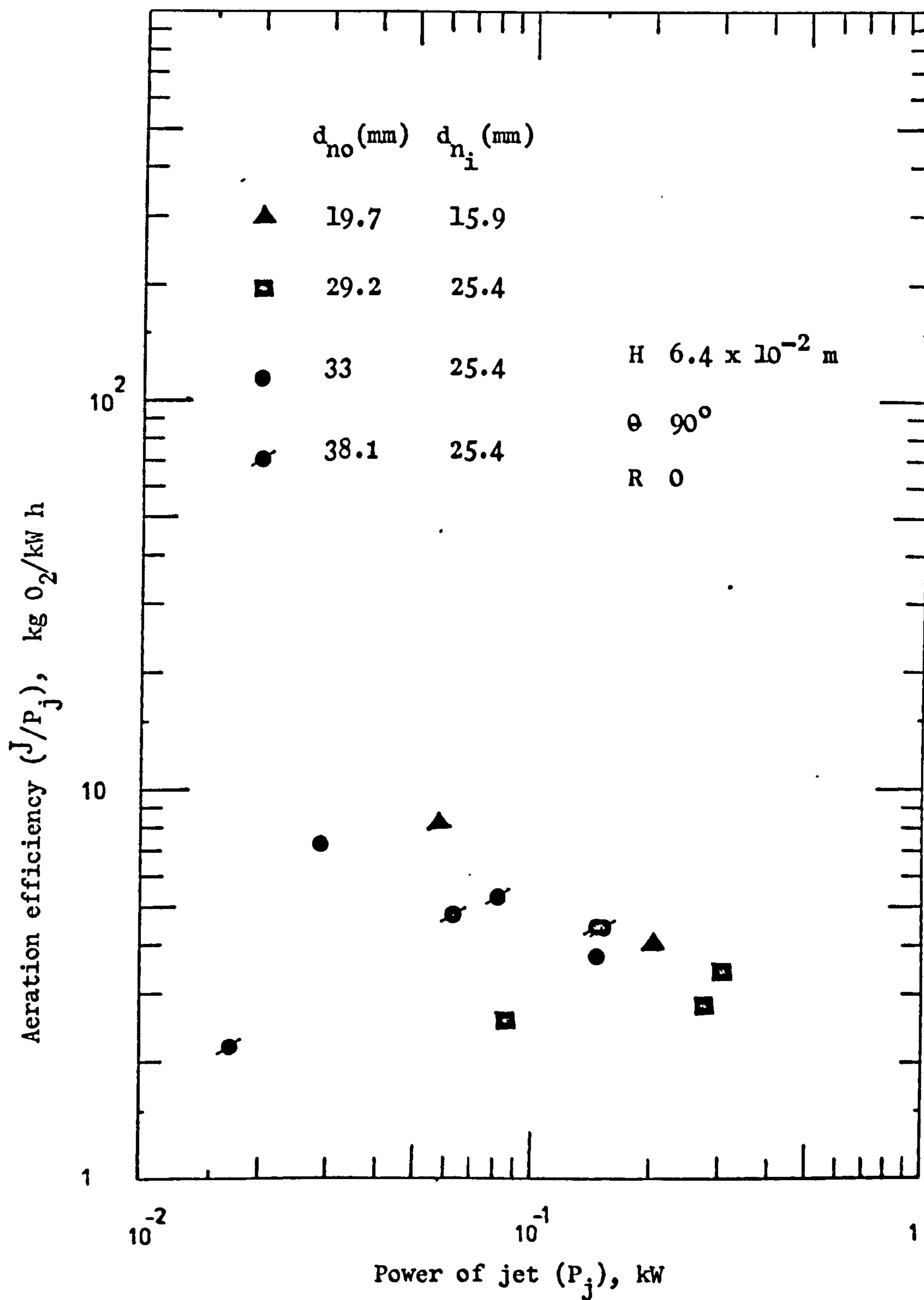


Figure 10.18. Effect of power of annular jets on aeration efficiency.

The air entrained by a plunging jet reaches the maximum depth of penetration in a short time. An approximate calculation, based on equations of motion, showed that the jet travelling at 11 m/s would bring the entrained air to maximum depth of 1 m in about one-sixth of a second. The entrained air is dispersed in the form of bubbles at the maximum depth of penetration. In fact, a two phase cone is set up around the submerged jet. Some bubbles would detach from the surface of the cone due to buoyancy effects. So these bubbles would reach the liquid surface quicker than the bubbles dispersed at the penetration depth. Due to circulation pattern set up in the liquid, the rising bubbles are caught in liquid eddies and are so circulated. The circulation of bubbles would increase the bubble retention time. Furthermore, the bubble rise path depends upon the bubble diameter, as reported by Levich (61).

In view of these complications, the assumption that the average height through which a bubble rises is the maximum penetration depth of bubbles is, in fact, an over-simplification of the problem.

Based on the above assumptions, the average bubble diameter in m is calculated in Appendix III and is given by the equation:

$$\bar{d}_b = 1.158 \left( \frac{K_g h}{\alpha} \right)^{\frac{2}{3}} \quad \text{III - 12}$$

where  $h$  is maximum penetration depth of bubbles in m (equation 5.14),  $k_g$  is gas-film mass transfer coefficient equal to  $1.458 \times 10^{-5}$  m/s (10.42), and  $\alpha$  is a fraction of oxygen in entrained air ( $Q_a$ ) absorbed which is calculated from the entrainment data and the oxygen transfer correlation shown in Fig. 10.14. All variables on



the right hand side of the equation III-12 are known for any jet condition within the experimental range of this work, and hence average bubble diameter  $\bar{d}_b$  can be calculated.

Mean bubble diameter ( $\bar{d}_{bm}$ ) is defined as:

$$\bar{d}_{bm} = \left( \frac{\sum_{i=1}^N d_{bi}^3}{N} \right)^{\frac{1}{3}} \quad 10.10$$

where  $d_{bi}$  is bubble diameter in m, and N is number of bubbles. Gal-Or (42) report that for air-tap water system, the mean bubble diameter is related to average bubble diameter by the equation:

$$\bar{d}_{bm} = \frac{\bar{d}_b}{1.27} \quad 10.11$$

Bubble frequency (n), bubble rise velocity (U) and bubble retention time ( $t_b$ ) for mean bubble diameter are calculated from the following equations:-

$$n = \frac{6}{\pi} \frac{Q_a}{\bar{d}_{bm}^3} \quad \text{III - 1}$$

$$U = 2 \sqrt{\frac{g \bar{d}_{bm}}{1.8}} \quad \text{III - 8}$$

$$t_b = \frac{h}{U} \quad \text{III - 9}$$

In addition, gas hold up ratio is calculated as follows:

$$\psi = \frac{V_g}{V} \quad 10.12$$

where  $\psi$  is gas hold up ratio,  $V_g$  is gas hold up in  $m^3$  and V is liquid volume in the reactor. Equation 10.12 can be written as:

$$\psi = \frac{\pi \bar{d}_{bm}^3 n t_b}{6 V} \quad 10.13$$

One can ask why the gas hold up is being calculated here when it could have been measured. The answer is that unfortunately during experimentation there was no intention to determine the bubble size. However, equation 10.13 gives the gas hold up ratio within the accuracy of above analysis and results.

A computer programme was written to solve the relevant equations and print out  $\bar{d}_{bm}$ ,  $n$ ,  $\alpha$ , and  $t_b$  for measured air entrainment rates at 1.05 m jet length.

Figs. 10.19 through 10.22 show the relations of  $\bar{d}_{bm}$ ,  $\alpha$ ,  $\psi$  and  $n$  with air entrainment rates. In Fig. 10-23 the mean bubble retention time ( $t_b$ ) is plotted against mean bubble diameter ( $\bar{d}_{bm}$ ). These results are plotted for vertical jets from 12.7, 22.2, 28.6 and 38.1 mm diameter cylindrical nozzles.

Fig. 10.19 shows that the mean bubble diameter depends on jet diameter. The mean bubble diameter increases with the increase of nozzle diameter. With the increase of entrainment rates, the mean bubble diameter increases and then decreases, thus giving a maximum mean bubble diameter for each nozzle diameter. The results of 38.1 mm nozzle are scattered. In fact, the results of this nozzle are subject to large errors, since the jet velocities for most of the data points are less than 5 m/s. The value of penetration depth predicted by equation 5.14 is subject to large deviations for jet velocities less than 5 m/s.

Because of the apparent dependency of mean bubble diameter on nozzle diameter, the results are replotted in Fig. 10.24. Here the ratio of mean bubble diameter to nozzle diameter ( $\frac{\bar{d}_{bm}}{d_n}$ ) is plotted against entrainment ratio ( $\frac{Q_a}{Q_l}$ ). The plot confirms the

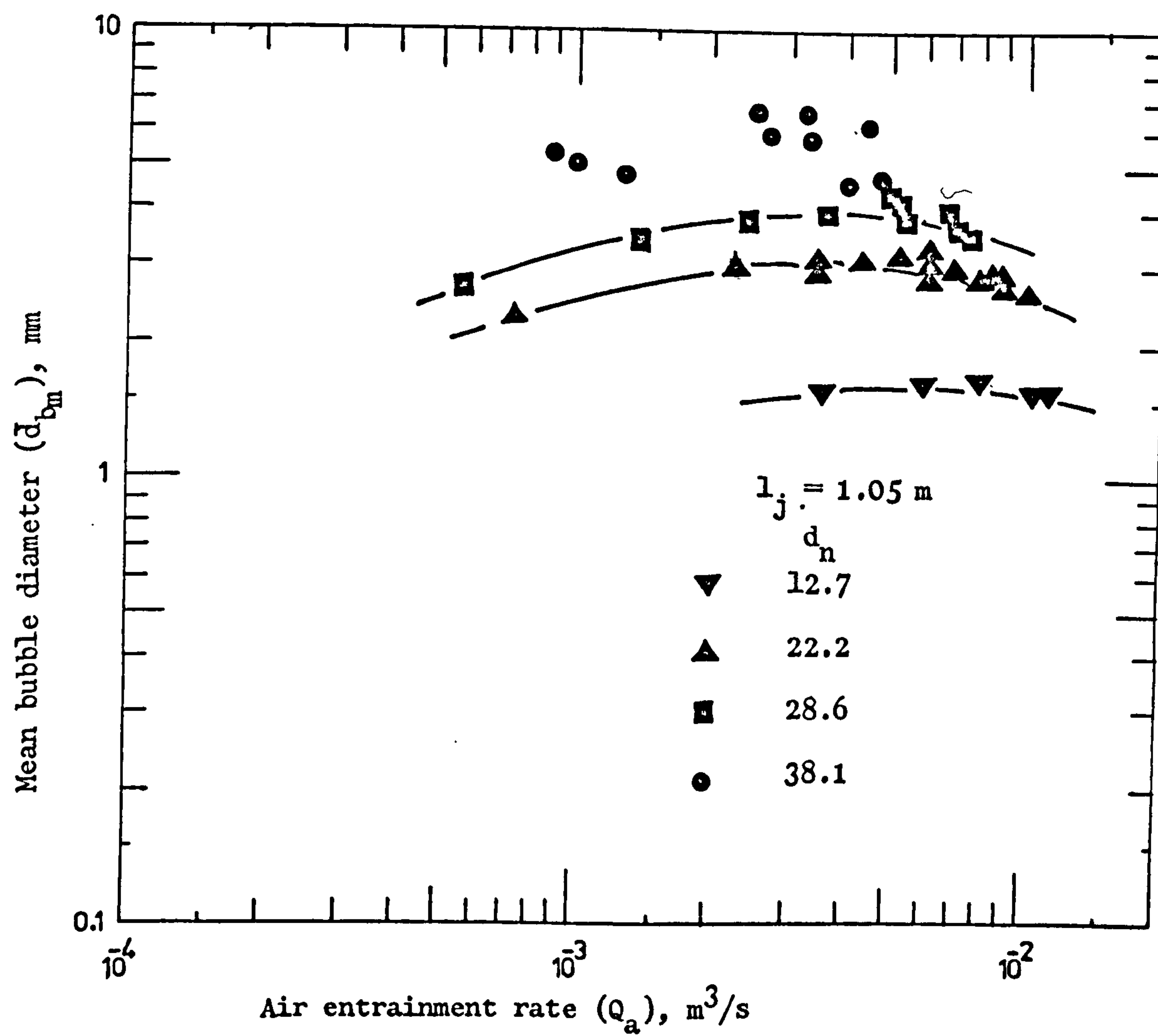


Figure 10.19. Relation of mean bubble diameter with air entrainment for various nozzle diameters.

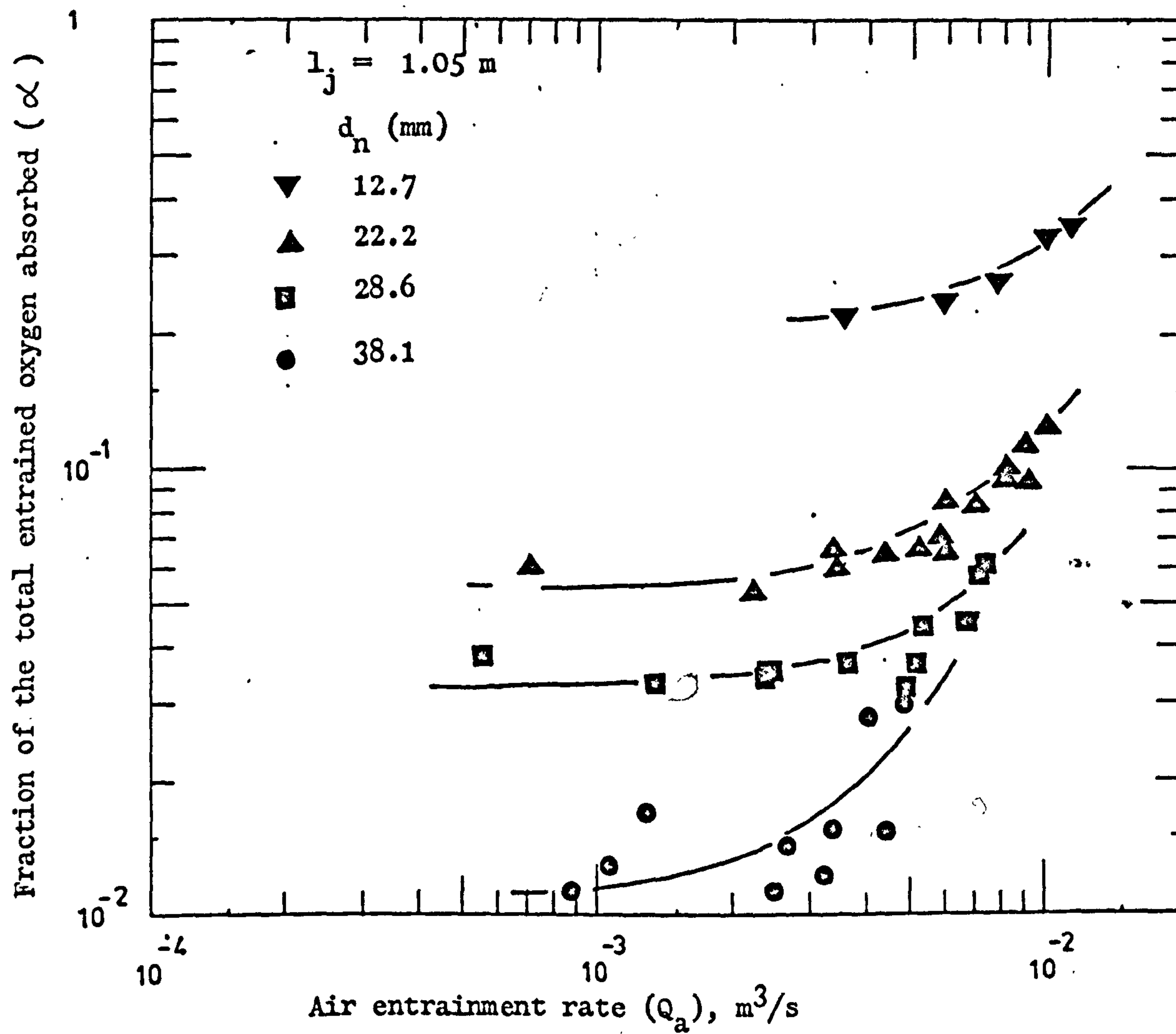


Figure 10.20. Relation of the fraction of the total entrained oxygen absorbed with air entrainment rate.



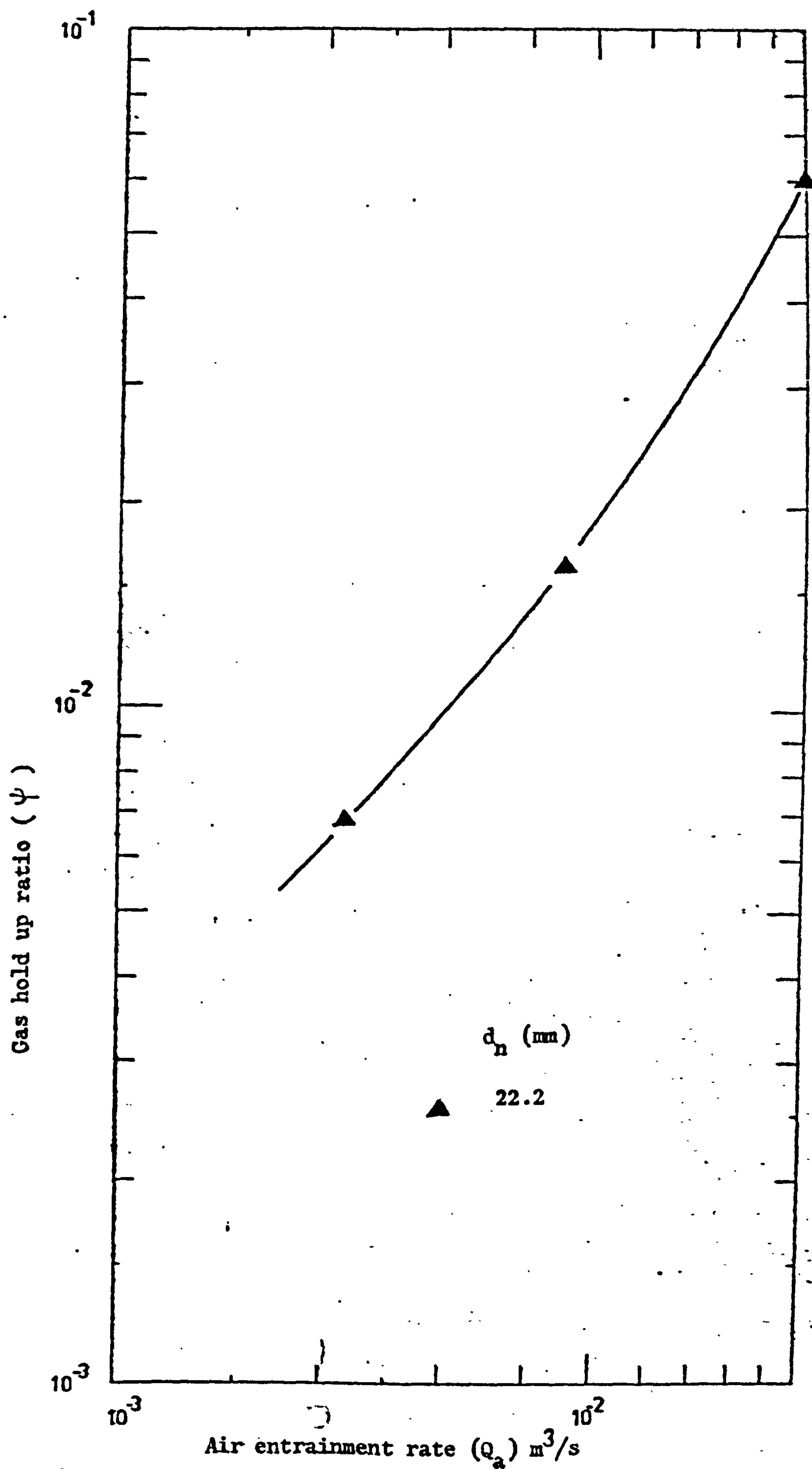


Figure 10.21. Relation of gas hold up ratio with air entrainment rate.

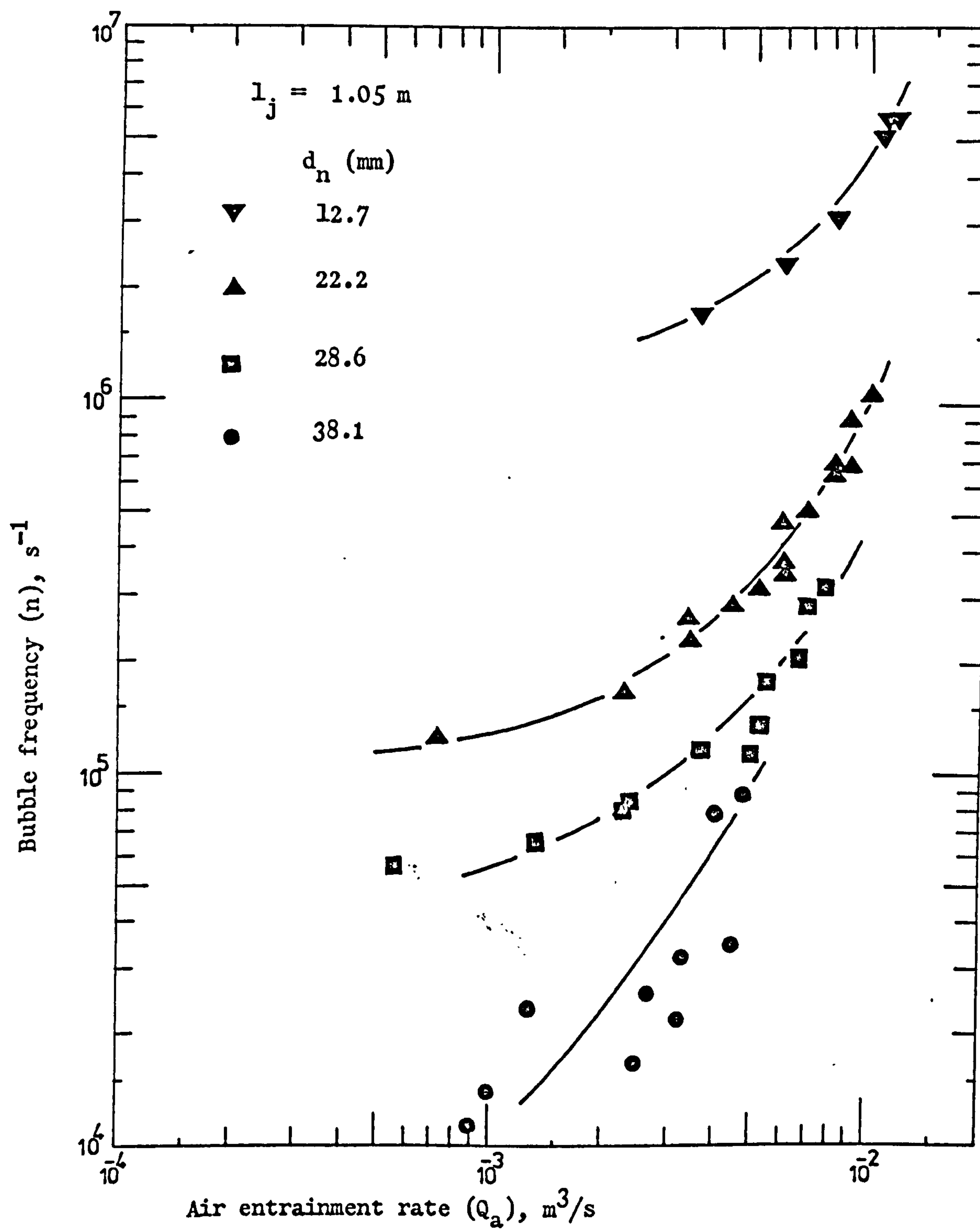


Figure 10.22. Relation of bubble frequency with air entrainment rate.

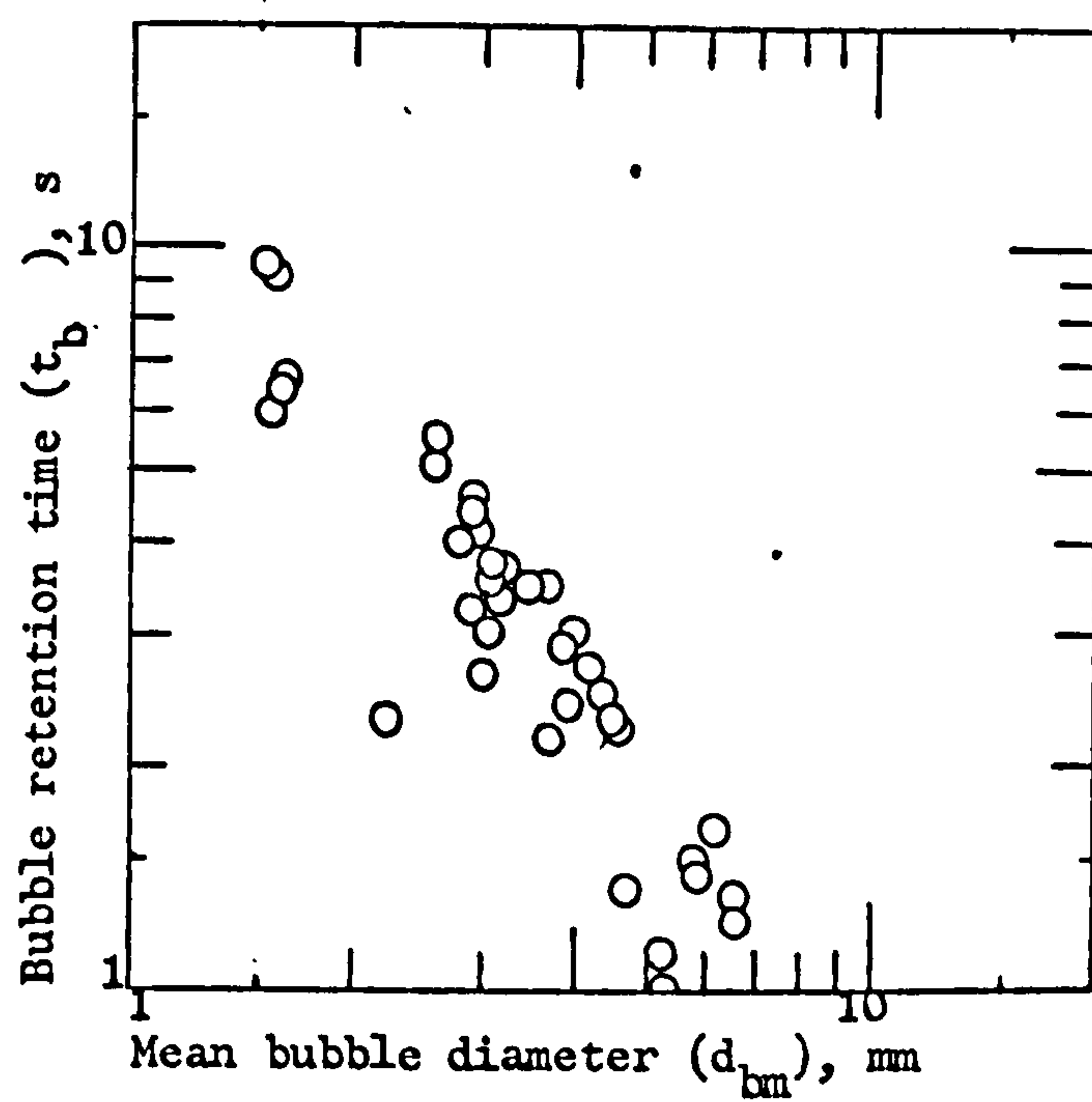


Figure 10.23. Relation of mean bubble diameter with bubble retention time.

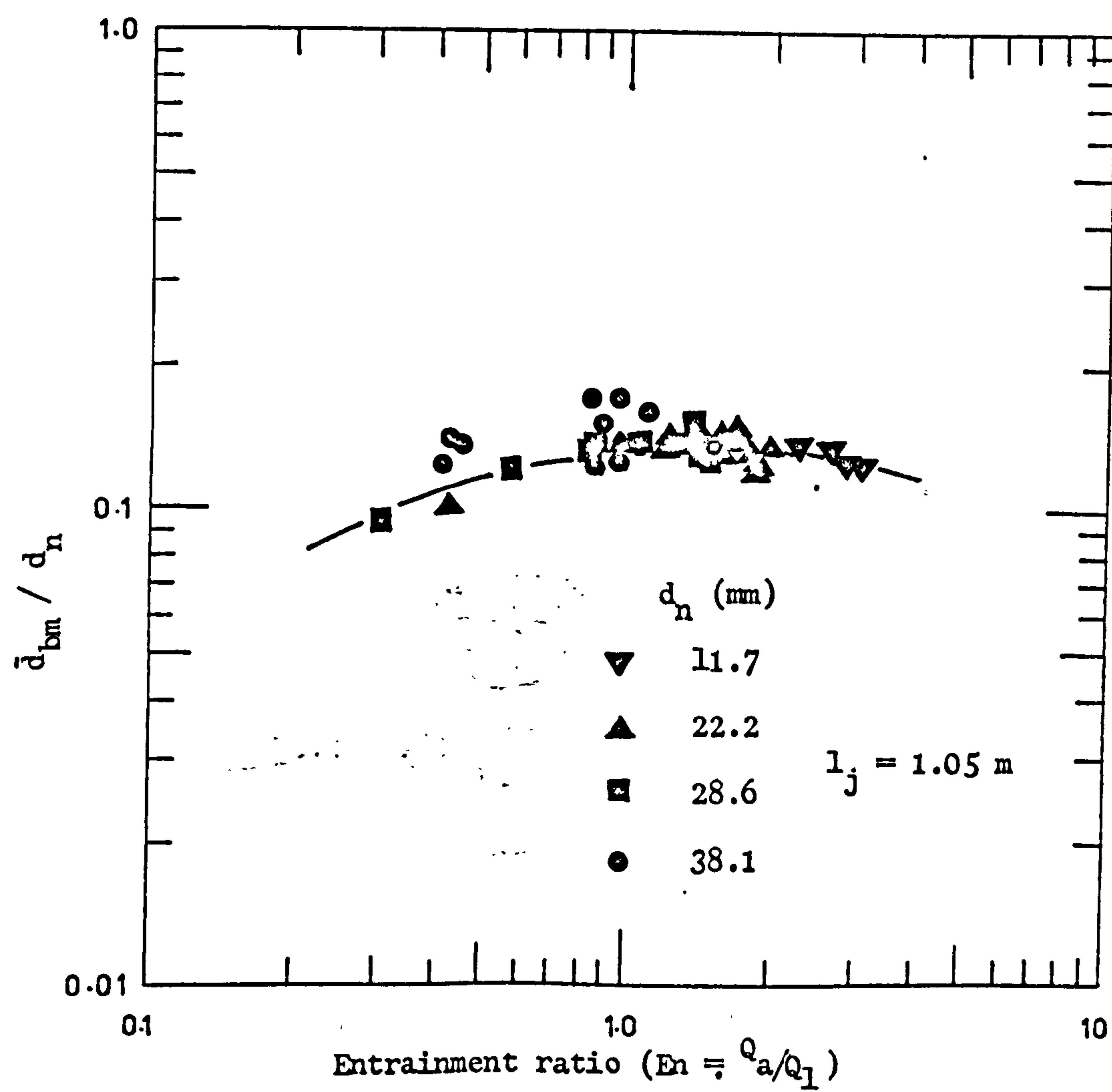


Figure 10.24. Relation of the ratio of mean bubble diameter to nozzle diameter with entrainment ratio.



diameter dependency and shows a maximum value of  $\frac{\bar{d}_{bm}}{d_n}$  approximately equal to 1.3.

The calculated range of mean bubble diameter is from 1.5 to 6.6 mm. The range of average bubble diameter would be 1.9 to 8.37 mm. The large values belong to 38.1 mm diameter nozzle which, as pointed out earlier, are subject to considerable error.

Below Table 10.1 shows the ranges of average bubble diameters for various systems reported in the literature. It is striking to note that the average bubble diameter range obtained from above analysis (1.9 - 8.37 mm) is in the same order of magnitude as the values reported in Table 10.1.

TABLE 10.1  
Bubble Sizes in Various Air-Liquid Systems by  
Various Investigators

Investigator	Average Bubble Dia. (mm)	System
Astarita (2)	2 - 6	air-water
Calderbank and Moo-Young (19,21)	3 - 5	air-water (15°C)
Ciborowski and Bin (25)	1.3 - 3.6	air-water
Ciborowski and Bin (25)	0.6 - 1.7	air - 40% glycerol
Van De Sande (121)	<1.4 - 3.8	air-water
Westerterp et al. (130)	1 - 5	air-sulphite (30°C)
Yoshida and Miura (136)	1.5 - 4.5	air-water

With the increase of air entrainment rate the per cent oxygen absorption (oxygen absorption efficiency) increases in the manner shown in Fig. 10.20, for different jet diameters. For entrainment rates less than  $5 \times 10^{-3} \text{ m}^3/\text{s}$ ,  $\alpha$  is stagnant for each jet. The smaller jets improve the oxygen absorption efficiency probably due to increase in interfacial area per unit volume due to smaller bubble

size distribution. However, at higher entrainment rates, it seems likely from Fig. 10.20 that the diameter dependency might disappear. From Fig. 10.21 gas hold up ratio also increases with the increase of entrainment rate. So from Figs. 10.20 and 10.21 it follows that per cent oxygen absorption is directly related to gas hold up. Westerterp et al. (130) and Burgess et al. (17) report that the increase of oxygen transfer is mainly due to increase in gas hold up ( $V_g$ ) rather than the decrease in bubble size, and that the average bubble diameter is essentially unaffected by the turbulence in the liquid.

From Fig. 10.20, the per cent oxygen absorption lies in the range, 1.1 to 36%. The range of per cent oxygen absorption in various commercial air diffusion units is in the range 2 to 14% (4.2.1.8). So the oxygen absorption efficiency not only agrees, but increases to two and a half-fold of the existing diffuser units. Further increase in per cent oxygen absorption is expected with smaller diameter nozzles and higher entrainment rates.

Since the gas hold up increases with the increase of air entrainment rates and the bubble size is not affected much eventually the frequency of bubbles increases as a result of the increase in air entrainment rate. This is shown in Fig. 10.22.

Another aspect is the relation of average bubble retention time with mean bubble diameter (with the increase of bubble diameter the retention time decreases because the bubble rise velocity increases. The range of average bubble retention time is 1 to 9.5 seconds for the bubble size range 1.5 to 6.6 mm diameter. The retention times within this range can be expected. Hankart et al.(45)

report that maximum possible average residence time of the gas in the dispersions is 7 seconds for a dispersion height of 90 cm. This was observed for air flow rate of  $1.1 \times 10^{-3}$  to  $3.32 \times 10^{-3} \text{ m}^3/\text{s}$  and impeller speeds of 100 and 1200 rpm. The air flow rates used by Hanhart et al. are within the range of air entrainment rates in this work. Also the liquid height in the reactor was about a metre. Hence, the average retention time of 9.5 seconds is not very far from the maximum retention of 7 seconds.

Although this calculation of bubble diameter is not rigorous due to the simplifying assumptions made and empirical correlations used the results agree remarkably with the results reported in the literature regarding average bubble diameter, average bubble retention time and per cent oxygen absorption.

## Chapter 11



## 11. AERATION OF BIOLOGICAL SYSTEM IN PLUNGING LIQUID JET REACTOR

This chapter deals with the second phase of the investigation: the aeration of a biological system. Defibred pig slurry (raw slurry filtered through 1.6 mm diameter holes) was used to represent the biological system.

Aeration of slurry produced persisting foam which caused several problems. Therefore, the chapter begins with a complete analysis of foam problems and its solution found in this work. Moreover, the effects of various parameters on the oxygen transfer in a biological system are studied. Oxygen transfer in the biological system is correlated with air entrainment rate as well as with power of jet. Finally, the results on the performance of a jet reactor as a "Continuous Biological Reactor" at 28 hours and 10 days retention times are presented and discussed.

### 11.1 FOAM PROBLEM

#### 11.1.1 Causes of Foaming

Foam is a congregation of gas bubbles separated by their films of liquid. It is always produced when a gas is dispersed into an impure liquid. Broadly speaking, a foam could be either stable like the head on the beer or unstable like the sea foam. The life of foam is finite - it could range from a few seconds to years (Perry (86)). Gaden et al. (41) define a foam as either "rigid" (high gas to liquid ratio) or "fluid" (low gas to liquid ratio).

Soap is the well known foaming agent. Others include protein,

amino acids, alcohols, esters, acids having long chains of carbon and hydrogen atoms, synthetic detergents and colloids. Pilpel (88) reports that the molecules of nearly all these compounds are so arranged that one end contains hydroxyl ( $-OH$ ), carboxyl acid ( $-COOH$ ) group and is water soluble (hydrophilic), while the other end is made up of a long chain of carbon and hydrogen atoms and is water insoluble but oil soluble (hydrophobic). Orr (82) says that these molecules migrate to gas liquid interface and orient themselves with their hydrophilic portion buried in the liquid phase, while the hydrophobic portion remains in the gas. Since this leads to the most stable molecular configuration, the molecules of the foaming agent concentrate on to the surface layer and reduce the surface tension and increase the viscosity of the surface layer as compared to the bulk liquid.

Foams are generally persistent in the case of organic and colloidal solutions. Colloids strongly adsorb at the surface layer or interfacial film.

Finely divided solids also collect on to the interface film and stabilize the foam by reducing the bubble coalescence (86, 41). An optimum particle size exists since too large and too small particles are less effective stabilizers (86).

Consequent reduction in surface tension by the foaming agent is not the essential requirement for the formation of stable foams. In fact, the key factor is the inherent elasticity of bubble films. In other words, the film should be able to vary its surface tension during a change (expansion or contraction of film), to counteract the force producing the change. When a bubble film is stretched at

some point, the concentration of foaming agent is decreased in the stretched zone. The decrease of foaming agent concentration increases the surface tension in the stretched zone. This increased surface tension counteracts the stretching force and may prevent the bubble rupture. Conversely, if the film is contracted, then the concentration of foaming agent in the zone being contracted would increase. This would decrease the surface tension in the zone of contraction, and would allow the film to expand on its own elsewhere, again without rupture. This film elasticity is, in fact, responsible for the formation of stable and persistent foams. Thus, two bubbles would bounce away from each other after collision due to elasticity of their films and thus bubble coalescence would be reduced (82).

Stables and Wilson (112) report that liquids having high surface viscosities also produce stable foams. In fact, with the increase of viscosity the velocity of approach of the bubbles is reduced and hence bubble coalescence is reduced.

In addition the foam persistence also depends upon the bubble size: smaller bubbles produce more stable foams.

As the liquid temperature rises, the foam persistence decreases owing to decrease in the viscosity and increase in pressure of the gas inside the bubbles (41).

Aeration of defibred pig slurry by a plunging jet produced a persistent foam. The presence of such factors as: higher liquid viscosity (refer to Fig. 11.4, page 230), fine solids (Baines et al.(5)); proteins (Glover (43)); colloids (5); and surface active

agent were responsible for the persistent foam. The bubble coalescence was visually observed to be reduced by the elasticity of the film. With raw slurry the foam was found to be "fluid" and the bubbles entrained substantial amount of liquid. The persistence of foam decreased to some extent after aeration for a few days. The foam changed from fluid to a rigid and fluffy foam. The decrease in persistence could be due to increase in temperature, reduction in fine solids and colloids (adsorption of fine solids and colloids on cells). The observations on the batch treatment of slurry showed the longer the liquid is aerated the lesser the persistence is.

#### 11.1.2 Foam Control

Foams produced by a chemical process may either please or annoy a chemical engineer. But often they annoy (as it did in this work) and require to be destroyed. Generally speaking, the foam can be destroyed mechanically or chemically.

##### 11.1.2.1 Mechanical methods

If the bubble film fails to counteract a mechanical shock applied to it, it would be ruptured and the bubble would disappear. Hence, in all mechanical methods of foam prevention sudden stresses are applied to foam films by mechanical means. Thus foam is destroyed by:

- (a) Beating the foam with blades or bars on a rotating shaft (41);
- (b) Compressing foam through grid or mesh (41);
- (c) Spraying the liquid over the foam (41);



- (d) Impinging liquid or gas jets over the foam (41);
- (e) Centrifuging the foam (Solomons (110));
- (f) Accelerating the foam and effluent air through a convergent nozzle (110)).

When the foam is separated into liquid and air by centrifuging or accelerating it through a nozzle, the liquid is returned back to aeration vessel and air is vented off.

In Waldhof's system (4.2.2.10), the foam is spilled over into a draft tube along with the liquid. Then it is sucked and destroyed by an impeller rotating just below the draft tube. This method works only with liquids having low foaming "potential".

Sudden pressure changes may also break the foam. Thus rapid succession of pressure waves produced by sirens and whistle may cause bubble rupture and prevent foaming (41,86).

#### 11.1.2.2 Chemical methods

Anti-foam agents effectively suppress foaming. Their use is not as economical as that of mechanical methods. Moreover, they contaminate the product. As a result of high surface activity they replace the foam producing substances and thus monopolize the surface film. As they do not support foaming, their presence at the liquid films would suppress foaming. A list of important antifoam agents is given by Solomons (110).

### 11.1.2.3 Foam control in this work

The foam produced by aeration of slurry spilled over the tank resulting in considerable loss of liquid (Fig. 11.1). The loss of liquid after the start of aeration was found by measuring the liquid level in the tank at equal intervals of time. A 6.4 mm polythene tube was filled with water and one end was dropped deep into the liquid and the remaining length was bent into a U-shape and was clipped on to a wooden board. The liquid level in the tank was indicated by the level of water in the U-tube.

In addition to loss of liquid, foam also reduced the oxygen transfer. The jet penetrated through a thick layer of foam and the foam surrounding the jet offered resistance to the flow of the air being entrained. Also the jet might be entraining into the liquid some of the foam. The resultant effect of foaming was the reduction in oxygen transfer (Fig. 11.2). The oxygen transfer in Fig. 11.2 finally reduced to an equilibrium value equal to the respiration rate of organisms.

At the end of 76 minutes aeration was stopped by closing the valve controlling the liquid flow through the jet. This resulted in sudden increase in dissolved oxygen concentration as shown in Fig. 11.2. This is explained by the fact that the increase in pressure head at the pump outlet due to the closure of the main valve caused increased dissolution of oxygen from the small entrained bubbles in the pump casing (partial pressure of oxygen increased due to increase in pressure head).

The loss of liquid due to spilling of foam from aeration tank

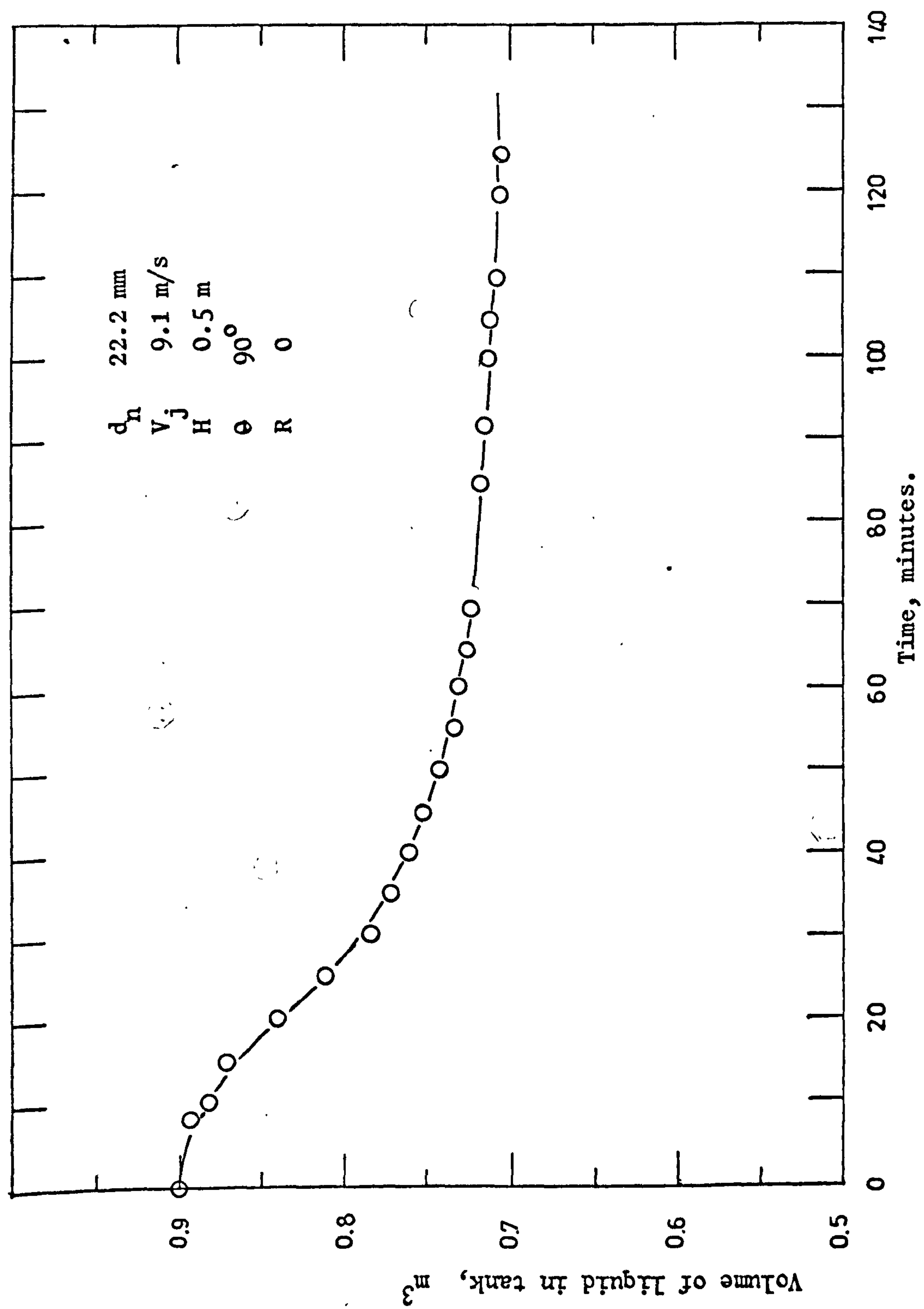


Figure 11.1. Liquid loss due to foaming.





was prevented by fixing a wooden rectangular trough (4.25 m x 1.9 m x 0.8 m) to the aeration tank (Fig. 11.3). The foam spread in the trough and the liquid in the foam drained back into the aeration tank. The effect of foam on oxygen transfer was eliminated by aerating the liquid with concealed jets (9.1). Fig. 11.2 shows that with concealed jet oxygen transfer rate did not decrease.

The liquid was sprayed over the foam in order to destroy it. Five Uniswirl nozzles (Delavan-Watson Ltd., Widnes, England), separated from each other by equal distances were connected to a 2 inch pipe clamped to the top of the trough lengthwise, so that the apexes of the hollow spray cones lie along the centre line (Fig. 11.3). One end of this pipe was sealed while the other was connected to the spray pump. The liquid from the aeration tank was sprayed over the foam through the spray nozzles. The nozzles as bought from the manufacturer produced a very fine spray and sometimes were clogged. The inlet and the orifice diameter of the nozzle were drilled to  $\frac{3}{8}$  inch and  $\frac{5}{16}$  inch respectively, so as to avoid clogging as well as to produce a coarse spray.

Foam control by antifoam agent imposes an additional cost to the cost of aeration. Moreover, just one dose of anti-foam agent does not completely solve the problem. But instead anti-foam has to be added intermittently whenever the foam height reaches some critical height. Anti-foam has considerable effect on  $K_L$  (2.2.2). Sometimes anti-foam oil might have undesirable effect on biological populations during a treatment process. Thus, for research purposes it was not advisable to use anti-foam agent particularly when the effect of anti-foam agent on  $K_L$  and organisms was not known quantitatively.

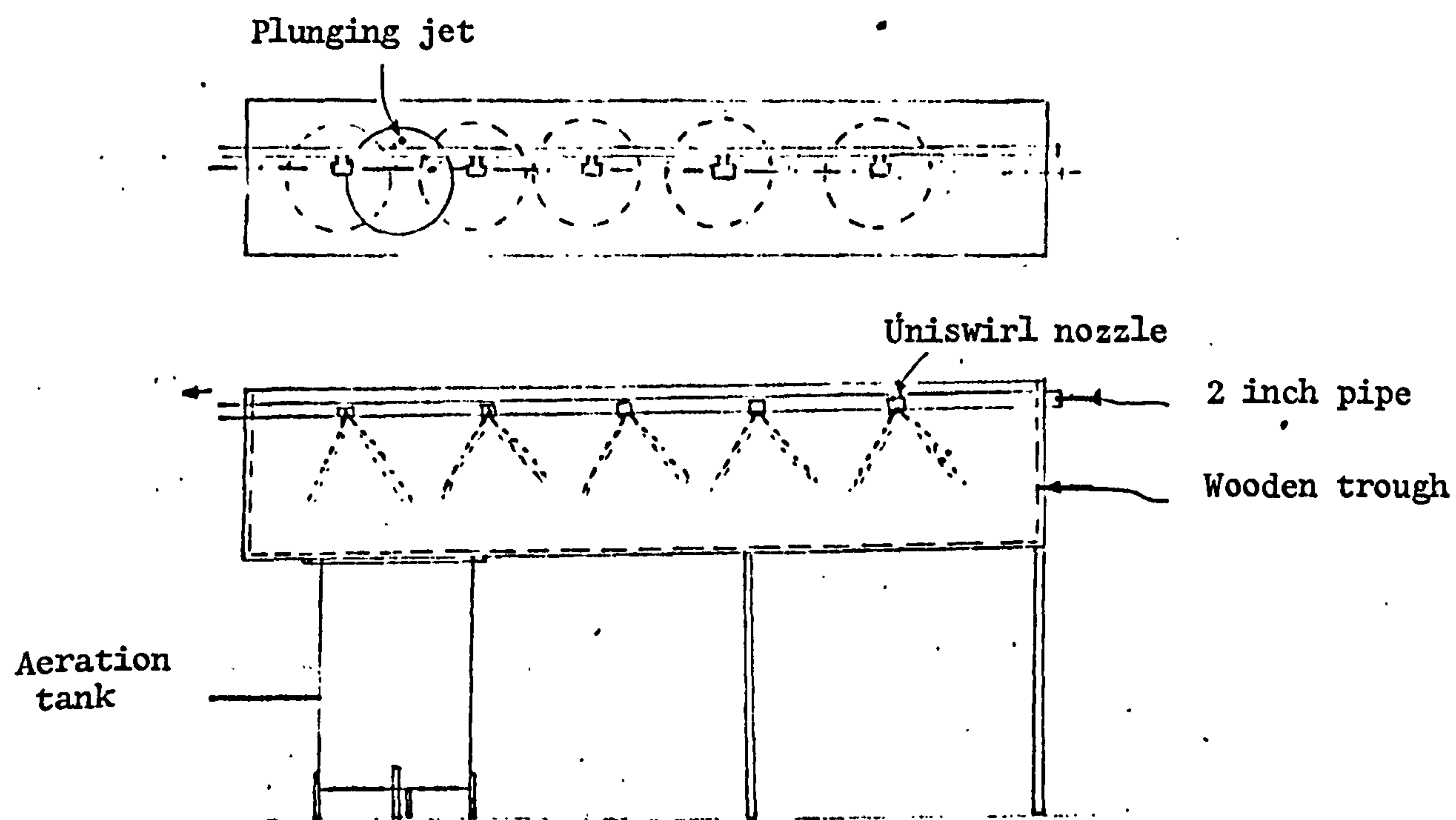


Figure 11.3. Foam control by liquid sprays.

## 11.2 OXYGEN TRANSFER IN BIOLOGICAL SYSTEM

### 11.2.1 Experimental

The experimental set up described in 9.1 was used again along with some necessary modifications.

Some practical problems were created by the liquid used to represent the biological system which was defibred pig slurry. As a matter of interest shear rate versus shear stress diagram was plotted for pig slurry and water using the Brookfield viscometer (Brookfield Engineering Laboratories, Stoughton, Mass., USA.). From the resulting plot (Fig. 11.4) it appears that the liquid was pseudo-plastic. Moreover, the liquid contained suspended solids ranging from colloidal particles to coarse particles of about 1 mm in size. The pump employed for the experiment with sulphite solution failed to pump the slurry, and was replaced by a new pump described in 9.1.

As the liquid was viscous and contained solids, it was suspected that these solids might block the pressure taps for the orifice plate. Therefore, for accurate measurement of flow rate cleaning of these pressure taps was necessary. A complete cleaning system for the orifice manometer and orifice pressure taps was designed.

Fig. 11.5 shows the system for cleaning of (1) clogged pressure taps, (2) clogged polythene tube in the system itself, and (3) for removing the slurry or solids accumulated in the limbs of mercury manometer. A manifold with four outlets was used. Each outlet had a simple on-off valve. The same valves were also connected to pressure taps. The outlets of the manifold were connected to the

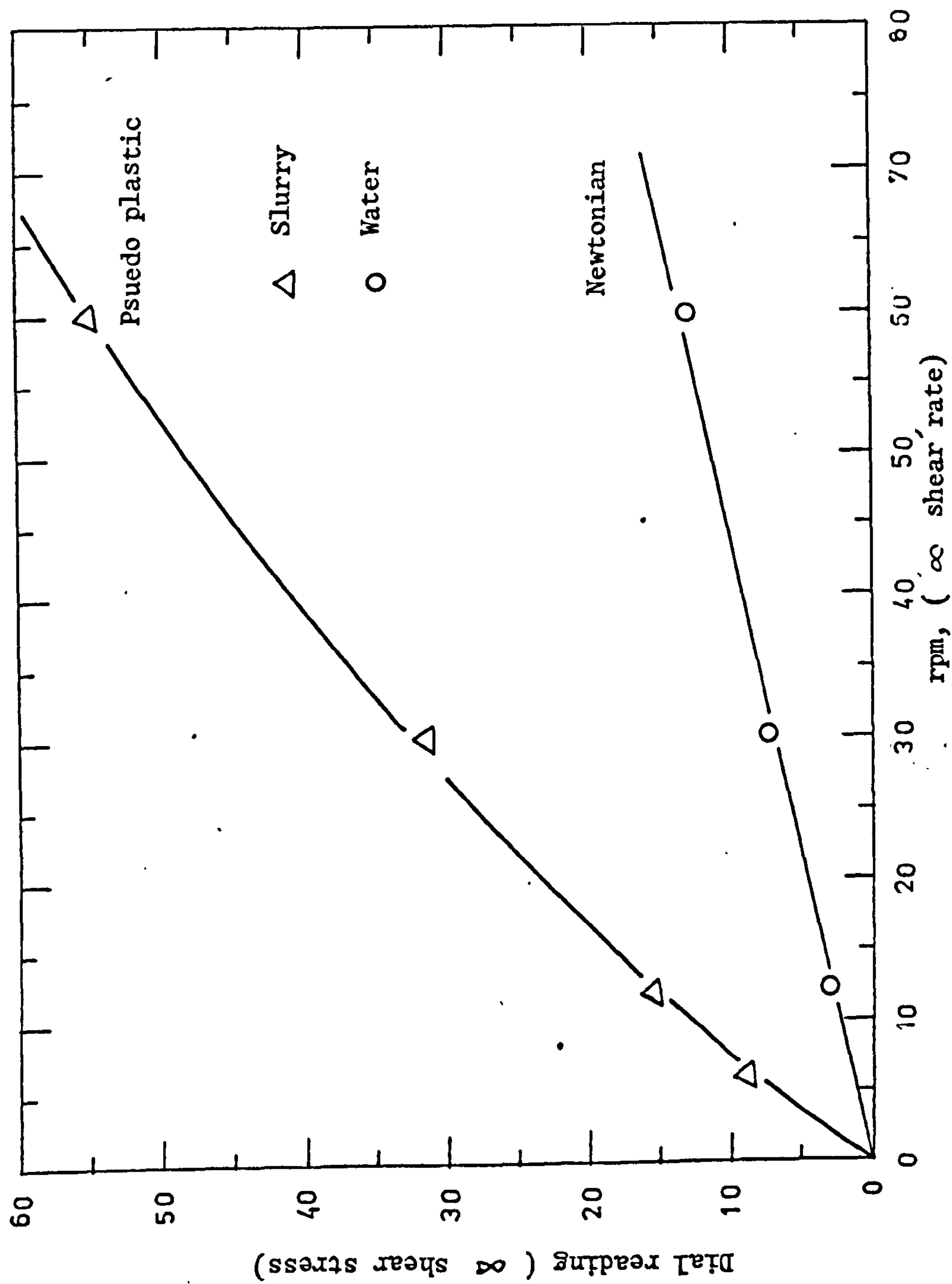


Figure 11.4. Viscosity diagram for water and slurry obtained by Brookfield viscometer.



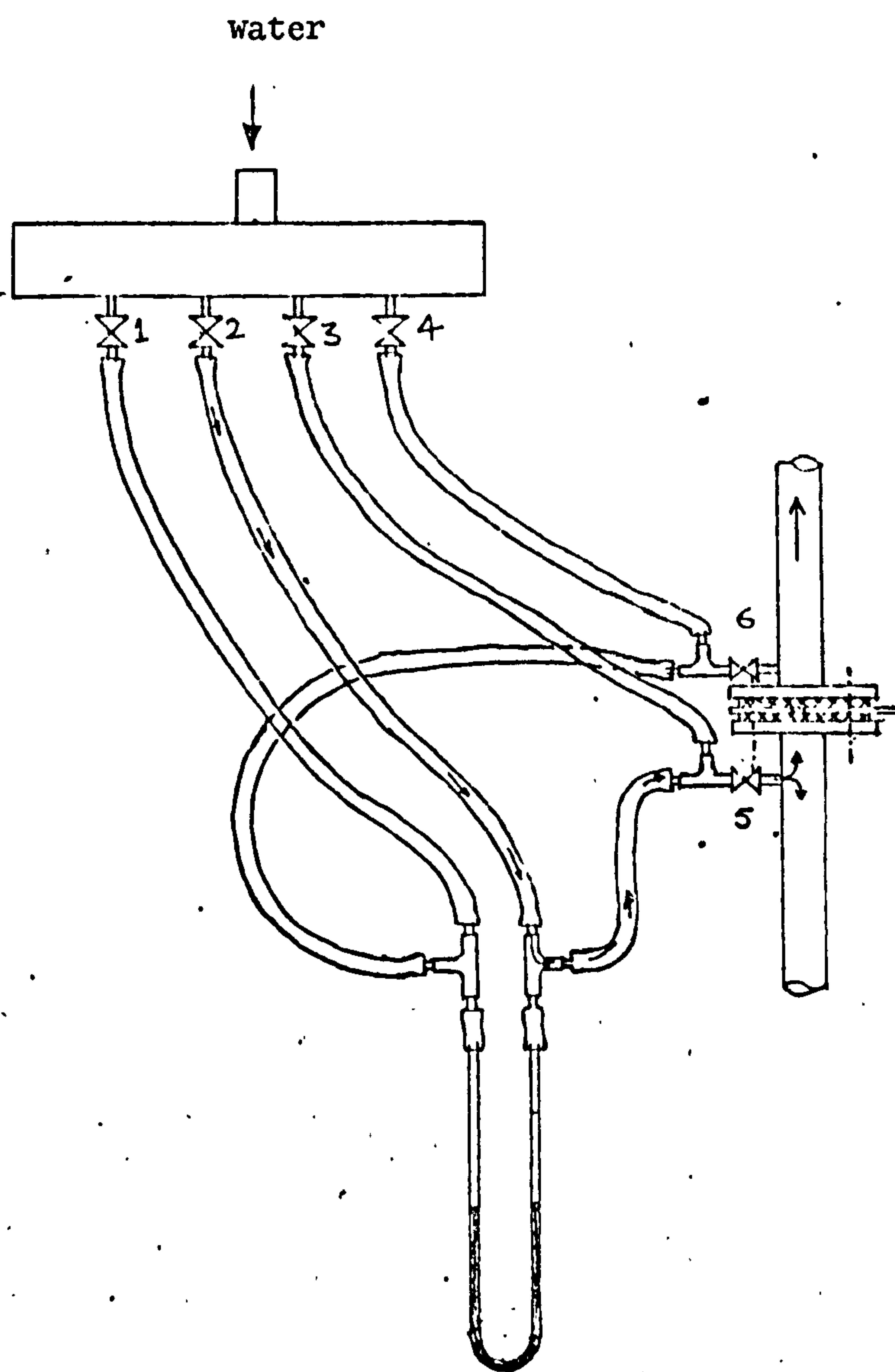


Figure 11.5. Flow diagram of cleaning system.

limbs of manometer and to the pressure taps in such a way so as to accomplish complete cleaning of the system. The valves at the manifold outlets were always kept closed. Any of these valves would be opened only when needed for the cleaning operation; however, valves 5 and 6 were usually open as it was necessary for the measurement of differential head.

For cleaning the upstream pressure tap valve 6 was closed and valve 5 was left open. The supply of tap water was turned on. By opening valve 3, the water flowing through valve 3 would be forced to flow through the blocked press tap into the main pipe. Similarly, when cleaning the downstream blocked pressure tap, valve 5 was closed and valve 6 was left open. Opening of valve 4 would clean the pressure tap.

When suspended solids or slurry had accumulated in the limbs of the manometer they were removed as follows. Suppose the slurry accumulated in the right limb was to be removed. Valve 6 was then closed and valve 5 was left open. Valve 2 was opened slightly for tap water to flow via the route shown by arrows into the main pipe. Valve 1 was then opened as much as required to raise the column of slurry in the right limb to the point where it would hit the flowing tap water and would be carried away by the flowing tap water. The operation required careful and intelligent handling of the valves 1 and 2, otherwise mishandling might result in washing out of mercury from the manometer.

The blocking of taps was rare and therefore cleaning was required on only few occasions.

For the study of the effect of suspended solids on oxygen transfer, flocculated and dried sludge was mixed with tap water.

The sludge flocs dispersed in water and did not foam on aeration. Sludge in different quantities was added to give different suspended solid concentrations.

A few experiments were also performed with deoxygenated tap water. The water was deoxygenated by adding sodium sulphite and cobaltous sulphate ( $4 \times 10^{-6}$  kmol/m<sup>3</sup>) solutions. To check whether all the sulphite was oxidized before the oxygen concentration started increasing from zero as a result of aeration, a sample was taken just at the point where the dissolved oxygen began to increase from zero. The sample was then analysed for the presence of sodium sulphite, but no sulphite was found in the sample. Therefore, all sulphite was oxidized when dissolved oxygen concentration began to increase from zero.

The slurry deoxygenated itself when left unaerated for some time owing to the respiration of micro-organisms. For the sludge-water system the respiration rate was so low that the liquid was left for several hours to get complete depletion of oxygen.

The concentration of dissolved oxygen in the liquid being aerated was measured by Model 1520 EIL portable dissolved oxygen meter (Electronic Instruments Ltd., Chertsey, Surrey, England). The meter was calibrated as described in EIL instruction manual. The meter was checked for accuracy after every two weeks and if necessary was recalibrated.

The meter probe was inserted in a cell (Fig. 11.6). The inlet tube of the cell was connected to a pressure tap at pump outlet and the outlet tube of the cell drained into the tank. Thus the tank liquid was circulated through the cell and the probe

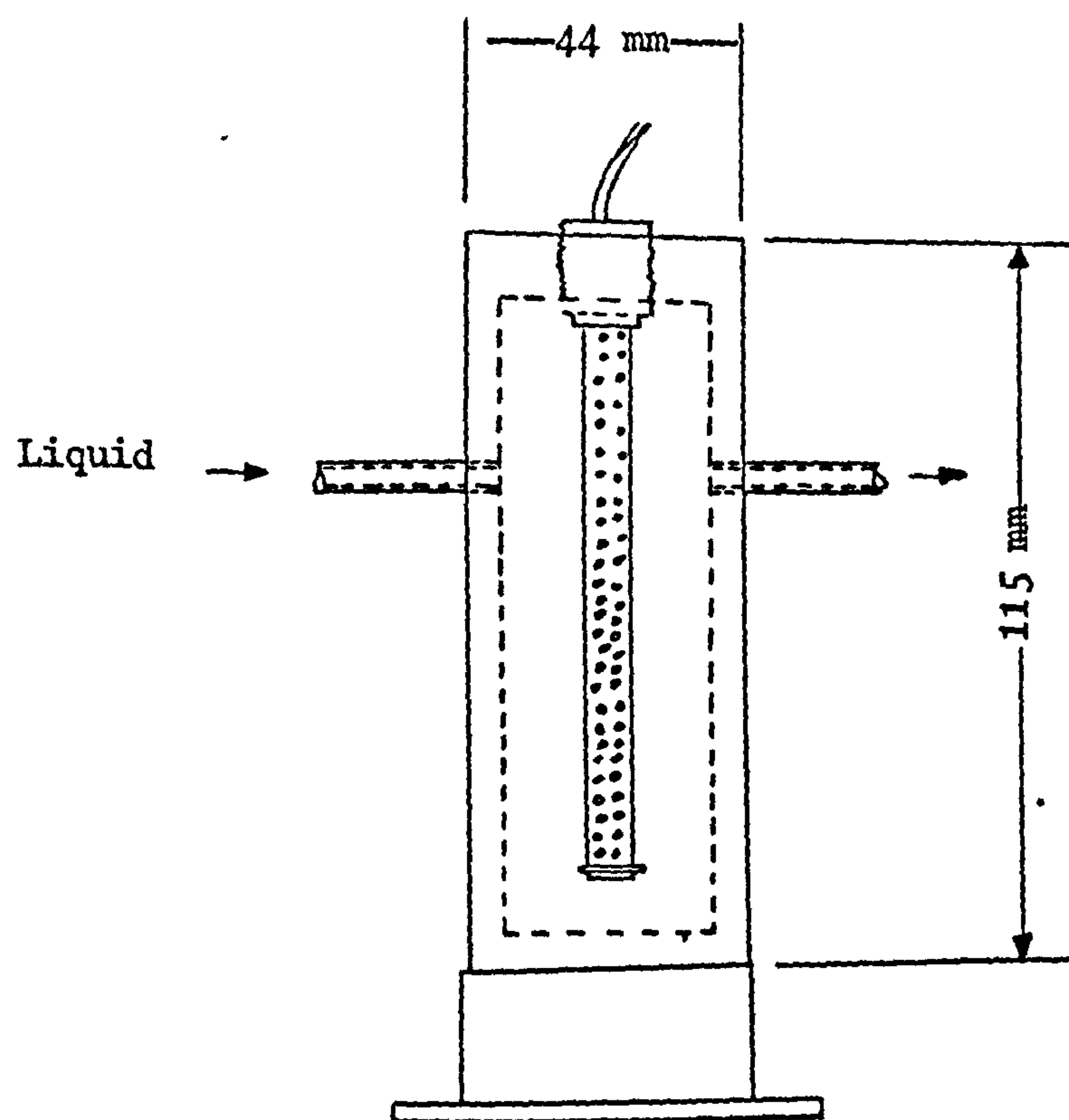


Figure 11.6. Probe cell.



measured the dissolved oxygen concentration of the liquid flowing past the probe.

The error in measurement by the meter is specified by the manufacturer as 1% for each 10°C rise in liquid temperature. In addition, Van De Sande (121) has shown that the response time of the electrode has no significant effect on the measurements.

#### 11.2.2 Measurement of Oxygen Transfer Coefficient

The oxygen transfer was measured by the method of unsteady-state aeration of deoxygenated tap water or slurry.  $K_L a$  in the tap water experiments was calculated by the method described in 6.1. Fig. 11.7 shows a record of the increase in per cent oxygen saturation with time and the decrease in per cent oxygen saturation due to respiration after the termination of aeration. The per cent oxygen saturation values at intervals of 3, 6 or 12 seconds, depending upon the aeration time were noted from the aeration records.

Since the respiration rates ( $r$ ) were very small as compared to oxygen transfer rates the dissolved oxygen concentration reached nearly to saturation value in most of the experiments. Also,  $r$  remained approximately constant when the dissolved oxygen decreased from 100% saturation value to about 5% saturation value, which means that the  $r$  was independent of oxygen saturation values greater than 5%. Respiration rate was measured by noting the decrease in dissolved oxygen concentration after the termination of aeration. In a series of several experiments it was found that the respiration rate remained approximately constant during the experiments.

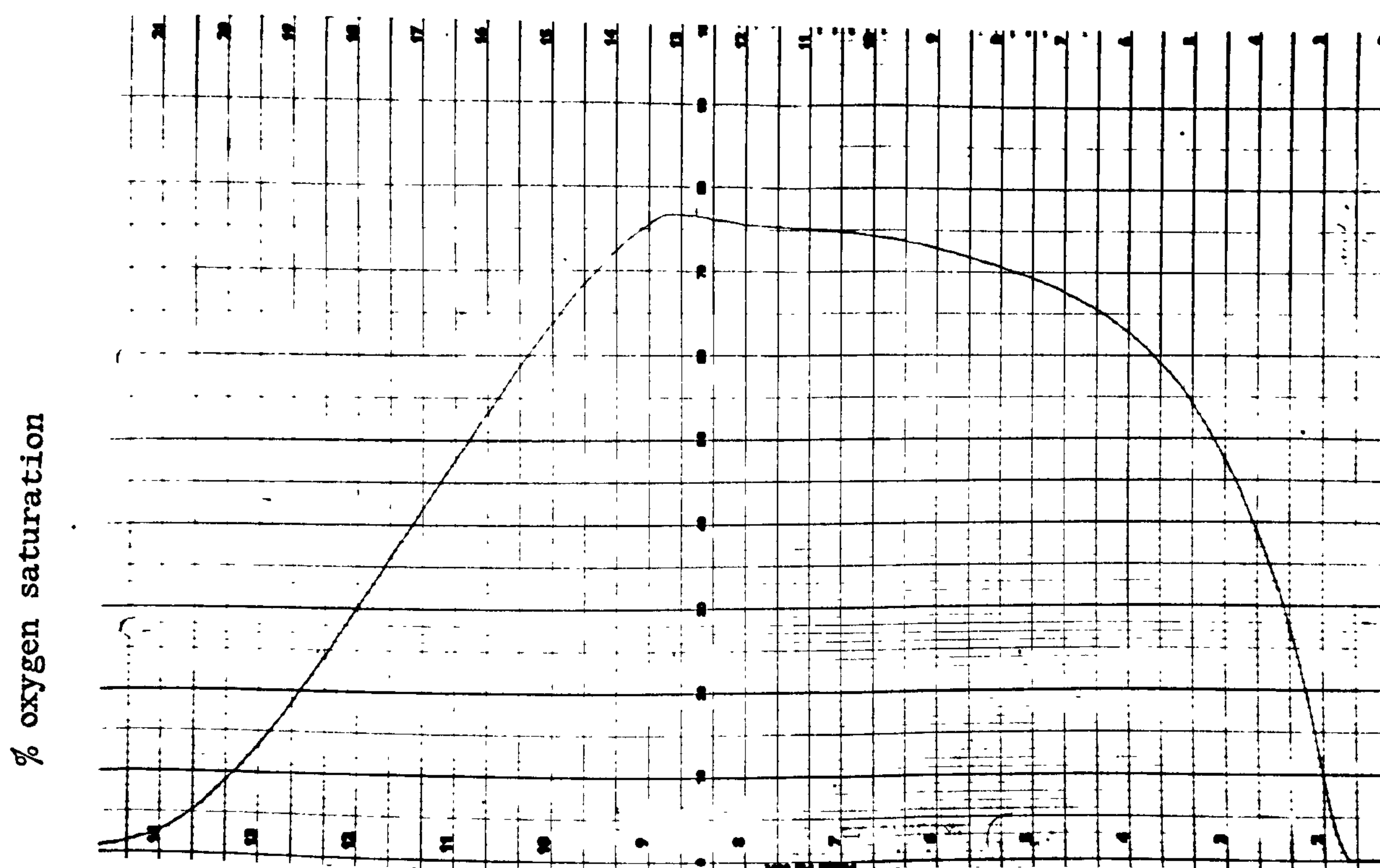


Figure 11.7. Record of dissolved oxygen concentration with time for aeration of slurry.

$d_n$  12.7 mm

$V_j$  16 m/s

Chart speed 25 mm/min.

Scale 1 cm. —

It was not possible to measure the effect of turbulence (during aeration) on the respiration rate. It was expected that the respiration rate would be higher in highly turbulent liquids since the larger surface area of organisms would be in contact with food and oxygen due to liquid turbulence.

From 2.1.1, the true exponential curve in Fig. 11.7 is given by the equation:

$$\frac{dx}{dt} = K (x' - x) \quad 11.1$$

where  $x$  is dissolved oxygen concentration as per cent oxygen saturation,  $x'$  is apparent saturation concentration as per cent of saturation concentration, and  $K$  is oxygen transfer coefficient ( $= K_L a$ ) in  $1/s$ .

Integrating equation 11.1 between the limits:

$$\text{at } t_1 = 0, \quad x = \bar{x}$$

$$\text{and } t_2 = t, \quad x = x$$

we get:

$$\left( \frac{x - x'}{\bar{x} - x'} \right) = e^{-Kt} \quad 11.2$$

or:

$$x = x' - (x' - \bar{x}) e^{-Kt} \quad 11.3$$

The equation is of the form:

$$x = A - B e^{-Kt} \quad 11.4$$

where  $A$  and  $B$  are constants.

Let  $\bar{x}^*$  be the observed value at time  $t$ , then the error is:

$$\epsilon = \bar{x}^* - x' + (x' - \bar{x}) e^{-Kt} \quad 11.5$$

A computer program was used to evaluate the constants of equation 11.4 on the basis of maximizing the probability that each data point



fitted the equation. A computer print out of the fitted curve to experimental points is shown in Fig. 11.8. All  $K$  values were converted to values at  $20^{\circ}\text{C}$  by using the equation 2.8. Maximum oxygen transfer rate was then calculated by multiplying  $K$  with volume of liquid and oxygen saturation concentration ( $C^*$ ) at standard conditions.

The measurement of  $K_L a$  by the equation 6.11 seems to be the accurate and quickest method. But in this work it was not practical to use this method since in most experiments the dissolved oxygen concentration reached approximately 100% saturation value due to very low respiration rates of raw slurry. However, for Run J15, oxygen transfer was calculated by using equation 6.11.

There are some limitations to the use of equation 6.11. It requires accurate measurement of respiration rate which is often difficult particularly when the turbulence has significant effect on respiration rate. Moreover, as pointed out in 6.3, small differences in  $C^*$  and  $C'$  induce large errors in  $K$  values. There is some evidence that the steady equation 6.11 gave tremendous scatter in the results and gave values somewhat 30% higher than measured by direct oxygen mass balance on the aerator (Lister and Boon (66)). On the other hand, a good agreement between  $K$  from equation 6.11 and from unsteady-state method has been reported by Kayser (57).

Measurement of  $K$  by plotting  $\frac{dC}{dt}$  against  $C$  did not seem to be a promising method, since it involved the tedious work of drawing tangents at various points on the dissolved oxygen concentration curve. The drawing of tangents would also be inaccurate since some of the curves were not smooth.



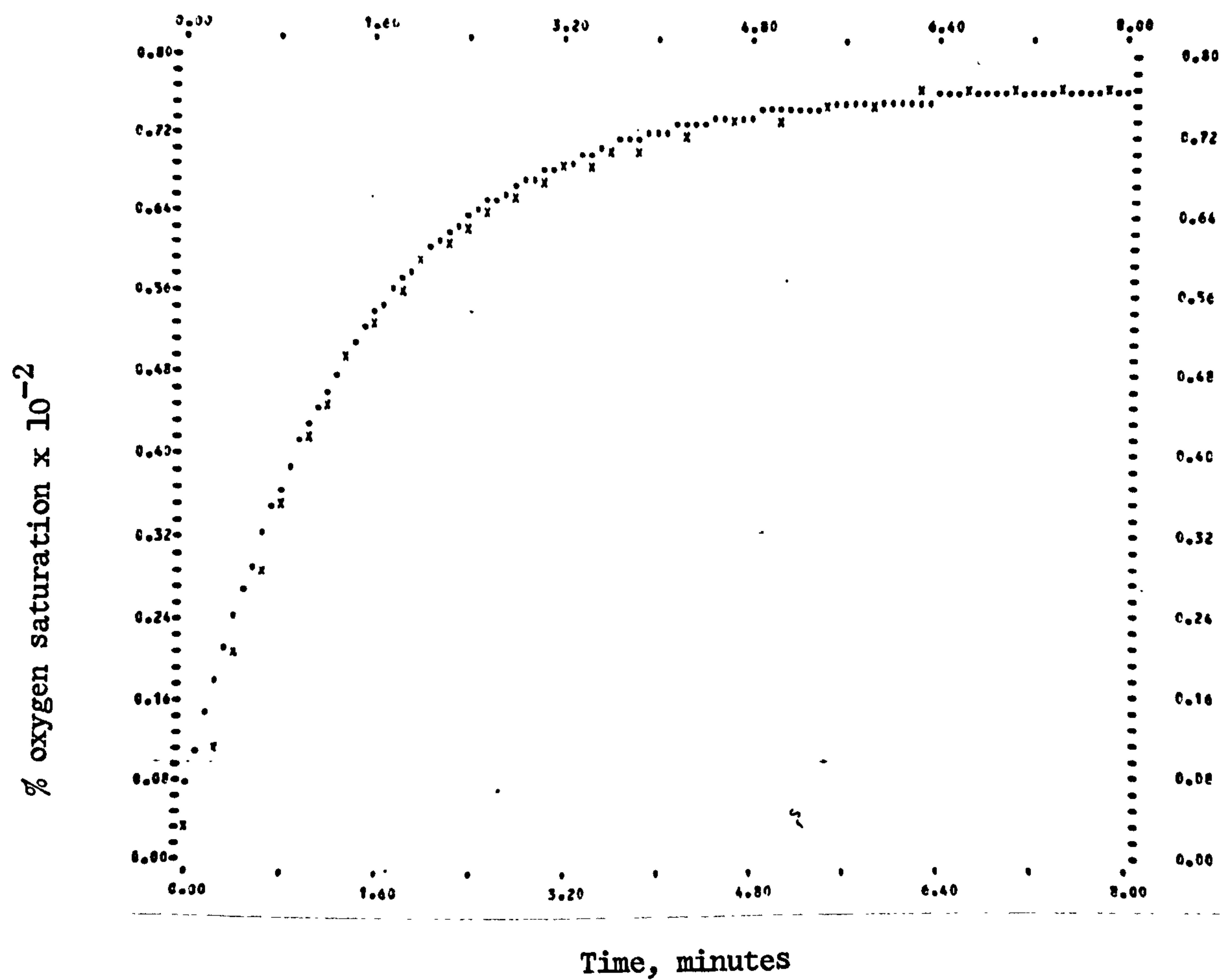


Figure 11.8. A computer print out of the fitted curve to the experimental curve of Figure 11.7.

Hence, by considering the above facts, the fitting of equation 11.4 to the experimental data was thought to be the more accurate and reliable method to determine oxygen transfer coefficient (K).

### 11.2.3 Results and Discussion

#### 11.2.3.1 Effect of suspended solids on oxygen transfer rate

The experiments were performed with the 22.2 mm diameter nozzle and at a constant jet velocity of 10 m/s. The suspended solids were represented by dispersed flocculated sludge (11.2.1). The concentration of suspended solids was varied from 1 to 8.3 kg (dry) solid/m<sup>3</sup>. Thus the effect was investigated over a wide range of suspended solids concentration. The particle size analysis was performed on a sample of suspension by a coulter counter. Particle size distribution is plotted in Fig. 11.9 which shows the per cent cumulative undersize of particle ranging from 7 to 1000  $\mu$ m.

The results plotted in Fig. 11.10 clearly show that the presence of suspended solids in the liquid phase has no appreciable effect on oxygen transfer rate. This holds for particle sizes ranging from fine to coarse dimension 7 to 1000  $\mu$ m. In fact, the turbulence in the aeration tank is quite high and with this consideration the results agree with Von Der Kroon (127), who found that at higher degrees of turbulence the gas transfer coefficient is not affected by the presence of solids.

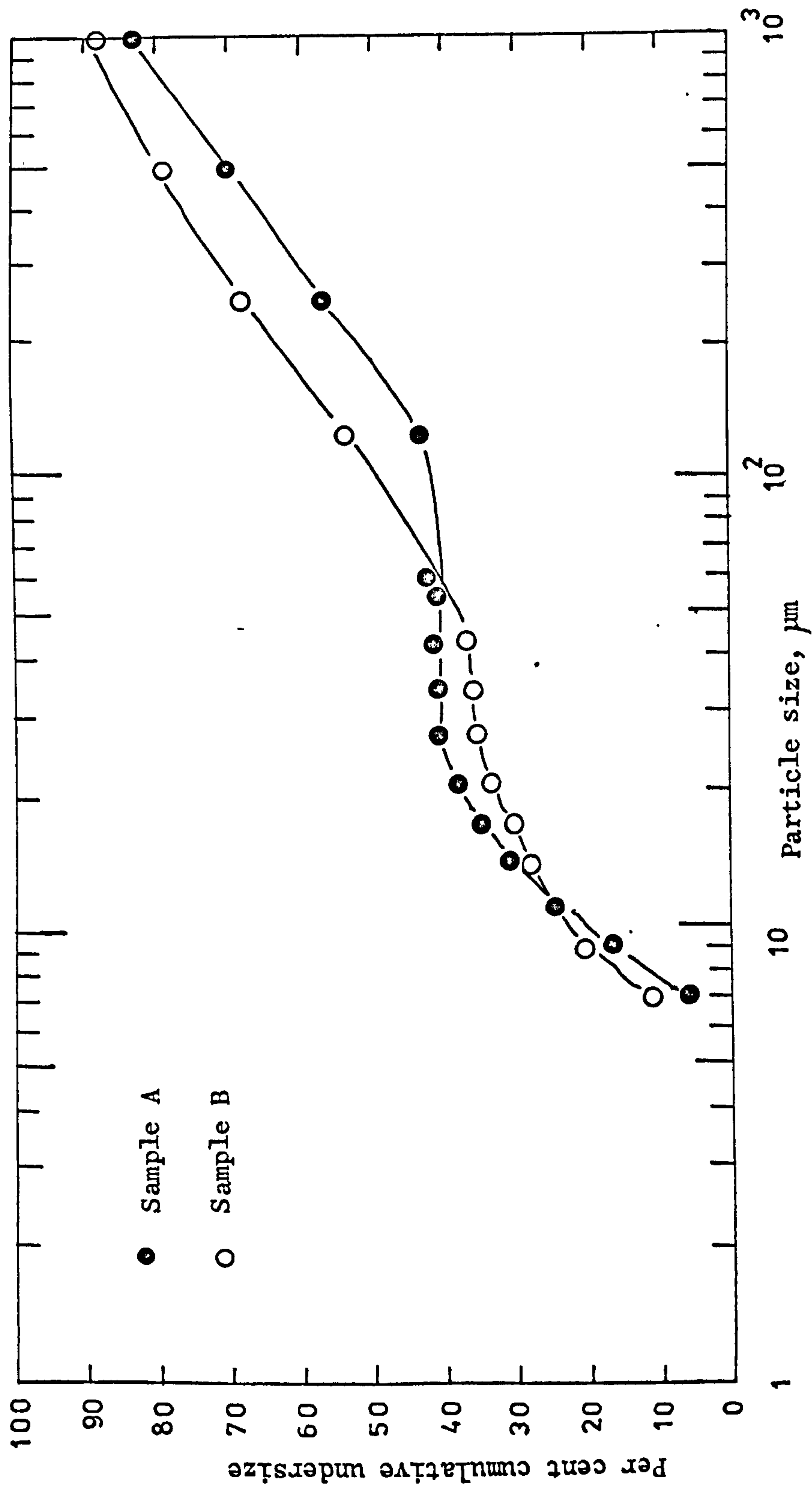


Figure 11.9. Particle size distribution of suspended solids of dispersed sludge flocs.

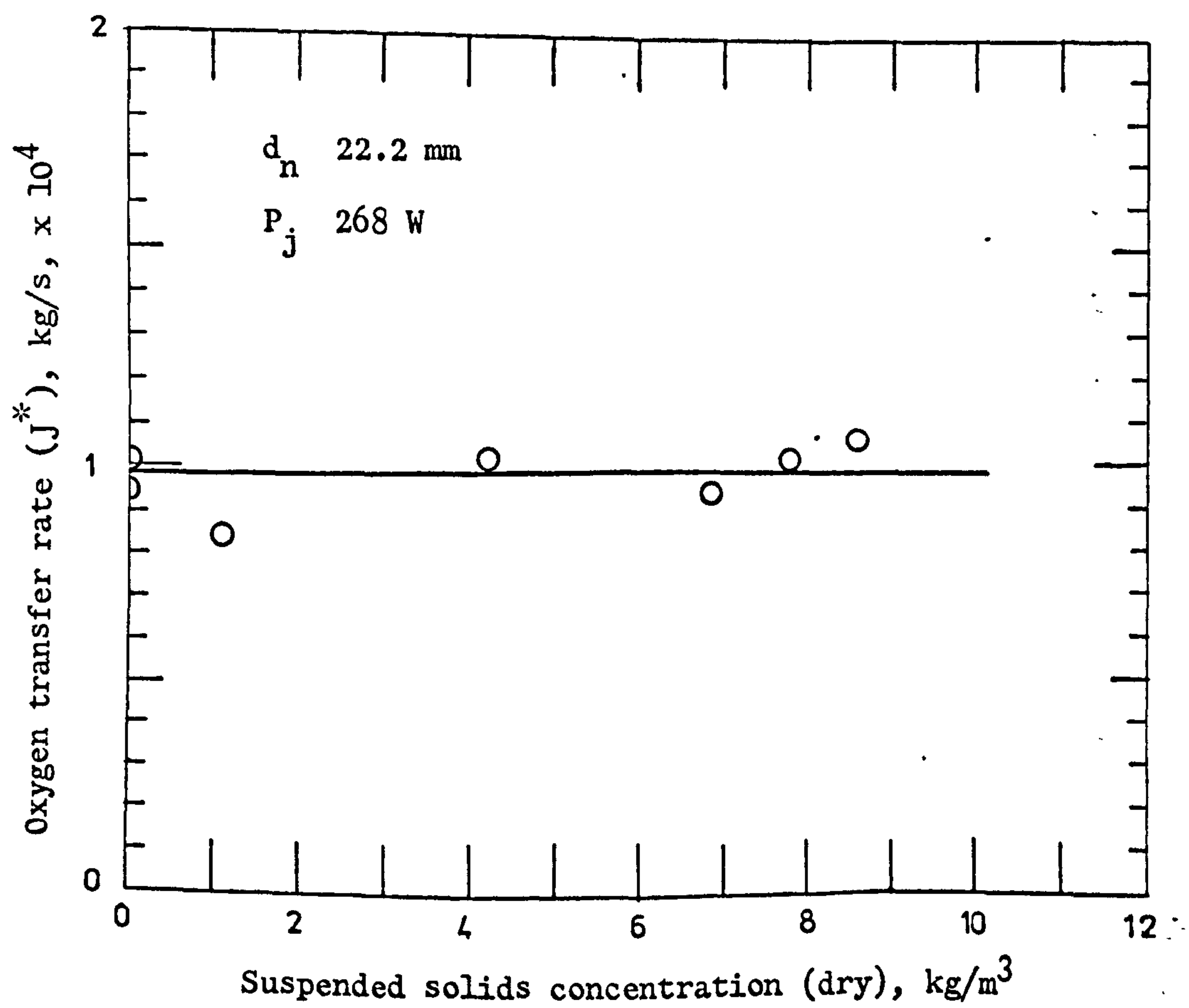


Figure 11.10. Effect of suspended solids on oxygen transfer rate.



#### 11.2.3.2 Effect of jet velocity and nozzle diameter on oxygen transfer rate

Fig. 11.11 shows the effect of jet velocity on oxygen transfer rates for the jets obtained from different diameter nozzles. It is obvious from the Fig. 11.11 that the oxygen transfer rate in biological system increases qualitatively like in sulphite system with the increase of jet velocity and/or nozzle diameter.

The scatter because of non-reproducibility of the results is expected in complex biological systems. As pointed out earlier, the liquid contains various soluble inorganic and organic substances, proteins, colloids, and suspended solids; also, the liquid produced persisting foams.

Complications caused by the complex nature of the waste liquid do not allow the interpretation of the results in terms of the factors which influence oxygen transfer rate in gas liquid dispersion. For instance, surface active agents have a tendency to collect at the air-liquid interface. Surface covered by the agents will offer additional resistance to oxygen transfer. But, on the other hand, the surface active agents also increase the oxygen transfer by increasing the bubble retention time, since they collect at the rear of a rising bubble and offer a downward drag. Proteinous matter concentrates at the bubble surface and may block some of the surface area. High liquid viscosity would increase the bubble retention time and would tend to increase the oxygen transfer. Generally speaking, some factors might be tending to increase the oxygen transfer while the other would have decreasing effect.

Although no bubble size measurements were made qualitatively,

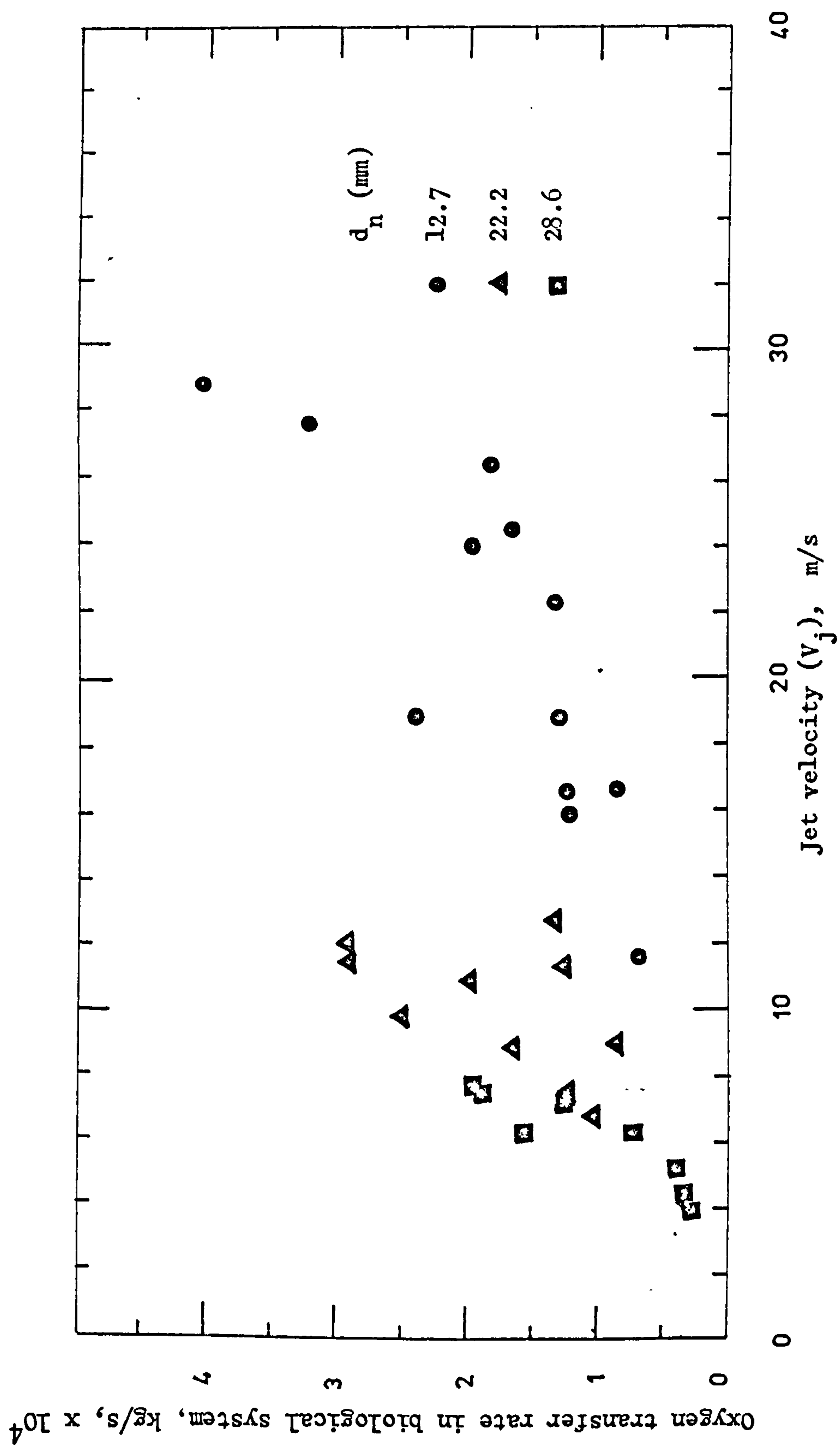


Figure 11.11. Effect of jet velocity on oxygen transfer rate in biological system for different nozzle diameters.

the bubble size distribution seemed to be affected by the nature of the liquid. The viscosity, surface tension and the film elasticity all affect the bubble size and the coalescence of bubbles. Bubble sizes ranging from extremely fine to large ( $\approx 10$  mm) were visually observed.

The short experimental time could have also contributed to the scatter of the results. The usual aeration time was in the range of 3 to 5 minutes. In a few experiments the aeration time was less than one minute. Generally speaking, as the experimental time is increased, the error caused by the lack of equilibrium of the interactions of various factors in the system is minimized. In fact, it is the same as saying that samples taken from longer time experiments would be more realistic than samples taken from shorter time experiments.

#### 11.2.4 Correlation of Oxygen Transfer with Power of Jet

The ratio of oxygen transfer rate ( $J^*$ ) in biological system to nozzle diameter ( $J^*/d_n$ ) is correlated with the power of jet ( $P_j$ ) in Fig. 11.12. The scatter is evenly distributed on either side of the regression line for each nozzle diameter. The correlation coefficient of this plot is 0.87.

Fig. 11.12 gives the correlation equation as

$$\frac{J^*}{d_n} = 1.96 \times 10^{-2} (P_j)^{0.72} \quad 11.6$$

where  $J^*$  is in kg/s,  $d_n$  is in m, and  $P_j$  is in kW.

In contrast, the oxygen transfer in the sulphite system is directly proportional to power of jet and the relation does not contain a  $d_n$  term.

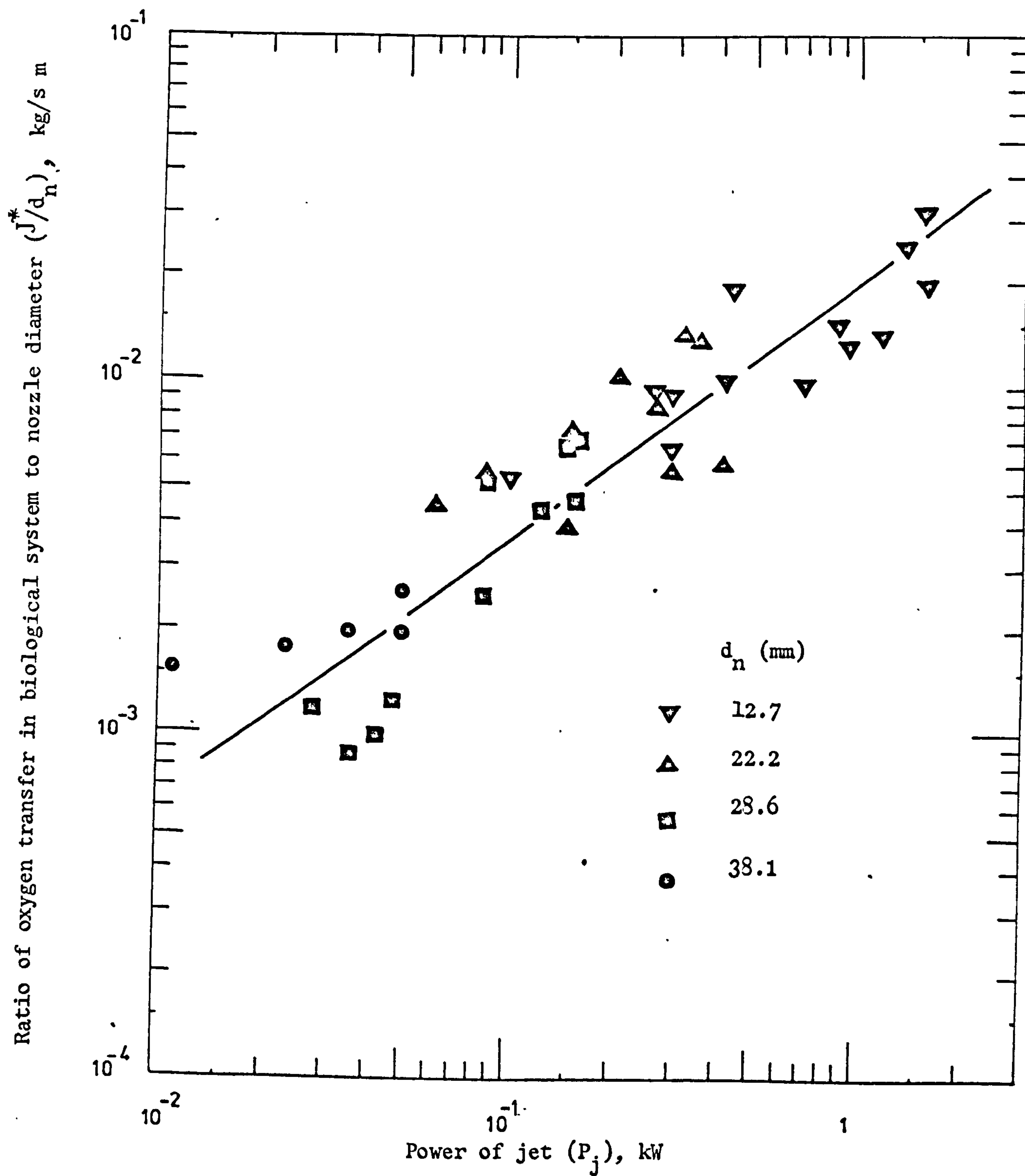


Figure 11.12. Correlation of oxygen transfer in biological system with power of jet.



The aeration efficiency ( $\text{kg O}_2/\text{kW h}$ ) is plotted against power of jet in Fig. 11.13.

With the increase of jet power there is a marked reduction in the aeration efficiency for the biological system. In contrast, for sulphite system there is very slight decreasing trend in aeration efficiency with the increase of jet power.

In general, it can be concluded that the lower the power of the jet the higher is the aeration efficiency. The optimum lowest power would be determined by the mixing and the oxygen demand of the biological system in any practical situation.

#### 11.2.5 Comparison of Oxygen Transfer in Tap Water, Sulphite Solution and Biological System

From the preceding discussion, it is clear that the behaviour of oxygen transfer with the increase of jet power is not the same for sulphite and biological system. A rough comparison between the oxygen transfer rates in water, sulphite and biological system is as follows:

At  $P_j$  equal to 0.268 kW:

Oxygen transfer rate in water (Fig. 11.10) =  $9.72 \times 10^{-5} \text{ kg/s}$ ,

Oxygen transfer rate in sulphite system =  $3 \times 10^{-4} \text{ kg/s}$ ,

Oxygen transfer rate in biological system =  $1.7 \times 10^{-4} \text{ kg/s}$ .

The comparison is possible at one power of jet since the oxygen transfer rate in the tap water was obtained only at 0.268 kW of jet. Therefore, from the above oxygen transfer rates it is estimated that at  $P_j$  equal to 0.268 kW,

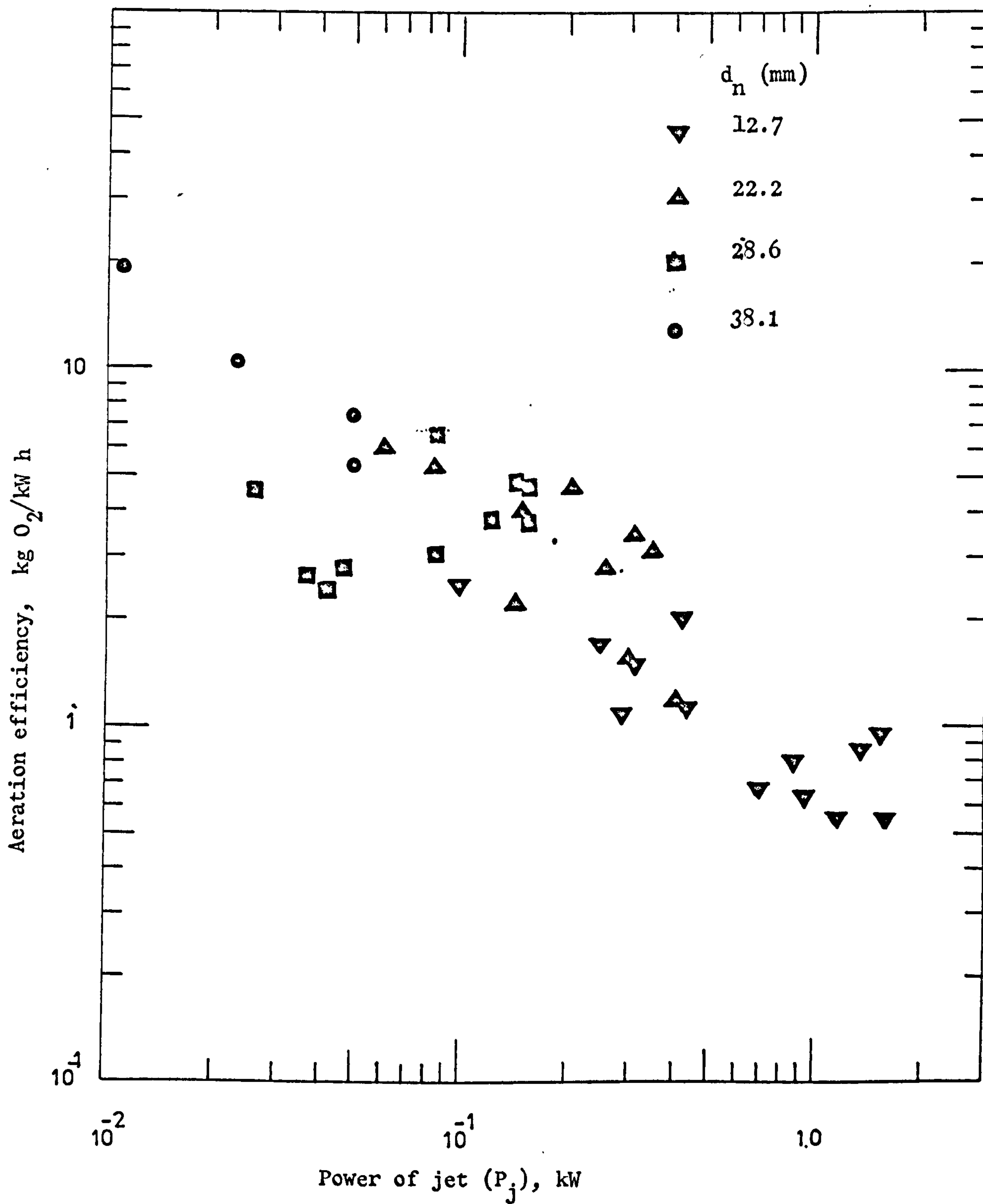


Figure 11.13. Relation of aeration efficiency with power of jet in biological system.

$$J_{\text{biol.}} = 1.75 J_{\text{H}_2\text{O}},$$

$$J_{\text{SO}_3} = 1.76 J_{\text{biol.}},$$

$$J_{\text{SO}_3} = 3 J_{\text{H}_2\text{O}}.$$

So the oxygen transfer rate in a biological system at 0.268 kW jet power is roughly 1.75 times higher than that of water. This, in fact, militates against the common practice of halving the oxygen transfer coefficient obtained with water when dealing with biological system; for instance, Robertson (97) favours this practice.

The oxygen transfer rate in biological system is higher than that in tap water due to the predominance of the factors described in 4.1, which enhance the oxygen transfer rate.

In the context of the present discussion, it should be noted that under zero dissolved oxygen concentration in a biological system, there is evidence to show that the oxygen transfer rate in biological system and the cobalt catalysed sulphite solutions are about the same. Table 11.1 compares the maximum biological oxygen transfer to sulphite oxygen transfer obtained with various organisms. It is obvious that under zero dissolved oxygen concentration (oxygen demand > oxygen supply) the maximum biological oxygen transfer can be approximated by the maximum oxygen transfer in cobalt catalysed sulphite solution. Similar results were obtained by Hunt et al. (53) who found that in a two impeller fermentor the oxygen transfer rates in sulphite and biological system (under oxygen limitation) were within 5% of one another.

TABLE 11.1

Ratio of Maximum Biological Oxygen Transfer Rate to  
Oxygen Transfer Rate in Cobalt Catalysed Sulphite  
Solution for Various Organisms Under Zero Dissolved  
Oxygen Concentration.

Organism	$O_2$ Transfer (Biol. System)	Investigator
	$O_2$ Transfer (Sulphite System)	
Serratia	0.97	Smith (109)
Aerobacter	1.62	Pirt ( 89)
Aerobacter	0.95	Pirt ( 89)
Azobacter	1.298	Owen and Johnson (83)
Saccharomyces	1.25	Maxon and Johnson(70)
Saccharomyces	1.02	Maxon and Johnson(70)
Saccharomyces	0.95	Maxon and Johnson(70)

However, the matter is still debatable, since Hirose et al. (51) found that the bacterial suspension, yeast suspensions in fermentation broth and sulphite system, all behaved differently in relation to oxygen transfer rate. They concluded that this different behaviour was due to the effect of the liquid properties on the liquid-film mass transfer coefficient ( $K_L$ ), and specific interfacial area ( $a$ ) as a result of change in bubble sizes.

In this work oxygen transfer rates in a biological system were obtained by reaeration and not under oxygen limiting conditions. In practice, aeration is performed at above critical oxygen concentration, so the results obtained in this work have more practical value.



### 11.2.6 Correlation of Oxygen Transfer Rate with Entrainment Rate

The oxygen transfer rate is correlated with the power of jet by the equation

$$\frac{J^*}{d_n} = 1.96 \times 10^{-2} (P_j)^{0.72} \quad 11.6$$

The data for the above correlation were obtained at 1.05 m jet length.

In 9.2.5 it has been shown that air entrainment in water and biological system is the same and is given by the equation:

$$\frac{Q_a}{d_n} = 0.855 P_j^{0.67} \quad 9.1$$

Equation 11.6 and 9.1 seem to be identical equations. The powers of  $P_j$  in the two equations are not significant from each other at 5% probability level.

Therefore,  $P_j$  can be eliminated from equations 11.6 and 9.1. Now the resulting equation is

$$J_{\text{biol.}}^* = 2.3 \times 10^{-2} Q_a \quad 11.7$$

Equation 11.7 shows that in a biological system the oxygen transfer coefficient or the oxygen transfer rate is directly proportional to the air entrainment rate. From this it also follows that the average bubble diameter remains constant for a certain biological system. This holds within the accuracy of the results presented here.

Oxygen transfer rate in sulphite system is given by

$$J_{\text{SO}_3} = 1.11 \times 10^{-3} P_j \quad 10.9$$

where  $J_{\text{SO}_3}$  is in kg/s and  $P_j$  is in kW.

Elimination of  $P_j$  from equations 10.9 and 9.1 gives

$$\frac{Q_a}{d_n} = 81.2 (J_{SO_3})^{0.67} \quad 11.8$$

Or:

$$J_{SO_3} = 1.43 \times 10^{-3} \left(\frac{Q_a}{d_n}\right)^{1.49} \quad 11.9$$

The equations 11.7 and 11.9 show that:

- (1) Oxygen transfer in sulphite system increases at a faster rate than that in biological system when the entrainment increases.
- (2) In a biological system nozzle diameter has no effect on the relationship of oxygen transfer rate with air entrainment rate; however, in sulphite system, at constant entrainment rate the oxygen transfer increases with the decrease of nozzle diameter.

### 11.3 PERFORMANCE OF PLUNGING JET REACTOR AS CONTINUOUS BIOLOGICAL REACTOR

#### 11.3.1 Experimental

The experimental apparatus described in 9.1 was converted to a biological continuous reactor by connecting a liquid overflow to the tank (Fig. 11.14) and feeding the liquid to the tank at constant flow rate.

For the 10 days retention time, small volumes of the liquid were fed intermittently by the small bucket feeding system (Plate XIII). A litre capacity tipping bucket was made of steel. The bucket rested on two supports and above the liquid sump. It was pivoted on the front support and could be tipped by lifting the rear end. The tipping was accomplished by connecting a swivel a little away from the periphery of the 20 cm diameter disc to the rear of the

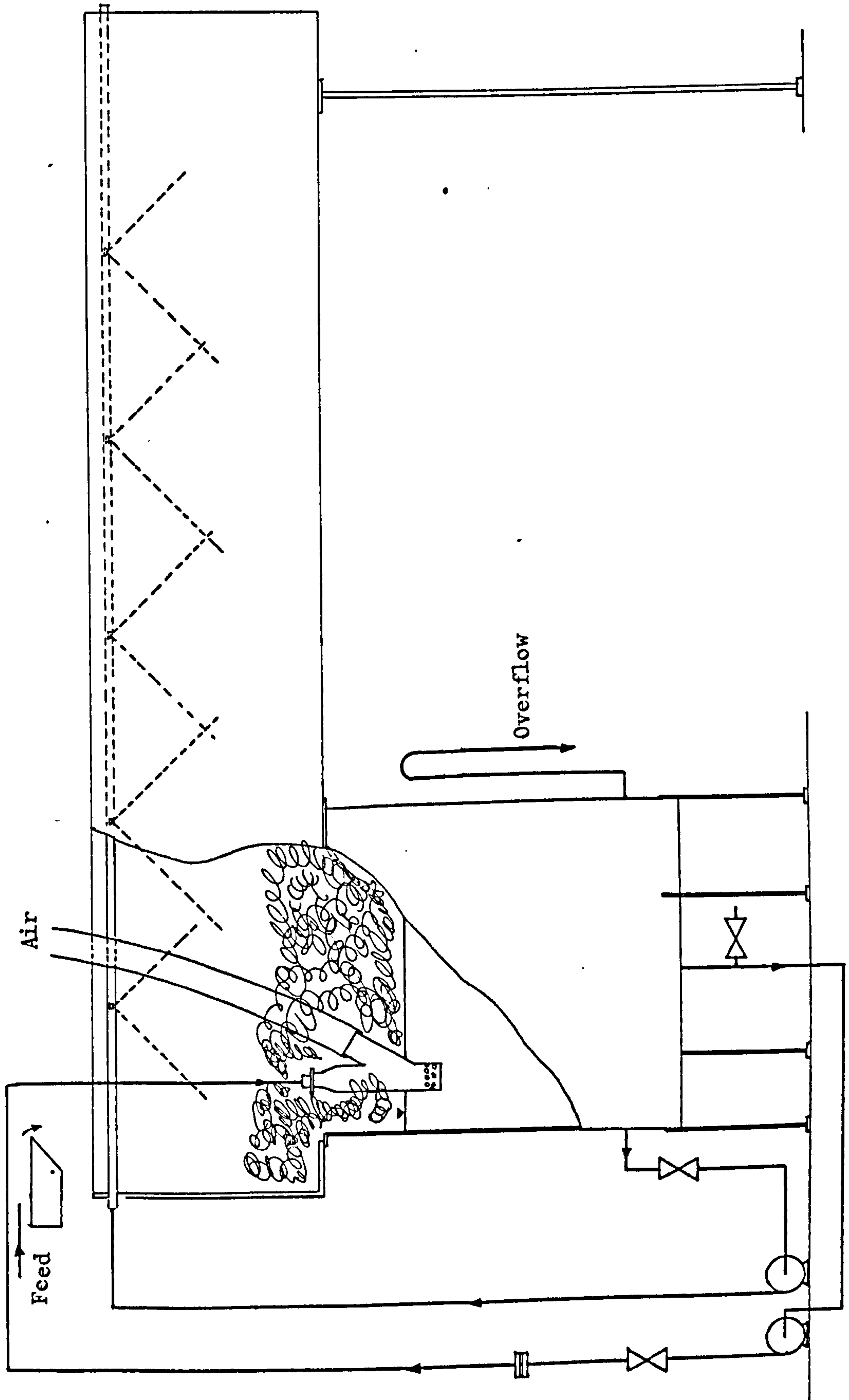


Figure 11.14. Flow diagram for continuous biological reactor plant.

bucket by a string and rotating the disc through one revolution. Hence, in one revolution the bucket was tipped and brought back to its horizontal position.

The liquid was not fed directly into the bucket. But, in fact, it was poured on a small hole in a 2 inch pipe connected to one side of the bucket. The other end of this pipe was closed. A small portion of liquid being pumped passed through the small hole into the 2 inch pipe and then accumulated in the bucket; the rest dropped into the sump and then drained into the storage tank. The flow of liquid into the bucket was obstructed by a shield. The shield was fixed to the wall connected to 2 inch pipe and  $\frac{1}{8}$  inch gap was kept between the shield and the wall. The liquid flowing into the bucket was diverted downwards by the shield.

The probe in the bucket sensed the liquid level in the bucket and stopped the feed pump. The bucket was calibrated to meter 900 ml of liquid, by adjusting the probe to sense the level of 900 ml liquid in the bucket. The liquid was then fed to the bucket by the feed pump and the volume collected in the bucket was measured by a measuring cylinder. The mean of 14 calibration experiments was 907 ml and the standard deviation was  $\pm 21.8$  ml. The bucket feeding system was fixed over the aeration tank and the bucket tipped the liquid directly into the tank.

A disc was connected through a flexible shaft to a  $\frac{1}{4}$  horse power geared motor, with an output speed range of 3 to 27 rpm (Allspeak Ltd., Accrington, England). The metered liquid was fed at predetermined time intervals by the automatic control circuit



shown in Fig. 11.15 and Plate XIV. A timer unit (Programmable Drum Timer 554H240V 2 Contact 1 hour, Electroplan Ltd., Royston, England) was set to operate the pump after every 15 minutes. The feed pump was stopped as the probe sensed the liquid level in the bucket and the geared motor started automatically to tip the bucket. A roller type limit switch (Limit switch H 530/H001 10 Amps/120 volt 6 amps/5 volt, P.S.J. Controls and Panels, Electrical, Bedford, England) was actuated by a cam fixed to the motor shaft so as to stop the motor at the end of one revolution. The tipping of bucket was accomplished automatically after whenever the feed pump filled the bucket with liquid.

907 mls of liquid were fed intermittently after an interval of 15 minutes and thus liquid feed rate was 3.63 lt./h. The volume of liquid in the aeration tank was  $0.88 \text{ m}^3$ .

For short residence time (28.4 hours) the liquid was fed to the tank by a syphon feeding system (Fig. 11.16). A siphon made of 2 inch pipe connections was connected to the base of a rectangular tank  $0.6 \text{ m} \times 0.43 \text{ m} \times 0.43 \text{ m}$ . The slurry from a storage tank was pumped to a circular settling tank from where it overflowed into the feed tank. When the liquid column in the tank rose to a point where the siphon began to work, the probe sensed the liquid level and stopped the feed pump. The height of the liquid column required for the siphon to work was critical. A fraction of liquid column ( $\Delta h$ ) was siphoned to the tank as the feed. The inlet of the siphon was well above the tank base and hence the settled solids even after several weeks could not block the inlet of the siphon.

The feed pump was connected electrically to a timer unit. The timer was set to operate the pump once each hour. Thus 5.27 gallons

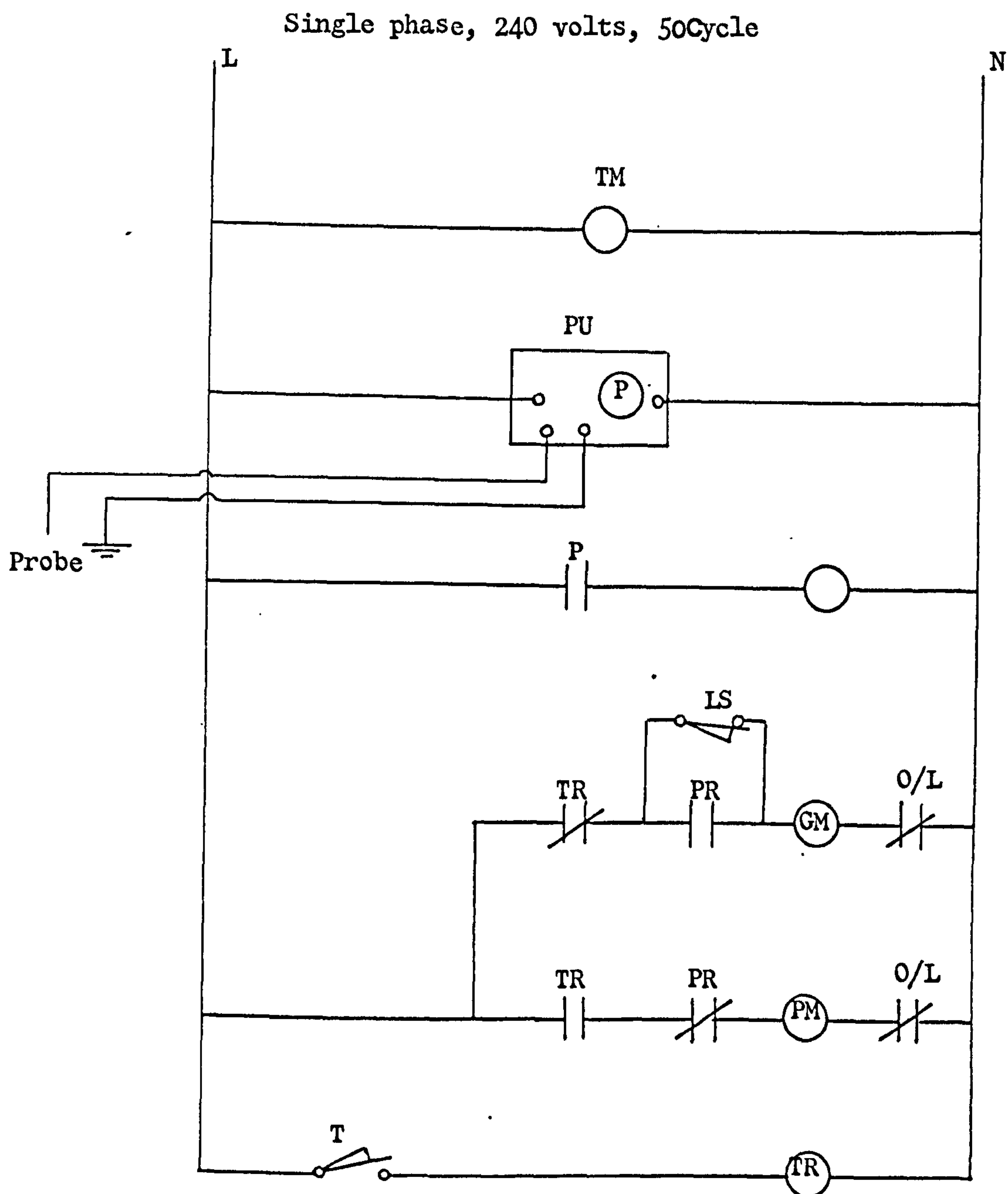


Figure 11.15. Control circuit for intermittent bucket feeding.

TM Timer motor  
 PR Probe relay  
 P Relay in probe unit.  
 LS Limit switch  
 TR Timer relay  
 T Timer switch  
 GM Geared motor  
 PM Pump motor  
 PU Probe unit

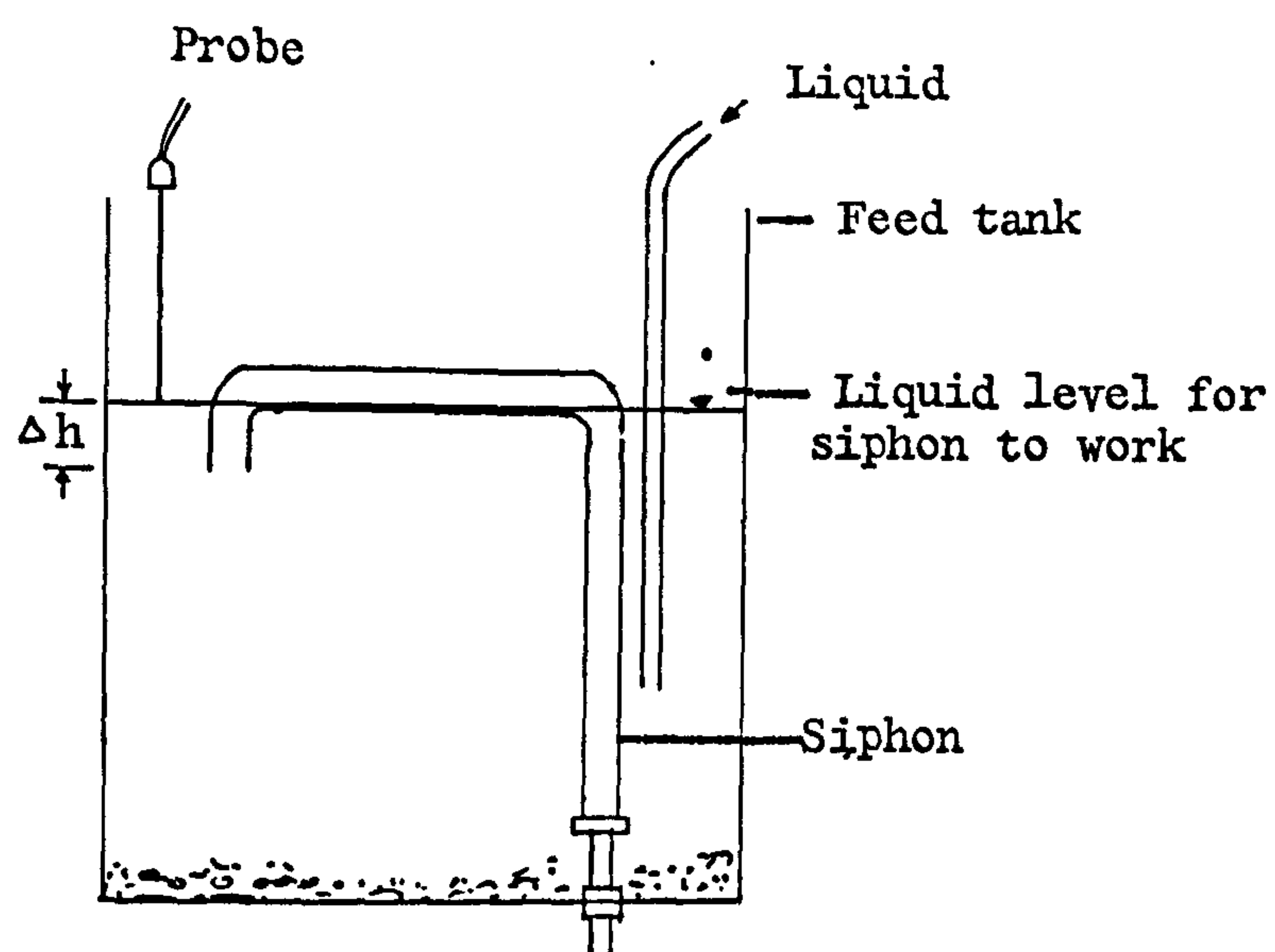


Figure 11.16. Syphon feeding system.

of liquid was fed to the tank at the start of each hour. Because of this intermittent feeding, the aeration process was on a semi-continuous basis; the reactor operated as a batch reactor for about an hour after every feed.

The ambient temperature and the liquid temperature in the aeration tank were measured by the thermocouples and were recorded continuously. Fig. 11.17 shows the calibration curve for the thermocouples.

The concentration of dissolved oxygen in the aeration tank was measured by EIL dissolved oxygen meter and was recorded continuously. In continuous experiments the dissolved oxygen meter probe was in the tank.

During the continuous operation of the aeration plant, the foam was controlled by liquid sprays (11.1.2.3). The pump used for the liquid sprays was smaller (68 feet head, 4000 gallons/hour flow rate) than that used for the plunging jet (95 feet head, 10000 gallons/hour flow rate). It was observed that the spray pump was not able to spray, while the jet pump was working as explained later.

In order to control the foam, the liquid was aerated for 45 minutes and foaming was allowed to occur uncontrolled by stopping the spray pump. The jet pump was then stopped and the spray pump was started to break the foam for the next 15 minutes. Hence a 45 minutes aeration and 15 minutes defoaming cycle was repeated every hour and was controlled automatically by two timer units. The wooden trough was allowing the foam to spread as well as storing the foam built up during aeration. Later, the cycle was



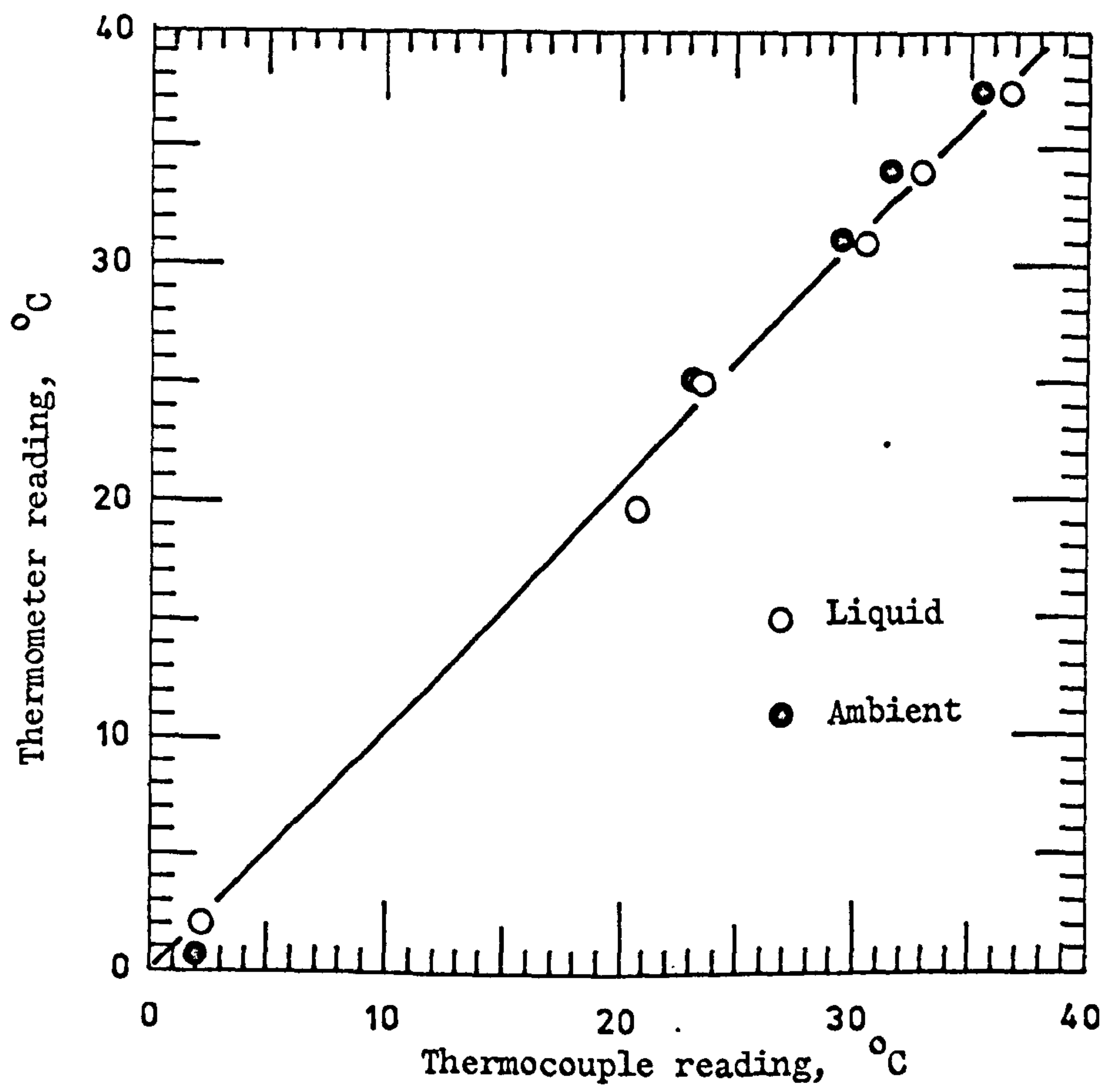


Figure 11.17. Thermocouples calibration curve.



**Total Solids:** The residue remaining when the water is evaporated from a sample of water, sewage, other liquids, or semi-solid masses of material and the residue is then dried at a specified temperature (usually  $103^{\circ}\text{C}$ ). The weight of residue as percentage of the weight of sample prior to evaporation is expressed as per cent dry matter (% DM).

The pollution parameters were determined by the standard methods (79, 113). The procedures of these methods are described in Appendix IV.

Since a waste sample is a mixture of water, dissolved solids and suspended solids, it was thought interesting to determine the individual COD and BOD of the soluble and insoluble solids for feed and product samples.

For this purpose, the samples were also centrifuged to separate liquid from solids. Liquid-solid separation could not be obtained for actual samples by using the available 2000 g laboratory centrifuge. The separation was found to be possible on 1:10 diluted feed samples and 1:5 diluted product samples. So the procedure was to take 10 ml of feed sample and 20 ml of product sample and then dilute them by their respective dilution factors. 35 ml of the diluted sample was centrifuged in duplicate. The centrifuged liquid was then filtered through a Millipore filter of 47 mm diameter and  $0.8\text{ }\mu\text{m}$  pore size. So the filtrate did not contain any solids greater than approximately  $1\text{ }\mu\text{m}$  in size. The product liquid passed through the filter easily leaving behind negligible fine solids on the filter paper as compared to the liquid from the feed sample. This, in fact, shows that a considerable portion of fine



solids in the feed is removed either by degradation or by adsorption during biological treatment.

The BOD (casual measurements) and COD analyses were performed on 5 ml of the filtrate liquid. The results were adjusted for the dilution by multiplying the results with the dilution factors.

Oxygen demand by solids (dissolved or suspended) in kg/kg of solids (dissolved or suspended) was calculated for feed and product liquid by the method illustrated in Appendix IV.

The statistical analysis of the results of a planned experimental program to determine the accuracy of COD analyses showed that a difference of 500 ppm is practical level of tolerance between paired routine analyses (Departmental Note: DN/HC/173/3000, National Institute of Agricultural Engineering, Silsoe, Beds., England). In part of the work COD analyses were performed in duplicate and the mean was adopted.

In experiments aimed at determining the effect of pH on foam, ammonia and nitrate nitrogen were also determined two times per week on product samples. The methods of determination of ammonia and nitrate nitrogen are described in Appendix IV.

The pH of the tank liquid was also recorded when investigating the effect of pH on foam production.

All experimental results of this part of the work are tabulated in Appendix V.



### 11.3.2 Results and Discussion on the Performance of Plunging Jet Reactor as a "Biological Continuous Reactor"

Before discussing the actual results, it seems important to discuss the operational aspects of the continuous plant. Continuous operation of the biological reactor on a pilot plant scale posed several practical problems. Break-downs happened during continuous running due to one reason or another, as happens with other plants in practice. Obviously, this was detrimental to the continuous data collected in a continuous experiment. It is easy to control the variables when the experimental run time is in hours but it is far more difficult to maintain uniformity among various variables for continuous experiments lasting for several days or even months. In addition, physical or chemical changes which are unnoticed in short duration experiments are considerably magnified in long term continuous experiments.

For instance, foaming which was not a problem as regards plant operation in reaeration experiments, became a severe problem in continuous experiments. Solution of this problem in itself resulted in additional problems. For example, the spray nozzles were found to be clogged after a few days of operation. So the plant had to be shut down. The nozzles were redrilled with a larger hole. In addition, the baffle plate was covered by a filter having a shape of a cylindrical cap, and made of steel sieve plate, with numerous 3 mm diameter holes. Initially, a fraction of liquid flow was tapped from the outlet piping of the aeration pump for spray purposes. With this arrangement only one or two nozzles were able to produce spray and the liquid just poured out through the remaining nozzles. This was due to

inadequate pressure head at the inlets of the spray nozzles. So the spray system was modified. A separate pump was used for the liquid sprays.

Though a separate pump was being used for the spray nozzles, the sprays were still not effective during the aeration. At the start of the aeration, the sprays were produced with full pressure, but after a while the liquid came out of the nozzles in the form of conical sheets which later disintegrated and sprinkled drops over the foam. This could be explained as follows. In air-water system the most of the entrained bubbles rise to liquid surface and burst at the liquid surface, thus releasing the air to atmosphere. On the contrary, when foam is formed, the bubbles are prevented from bursting and the surface bubbles are more prone to be recirculated in the system. This would increase the gas hold up. Lack of coalescence would increase the population of finer bubbles due to shearing action of the jet. A liquid sample from the aeration tank showed the existence of extremely fine bubbles. Under these conditions, a substantial amount of air in the form of fine air bubbles passing through the pumps would reduce the liquid flow rate. This was found true in continuous experiments. The liquid flow rate dropped from its initial setting. This substantial amount of air flowing through the pump caused poor sprays.

On a few occasions, the spray pump failed to pump any liquid due to an air lock in the suction piping. This was really surprising. When the spray pump was switched off for a moment and then restarted, the sprays came into action. By stopping the pump, in fact, the suction pipe was refilled with liquid from the tank by gravity and the air lock was removed.



The foaming was then controlled by separating foaming (aeration) and defoaming operations. The spray pump was stopped during aeration (foaming) and the foam accumulated into the wooden trough. When the wooden trough was filled up to the top with foam, the aeration was stopped and the spray pump started for defoaming. So the foaming and defoaming cycle was repeated automatically. This, in fact, provided an effective and practical solution to foam problems. In any situation defoaming time should be minimum and aeration time should be maximum.

Foaming and defoaming times entirely depend upon:

- (a) Foam storage capacity;
- (b) Air entrainment rates;
- (c) Defoaming efficiency of the spray system;
- (d) Stability of foam.

For a given plant air entrainment rate and the foam storage capacity will determine the aeration or foaming time. Stability of the foam and the defoaming efficiency of the spray system will determine the defoaming time.

Foam storage capacity depends upon the design of aeration tank and on the additional cost involved in adding foam storage to the aeration vessel. If underground aeration is used, then the storage of foam on level ground would be simple.

Air entrainment rate will depend upon oxygen requirements. During aeration dissolved oxygen concentration rises and during defoaming it falls. Under optimum aeration conditions, it is possible that the dissolved oxygen concentration would be zero. Thus the effect of both zero dissolved oxygen concentration and its

duration on the micro-organisms should be considered while deciding on oxygen transfer rates and defoaming time. Short durations (a few minutes) have no significant effect on microbial populations (98). Similarly, zero dissolved oxygen concentration for such short duration will not have any significant harmful effect on organisms. If there happens to be some small effect, this has to be accepted in the larger interest of economic plant operation. In the present work the dissolved oxygen concentration fell to zero during defoaming at 28 hours retention time. But for 10 days retention time, the dissolved oxygen concentration was never zero during defoaming. Moreover, the dissolved oxygen concentration was usually near saturation in 10 days retention time experiments. It was not possible to reduce the concentration of oxygen by reducing the jet liquid flow since the flow was already considerably throttled. Further throttling of flow would definitely ruin the pump seal.

Defoaming efficiency of the spray system will depend upon the spray pump capacity, number of nozzles and the design of spray nozzle. In this work, hollow cone spray nozzles were selected because they are less susceptible to clogging. However, solid cone sprays would be more efficient in defoaming. But this requires a special design of this nozzle which could handle slurry without clogging.

In this work it was observed that the stability of foam depended upon the loading rate. With the high loading rate the foam was persisting, whereas with the low loading rate the foam was easy to control. So, the loading rate is also a key factor in the design of a foam control unit.



In fact, the exact and quantitative relationship between the above factors invites a systematic long term research work. The present work suffices to give a practical solution to the foam problem and points out the important factors involved in this solution.

Design of a continuous feed system also posed some problems. Initially, siphon feeding was designed and a siphon made of one inch steel piping was used. It worked well for a few days and then clogged. It seemed that the solids settled in the horizontal part of the tube and thus increased the critical liquid column height at which the siphon begins to work. Moreover, when some stray foam bubbles on the liquid surface contacted the probe, the feed pump was stopped. So the liquid could not reach the actual height at which the siphon begins to work. These problems were solved by using a 2 inch pipe siphon and feeding the liquid to the feed tank gently so that no foam or bubbles were produced. After this modification, the siphon feeding system worked for several days without any break-down. The siphon feeding system could only be used for the short retention time for the volume of aeration tank used in this work.

For the long retention time, the small volume bucket feeding system was designed and has been described in 11.3.1.

The point to be stressed here is that a considerable time and effort were spent in making the continuous biological system work for research as well as for practical purposes. So the results presented in this part of the work lack high precision because of the difficulty in maintaining constant plant condition over long periods of time. This is left for future workers to

operate the plant with better control of the variables involved.

In the present work the performance of the continuous reactor at 28 hours and 10 days retention times was studied and the results along with discussion are presented in the following paragraphs.

Figs. 11.18 and 11.19 show the COD of feed and product for 28 hours and 10 days retention times, respectively. The results are highly scattered and prevent the drawing of any definite conclusions. However, there is an indication which will be described later that steady conditions were reached after 5 days for 28 hours retention time and after 15 days for 10 days retention time.

For 28 hours retention time the COD of feed was in the range of 60,000 to 84,000 mg/lt, whereas for 10 days retention time was in the range 31,000 - 41,000 mg/lt. The variations in feed COD for 28 hours retention time are much greater than those for 10 days retention time. It is obvious that feed COD was not uniform in either case.

It should be noted here that the first experiment was performed with 28 hours retention time. The feed was taken from a storage tank which used to serve as a source of feed for some other full scale treatment plants. Because of the high feed consumption of these other large scale plants the storage tank was refilled frequently with fresh liquid, which did not always have the same composition. This fact is manifested in the large variations in COD of feed samples.

The variations in feed liquid composition were avoided by taking a feed from a separate storage tank which was filled only

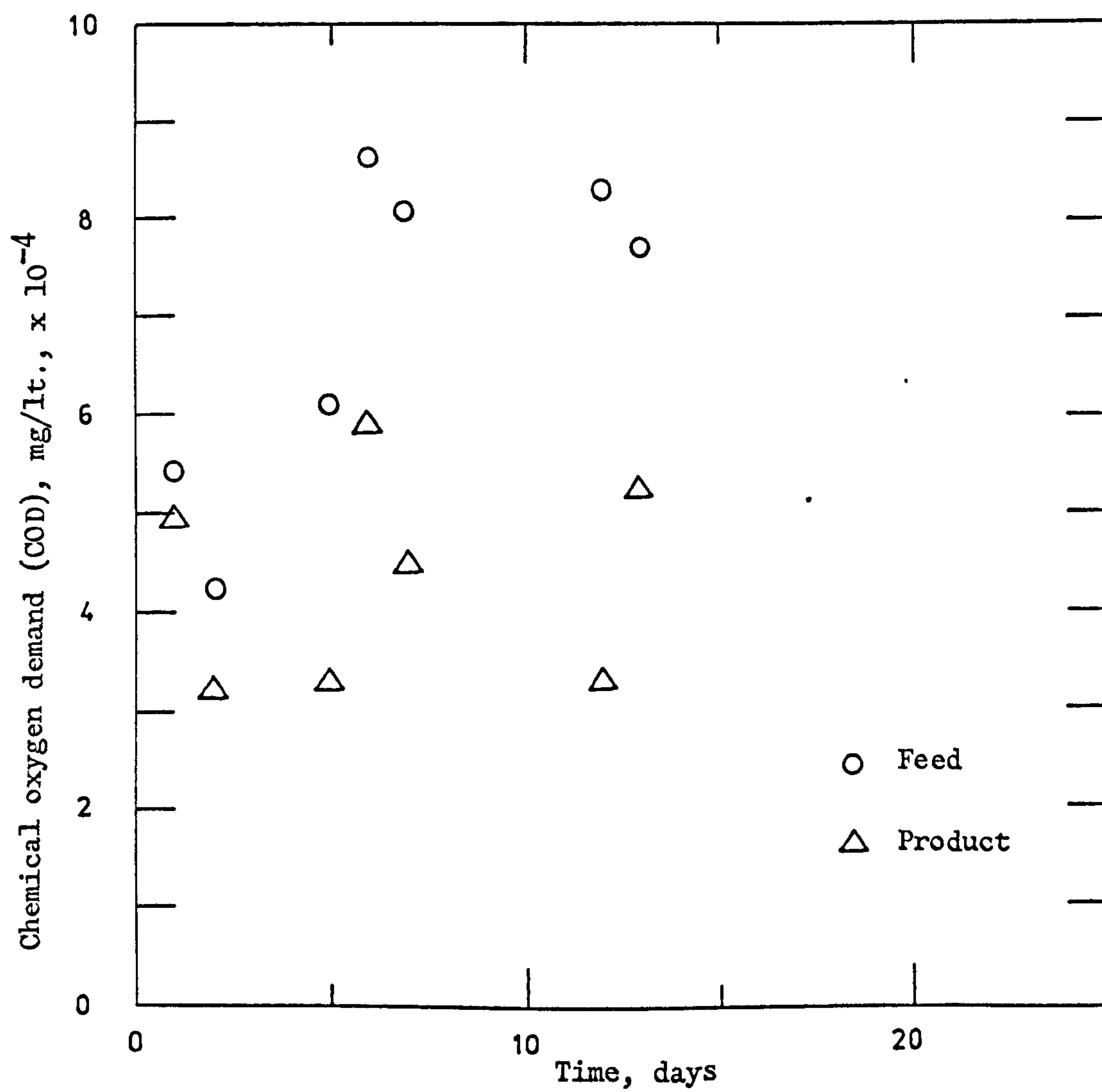


Figure 11.18. Variations in COD of feed and product in continuous biological reactor (retention time 28 hours).

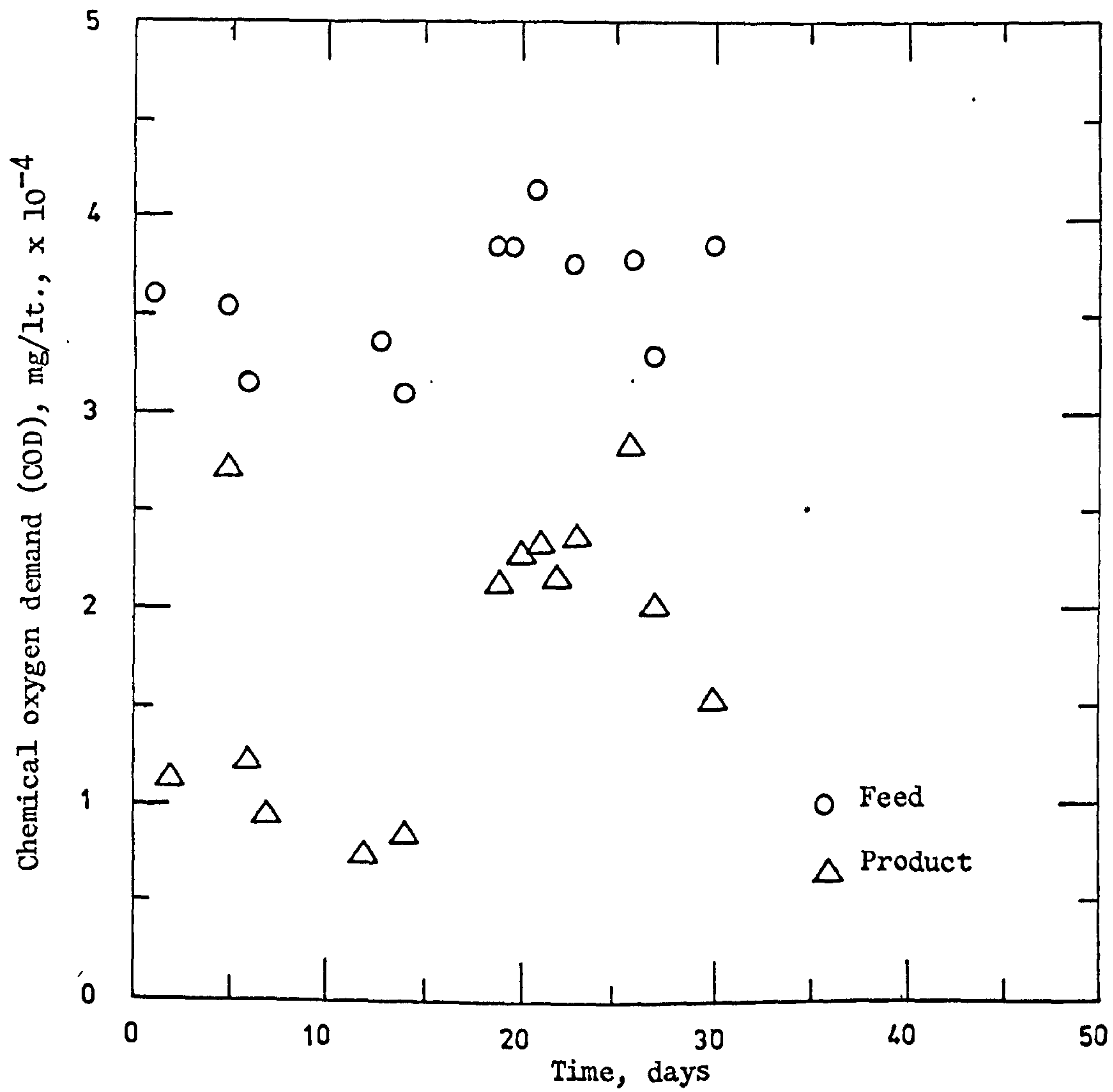


Figure 11.19. Variations in COD of feed and product in continuous biological reactor (retention time 10 days).



once at the start of the experiment. Experiments at 10 days retention time were performed with this improvement. Fig. 11.19 shows the reduction in scatter in COD of feed.

In Fig. 11.18, after 5 days the feed CODs are roughly consistent. By taking mean of feed CODs and mean of product CODs, the percentage reduction in total COD for 28 hours retention time is 41%. This is a rough estimate.

Similarly, for 10 days retention time (Fig. 11.19), by taking mean of feed CODs and product CODs at steady conditions (after 15 days) the reduction in COD is 45%. It is surprising that the per cent reduction in COD for 28 hours and 10 days retention time is nearly the same.

Figs. 11.20 and 11.21 show the variations of liquid CODs in feed and product at 28 hours and 10 days retention time respectively. There is negligible scatter in Fig. 11.21. Also the scatter is not much in the liquid COD of the product at 28 hours retention times. From these results it is concluded that the presence of suspended solids causes considerable scatter in the results shown in Figs. 11.18 and 11.19. As already stated that the scatter in the liquid feed COD for 28 hours retention time is, in fact, due to daily variations in the quality of liquid in feed storage tank.

It is worth noticing that the variations of liquid CODs in the feed have not greatly affected the liquid COD of the product. From this it can be concluded that the completely mixed continuous system has a great affinity towards equilibrium conditions, and has the ability to absorb shock loadings due to sudden variations in feed strength to some extent.

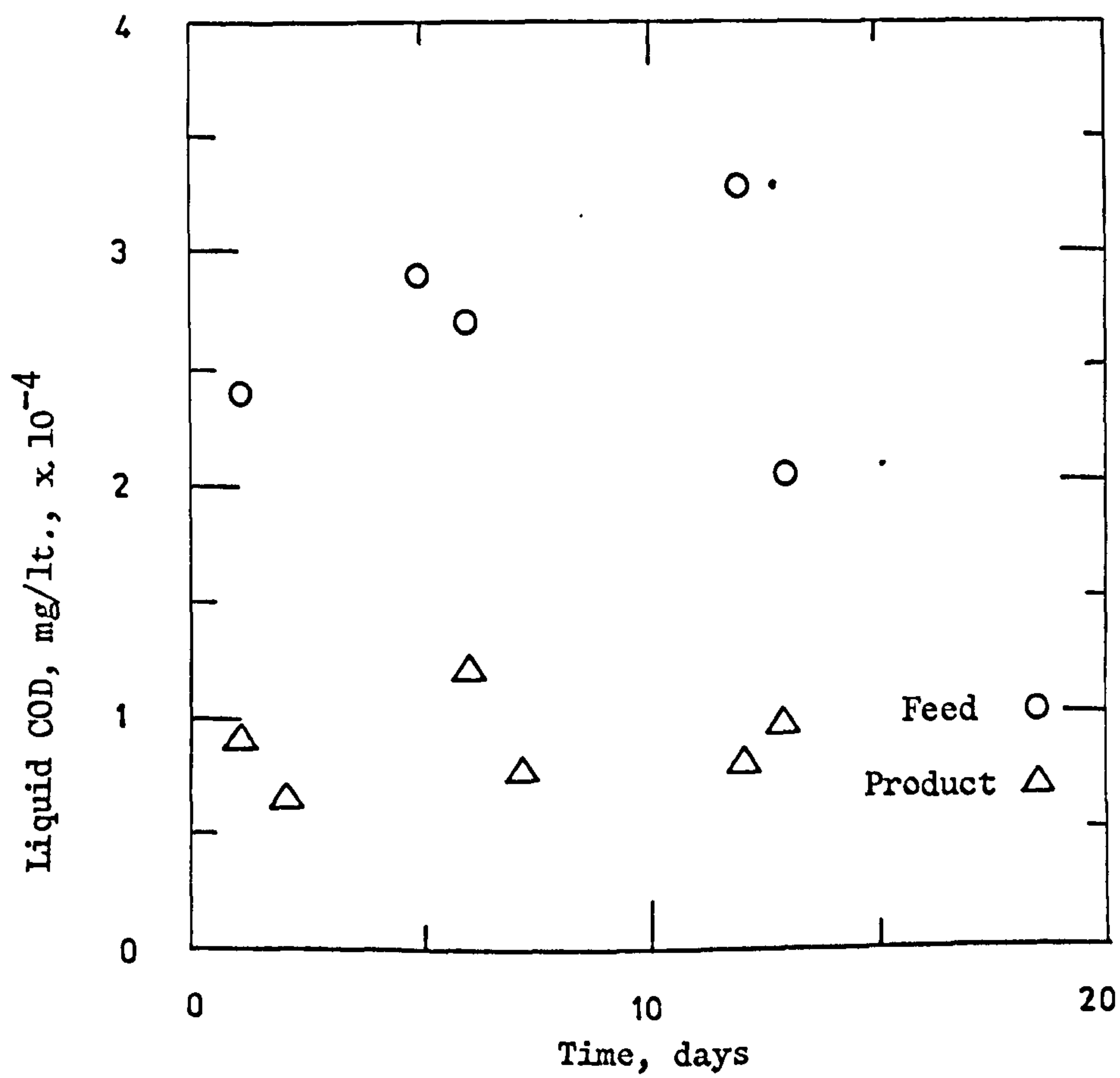


Figure 11.20. Variations in liquid COD of feed and product in continuous biological reactor (retention time 28 hours).

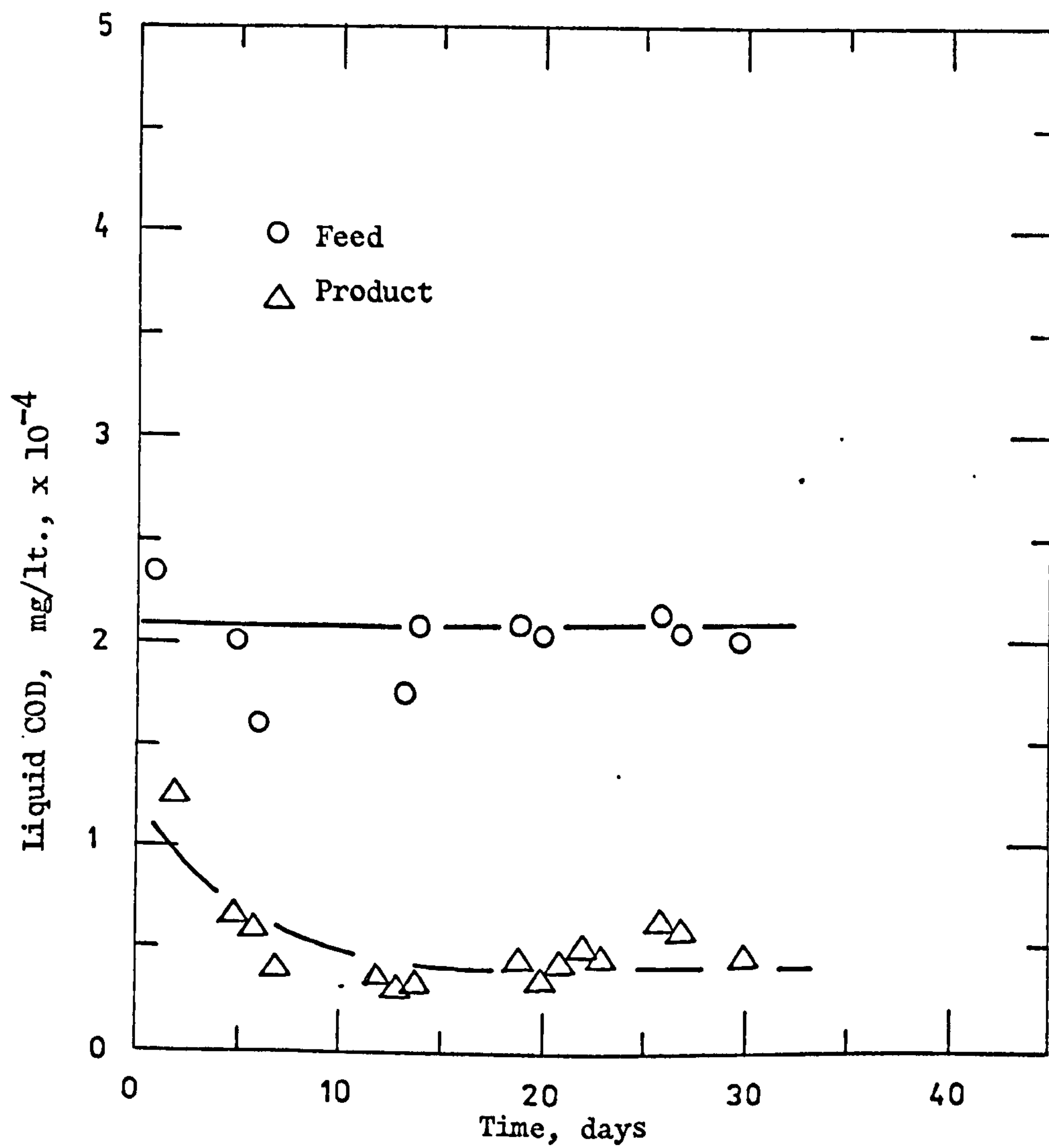


Figure 11.21. Variations in liquid COD of feed and product in continuous biological reactor (retention time 10 days).

At steady state the reduction in liquid COD is 64% and 78.6% for 28 hours and 10 days retention time respectively.

Figs. 11.22 and 11.23 show the variations in CODs of dissolved and suspended solid fractions in feed and product at 28 hours and 10 days retention time respectively. Again, the scatter in the results is high. Also no definite conclusions can be drawn.

However, a rough estimate can be obtained. Note that the scatter is considerably reduced in case of dissolved solids in the product.

The results show that kg COD in dissolved solids per kg of dissolved solid in the product is approximately equal to 0.8 for 28 hours retention time, and 0.5 for 10 days retention time.

From Fig. 11.22 at 28 hours retention time:

For feed (dry basis):

$$\text{Mean kg COD of dissolved solids/kg dissolved solids} = 2 \text{ (SD = } \pm 0.92 \text{)}$$

$$\text{Mean kg COD of suspended solids/kg suspended solids} = 1.48 \text{ (SD = } \pm 0.2 \text{)}$$

For product (dry basis):

$$\text{Mean kg COD of dissolved solids/kg dissolved solids} = 0.88 \text{ (SD = } \pm 0.5 \text{)}$$

$$\text{Mean kg COD of suspended solids/kg suspended solids} = 1.36 \text{ (SD = } \pm 1.07 \text{)}$$

SD stands for standard deviation.

Similarly from Fig. 11.23 at 10 days retention time:

For feed (dry basis):

$$\text{Mean kg COD of dissolved solids/kg of dissolved solids} = 1.92 \text{ (SD = } \pm 0.52 \text{)}$$

$$\text{Mean kg COD of suspended solids/kg of suspended solids} = 2.36 \text{ (SD = } \pm 1.62 \text{)}$$



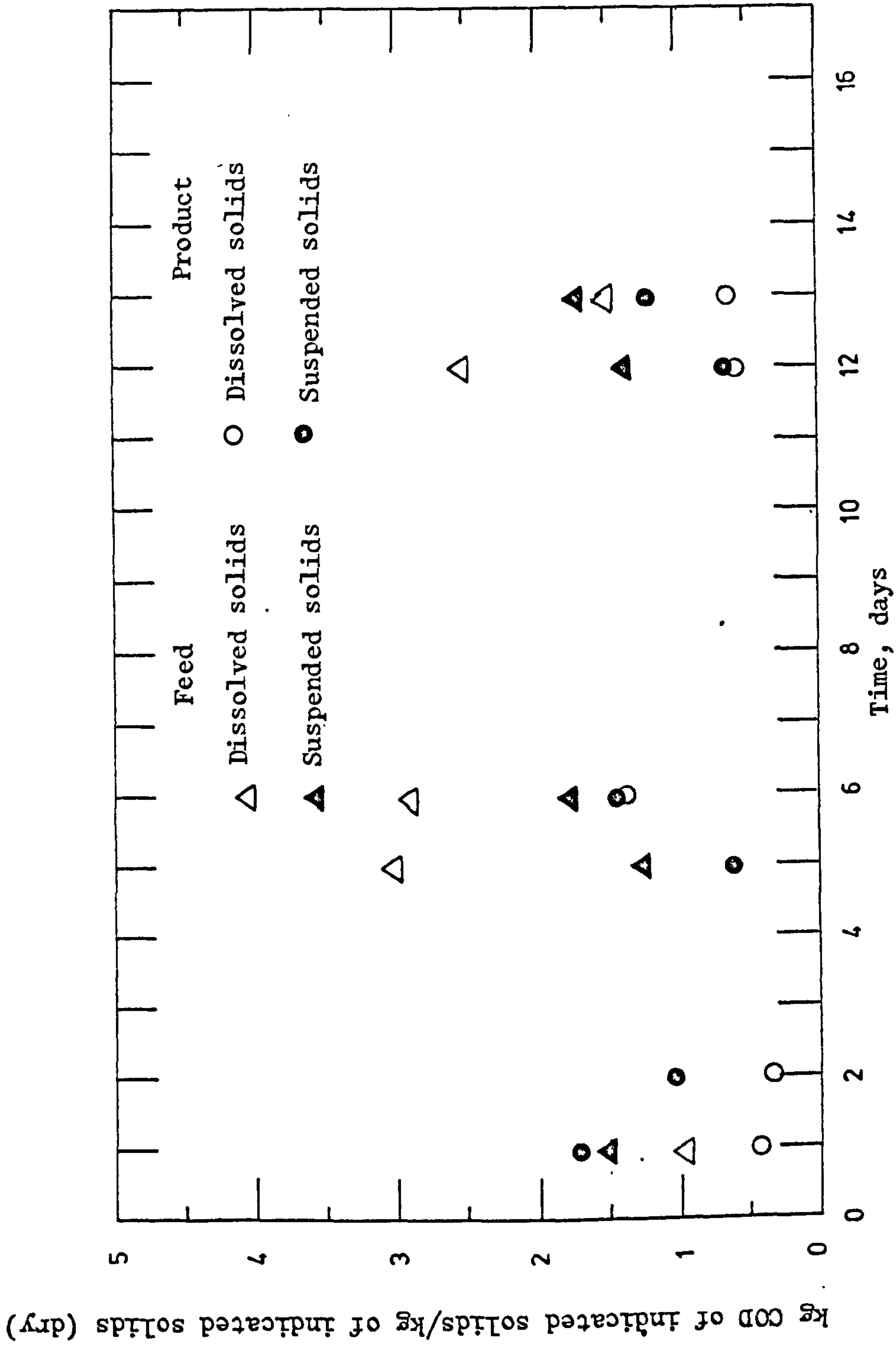


Figure 11.22. Variations in solid COD per kg of dry solids in feed and product samples for dissolved and suspended solids (retention time 28 hours).

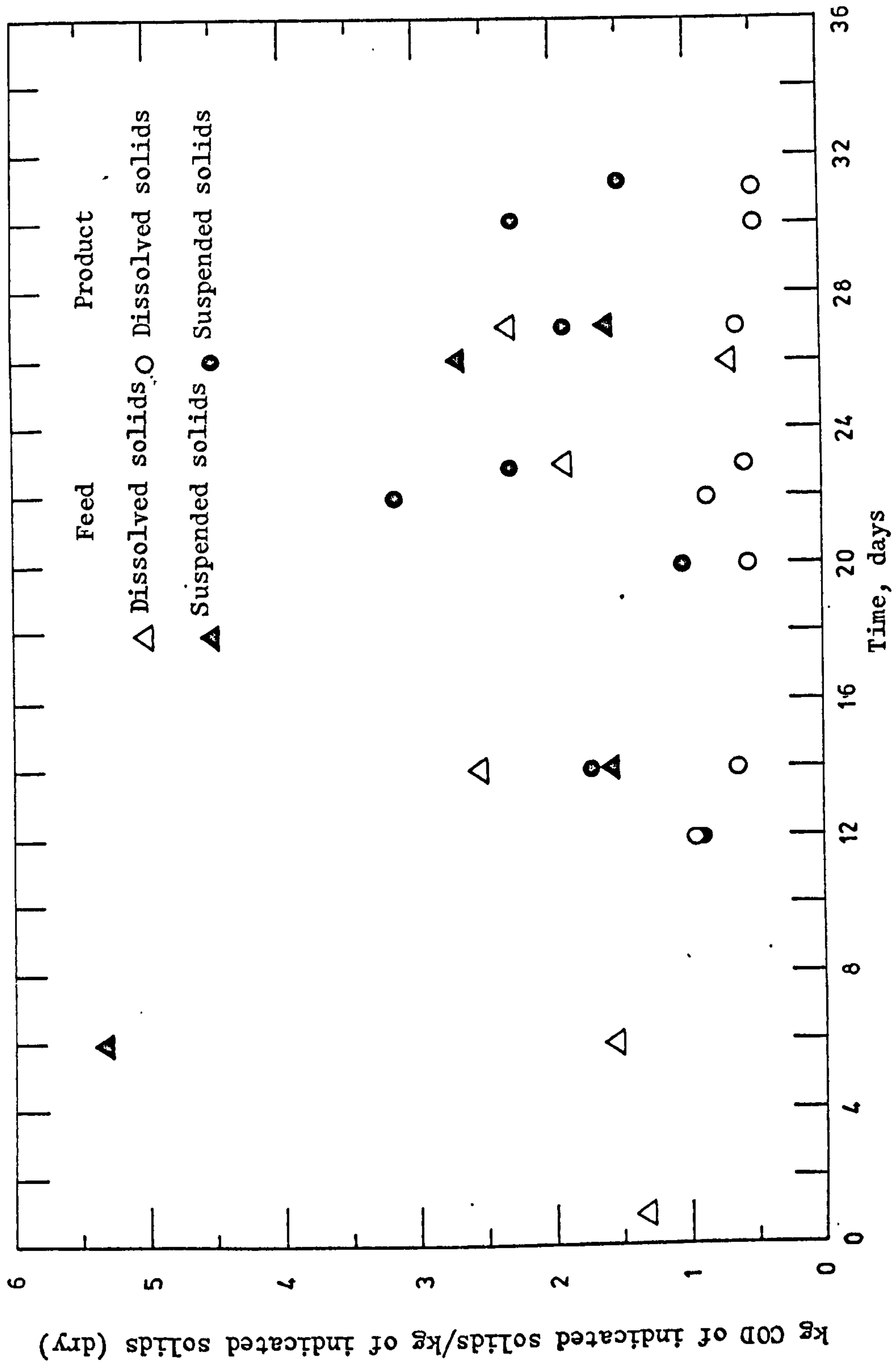


Figure 11.23. Variations of solid COD per kg dry solid in feed and product samples for dissolved and suspended solids (retention time 10 days).

For product (dry basis):

$$\text{*Mean kg COD of dissolved solids/kg of dissolved solids} = 0.6 \text{ (SD} = \pm 0.14 \text{)}$$

$$\text{*Mean kg COD of suspended solids/kg of suspended solids} = 2.12 \text{ (SD} = \pm 1.42 \text{)}$$

\* Mean values obtained from data after 15 days - at steady-state conditions.

From the above results, there is 68 and 32% reduction in COD of dissolved solids/kg of dissolved solids (dry) in feed for 10 days and 28 hours retention time respectively. In contrast, there is no significant reduction in COD of suspended solids at both retention times.

From the knowledge of BOD and COD data of feed and product at steady conditions, the following approximate estimates of BOD and COD removal efficiencies were made:

At 28 hours retention time:

$$\text{kg COD removed/kW h} = 4.9$$

$$\text{kg BOD removed/kW h} = 2.3$$

At 10 days retention time:

$$\text{kg COD removed/kW h} = 3.3$$

$$\text{kg BOD removed/kW h} = 2.3$$

The results at 28 hours retention time are not so accurate as those of 10 days retention time because of large deviations in feed COD. Efficiency in terms of BOD is expected to be low because BOD removed is on 5 day basis and also BOD is physically different from COD.

The variations of concentration of suspended solids in the biological continuous reactor for 28 hours and 10 days retention

times are shown in Figs. 11.24 and 11.25. The steady state value of suspended solid concentrations at 28 hours and 10 days retention times are  $3 \times 10^{-2}$  and  $1.5 \times 10^{-2}$  kg SS (dry)/kg mixed liquor. The suspended solids concentration increased to 120% and 125% in 28 hours and 10 days retention times respectively.

The reactor liquid temperature varied from 26 to 40°C and 4 to 19°C for 28 hours and 10 days retention time, respectively. Similarly ambient temperature varied from 8 to 17°C but for most of the period the ambient temperature was about 10°C in case of 28 hours retention time. These experiments were performed in summer. The experiments on 10 days retention time were performed in winter and the ambient temperature was in the range - 5 to 8 °C and for most of the period the temperature was about 4°C. The experiments with 28 hours retention time were performed over a period of 18 days whereas with 10 days retention time the period was 30 days.

Typical records of the variations of:

- (a) Tank liquid temperature;
- (b) Ambient temperature and
- (c) Dissolved oxygen concentration;

are shown in Figs. 11.26, 11.27 for 28 hours and 10 days retention time respectively.

For 28 hours retention time, the liquid was fed to tank at the end of each hour by siphon feeding system. Fig. 11.26 shows that as the liquid is fed the dissolved oxygen concentration drops to 1% saturation value and the temperature rises to its peak value. It stays at its peak value as long as the dissolved oxygen concentration stays at its lowest value. Then as the dissolved oxygen rises



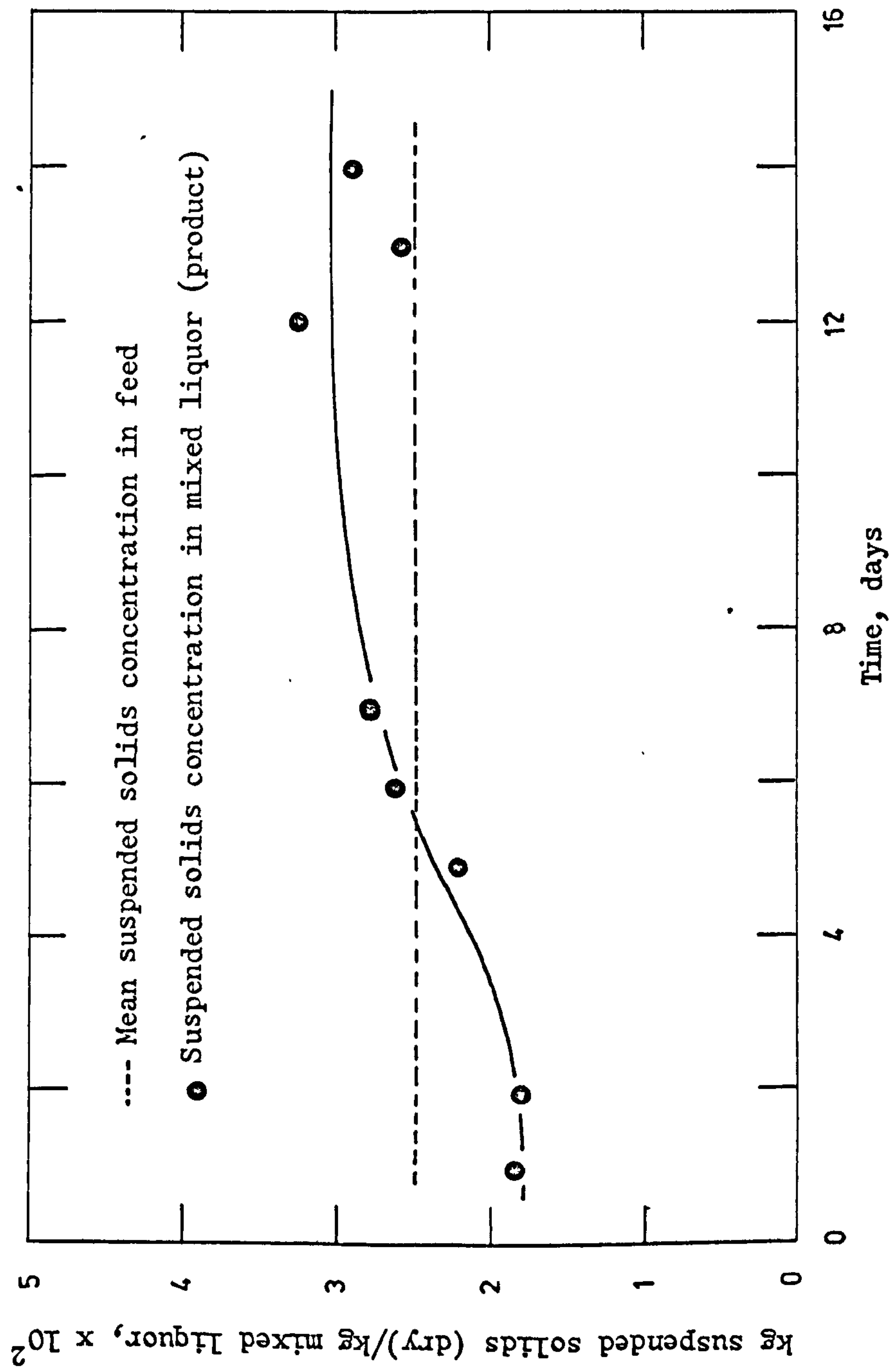


Figure 11.24. Variations in suspended solid concentration in mixed liquor (retention time 28 hours).

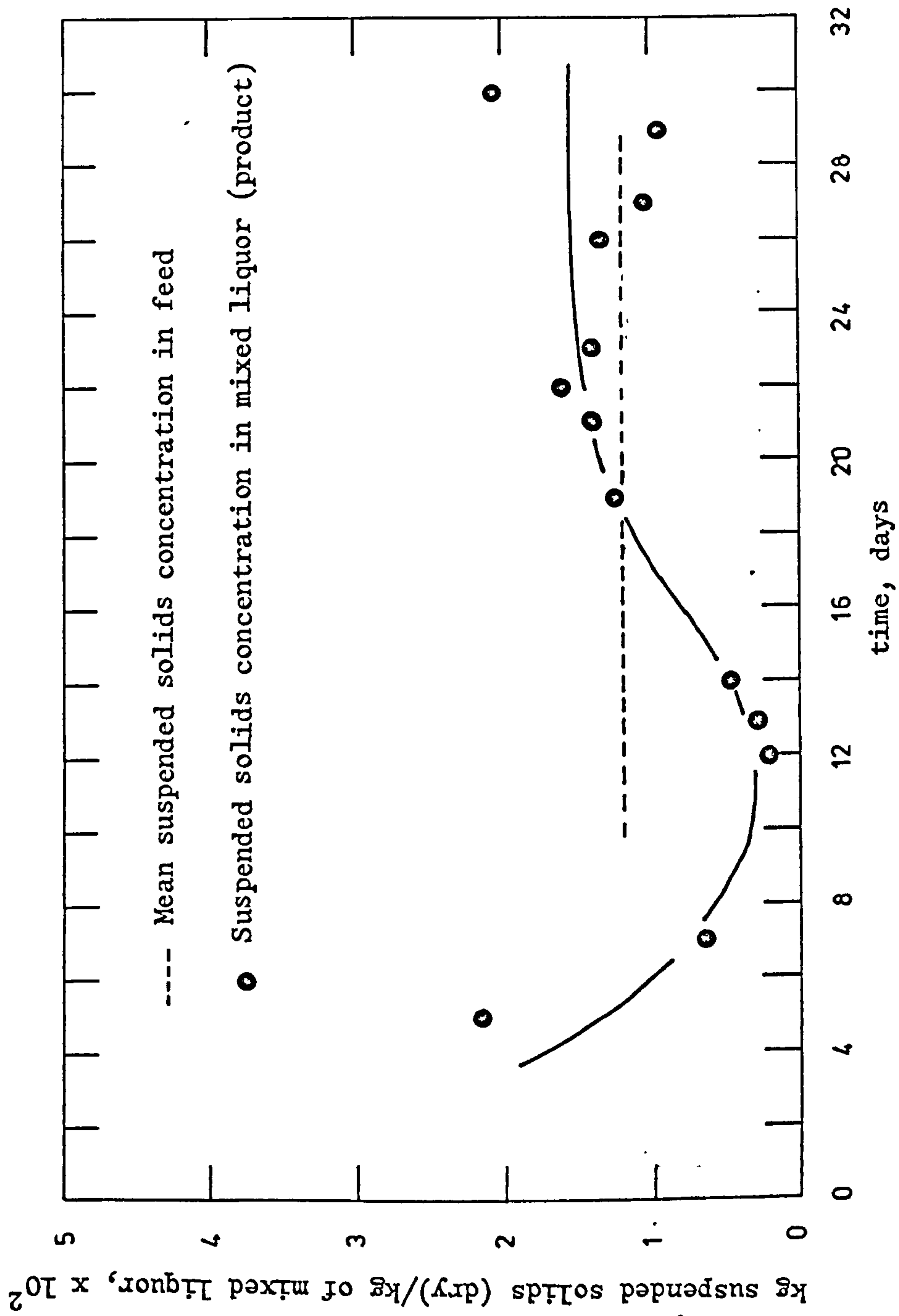


Figure 11.25. Variations in suspended solids concentration in mixed liquor  
(retention time 10 days)



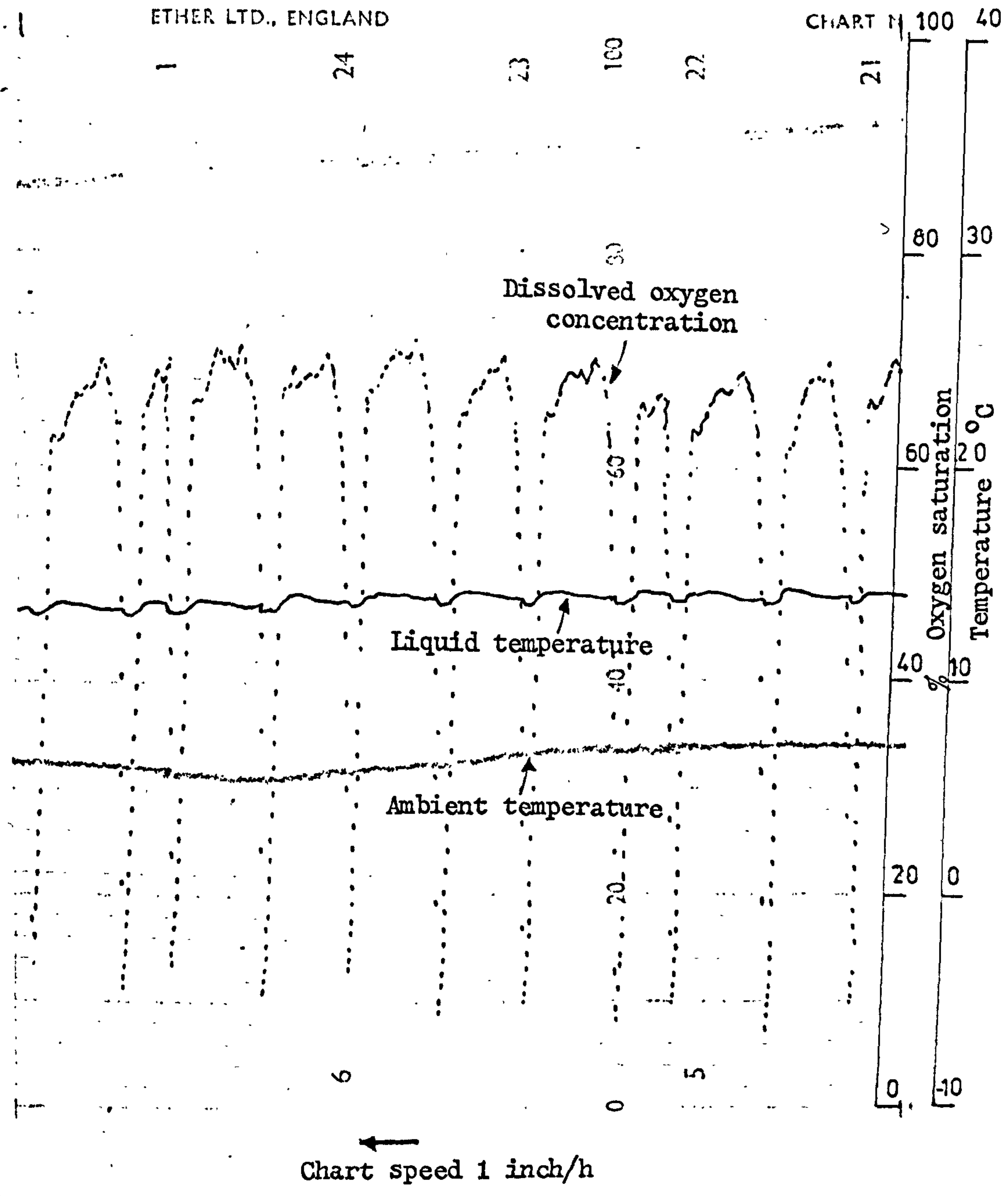


Figure 11.27. Typical record of 10 days retention time showing variations with time of dissolved oxygen concentration, liquid temperature and ambient temperature.



nonlinearly, similarly the temperature drops nonlinearly. The cycle is repeated on the next feed of the liquid. Here aeration was not stopped for defoaming as this record belongs to preliminary experiments. The record in Fig. 11.26 was chosen on the ground that it clearly shows the effect of intermittent high loading rate on the behaviour of dissolved oxygen and temperature of liquid.

The small wavy fluctuations in ambient and liquid temperatures are due to instrumental error. A thermostat-controlled fan was maintaining constant temperature in the control room. Variations in control room temperature affected the thermocouple amplifiers. These fluctuations were later eliminated by better insulation of the amplifiers.

Fig. 11.28 shows that the fluctuations in tank liquid temperature are not observed when the dissolved oxygen concentration is zero but begins to appear with the increase of dissolved oxygen concentration.

From these results it appears that the substrate utilization is a rapid process at high loading rate. In fact, biochemical reaction rate increases with the increase of BOD load (kg of BOD feed/kg of suspended solids in mixed liquor). As the liquid is fed to the reactor, the metabolic activity accelerates rapidly to degrade the incoming substrate; this gives rise to rapid increase in temperature (exothermic reaction) and high oxygen demand which in turn decreases the oxygen concentration at the same speed as the increase of temperature. Metabolic activity proceeds at its optimum value (lowest dissolved oxygen concentration and maximum

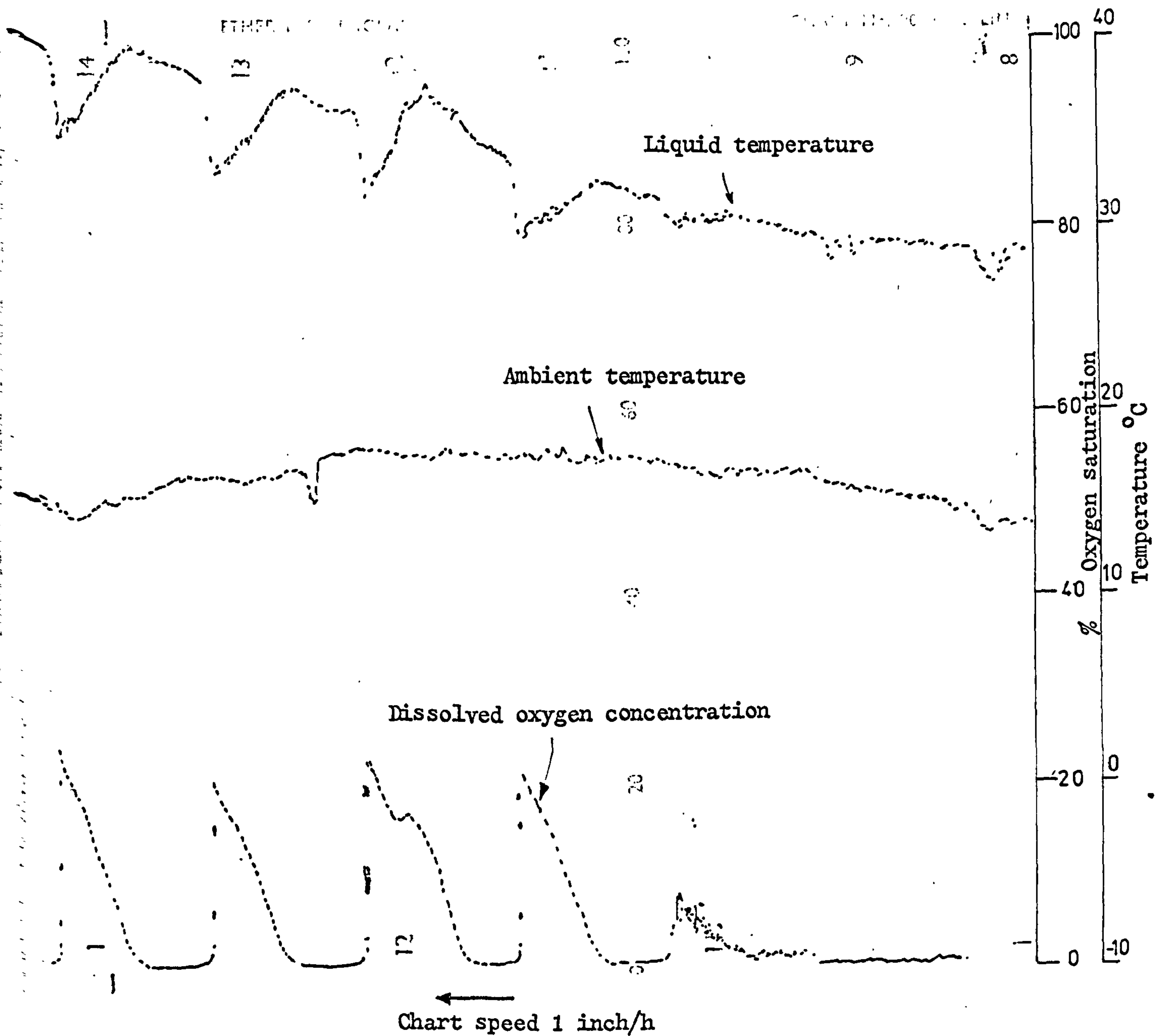


Figure 11.28. Record from 28 hours retention time experiments showing that under limiting oxygen concentration liquid temperature variations are not observed. Temperature variations appear when oxygen supply is increased.

temperature). After the utilization and incorporation into cell material of possibly the easily biodegradable matter the metabolic activity decreases and hence the dissolved oxygen concentration increases. So also the temperature decreases. In Fig. 11.28 when the dissolved oxygen concentration is zero at the time of liquid feed to the reactor, the temperature of liquid does not rise since the metabolic activity is limited by the limiting dissolved oxygen concentration. Thus in abundant oxygen supply metabolic activity is not limited and a rapid degradation of waste takes place.

Fig. 11.27 shows the variations in liquid temperature for 10 days retention time. The temperature did not vary in the same fashion as it varied with 28 hours retention time. It increased or decreased rather smoothly. This points out that at low feed rates there are no drastic changes in metabolic activity.

The results of 28 hours retention time are so scattered that only speculations can be made. So if in Fig. 11.22 (page 275) the reading on the 6th day for COD of dissolved solids/kg of dissolved solids equal to 1.4 is omitted, then the remaining four readings are consistent and nearly coincide with the COD of dissolved solid for 10 days retention time. Similarly, reduction in liquid COD and total COD is of the same order within the range of scatter. Also the increase in suspended solids concentration is nearly equal at the two retention times. From these facts, it can be concluded that with the assurance of abundant supply of dissolved oxygen so that metabolic activities proceed without hinderance, the performance as regards purification of waste is the same irrespective of the retention time in a completely mixed biological reactor.



There is a belief (98) that at pH 6.5 foaming does not occur. This theory was not confirmed in the present work. To confirm that foaming is reduced at pH 6.5, the liquid was aerated on a batch basis so as to encourage nitrification. The nitrifying bacteria convert the ammonia nitrogen to nitrate nitrogen and so the pH of solution decreases due to the lower concentration of  $\text{NH}_4^+$  in solution as reported by Owen et al. (84). Montgomery and Borne (75) report that growth of nitrifying bacteria is very slow. Therefore the decrease of pH was incredibly slow. However, after 62 days of aeration (35 days batch and 27 days continuous) pH 6.4 was recorded but foaming was unchanged.

#### 11.4 TECHNOLOGICAL POTENTIAL OF PLUNGING JET REACTOR

This study has proved that a plunging jet aeration system has great potential in chemical waste treatment and fermentation processes since it is comparable or superior to existing gas-liquid contactors as regards aeration efficiency (refer Table 4.1, page 43). This section aims at emphasizing this aspect. For waste treatment purposes, the jet aeration system is robust and free from the operational difficulties such as clogging in air diffusers, limitation of speed of surface aerator by the tank width, poor mixing in the lower region of tank in brush aeration. In the jet aeration system all parts are easily accessible. The aeration and mixing is achieved by the jet itself and no separate stirring device is needed. Concentrated wastes for instance farm and industrial wastes can be aerated by the jet aeration system without any operational difficulty. Moreover, from the design and the degree of turbulence



produced in conventional devices, except the Simplex Hi-Cone, it appears that these devices fail to provide good mixing of solids. However, apart from the good turbulence produced by high velocity jets in the jet aerator which keeps the solids in suspension, the solids near the tank bottom are circulated by the pump and are dispersed into the bulk liquid by the jet. For very large tanks multiple jets can be used and the oxygen can be supplied where desired by arranging the jets.

With 12.7 mm diameter nozzle entraining air at a rate of  $0.01 \text{ m}^3/\text{s}$  the interfacial area per unit volume of gas hold up is  $5 \text{ cm}^{-1}$  which is of the same order of magnitude as that of other conventional gas-liquid contactors, as shown in Table 11.1

TABLE 11.1

Interfacial Area per Unit Volume of Gas Hold Up  
for Various Gas-Liquid Contactors.

Gas-liquid Contactor	Interfacial area per unit volume of gas hold up ( $\text{cm}^{-1}$ )	Investigator
Bubble-cap plate	1.5	Porter et al.(93)
Sieve plate	1 - 8 2 - 5	Calderbank (18) Sharma and Gupta (104)
Bubble column	1 - 6	Sharma and Mashelkar (105)

As is obvious from the results presented in 10.4.6, this value is not maximum and can be further increased by increasing the jet velocity; although the aeration system is more efficient in terms of

- . aeration efficiency at low jet velocity than at high jet velocity for a biological system - the aeration efficiency decreases with the increase of jet power.

### CONCLUSIONS

The main conclusions from this work are condensed below.

- (1) The air entrainment rate by cylindrical jets having jet lengths greater than 0.66 m can be predicted by the dimensionless equation.

$$En = 8.7 \times 10^{-5} (Re_j)^{0.77} (We)^{0.15}$$

The equation is obtained with water, hence the effect of the liquid properties on the entrainment cannot be stated conclusively.

- (2) For nozzle diameters less than 22.2 mm, the experimental results on entrainment agree in general with the Van De Sande's theory, although there are some discrepancies which could be due to nozzle design. In this work  $\frac{1}{d_n}$  varies and is much less than 50. For the nozzle diameters greater than 28.6 mm there is sheer disagreement between the theory and experiments.
- (3) The short time exposure photograph of the high velocity jet clearly showed the central core of the jet surrounded by the diverging jet envelope. This supports the theory of Van De Sande that the air is captured between the central core and the outer envelope of the jet.
- (4) The air entrainment is independent of jet length for cylindrical jets longer than 0.66 m; and below this length the entrainment increases with the increase of jet length. However, the entrainment was studied for only three jet lengths,

therefore, the true behaviour of the entrainment with the jet length cannot be stated conclusively.

- (5) A transition region - between a low velocity region ( $V < 5$  m/s) and a high velocity region (begins at  $We = 10$ ) — which appears with small diameter nozzles ( $d_n < 10$  mm) does not appear with large diameter nozzles ( $d_n > 12.7$  mm).
- (6) In a stirred catalysed sulphite solution undergoing chemical reaction with the oxygen from the gaseous phase when the sulphite concentration is greater than  $6 \times 10^{-2}$  kmol/m<sup>3</sup> or catalyst ( $C_o^{++}$ ) concentration is greater than  $2 \times 10^{-5}$  kmol/m<sup>3</sup>, the oxidation reaction is independent of chemical kinetics and oxygen transfer takes place at maximum rate.
- (7) Under above conditions, the reaction is virtually instantaneous at the interface and the mass transfer is controlled by the gas film.
- (8) For cylindrical jets the oxygen transfer is independent of jet length when the jet length is in the range 0.15 to 0.7 m, but below this range it decreases linearly with the decrease of the jet length. However, for annular jets the oxygen transfer rate is independent of the jet lengths in the range 0.025 to 0.4 m.
- (9) Oxygen transfer by virtue of entrainment is related to power of the jet by the correlation

$$J = 4 P_j$$

where  $J$  is in kg/h and  $P_j$  in kW. The relation is independent of the jet position and the jet cross-section (cylindrical or annular), but for cylindrical jets, the jet length should be



greater than 0.15 m.

- (10) The oxygen absorption efficiency of the plunging jet reactor (1.1 - 36%) is comparable and even higher than those of existing commercial units (6 - 11%).

- (11) The oxygen transfer rate in biological system is correlated by the equation:

$$\frac{J^*}{d_n} = 1.96 \times 10^{-2} (P_j)^{0.72}$$

where  $J^*$  is in kg/s,  $d_n$  in m, and  $P_j$  in kW.

- (12) For turbulent liquids, the presence of suspended solids has no influence on gas mass transfer rates.
- (13) The oxygen transfer in the biological system is significantly higher than that in tap water. This conclusion militates against some practices of halving the oxygen transfer coefficient obtained with the tap water experiments.
- (14) The aeration of the waste liquid (defibred pig slurry) in a continuous biological reactor at short (28 hours) and long retention time (10 days) gave approximately the same reduction in total COD of the feed (41 and 45%).
- (15) From the analysis of the liquid and solid phases of pig slurry in the feed and product of a continuous reactor, it is concluded that only reduction in the COD of the dissolved solids takes place. The COD of the suspended solids in the feed and the product remains nearly the same.

- (16) The steady state concentration of the suspended solids in the continuous reactor increased by nearly the same factor (20 and 25%) at both short (28 hours) and long (10 days) retention time.
- (17) The presence of the suspended solids causes error in analytical methods, hence the results on continuous biological reactor are scattered.
- (18) The calculated mean bubble diameter in plunging jet reactor is in the range 1.5 to 6.6 mm. This range is in the same order of magnitude of the bubble sizes as reported in the literature (see Table 10.1 on page 215 ).
- (19) The calculated bubble retention time is in the range 1 to 9.5 seconds and agrees with the reported results.
- (20) The bubble size decreases with the decrease of nozzle diameter. The ratio of the mean bubble diameter to the nozzle diameter ( $\frac{\bar{d}_{bm}}{d_n}$ ) correlates well with the entrainment ratio. The correlation indicates a maximum value of 0.13 for  $\frac{\bar{d}_{bm}}{d_n}$  which means that the maximum mean bubble diameter is about 13% of the nozzle diameter.
- (21) The aeration of a biological system in the plunging jet aerator may pose two great problems as a result of foaming. One is the loss of the liquid from the aeration tank, and the other is the reduction in the oxygen transfer rate.
- (22) In a continuous plunging jet aeration system foaming can be controlled by storing the foam produced during aeration and

then collapsing it by spraying the liquid over the foam through nozzles. By using a control circuit, the aeration (foaming) and defoaming operations can be automatic for a continuous plant. The reduction in the oxygen transfer because of foam can be prevented by concealing the jet and the nozzle.

### RECOMMENDATIONS FOR FURTHER WORK

The following are the recommendations or suggestions to be considered in a further study on the subject of this dissertation.

1. The effect of the liquid properties such as viscosity, surface tension, density, should be individually considered and the validity of the dimensionless correlations for varying liquid properties should be tested.
2. The effect of the jet length on the entrainment rate should be thoroughly investigated by obtaining the data at various jet lengths.
3. The nozzles should be remade with  $\frac{1}{d_n}$  greater than 50 to minimize the induced turbulence in the jet stream. A set of the data should be obtained for different jet diameters as obtained in this work. Then the significance of the data fitted to the dimensionless correlations should be tested statistically.
4. The work should be extended to jet diameters greater than 38.1 mm since large diameter jets are of more practical value.
5. The liquid flow pattern and the relation of these flow patterns on the bubble motion should be studied by performing experiments in a transparent tank.
6. It might be interesting to work with different jet cross-sections such as square, triangular and elliptical.



7. The effect of tank geometry and dimensions on mass transfer aspects might also be an interesting exercise.
8. With large tanks the mixing might be the problem. This might be overcome by using multiple angular jets off-centred and impacting on liquid surface in opposite directions. These jets would tend to rotate the whole bulk and would help in good mixing. So the work should also be done on this aspect using multiple jets.
9. A quantitative interrelationship between the parameters involved in foam control should be studied experimentally.
10. The performance of the biological reactor should be investigated at hydraulic retention time other than that used in this work.

## BIBLIOGRAPHY

1. AHMED, A., and GLOVER, J. Paper presented at Farm Waste Disposal Conference, 12 to 14 September, 1972, Glasgow: Agricultural Research Council.
2. ASTARITA, G. Mass Transfer with Chemical Reaction. Amsterdam; Elsevier Publishing Company, 1967.
3. ASTARITA, G., MARRUCCI, G., and COLETI, L. *Chemica Ind.*, Milano, 46, 1964, 1021.
4. BASSETT, H., and PARKER, W. *J. Chem. Soc.*, 1951, 1540.
5. BAINES, S., EVANS, M.R., HISSET, R., and HEPHERD, R.Q. *The Agricultural Engineer*, 28, 1973, 77.
6. BARRON, H.G., and O'HERN, H.A. *Chem. Eng. Sci.*, 21, 1966, 397.
7. BARTHOLOMEW, W.H., KAROW, E.O., SFAT, M.R., and WILHELM, R.H. *Ind. Eng. Chem.*, 42, 1950, 1801.
8. BASSETT, H., and PARKER, W. *J. Chem. Soc.*, 1951, 1540.
9. BEWTRA, J.K., and NICHOLAS, W.R. Paper presented at the Seventeenth Annual Purdue Industrial Waste Conference. Cited in reference 60.
10. BÖHNKE, B. Advances in Water Pollution Research, Proceedings of Fifth International Conference held in San Francisco and Hawaii 1970, edited by S.H. Jenkins, Oxford: Pergamon Press, 1971, Paper II-9.
11. BOWERS, R.H. *J. Appl. Chem.*, 5, 1955, 542.
12. BRIERLEY, M.R., and STEEL, R. *Appl. Microbiol.*, 7, 1959, 57.
13. BROWN, W.E., and PETERSON, W.H. *Ind. Engng. Chem.*, 42, 1950, 1823.
14. BUCKINGHAM, E. *Trans. ASME*, 37, 1915, 263.

15. BUELTMAN, C., WESSON, C.G., TERMINI, J., and KINGSBURY, W.  
In: Advances in Biological Waste Treatment, edit.  
by W. W. Eckenfelder, Jr., and B. J. McCabe, New  
York: Pergamon Press, 1963, 175.
16. BURGESS, J.M., MOLLOY, N.A., and MCCARTHY, M.J. Chem. Engng.  
Sci., 27, 1972, 442.
17. BURGESS, J.M., and MOLLOY, N.A. Chem. Engng. Sci., 28, 1973,  
183.
18. CALDERBANK, P.H. Trans. Instn. Chem. Engrs., 37, 1959, 173.
19. CALDERBANK, P.H. Trans. Instn. Chem. Engrs. (London), 36,  
1958, 443.
20. CALDERBANK, P.H. In: Biochemical and Biological Engineering  
Science, Vol. 1, edit. by N. Blakebrough, London:  
Academic Press, 1967.
21. CALDERBANK, P.H., and MOO-YOUNG, M.B. Chem. Engng. Sci.,  
16, 1961, 39.
22. CALDERBANK, P.H., JOHNSON, D.S.L., and LONDON, J. Chem.  
Engng. Sci., 25, 1970, 235.
23. CARPANI and ROXBURG, J.M. Can. J. Chem. Engng. 36, 1958, 73.
24. CHAIN, E.B., PALADINO, S., CALLOW, D.S., UGOLINI, F., and Van  
Der SLUIS, J. Bull. World Hlth. Org., 6, 1952, 73.
25. CIBOROWSKI, J., and BIN, A. Pr. Inst. Inz. Chem. Politech.  
Warszaw, 1 (3), 1972, 247.
26. COOPER, C.M., FERNSTORM, G.A., and MILLER, S.A. Ind. Engng.  
Chem., 36, 1944, 504.
27. DANCKWERTS, P.V. Ind. and Engng. Chem., 43, 1951, 1460.
28. DANCKWERTS, P.V. Gas Liquid Reaction. London: McGraw-Hill  
Book Company, 1970.



29. DEINDOERFER, F.H., and GADEN, E.L., Jr. Appl. Microbiol.  
3, 1955, 253.
30. DANG, V., GILL, W.N., and RUCKENSTEIN, E. Can. J. Chem.  
Engng., 50, 1972, 300.
31. de FRATE, L., and RUSH, F. Selected Papers Symposium  
Part II, 64th National Meeting of the AIChE, New  
Orleans, Louisiana, March 16 to 20, 1969.
32. de WAAL, K.J.A., and OKESON, J.C. Chem. Engng. Sci., 21,  
1966, 559.
33. DOBBINS, E.W. In: Advances in Water Pollution Research,  
Proceedings of the International Conference, edit.  
by W. W. Eckenfelder, Jr., Vol. 2, London: Pergamon  
Press, September 1962, 61.
34. DREIR, D.E. In: Advances in Biological Waste Treatment,  
edit. by W.W. Eckenfelder, Jr., and B.J. McCabe,  
New York: Pergamon Press, 1963, 186.
35. ECKENFELDER, W.W., Jr., and O'CONNOR, D.J. Biological Waste  
Treatment, London: Pergamon Press, 1961, 97.
36. ECKENFELDER, W.W., Jr. Industrial Water Pollution Control.  
McGraw-Hill Book Company, 1966, 76.
37. ECKENFELDER, W.W., Jr., and FORD, D.L. In: Advances in  
Water Quality Improvement, edit. by E.F. Gloyna and  
W.W. Eckenfelder, Jr., University of Texas Press,  
1968, 215.
38. ECKENFELDER, W.W., Jr., and MOORE, T.L. Chem. Engng.,  
September 1955, 189.
39. ECKENFELDER, W.W., Jr., and BARNHART, E.L. J. AIChE, 7(4),  
December 1961, 631.



40. FINN, R.K. Bact. Rev., 18, 1954, 254. Cited in the reference 95.
41. GADEN, E.L., Jr., and KEVORKIAN, V. Chem. Engng., 63, October 1956, 173.
42. GAL-OR, B. In: Advances in Chemical Engineering, edit. by T.B. Drew and others, Vol. 7, London: Academic Press, 1968, 310.
43. GLOVER, F.A. Paper Presented at Farm Waste Disposal Conference, 12 to 14 September 1972, Glasgow: Agricultural Research Council.
44. GLOVER, J., and THORLEY, R.K. (Mrs.). Unpublished Work, Chemical Engineering Department, Loughborough University of Technology, Loughborough, 1973.
45. HANHART, J., KRAMERS, H., and WESTERTEP, K.R. Chem. Engng. Sci., 18, 1963, 503.
46. HAUSER, E.A. Colloidal Phenomena. New York: McGraw Hill Book Company, Inc., 1939, 117.
47. HAUXWELL, G.D. Ph. D. Dissertation, Corvallis, Oregon State University, 1972.
48. HENDERSON, J.B., MCCARTHY, M.J., and MOLLOY, N.A. Proc. Chemeca, Australia, 1970, 86.
49. HIGBIE, R. Trans. AIChE, 31, 1935, 365.
50. HINSHELWOOD, C.N. The Chemical Kinetics of the Bacterial Cell, Oxford: Clarendon Press, 1946, 5.
51. HIROSE, Y., YAMANAKA, S., OKADA, H., and KINOSHITA, K. Agr. Biol. Chem., 29, 1965, 989.
52. HIROSE, T., and MOO-YOUNG, M. Can. J. Chem. Engng. 47, 1969, 265.

53. HUNT, G., REISMAN, H.B., and LAGO, J. Paper presented at Sixty-second Annual Meeting, AIChE: Washington D.C., November 16-20, 1969.
54. HURWITZ, E., GLOPPEN, R.C., and ROEBER, J. Advances in Biological Waste Treatment, edit. by W. W. Eckenfelder, Jr., and B.J. McCabe, New York: Pergamon Press, 1963, 399.
55. IMHOFF, K. Taschenbuch der Stadtent-wässerung 22 Auflage, München Wien, 1969. Cited in the reference 116.
56. JORISSEN, W. P. Z. Phys. Chem., 22, 1897, 54.
57. KAYSER, R. Advances in Water Pollution Research - Proceedings of the Fourth International Conference held in Prague, 1969, edit. by S.H. Jenkins, Pergamon Press, 1969, 477.
58. KISHINEVSKI, M. J. Appl. Chem. (of USSR), 28, 1955, 881.
59. KNOP, E., and KALBSKOPF, K.H. Advances in Water Pollution Research - Proceedings of the Fourth International Conference held in Prague, 1969, edit. by S.H. Jenkins, Pergamon Press, 1969, 497.
60. LAMB, M. Discussion. In: Advances in Water Pollution Research, Proceedings of the International Conference held in London Sept. 1962, Vol. 2, edit. by W. W. Eckenfelder, New York: Pergamon Press, 1964, 76.
61. LEVICH, V. Physicochemical Hydrodynamics. Englewood Cliffs, New Jersey: Prentice-Hall Inc., 1962, 450.
62. LEWIS, W.K., and WHITMAN, W. G. Ind. and Engng. Chem., 16, 1924, 1215.
63. LIN, T. J., and DONNELLY, H. G. AIChE, 12 (3), May 1966, 563.
64. LINEK, V. Chem. Engng. Sci., 26, 1971, 491.

65. LINEK, V. Chem. Engng. Sci., 27, 1972, 627.
66. LISTER, A.R., and BOON, A.G. Water Pollution Control, London, 72, 1973, 590.
67. LINEK, V., and MAYRHOFEROVAJ. Chem. Engng. Sci., 25, 1970, 787.
68. MANCY, K.H., and BARLAGE, W.E., Jr. In: Advances in Water Quality Improvement, edit. by E.F. Glyona and W.W. Eckenfelder, Jr. Austin: University of Texas Press, 1968, 262.
69. MANCY, K.H., and OKUN, D.A. Discussion in the reference 127.
70. MAXON, W.D., and JOHNSON, M.J. Ind. and Engng. Chem., 45, 1953, 2554.
71. MCCARTHY, M.J., KIRCHNER, W.G., MOLLOY, N.A., and HENDERSON J.B. Trans. Instn. Min. Metall., 78, 1969, 239.
72. McKEOWN, J.J., and OKUN, D.A. Progress Report Research Grant RG 3720 (C4) National Inst. Hlth. 1953, Cited in the reference 39.
73. MERTES, A.T. Patent 2,128,311 United States Patent Office, 1938.
74. MIYAMOTO, S. Bull. Chem. Soc., Japan, 7, 1931, 8.
75. MONTGOMERY, H.A.C., and BORNE, B.J. J. Proc. Inst. Sew. Purif. 1966, 357.
76. MOO-YOUNG, M., and HIROSE, T. Ind. Engng. Chem., Fundament., 11, 1972, 281.
77. MORGAN, P.F. and BEWTRA, J.K. Water Pollution Control Federation, Journal, 32, 1960, 1047.
78. MORGAN, P.F., and BEWTRA, J. In: Advances in Biological Waste Treatment, edit. by W.W. Eckenfelder, Jr., and B.J. McCabe, New York: Pergamon Press, 1963, 181.



79. Official Standardized and Recommended Methods of Analyses.  
Cambridge: W. Heffer and Sons Ltd., 1963.
80. OHYAMA, Y., TAKASHIMA, T., and IDEMURA, H. Science Research  
Institute Reports (Japan), 29, November 1953, 344.  
Not available. Cited in the reference 48.
81. ONDA, K., TAKEUCHI, H., and MAEDA, Y. Chem. Engng. Sci., 27,  
1972, 449.
82. ORR, C., Jr., Particulate Technology, New York: The Macmillan  
Co., 1966, 376.
83. OWEN, S.P., and JOHNSON, J.J. Agr. and Food Chem., 3, 1955,  
606.
84. OWENS, J.D., EVANS, M.R., THACKER, F.E., HISSET, R., and BAINES, S.  
Water Research, 7, 1973, 1745.
85. PASVEER, A. In: Advances in Biological Waste Treatment, edit.  
by W.W. Eckenfelder, Jr., and B.J. McCabe, New York:  
Pergamon Press, 1963, 291.
86. PERRY, J.H. Chemical Engineers Handbook. New York:  
McGraw-Hill Book Company, 1963.
87. PHILLIPS, D.H., and JOHNSON, M.J. Ind. and Engng. Chem., 51,  
1959, 83.
88. PILPEL, N. Chem. & Process Engng., October 1956, 349.
89. PIRT, S.J. J. Gen. Microbiol., 16, 1957, 59.
90. POON, P.C., CALVIN and CAMPBELL, H. Water and Sew. Wrks.,  
114, 1967, 461.
91. <sup>"</sup>POPEL, F. Landt. Forsch., 18, 1970, 138. Cited in the  
reference 116.
92. <sup>"</sup>POPEL, F. Landt. Forsch. 18, 1970, 140. Cited in the  
reference 116.



93. PORTER, K.E., KING, M.B., and VARSHNEY, K.C. Trans. Instn. Chem. Engrs., 44, 1966, T274.
94. REITH, T. A Doctoral Dissertation, Technische Hogeschool Delft, 1968.
95. RICHARDS, J.W. Progress in Industrial Microbiology, 3, 1961, 143.
96. ROBERTSON, A.N. Scottish Farm Bldgs. Progress, (32), 1973, 13.
97. ROBERTSON, D.G.C., O'SHAUGHNESSY, D.P., and MOLLOY, N.A. Chem. Engng. Sci., 28, 1973, 1635.
98. ROBINSON, K. Private Communication, 1973.
99. ROXBURGH, J.M. Can. J. Chem. Engng., 40, 1962, 127.
100. SAWICKI, J.E., and BARRON, C.H. Chem. Engng. J., 5, 1973, 153.
101. SCHULTZ, J.S., and GADEN, E.L., Jr. Ind. and Engng. Chem. 48, 1956, 2209.
102. SCHERB, K. Vergleichende Untersuchungen über das Sauerstoffeintragsvermögen Verschiedener Belüftungssysteme auf dem Münchener Abwasserversuchsfeld. Münchener Beiträge Zur Abwasser - Fischereireinund Flussbiologie (Hrg. Liebmann) Bd. 12, München 1965, 330.
103. SEELIGER, R. Naturwiss. 36, 1949, 41.
104. SHARMA, M.M., and GUPTA, R.K. Trans. Instn. Chem. Engrs., 45, 1967, T 169.
105. SHARMA, M.M., and MASHELKAR, R.A. Paper presented to Tripartite Chemical Engineering Conference, Montreal, 1968, Symposium on Mass Transfer with Chemical Reaction. Cited in the reference 28 on page 236.
106. SHERWOOD, T.K., and PIGFORD, R.L. Absorption and Extraction, New York: McGraw-Hill Book Company, Inc., 1952, 317.
107. SHIRLEY, R.W. Master's thesis, University of Iowa, 1950.

120a. VALENTIN, F.H.H. Absorption in Gas-liquid  
Dispersions. E. and F.N. SPON LTD.,  
London, 1967.

108. SHIROTSUKA, T., and KAWASE, Y. J. Chem. Engng., Japan, 6,  
1973, 432.
109. SMITH, G.G. Ph.D. Dissertation, University of Wisconsin.  
Not available. Cited in the reference 95.
110. SOLOMONS, G.L. Materials and Methods in Fermentation.  
Academic Press, 1969, 133.
111. Solubility of Atmospheric Oxygen in Water, Proc. Paper, J. San.  
Engng. Div. ASCE, 86 (SA4), July 1960, 41.
112. STABLES and WILSON. Phil. Mag., 15, 1883, 406.
113. Standard Methods for the Examination of Water and Waste Water.  
American Public Health Association, 1971.
114. SWIGGETT, G.E. Ph.D. Dissertation, Corvallis: Oregon State  
University, 1969. Cited in the reference 47.
115. SZEKELY, J. Trans. of the Metall. Soc. AIME, 245, 1969, 341.
116. THAER, R. Landt. Forsch., 19, 1971, 159.
117. TODTENHAUPT, E.K. Chem. Ing. Techn., 43, 1971, 336.
118. TRUESDALE, G.A., and VANDYKE, K.G. Wat. Waste Treat. J., 7,  
1958, 9. Cited in the reference 66.
119. TSAO, G.T. Biotech., and Bioengng. 10, 1968, 765.
120. TYLER, E., and RICHARDSON, E.G. Proc. Phys. Soc., London,  
37, 1925, 279.
121. Van De SANDE, E. Ph.D. Dissertation, Technische Hogerschool  
Delft, 1974.
122. Van De SANDE, E., and SMITH, J.M. Unpublished Paper, 1973.
123. Van De SANDE, E., and SMITH, J.M. Chem. Engng. Sci. 28,  
1973, 1161.
124. Van De SANDE, E., and SMITH, J.M. Chem. Ing. Techn., 44,  
1972, 1177.
125. Van Der EMDE, W. Discussion. Advances in Water Pollution  
Research, Vol. 2, edit. by W.W. Eckenfelder, Jr.,  
Oxford: Pergamon Press, 1964, 87.



126. Van Der EMDE, W. In: Advances in Water Quality Improvement, edit. by E. F. Gloyna and W.W. Eckenfelder, Jr., University of Texas Press, 1968, 238.
127. Von Der KROON, G.T.M. Advances in Water Pollution Research, Proceedings of the Fourth International Conference held in Prague, 1969, edit. by S.H. Jenkins, Pergamon Press, 1969, 219.
128. WELLEK, R.M., and HUANG, C. Ind. Engng. Chem., Fundamental. 9, 1970, 480.
129. WESSELINGH, J.A., and VAN'T HOOG, A.C. Trans. Instn. of Chem. Engrs., 48, 1970, T 69.
130. WESTERTEP, K.R., Van DIERENDONCK, L.L., and De KRAA, J.A. Chem. Engng. Sci., 18, 1963, 157.
131. WESTON, R.F., and STACK, V.T. Jr., In: Advances in Biological Waste Treatment, edit. by W.W. Eckenfelder and B.J. McCabe, New York: Pergamon Press, 1963, 149.
132. WHEATLAND, A.B. Farm Waste Disposal Papers presented at the Poultry Waste Conference, Summingdale Park, 17.
133. WINZLER, R.J. J. Cell. Comp. Physiol., 17, 1941, 263.  
Cited in the reference 95.
134. YAGI, S., and INONE, H. Chem. Engng. Sci. 17, 1962, 411.
135. YOSHIDA, F., IKEDA, A., IMAKAWA, S., and MIURA, Y.  
Ind. Engng. Chem., 52, 1960, 435.
136. YOSHIDA, F., and MIURA, Y. Ind. Engng. Chem. Process Design and Develop., 2, 1963, 263.
137. ZEPER, J., and De MAN, A. Advances in Water Pollution Research, San Fransisco and Hawaii, Vol. 1, Paper II-8, 1970.
138. ZIOKARNIK, M. Chem.-Ing.-Techn., 38, 1966, 357.
139. ZLOKARNIK, M. Chem.-Ing.-Techn., 38, 1966, 717.
140. ZLOKARNIK, M., and JUDAT, H. Chem.-Ing.-Techn., 39, 1967, 1163.



## Appendices

## APPENDIX I

### CALCULATION OF OXYGEN TRANSFER RATES BY IODOMETRIC TITRATION OF SAMPLES FROM SULPHITE OXIDATION EXPERIMENTS

The appendix is divided into two sections. Section I.1 deals with the laboratory method used for iodometric titrations, and section I.2 presents formulas for calculation of oxygen transfer rates from titration results.

#### I.1 Procedure for Iodometric Titrations

To perform the chemical analysis on sulphite samples obtained from a sulphite oxidation experiment several 500 ml conical flasks were made ready to accept the samples by pipetting a constant volume of 0.1 normal iodine ( $.1N I_2$ ) solution into each flask. The constant volume of iodine was chosen in excess so that some iodine should be left to make titrations possible after the addition of sulphite sample. The volume of iodine used was in the range 20 to 100 ml. In many experiments 50 ml of iodine solution was pipetted.

Samples were collected by a nominal 10 ml syringe which actually delivered 10.6 ml liquid (found by weighing the 10 ml liquid from the syringe), so 10.6 ml of samples were added gently to flasks containing  $I_2$  solution. 2 ml of glacial acetic acid was also added.

After 5 minutes, the unreacted iodine was titrated against 0.1 normal sodium thiosulphate solution to the straw colour. Two or three drops of freshly prepared starch solution were added to the flask and the solution was titrated to end point.

The volume of thiosulphate used in titration was noted in ml.

## I.2 Calculation of Oxygen Transfer Rate in Continuous and Batch Experiments

The formulas for oxygen transfer rate in continuous and batch experiments are derived separately as follows:

### (a) Continuous Experiments

Let:

$$\begin{aligned} \text{Volume of liquid in the reactor} &= V \text{ m}^3 \\ \text{Sodium sulphite concentration in the feed} &= C_{\text{SO}_3} \text{ kmol/m}^3 \\ \text{Sodium sulphite concentration in the product at steady state} &= C'_{\text{SO}_3} \text{ kmol/m}^3 \\ \text{Liquid flow rate of the feed and the product} &= q \text{ m}^3/\text{s} \\ \text{Sulphite oxidation rate} &= r' \text{ kmol/m}^3/\text{s} \end{aligned}$$

Mass (molal) balance on the reactor at steady state gives

mols of sulphite in = mols of sulphite out + mols of sulphite reacted

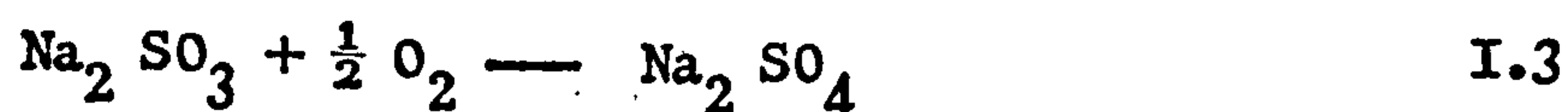
Or mathematically,

$$q C_{\text{SO}_3} = q C'_{\text{SO}_3} + (r') V \quad \text{I.1}$$

Therefore mols of sulphite reacted,

$$(r') V = q (C_{\text{SO}_3} - C'_{\text{SO}_3}) \quad \text{I.2}$$

Sodium sulphite is oxidized according to equation



Hence:

$$\text{Mols of oxygen reacted} = \frac{1}{2} (\text{Mols of sulphite reacted})$$

Therefore:

$$\text{Oxygen transfer rate} = \frac{1}{2} (r') V \quad \text{I.4}$$

$$= \frac{1}{2} q (C_{\text{SO}_3} - C'_{\text{SO}_3}) \quad \text{I.5}$$

Equation I.5 can also be expressed in terms of volume of thiosulphate titrations as shown by the following analysis.

Let:

Normality of iodine solution	= z N
Normality of sodium thiosulphate solution	= y N
Volume of the sample from the reactor	= S ml
Volume of iodine to which sample is added	= $v'$ ml
Volume of thiosulphate titrations of feed sample	= $W_0$ ml
Volume of thiosulphate titrations of product samples	= W ml

Now:

$$W_0 \text{ ml of } y \text{ N thiosulphate} = W_0 \left(\frac{Y}{Z}\right) \text{ ml of } z \text{ N } I_2 \quad \text{I.6}$$

$$\begin{aligned} \text{Volume of } z \text{ N } I_2 \text{ reacted on addition of } 5 \text{ ml sample} \\ = v' - W_0 \left(\frac{Y}{Z}\right) \end{aligned} \quad \text{I.7}$$

Hence:

$$\begin{aligned} \text{Normality of sulphite solution in the feed} \\ = z \frac{v' - W_0 \left(\frac{Y}{Z}\right)}{S} \end{aligned} \quad \text{I.8}$$

Since 1N sodium sulphite ( $\text{Na}_2\text{SO}_3 \cdot 7 \text{ H}_2\text{O}$ ) solution contains  $\frac{1}{2}$  kmol of sodium sulphite/ $\text{m}^3$ , therefore sulphite concentration in the feed is given as

$$C_{\text{SO}_3} = \frac{1}{2} z \cdot \frac{v' - W_0 \left(\frac{Y}{Z}\right)}{S} \text{ kmol/m}^3 \quad \text{I.9}$$

Similarly by following the above procedure, sulphite concentration in the product is given as

$$C'_{\text{SO}_3} = \frac{1}{2} z \cdot \frac{v' - W \left(\frac{Y}{Z}\right)}{S} \text{ kmol/m}^3 \quad \text{I.10}$$



From equations I.9 and I.10

$$C_{SO_3} - C'_{SO_3} = \frac{y}{2S} (W - W_0) \quad I.11$$

Elimination of  $C_{SO_3} - C'_{SO_3}$  from equation I.5 by using equation I.11 gives the oxygen transfer rate as

$$J^* = \frac{8 q y}{S} (W - W_0) \text{ kg/s} \quad I.12$$

For several feed and product samples  $W$  and  $W_0$  will be the mean values.

#### (b) Batch Experiments

For this case oxygen transfer rate is simply given by

$$J^* = \frac{1}{2} (r') V \text{ kmol/s} \quad I.13$$

In terms of sulphite concentration the equation I.13 can be written as

$$J^* = \frac{1}{2} V \cdot \frac{dC_{SO_3}}{dt} \quad I.14$$

$$\text{Since } r' = \frac{d C_{SO_3}}{dt} \quad I.15$$

Representing  $\frac{d C_{SO_3}}{dt}$  in terms of the volume of thiosulphate titrations by using equation I.11, the equation I.14 can be written as

$$J^* = \frac{Vy}{4S} \left( \frac{dW}{dt} \right) \text{ kmol/s} \quad I.16$$

Or:

$$J^* = \frac{8 Vy}{S} \left( \frac{dW}{dt} \right) \text{ kg/s} \quad I.17$$

where  $\left( \frac{dW}{dt} \right)$  is the rate of increase of volume of thiosulphate titrations in ml/s. When volumes of thiosulphate titrations are plotted against the sampling time in seconds,  $\left( \frac{dW}{dt} \right)$  is the slope of the line given by regression analysis of the plot.

## APPENDIX II

### DIMENSIONAL ANALYSIS AS APPLIED TO ENTRAINMENT PHENOMENON

A more general approach has been made in the following analysis, that is, the entrainment of a fluid (gas or liquid) whose physical properties are different from the pool liquid is considered. In addition, the analysis applies to vertical jets.

According to the Buckingham  $\Pi$  theorem (14), in a physical problem, if there are  $n$  quantities involved having  $m$  dimensions, then the quantities may be arranged in  $(n - m)$  dimensionless groups. The quantities involved in an entrainment problem are the following:

- (1) Fluid entrainment rate,  $Q_f$
- (2) Nozzle diameter,  $d_n$
- (3) Jet length,  $l_j$
- (4) Jet velocity at nozzle exit,  $V_j$
- (5) Pool liquid density  $\rho_l$
- (6) Fluid density,  $\rho_f$
- (7) Pool liquid viscosity,  $\eta_l$
- (8) Fluid viscosity,  $\eta_f$
- (9) Pool liquid surface tension  $\sigma_l$
- (10) Fluid surface tension  $\sigma_f$

Ten quantities are involved having three dimensions, L, M and T. Since all these quantities are related, therefore some functional relationship must exist, so:

$$f(V_j, d_n, \rho_l, \rho_f, \eta_l, \eta_f, l_j, \sigma_l, \sigma_f, Q_f) = 0 \quad \text{II.1}$$

According to  $\Pi$  theorem, these quantities can be grouped in 7 dimensionless groups represented by the equation

$$f(\Pi_1, \Pi_2, \Pi_3, \Pi_4, \Pi_5, \Pi_6, \Pi_7) = 0 \quad \text{II.2}$$

The method of applying this theorem is to select variable quantities equal in number to dimensions involved and one new variable from the remaining variables for each new dimensionless group. Following this instruction, 3 variables  $V_j$ ,  $d_n$ , and  $e_1$  are selected since they contain the three dimensions M, L and T. To form a first dimensionless group  $\Pi_1$ , variable  $e_f$  is combined to the selected variables and the equation for  $\Pi_1$  is written as

$$\Pi_1 = V_j^{x_1} d_n^{y_1} e_1^{z_1} e_f \quad \text{II.3}$$

Similarly:

$$\Pi_2 = V_j^{x_2} d_n^{y_2} e_1^{z_2} n_1 \quad \text{II.4}$$

finally

$$\Pi_7 = V_j^{x_7} d_n^{y_7} e_1^{z_7} q_f \quad \text{II.9}$$

In the preceding equations exponents are determined so that each  $\Pi$  is dimensionless. Substituting the corresponding dimensions in the equations,

$$\Pi_1 = \left(\frac{L}{T}\right)^{x_1} (L)^{y_1} \left(\frac{M}{L^3}\right)^{z_1} \left(\frac{M}{L^3}\right) = M^0 L^0 T^0 \quad \text{II.10}$$

$$\Pi_2 = \left(\frac{L}{T}\right)^{x_2} (L)^{y_2} \left(\frac{M}{L^3}\right)^{z_2} \left(\frac{M}{LT}\right) = M^0 L^0 T^0 \quad \text{II.11}$$

$$\Pi_7 = \left(\frac{L}{T}\right)^{x_7} (L)^{y_7} \left(\frac{M}{L^3}\right)^{z_7} \left(\frac{L^3}{T}\right) = M^0 L^0 T^0 \quad \text{II.16}$$

By equating the exponents of L, M, and T to zero the equation

II.10 gives:

$$\text{for L, } x_1 + y_1 - 3z_1 - 3 = 0 \quad \text{II.17}$$

$$\text{for M, } z_1 + 1 = 0 \quad \text{II.18}$$

$$\text{for T, } -x_1 = 0 \quad \text{II.19}$$

These equations give:

$$x_1 = 0$$

$$y_1 = 0$$

$$z_1 = -1$$

Substitution of values of  $x_1$ ,  $y_1$  and  $z_1$  in equation II.3 gives

$$\Pi_1 = \frac{\ell_f}{\ell_1} \quad \text{II.20}$$

Following the above procedure,  $\Pi_2, \Pi_3, \dots, \Pi_7$  are obtained as:

$$\Pi_2 = \frac{\eta_1}{v_j d_n \ell_1} \quad \text{II.21}$$

$$\Pi_3 = \frac{\eta_f}{v_j d_n \ell_1} \quad \text{II.22}$$

$$\Pi_4 = \frac{l_j}{d_n} \quad \text{II.23}$$

$$\Pi_5 = \frac{\sigma_1}{v_j^2 d_n \ell_1} \quad \text{II.24}$$

$$\Pi_6 = \frac{\sigma_f}{v_j^2 d_n \ell_1} \quad \text{II.25}$$

$$\Pi_7 = \frac{Q_f}{v_j d_n^2} \quad \text{II.26}$$



Therefore equation II.2 becomes:

$$f \left[ \left( \frac{\ell_f}{\ell_1} \right), \left( \frac{\eta_1}{V_j d_n \ell_1} \right), \left( \frac{\eta_f}{V_j d_n \ell_1} \right), \left( \frac{l_j}{d_n} \right), \left( \frac{\sigma_1}{V_j^2 d_n \ell_1} \right), \right. \\ \left. \left( \frac{\sigma_f}{V_j^2 d_n \ell_1} \right), \left( \frac{Q_f}{V_j d_n^2} \right) \right] = 0 \quad \text{II.27}$$

Inversion of 2nd, 3rd, 5th and 6th group gives:

$$f \left[ \left( \frac{\ell_f}{\ell_1} \right), (Re_j)_{n_1}, (Re_j)_{n_f}, \left( \frac{l_j}{d_n} \right), \left( \frac{l_j}{d_n} \right), (We)_{\sigma_1}, \right. \\ \left. (We)_{\sigma_f}, \left( \frac{Q_f}{V_j d_n^2} \right) \right] = 0 \quad \text{II.28}$$

For air-water system  $\frac{\ell_f}{\ell_1}$  is a constant, also air has no surface tension, therefore,  $(We)_{\sigma_f}$  is cancelled. In addition the air viscosity would affect the jet envelope diameter as a result of viscous forces on jet surface; however, in experiments it was observed that for long jets ( $l_j > 0.66$  m) the length and hence the jet envelope did not affect the entrainment rate. From this reasoning  $(Re_j)_{n_f}$  and  $\left( \frac{l_j}{d_n} \right)$  can be cancelled. The resulting equation is

$$f \left( (Re_j)_{n_1}, (We)_{\sigma_1}, \frac{Q_f}{V_j d_n^2} \right) = 0 \quad \text{II.29}$$

On the basis of liquid properties; and  $Q_f = Q_a$

$$f \left( Re_j, We, \frac{Q_a}{V_j d_n^2} \right) = 0 \quad \text{II.30}$$

Or:

$$En = f ( Re_j, We ) \quad \text{II.31}$$

$$\text{where } En \propto \frac{Q_a}{V_j d_n^2}$$

Now:

$$En = K_o (Re_j)^{n_1} \times (We)^{n_2} \quad \text{II.32}$$

$$= K_o \left( \frac{V_j d_n \rho_l}{\eta_l} \right)^{n_1} \left( \frac{V_j^2 d_n \rho_l}{\sigma} \right) \quad \text{II.33}$$

For constant liquid properties,

$$En = K_o' (V_j)^{n_1 + 2n_2} (d_n)^{n_1 + n_2} \quad \text{II.34}$$

Or:

$$En = K_o' V_j^a d_n^b \quad \text{II.35}$$

$$\text{where } a = n_1 + 2n_2 \quad \text{II.36}$$

$$b = n_1 + n_2 \quad \text{II.37}$$

$$\log (En) = \log K_o' + a \log V_j + b \log d_n \quad \text{II.37}$$

For a given nozzle diameter

$$\log (En) = a \log V_j + C_k \quad \text{II.38}$$

$$\text{where } C_k = \log K_o' + b \log d_n \quad \text{II.39}$$

Equation II.38 is of the form

$$y = mx + C_k \quad (\text{equation of straight line on x-y co-ordinates})$$

where slope  $m$  is equal to  $a$ .

Hence the value of  $a$  was determined by a linear regression analysis of the entrainment data for 12.7 mm, 22.2 mm and 28.6 mm diameter nozzles for two jet lengths: 0.66 m and 1.05 m. The values of  $a$  so obtained are given below. The mean  $a$  value is 1.07.

	<u>a</u>	
$l_j$ (m)	0.66	1.05
$d_n$ (mm)		
12.7	0.96	1.06
22.2	0.78	1.24
28.6	0.88	1.52
<hr/>		
Mean a = 1.07		

Again, value of  $b$  in equation II.35 was found by the linear regression analysis of  $\log \left( \frac{En}{V_j^{1.07}} \right)$  against  $\log (d_n)$  for the data of three nozzles (12.7, 22.2 and 28.6 mm diameter) at two jet lengths (0.66 and 1.05 m). The value of  $b$  was found to be 0.92.

The values of  $n_1$  and  $n_2$  from equations II.36 and II.37 are found to 0.77 and 0.15 respectively. Substitution of these values of  $n_1$  and  $n_2$  in equation II.32 gives

$$En = K_o (Re_j)^{0.77} \times (We)^{0.15} \quad \text{II.40}$$

and hence the entrainment data for nozzle diameters 12.7, 22.2, and 28.6 mm for jet lengths 0.66 and 1.05 m are correlated by the dimensionless equation (by regression analysis).

$$En = 8.7 \times 10^{-5} (Re_j)^{0.77} \times (We)^{0.15} \quad \text{II.41}$$

This correlation is shown in Fig. 9.17, page 166.

## APPENDIX III

## CALCULATION OF AVERAGE BUBBLE DIAMETER

Air entrainment rate is related to average bubble diameter by the following equation:

$$Q_a = n \frac{\pi}{6} \bar{d}_b^3 \quad \text{III.1}$$

where  $Q_a$  is air entrainment rate in  $\text{m}^3/\text{h}$ ,  $\bar{d}_b$  is average bubble diameter in m, and  $n$  is bubble frequency in number of bubbles/h.

The rate at which interfacial area is generated is given by the equation:

$$A = n \pi \bar{d}_b^2 \quad \text{III.2}$$

where  $A$  is interfacial area generated in  $\text{m}^2/\text{h}$ .

Oxygen transfer rate due to entrainment is given by:

$$J = \alpha Q_a \hat{C} \quad \text{III.3}$$

where  $J$  is kg of  $\text{O}_2$  transfer/h,  $\alpha$  is fraction of oxygen in entrained air absorbed and  $\hat{C}$  is concentration of oxygen in air in  $\text{kg}/\text{m}^3$ .

Since the oxygen transfer takes place through the interfacial area  $A$  for a duration equal to the average retention time of bubble  $t_b$  (s), therefore:

$$J = K_g A \hat{C} t_b \quad \text{III.4}$$

where  $K_g$  is gas-film mass transfer coefficient in  $\text{m}/\text{s}$ .

Substitution of the value of  $A$  from equation III.2 into equation III.4 gives:

$$J = K_g n \pi \bar{d}_b^2 \hat{C} t_b \quad \text{III.5}$$



$$= \text{kg/h}$$

Equating the equations III.3 and III.5 as:

$$K_g n \pi \bar{d}_b^2 \cancel{\rho} t_b = \alpha Q_a \cancel{\rho}$$

gives:

$$n \pi \bar{d}_b^2 = \frac{\alpha Q_a}{K_g t_b} \quad \text{III.6}$$

Division of the equation III.1 by equation III.6 gives the formula for the average bubble diameter as

$$\bar{d}_b^2 = \frac{6 K_g t_b}{\alpha} \quad \text{III.7}$$

Bubble rise velocity  $U$  is given by the empirical equation (Levich (61)):

$$U = 2 \sqrt{\frac{g \bar{d}_b}{1.8}} \quad \text{III.8}$$

The empirical equation for maximum penetration depth of bubbles is:

$$h = 1.75 v_j^{0.85} d_j^{0.65} \quad 5.14$$

So, the average bubble retention time for a particular jet condition is:

$$t_b = \frac{h}{U} \quad \text{III.9}$$

Elimination of  $U$  from the equation III.9 using the equation III.8 gives:

$$t_b = \frac{h}{2 \sqrt{\frac{g \bar{d}_b}{1.8}}} \quad \text{III.10}$$

Substitution for  $t_b$  into the equation III.7 from equation III.10 gives:

$$\bar{d}_b = \frac{6 K_g}{\alpha} \frac{h}{2 \sqrt{\frac{g \bar{d}_b}{1.8}}} \quad \text{III.11}$$

On simplification equation III.11 becomes:

$$\bar{d}_b = 1.158 \left( \frac{K_g h}{\alpha} \right)^{\frac{2}{3}} \quad \text{III.12}$$

## APPENDIX IV

### METHODS FOR DETERMINATION OF POLLUTION PARAMETERS.

The laboratory methods described here and used in this work for the determination of pollution parameters are based on the standard methods of analysis (79, 113) with slight modifications.

#### IV.1 Determination of Chemical Oxygen Demand (COD)

Note that the method allows the determination of C.O.D. up to 500 mg/lt. Since CODs to be measured were much greater than 500 mg/lt., the samples were diluted prior to analysis.

The chemistry and the arithmetic involved will not be discussed and for this standard text books on inorganic chemical analysis should be referred to.

#### Reagents:

Potassium dichromate solution:- 7.662 gm/lt.

Ferrous ammonium sulphate solution:- 4.9 gm/lt.

containing 20 ml of concentrated M.A.R.

Sulphuric acid (sp. gr. 1.84).

Mercuric sulphate:- 20 gm in 100 ml of water

containing 10 ml of M.A.R. sulphuric acid (sp.gr. 1.84).

Silver sulphate/sulphuric acid solution:- 5 g

of silver sulphate added to a 500 ml of M.A.R. sulphuric acid (sp. gr. 1.84).

Indicator solution:- 1 : 10 phenanthroline

ferrous sulphate complex (B D H Ferroin indicator).

Apparatus:

Each unit consisted of round bottom Q and Q flask B 29/32, a condenser B 29/32 and a small beaker to invert over the top of the condenser to prevent dirt from getting into the dichromate solution. Assemblies of 6 units were built for either gas or electric heating.

Procedure:

To the 50 ml flask, 5 ml of diluted sample, 0.5 ml of mercuric sulphate, 2 ml of potassium dichromate solution (measured very accurately with Grade A pipette) and finally 7.5 ml of silver sulphate/sulphuric acid solution was added. The apparatus was assembled and the contents of the flasks were refluxed gently for 2 hours. The apparatus was allowed to cool for some time. Before removing the flasks, the insides of the condensers were rinsed with deionised water. The cooled mixture in the 50 ml flask was titrated against the standard ferrous ammonium sulphate solution using 2 drops of "Ferrouin" indicator with each batch of samples COD of one blank (5 ml tap water) was also determined.

The ferrous ammonium sulphate (FAS) solution was standardized against an acidified solution of potassium dichromate solution using "Ferrouin" indicator.

2 ml of  $K_2Cr_2O_7$  = 25 ml FAS

and: 1 ml of FAS = 20 mg COD.

Then: COD in mg/lt. = Titration (Test-Blank) ml. FAS x  
20 ml x Dilution.



Note that the dilution of the actual sample was such that it gave between 30 and 70 per cent reduction of the dichromate. To obtain the best dilution, it was necessary in the preliminary stage to prepare a range of samples at intervals of 1 : 10 or 1 : 50, until the best dilution was obtained. The experience later made the selection of dilution factor more easy. For instance, a dilution 1 : 200 was adopted for wastes having CODs between 20,000 and 40,000 mg/lt. and a dilution 1 : 20 for CODs between 3,000 and 5,000.

#### IV.2 Determination of Biological Oxygen Demand (BOD)

The method used was that developed by Water Pollution Research Laboratory (WPRL), Stevenage, England, and hence only the summary will be presented. For detail the reference should be made to official notifications of WPRL.

The test sample was mixed with a known volume of dilution water (deionized) which was saturated with air at 20°C. The diluted sample was divided into two portions and dissolved oxygen was determined immediately in one portion and in the other portion after storage in a completely filled bottle in the dark for 5 days at 20°C. The difference between the two concentrations of dissolved oxygen, corrected for the blank and multiplied by the dilution factor, is the BOD.

The amount of oxygen consumed was determined by the alkaline iodide azide reagents using N/8 sodium thiosulphate and starch indicator for the titrations.



#### IV. 3 Determination of Suspended Solids Concentrations (SS)

A diluted sample of waste liquid was filtered through a 7 cm fibre glass filter Grade GF/C with the aid of a vacuum pump. Before filtration the filter paper was dried in a forced draught oven at 100°C for 3 hours, cooled and weighed to 0.2 mg. A diluted sample of volume between 100 to 250 ml was poured into the assembled Hartley funnel and gentle vacuum was applied until all the sample had passed through the filter paper. The dilution was so chosen which allowed the filtration to be completed in less than an hour. The filter paper was further dried overnight at 105°C and after cooling was reweighed.

$$\text{SS in mg/lt.} = \frac{(\text{Total weight of filter paper with dry solids} - \text{weight of filter paper}) \text{ mg}}{\text{Volume of sample in ml}} \times \text{Dilution} \times 1000$$

#### IV. 4 Determination of Total Solids (% DM)

About 200 ml volumes of samples were poured into weighed shallow tins of about 30 cm in diameter. The samples were dried in a forced draught UNITHERM oven for 16 hours at 105°C. After this time the dried samples were allowed to cool and then reweighed.

The weight of the residue after evaporation is expressed as per cent of the initial weight of the sample and is termed as per cent dry matter.

#### IV. 5 Determination of Ammonia and Nitrate Nitrogen Concentration

Ammonia nitrogen was determined using an EIL (Electric Instruments Ltd., Surrey, England) ammonia specific ion electrode NO.8002-2.

The electrode can be used with any pH meter having an expanded scale. The EIL 7030 expanded pH scale meter allows direct read out of the ammonia concentration and is effective to 1 mg/lt. concentration.

50 ml of filtered sample was made alkaline with the addition of 1 ml 1N NaOH and the concentration of ammonia was read directly from the 3 decade concentration scales previously calibrated at 10, 100 and 1000 mg/lt. with ammonium chloride standards (3.819 gm of ammonium chloride = 1,000 mg/lt. ammonia nitrogen).

The technique of specific ion electrode measurement was similarly used for determining nitrate nitrogen using an Orion 92-07 electrode in conjunction with a potassium chloride reference electrode. Standards were prepared from sodium nitrate solution over the range 10 to 1,000 mg/lt. Test samples were made up in 1 : 10 solution of 0.1 M dihydrogen potassium phosphate buffer.

#### IV. 6 Waste Sample Material Balance

Let 1 kg of waste contain

$\ddot{x}$  kg of dry insoluble solids

and

$\ddot{z}$  kg of soluble solids

Also:

per cent dry matter of waste sample is  $\ddot{y}$

Since total solids are equal to sum of soluble and insoluble solids, therefore,

$$\ddot{y}/100 = (\ddot{x} + \ddot{z}) \quad \text{IV.1}$$

Let  $u$  be the dilution factor (volume basis) and  $w$  be per cent dry matter for the centrifuged liquid (diluted sample).

Hence, per cent dry matter of undiluted centrifuged liquid would be  $u \times w$ .

Fraction of dissolved solids in 1 kg waste,

$$\dot{z} = \frac{u w (1 - \ddot{x})}{100} \quad \text{IV.2}$$

By eliminating  $\ddot{x}$  using equation IV.1, the equation IV.2 can be written as

$$\dot{z} = \frac{u w (1 - 0.01 \dot{y})}{(100 - u w)} \quad \text{IV.3}$$

Also

$$\ddot{x} = 0.01 \dot{y} - \dot{z} \quad \text{IV.4}$$

Example calculations:

Run, L01, Day 13, Product

Dilution factor, u	= 5
Percent dry matter of centrifuged liquid, w	= 0.09
Per cent dry matter of waste sample, $\dot{y}$	= 0.69
Weight of 5 ml sample	= 4945 mg
Weight of 5 ml centrifuged liquid	= 4805 mg
Suspended solids concentration in waste	= 2600 mg/lt.
COD of waste sample	= 7050 mg/lt.
COD of centrifuged liquid (undiluted)	= 2800 mg/lt.

Fraction of dissolved solids,

$$\dot{z} = \frac{u x w (1 - 0.01 \dot{y})}{(100 - u x w)}$$

$$\dot{z} = \frac{5 \times 0.09 (1 - 0.0069)}{(100 - 5 \times 0.09)}$$

$$\dot{z} = 4.48 \times 10^{-3}$$

hence, fraction of insoluble solids from IV.4:

$$\ddot{x} = 2.42 \times 10^{-3}$$

$$\begin{aligned} \text{COD of waste} &= 7050 \text{ mg/lt.} \\ &= 7050 \text{ g/m}^3 \end{aligned}$$



and:

$$\text{weight of 5 ml sample} = 4.945 \text{ g}$$

Therefore:

$$\text{kg of COD per kg of waste} = \underline{7.13 \times 10^{-3}}$$

Similarly,

$$\begin{aligned} \text{COD of centrifuged liquid (corrected for dilution factor)} \\ = 2800 \text{ mg/lt.} \end{aligned}$$

and:

$$\text{Weight of 5 ml sample of liquid} = 4.805 \text{ g}$$

Therefore:

$$\text{COD of liquid in kg per kg of liquid} = 2.91 \times 10^{-3}$$

Hence:

$$\text{COD of } \frac{1}{2} \text{ kg of dissolved solids} = 2.91 \times 10^{-3} (1 - \frac{1}{2})$$

Or:

$$\text{Liquid COD in kg per kg of waste} = \underline{2.89 \times 10^{-3}}$$

$$\begin{aligned} \text{Dissolved solids COD in kg per kg of dissolved solids} &= \frac{2.89 \times 10^{-3}}{\frac{1}{2}} \\ &= \frac{2.89 \times 10^{-3}}{4.48 \times 10^{-3}} \\ &= \underline{0.645} \end{aligned}$$

COD of SS solids in 1 kg of waste

$$\begin{aligned} &= \text{COD in 1 kg of waste} - \text{COD of soluble fraction in} \\ &\quad \text{1 kg of waste.} \end{aligned}$$

$$= 7.128 \times 10^{-3} - 2.9 \times 10^{-3}$$

$$= \underline{4.23 \times 10^{-3}}$$



Suspended solids COD in kg per kg of suspended solids

$$= \frac{4.23 \times 10^{-3}}{\ddot{x}}$$

$$= \frac{4.23 \times 10^{-3}}{2.42 \times 10^{-3}}$$

$$= \underline{1.74}$$

Note:

When per cent dry matter for centrifuged liquid was not measured it was calculated from per cent dry matter of waste and suspended solid concentration.

## APPENDIX V

EXPERIMENTAL RESULTS  
IN  
TABULAR FORM

V.1	EXPERIMENTAL RESULTS ON SULPHITE OXIDATION	328
V.2	EXPERIMENTAL RESULTS ON AIR ENTRAINMENT	331 ,
V.3	EXPERIMENTAL RESULTS ON OXYGEN TRANSFER IN PLUNGING JET REACTOR WITH SULPHITE SYSTEM	341
V.4	EXPERIMENTAL RESULTS ON OXYGEN TRANSFER IN PLUNGING JET REACTOR WITH BIOLOGICAL SYSTEM	346
V.5	EXPERIMENTAL RESULTS ON BIOLOGICAL CONTINUOUS REACTOR	350

TABLE V.1.1.A Experimental Results on Sulphite Oxidation in Continuous Reactor

Reactor liquid volume - $4.4 \times 10^{-2} \text{ m}^3$ , Liquid temperature - $20 \pm 1^\circ\text{C}$							
Run	Feed and Product Rate $\text{m}^3/\text{s} \times 10^{-5}$	$\text{SO}_3^-$ Conc. in $\text{m}^3 \times 10^{-2}$ $\text{kmol}/\text{m}^3 \times 10^{-2}$	$\text{SO}_3^-$ Conc. Product in $\text{m}^3 \times 10^{-2}$ $\text{kmol}/\text{m}^3 \times 10^{-2}$	$\text{Co}^{++}$ Conc $\text{kmol}/\text{m}^3 \times 10^{-4}$	pH	Stirrer speed $\text{rpm} \times 10^3$	$\text{O}_2$ Transfer Rate $\text{kg}/\text{s} \times 10^{-5}$
A01	1.67	6.25	3.98	0.04	8.5	3.1	0.60
A02	1.67	0.92	0.043	0.04	8.5	3.1	0.23
A03	1.67	3.96	2.07	0.04	8.5	3.1	0.50
A04	1.67	15.7	12.8	0.04	8.5	3.1	0.78
A05	1.67	12.5	9.82	0.04	8.5	3.1	0.71
A06	1.67	15.8	12.5	0.04	8.5	3.1	0.88
A07	1.67	8.84	5.92	0.04	8.5	3.1	0.78
A08	1.67	3.85	2.68	0.04	5.65	3.3	0.44
A09	2.33	4.29	2.28	0.04	7.4	3.3	0.75
A10	2.33	5.09	1.56	0.04	10	3.3	1.32
A11	2.33	4.41	2.07	0.1	8.55	3.3	0.87
A12	2.33	4.27	1.52	0.2	8.55	3.3	1.01
A13	2.33	3.99	0.95	0.5	8.55	3.3	1.14
A14	2.33	4.38	0.92	1.0	8.55	3.3	1.29

TABLE V.1.B      Experimental Results on Sulphite Oxidation in Batch Reactor

Reactor liquid volume -- $4.4 \times 10^{-2} \text{ m}^3$ Liquid temperature -- $20 \pm 1^\circ\text{C}$						
Run	Initial $\text{SO}_3^{=}$ Conc. $\text{kmol/m}^3 \times 10^{-1}$	Final $\text{SO}_3^{=}$ Conc. $\text{kmol/m}^3 \times 10^{-1}$	$\text{C}_O^{++}$ Conc. $\text{kmol/m}^3 \times 10^{-5}$	pH	Stirrer Speed $\text{rpm} \times 10^3$	$\text{O}_2$ Transfer Rate $\text{kg/s} \times 10^{-5}$
B01	2.93	2.67	0.033	8.5	3.27	0.84
B02	3.18	3.02	0.1	8.5	3.27	0.63
B03	1.31	1.06	1.0	8.5	3.27	0.67
B04	2.94	2.66	8.0	8.5	3.1	0.94
B05	0.62	1.47	30	8.5	3.2	2.26
B06	0.96	0.79	30	8.5	0.66	0.65
B07	1.1	0.62	30	8.5	1.01	1.47
B08	1.13	0.87	30	8.5	1.7	1.22
B09	1.81	1.28	30	8.5	3.68	3.16



TABLE V.1.C   Experimental Results on Sulphite Oxidation in Batch Reactor with Pure Oxygen

Reactor liquid volume -  $4.4 \times 10^{-2} \text{ m}^3$        $C_o^{++}$  concentration -  $4 \times 10^{-6} \text{ kmol/m}^3$   
Liquid temperature -  $20 \pm 1 \text{ }^\circ\text{C}$   
Stirrer speed - 3100 rpm      pH - 8.5

Run	Initial $\text{SO}_3^{--}$ Conc. $\text{kmol/m}^3 \times 10^{-1}$	Final $\text{SO}_3^{--}$ Conc. $\text{Kmol/m}^3 \times 10^{-1}$	$\text{O}_2$ Pressure $\text{kN/m}^2 \times 10^2$	$\text{O}_2$ Transfer Rate $\text{kg/s} \times 10^{-5}$
C01	1.84	1.58	0.52	1.02
C02	1.39	6.48	0.78	2.86
C03	2.78	1.89	1.01	2.23
C04	1.97	1.23	1.01	2.44
C05	1.75	1.31	1.23	1.8
C06	2.76	1.45	1.44	4.3

TABLE V.2.Da      Experimental Results on Air Entrainment in the  
Plunging Jet System<sup>+</sup> with Cylindrical Nozzles.

Run	Jet Length 0.41 m							
	Nozzle Dia. mm.	Jet Liquid Flow Rate $\text{m}^3/\text{s} \times 10^{-3}$	Jet Velocity m/s	Entrain- ment Rate $\text{m}^3/\text{s} \times 10^{-3}$	Reynolds Number <sup>a</sup> (-) $\times 10^5$	Weber Number	Jet Power W	Entrain- ment Ratio <sup>b</sup>
D001	9.5	1.11	15.53	1.17	1.29	38	133	1.06
D002	9.5	1.47	20.69	2.76	1.73	68	315	1.87
D003	9.5	1.47	20.69	3.08	1.73	67	315	2.09
D004	9.5	1.47	20.69	2.84	1.73	68	315	1.93
D005	12.7	1.68	13.24	1.30	1.47	37	147	0.77
D006	12.7	2.46	19.43	2.84	2.16	79	464	1.15
D007	12.7	2.77	21.90	3.57	2.44	101	665	1.29
D008	12.7	3.11	24.56	4.66	2.73	127	938	1.5
D009	12.7	3.16	24.98	5.02	2.78	131	987	1.59
D010	12.7	3.41	26.97	5.71	3.	153	1242	1.67
D011	12.7	3.41	26.97	5.79	3.	153	1242	1.7
D012	12.7	3.51	27.73	5.67	3.08	162	1350	1.62
D013	22.2	2.10	5.42	1.05	1.06	11	31	0.50
D014	22.2	2.53	6.51	1.3	1.27	16	54	0.51
D015	22.2	2.53	6.51	1.62	1.27	16	54	0.64
D016	22.2	3.27	8.42	2.47	1.64	26	116	0.76
D017	22.2	3.56	9.18	3.	1.79	31	150	0.84
D018	22.2	3.74	9.65	3.65	1.88	34	174	0.98
D019	22.2	3.87	9.99	3.65	1.94	37	193	0.94
D020	22.2	4.32	11.15	4.62	2.17	46	269	1.07
D021	22.2	4.73	12.21	5.75	2.38	55	353	1.22
D022	22.2	4.77	12.3	6.08	2.39	56	361	1.27

<sup>a</sup>Based on nozzle diameter.

<sup>b</sup>Air entrainment rate ( $\text{m}^3/\text{s}$ ) / Jet Liquid flow rate ( $\text{m}^3/\text{s}$ ).

<sup>+</sup>Air-water system.

TABLE V.2. Da (continued)

Run	Jet Length 0.41 m							
	Nozzle Dia. mm.	Jet Liquid Flow Rate $\text{m}^3/\text{s} \times 10^{-3}$	Jet Velocity m/s	Entrainment Rate $\text{m}^3/\text{s} \times 10^{-3}$	Reynolds Number <sup>a</sup> (-) $\times 10^5$	Weber Number	Jet Power kW	Entrainment Ratio <sup>b</sup>
D023	28.6	2.32	3.63	0.57	0.91	6.2	15.3	0.24
D024	28.6	2.32	3.63	0.81	0.91	6.2	15.3	0.35
D025	28.6	2.53	3.94	1.13	0.99	7.4	19.6	0.45
D026	28.6	2.58	4.04	1.05	1.01	7.7	21.1	0.41
D027	28.6	2.89	4.51	1.22	1.13	9.6	29	0.42
D028	28.6	3	4.68	1.62	1.17	10.4	33	0.54
D029	28.6	3.32	5.17	2.19	1.29	12.7	44	0.66
D030	28.6	3.56	5.55	1.86	1.38	14.6	55	0.52
D031	28.6	3.65	5.7	2.43	1.42	15.4	59	0.67
D032	28.6	3.74	5.84	2.27	1.46	16	64	0.61
D033	28.6	3.92	6.11	2.59	1.53	18	73	0.66
D034	28.6	4.04	6.31	2.84	1.58	19	80	0.70
D035	28.6	4.20	6.56	3.32	1.64	20	90	0.79
D036	28.6	4.55	7.10	4.29	1.78	24	115	0.94
D037	28.6	4.66	7.27	4.54	1.82	25	123	0.97
D038	28.6	4.91	7.66	5.11	1.92	28	144	1.04
D039	28.6	4.94	7.71	4.62	1.93	28	147	0.93
D040	38.1	2.39	2.1	1.05	0.70	2.8	5.3	0.44
D041	38.1	2.59	2.27	0.49	0.76	3.3	6.7	0.19
D042	38.1	2.65	2.33	0.73	0.78	3.4	7.2	0.27
D043	38.1	2.77	2.43	1.38	0.81	3.7	8.2	0.50
D044	38.1	3.00	2.63	1.78	0.88	4.4	10.4	0.60
D045	38.1	4.73	4.15	2.19	1.39	10.9	41	0.46
D046	38.1	4.73	4.15	2.51	1.39	10.9	41	0.53



TABLE V.2.Db      Experimental Results on Air Entrainment in the Plunging  
 Jet System with Cylindrical Nozzles <sup>+</sup>

Run	Jet Length 0.66 m							
	Nozzle Dia. mm.	Jet Liquid Flow Rate $\text{m}^3/\text{s} \times 10^{-3}$	Jet Velocity m/s	Entrainment Rate $\text{m}^3/\text{s} \times 10^{-3}$	Reynolds Number <sup>a</sup> (-) $\times 10^5$	Weber Number	Jet Power 'W'	Entrain- ment Ratio <sup>b</sup>
D047	9.5	0.95	13.4	2.59	1.11	28	86	2.72
D048	9.5	1.24	17.4	4.42	1.45	48	188	3.57
D049	9.5	1.42	20	5.35	1.66	63	281	3.77
D050	12.7	1.47	11.64	2.11	1.29	29	100	1.43
D051	12.7	1.47	11.64	2.03	1.29	29	100	1.38
D052	12.7	1.86	14.68	3	1.63	45	200	1.61
D053	12.7	2.02	15.99	3.61	1.78	54	259	1.78
D054	12.7	2.18	17.21	4.38	1.91	62	323	2.01
D055	12.7	2.32	18.35	4.38	2.04	71	391	1.88
D056	12.7	2.46	19.43	5.19	2.16	79	464	2.11
D057	12.7	2.77	21.9	6.73	2.44	101	665	2.43
D058	12.7	2.83	22.37	7.37	2.49	105	709	2.6
D059	12.7	3.11	24.56	8.10	2.73	127	938	2.61
D060	12.7	3.37	26.58	11.1	2.96	149	1190	3.3
D061	12.7	3.37	26.58	10.01	2.96	149	1190	2.97
D062	22.2	1.47	3.8	1.3	0.74	5.3	11	0.88
D063	22.2	2.02	5.22	2.03	1.02	10	28	1
D064	22.2	2.25	5.81	2.23	1.13	12.4	38	1
D065	22.2	2.46	6.34	2.84	1.23	15	50	1.15
D066	22.2	3.37	8.68	5.59	1.69	28	127	1.67
D067	22.2	2.65	6.84	3.12	1.33	17.24	62	1.18
D068	22.2	2.65	6.84	3.24	1.33	17.24	62	1.22
D069	22.2	2.71	7	3.65	1.36	18	66	1.35
D070	22.2	2.95	7.6	3.61	1.48	21	85	1.22
D071	22.2	3.11	8.02	4.09	1.56	24	100	1.32
D072	22.2	3.16	8.16	4.66	1.59	25	105	1.48

<sup>a</sup> Based on nozzle diameter

<sup>b</sup> Air entrainment rate ( $\text{m}^3/\text{s}$ )/Jet Liquid Flow rate ( $\text{m}^3/\text{s}$ ).

<sup>+</sup> Air-water system.



TABLE V.2.Db (continued)

Run	Jet Length 0.66 m							
	Nozzle Dia. mm.	Jet Liquid Flow Rate $\text{m}^3/\text{s} \times 10^{-3}$	Jet Velocity m/s	Entrainment Rate $\text{m}^3/\text{s} \times 10^{-3}$	Reynolds Number <sup>a</sup> (-) $\times 10^5$	Weber Number	Jet Power W	Entrainment Ratio <sup>b</sup>
D073	22.2	3.41	8.81	5.39	1.71	29	132	1.58
D074	22.2	3.41	8.81	5.51	1.71	29	132	1.62
D075	28.6	1.77	2.76	1.38	0.69	3.6	6.7	0.78
D076	28.6	1.86	2.9	1.38	0.73	4	7.8	0.74
D077	28.6	2.02	3.16	1.62	0.79	4.7	10	0.8
D078	28.6	2.39	3.73	2.03	0.93	6.6	17	0.85
D079	28.6	2.46	3.84	2.43	0.96	7	18	1.0
D080	28.6	2.83	4.42	2.84	1.11	9.2	28	1
D081	28.6	3	4.68	3.36	1.17	10	33	1.12
D082	28.6	3.16	4.93	3.57	1.23	12	38	1.13
D083	28.6	3.32	5.17	4.54	1.29	13	44	1.37
D084	28.6	3.65	5.7	4.62	1.43	15	59	1.27
D085	28.6	3.92	6.1	5.55	1.53	18	73	1.42
D086	28.6	4	6.24	5.63	1.56	18	78	1.41
D087	28.6	4.51	7.04	7.5	1.76	23	112	1.66
D088	28.6	4.7	7.33	7.86	1.83	25	126	1.68
D089	28.6	4.77	7.44	8.71	1.86	26	132	1.83
D090	38.1	1.58	1.38	1.22	0.46	1.21	1.5	0.77
D091	38.1	2.1	1.85	1.62	0.62	2.2	3.6	0.77
D092	38.1	2.25	1.98	1.42	0.66	2.5	4.4	0.63
D093	38.1	2.39	2.1	1.86	0.70	2.8	5.3	0.78
D094	38.1	2.65	2.33	2.15	0.78	3.4	7.2	0.81
D095	38.1	2.77	2.43	1.86	0.81	3.7	8.2	0.67
D096	38.1	3.27	2.87	2.27	0.96	5.2	13.4	0.7
D097	38.1	3.27	2.87	3.28	0.96	5.2	13.4	1.01
D098	38.1	3.56	3.12	3.52	1.04	6.2	17	1
D099	38.1	3.83	3.36	2.8	1.12	7.1	22	0.73
D100	38.1	4.20	3.69	3.57	1.23	8.6	29	0.85
D101	38.1	4.44	3.9	3.85	1.3	9.6	34	0.87
D102	38.1	4.84	4.25	4.54	1.42	11.4	44	0.94
D103	38.1	4.84	4.25	4.38	1.42	11.4	44	0.91

TABLE V.2.Dc      Experimental Results on Air Entrainment in the Plunging  
Jet System with Cylindrical Nozzles <sup>+</sup>

Run	Jet Length 1.05 m							
	Nozzle Dia. mm	Jet Liquid Flow Rate m <sup>3</sup> /s x 10 <sup>-3</sup>	Jet Velocity m/s	Entrainment Rate m <sup>3</sup> /s x 10 <sup>-3</sup>	Reynolds Number <sup>a</sup> (-) x 10 <sup>5</sup>	Weber Number	Jet Power 'W'	Entrainment Ratio <sup>b</sup>
D104	12.7	2.10	16.61	3.65	1.85	58	290	1.74
D105	12.7	2.53	19.95	5.92	2.22	84	503	2.34
D106	12.7	2.89	22.82	7.90	2.54	110	753	2.74
D107	12.7	3.46	27.35	10.62	3.04	158	1296	3.07
D108	22.2	1.68	4.32	0.73	0.84	6.9	15.7	0.44
D109*	22.2	1.84	4.75	1.22	-	-	20	0.66
D110	22.2	2.36	6.08	2.35	1.18	13.6	44	1.0
D111	22.2	2.77	7.15	3.40	1.39	19	71	1.23
D112	22.2	2.89	7.45	3.48	1.45	20	80	1.21
D113*	22.2	2.91	7.48	3.50	-	-	86	1.21
D114	22.2	3.11	8.02	4.46	1.56	24	100	1.44
D115	22.2	3.32	8.55	5.27	1.66	27	121	1.59
D116*	22.2	3.41	8.78	5.3	-	-	130	1.56
D117*	22.2	3.41	8.78	6.1	-	-	130	1.79
D118	22.2	3.51	9.05	6.08	1.76	30	144	1.74
D119*	22.2	3.53	9.1	6.03	-	-	146	1.7
D120	22.2	3.56	9.18	6	1.79	31	150	1.69
D121	22.2	3.79	9.76	6.08	1.89	35	180	1.6
D122*	22.2	3.93	10.12	7.1	-	-	199	1.8
D123	22.2	3.96	10.21	7.05	1.99	38	206	1.78
D124*	22.2	4.33	11.04	8.3	-	-	264	1.92
D125	22.2	4.36	11.24	8.27	2.19	47	276	1.90
D126	22.2	4.40	11.35	8.27	2.21	47	283	1.88
D127	22.2	4.51	11.64	9.16	2.27	50	306	2.04
D128*	22.2	4.57	11.78	9.2	-	-	313	2.0
D129	22.2	4.80	12.39	9.12	2.41	57	369	1.90
D130	22.2	5.11	13.18	10.13	2.57	64	444	1.99
D131	28.6	1.86	2.90	0.57	0.73	4	7.8	0.31
D132	28.6	2.37	3.7	1.38	0.92	6.5	16.0	0.58

a Based on nozzle diameter.

b Air entrainment rate (m<sup>3</sup>/s)/Jet Liquid flow rate (m<sup>3</sup>/s).

+ Air-water system; however, runs marked \* are with air-biological system.



TABLE V.2.Dc (continued)

Run	Jet Length 1.05 m							
	Nozzle Dia. mm.	Jet Liquid Flow Rate $\text{m}^3/\text{s} \times 10^{-3}$	Jet Velocity m/s	Entrainment Rate $\text{m}^3/\text{s} \times 10^{-3}$	Reynolds Number <sup>a</sup> (-) $\times 10^5$	Weber Number	Jet Power 'W'	Entrain- ment <sup>b</sup> Ratio
D133	28.6	2.89	4.51	2.43	1.13	9.6	29	0.84
D134	28.6	3.16	4.93	3.0	1.23	11.5	38	0.95
D135	28.6	3.41	5.33	3.69	1.33	13.4	48	1.08
D136	28.6	3.65	5.7	5.11	1.43	15.4	59	1.4
D137	28.6	3.83	5.97	5.27	1.49	17	68	1.38
D138	28.6	4.12	6.43	5.43	1.61	20	85	1.32
D139	28.6	4.48	6.98	6.81	1.75	23	109	1.52
D140	28.6	4.91	7.66	7.13	1.92	28	144	1.46
D141	28.6	5.14	8.03	7.7	2.01	31	166	1.5
D142	38.1	2.10	1.85	0.89	0.62	2.2	3.6	0.42
D143	38.1	2.32	2.04	1.05	0.68	2.6	4.8	0.45
D144	38.1	2.74	2.4	1.3	0.80	3.7	8	0.42
D145	38.1	2.95	2.59	2.51	0.86	4.2	9.8	0.85
D146	38.1	3.32	2.91	3.24	0.97	5.3	14	0.98
D147	38.1	3.32	2.91	2.71	0.97	5.3	14	0.82
D148	38.1	3.65	3.20	3.32	1.07	6.5	19	0.91
D149	38.1	4	3.51	4.46	1.17	7.8	25	1.11
D150	38.1	4.73	4.15	4.05	1.39	11	41	0.86
D151	38.1	5.08	4.46	4.86	1.49	13	50	0.96
D152	38.1	5.11	4.49	4.46	1.50	12.7	51	0.87

TABLE V.2.E                      Experimental Results on Air Entrainment  
 through the Inner Tube of Annular  
 Nozzle at Various Jet Lengths

Annular nozzle - 33 mm outer dia., 25.4 mm inner dia., Air-water system					
Run	Jet Length $\text{m} \times 10^{-2}$	Jet Velocity $\text{m/s}$	Air Flow <sup>a</sup> Measured $\text{ft}^3$	Time <sup>b</sup> $\text{s}$	Entrainment Rate $\text{m}^3/\text{s} \times 10^{-3}$
E01	0.3	11	2	35	1.62
E02	0.3	9	2	44	1.29
E03	0.3	7.2	2	76	0.75
E04	2.5	11	2	41	1.39
E05	2.5	9	2	50	1.14
E06	2.5	7.2	2	89	0.64
E07	5.1	11	2	48	1.18
E08	5.1	9	2	56	1.02
E09	5.1	7.2	2	109	0.52
E10	7.6	11	1	34	0.84
E11	7.6	9	1	42	0.68
E12	7.6	7.2	1	71	0.4
E13	12.7	11	1	40	0.71
E14	12.7	9	1	54	0.53
E15	12.7	7.2	1	153	0.19
E16	17.8	11	1	36	0.79
E17	17.8	9	1	47	0.61

a and b                      The tabulated air flow was measured by a gas meter  
 during the tabulated time.



TABLE V.2.Fa      Experimental Results on Air Entrainment in Plunging  
Jet System    with Annular Nozzles <sup>+</sup>

Run	Jet Length 0.66 m						
	Nozzle <sup>a</sup>		Jet Liquid Flow Rate	Jet Velocity	Entrainment Rate	Jet Power	Entrainment Ratio
	Outer Dia. mm.	Inner Dia. mm.					
			m <sup>3</sup> /s x 10 <sup>-3</sup>	m/s	m <sup>3</sup> /s x 10 <sup>-3</sup>	W	
F01	19.7	15.9	1.76	16.55	2.93	242	1.67
F02	19.7	15.9	2.22	20.9	7.89	486	3.55
F03	19.7	15.9	2.29	21.5	9.76	531	4.26
F04	29.2	25.4	1.09	6.64	1.06	24	0.97
F05	29.2	25.4	1.22	7.46	0.814	34	0.67
F06	29.2	25.4	1.56	9.56	2.04	71	1.3
F07	29.2	25.4	1.76	10.77	2.19	102	1.25
F08	29.2	25.4	1.84	11.25	3.01	116	1.64
F09	29.2	25.4	2.08	12.7	3.74	169	1.8
F10	29.2	25.4	2.14	13.1	4.06	183	1.9
F11	29.2	25.4	2.5	15.39	6.67	296	2.67
F12	29.2	25.4	2.57	15.7	8.7	317	3.38
F13	29.2	25.4	2.84	17.39	12.2	432	4.3
F14	29.2	25.4	2.9	17.7	11.3	457	3.9
F15	29.2	25.4	3.07	18.79	13.68	538	4.45
F16	33	25.4	1.76	5.03	0.97	23	0.55
F17	33	25.4	2.24	6.4	2.2	46	0.98
F18	33	25.4	2.62	7.48	3.25	74	1.24
F19	33	25.4	3.15	9.0	4.46	130	1.42
F20	33	25.4	3.90	11.15	7.07	244	1.81
F21	33	25.4	4.13	11.8	8.54	289	2.07
F22	33	25.4	4.4	12.59	10.17	351	2.31
F23	33	25.4	4.4	12.59	9.16	351	2.08

<sup>a</sup>Outer and inner diameters of annular nozzle are defined in Fig.9.3, page 135

<sup>+</sup> Air-water System.

TABLE V.2.Fa (continued)

	Jet Length 0.66 m						
	Nozzle		Jet Liquid Flow Rate	Jet Velocity	Entrainment Rate	Jet Power	Entrainment Ratio
	Outer Dia. mm.	Inner Dia. mm.					
			$\text{m}^3/\text{s} \times 10^{-3}$	m/s	$\text{m}^3/\text{s} \times 10^{-3}$	!W!	
F24	38.1	25.4	2.02	3.19	1.14	10	0.56
F25	38.1	25.4	2.62	4.14	2.12	22	0.81
F26	38.1	25.4	3.03	4.78	2.93	34	0.97
F27	38.1	25.4	3.49	5.51	3.58	52	1.03
F28	38.1	25.4	3.90	6.16	4.06	74	1.04
F29	38.1	25.4	4.28	6.77	4.64	98	1.08
F30	38.1	25.4	4.94	7.79	6.18	148	1.25

TABLE V.2.Fb      Experimental Results on Air Entrainment in Plunging  
                                 Jet System, with Annular Nozzles.<sup>+</sup>

Run	Jet Length 0.98 m						
	Nozzle <sup>a</sup>		Jet Liquid Flow Rate	Jet Velocity	Entrainment Rate	Jet Power	Entrainment Ratio
	Outer Dia. mm	Inner Dia. mm					
			m <sup>3</sup> /s x 10 <sup>-3</sup>	m/s	m <sup>3</sup> /s x 10 <sup>-3</sup>		
F31	19.7	15.9	1.08	10.18	1.63	56	1.5
F32	19.7	15.9	1.77	16.6	6.18	243	3.5
F33	19.7	15.9	1.92	18	7.8	309	4.1
F34	19.7	15.9	2.22	20.8	11.38	481	5.13
F35	29.2	25.4	1.46	8.89	1.3	57	0.88
F36	29.2	25.4	1.77	10.8	3.5	103	1.98
F37	29.2	25.4	2.08	12.73	5.86	168	2.82
F38	29.2	25.4	2.52	15.4	10.59	299	4.20
F39	29.2	25.4	2.78	16.9	13	394	4.66
F40	29.2	25.4	3.07	18.8	17.1	539	5.56
F41	33	25.4	1.45	4.15	0.65	12.4	0.45
F42	33	25.4	1.57	4.47	0.81	16	0.52
F43	33	25.4	2.02	5.77	1.95	34	0.97
F44	33	25.4	2.08	5.95	2.03	37	0.97
F45	33	25.4	2.30	6.56	2.44	49	1.06
F46	33	25.4	2.62	7.5	3.83	74	1.46
F47	33	25.4	2.90	8.3	4.56	100	1.57
F48	33	25.4	3.1	8.84	4.88	120	1.58
F49	33	25.4	3.13	8.95	5.7	125	1.82
F50	33	25.4	3.66	10.46	8.14	199	2.22
F51	33	25.4	3.9	11.18	9.76	244	2.5
F52	33	25.4	4.1	11.72	10.5	281	2.56
F53	33	25.4	4.27	12.23	11.64	319	2.72
F54	33	25.4	4.35	12.45	12.2	336	2.80
F55	38.1	25.4	2.24	3.53	1.3	14	0.58
F56	38.1	25.4	2.66	4.19	2.11	23	0.79
F57	38.1	25.4	3.13	4.95	2.76	38	0.88
F58	38.1	25.4	3.49	5.51	3.26	52	0.94
F59	38.1	25.4	3.90	6.16	4.06	66	1.04
F60	38.1	25.4	4.15	6.56	4.88	74	1.18
F61	38.1	25.4	4.54	7.17	5.45	116	1.2

<sup>a</sup>Outer and inner diameters of annular nozzle are defined in Fig. 9.3 page 135

<sup>+</sup>Air-water system.



TABLE V.3.G

Experimental Results on Aeration of Sulphite System in a Plunging Jet Reactor with Cylindrical Jets.

Liquid volume - 0.9 m<sup>3</sup>, SO<sub>3</sub><sup>==</sup> concentration - > 0.06 kmol/m<sup>3</sup>, C<sub>O</sub><sup>++</sup> concentration - 4 x 10<sup>-6</sup> kmol/m<sup>3</sup>

Run	Nozzle Position (H, $\theta$ , R) <sup>a</sup>	Nozzle Dia. mm	Jet <sup>b</sup> Velocity m/s	Measured Power <sup>c</sup> W	Jet Reynolds Number <sup>d</sup> (-) x 10 <sup>5</sup>	Jet Power W	O <sub>2</sub> Transfer Rate kg/s x 10 <sup>-4</sup>	Aeration <sup>f</sup> Efficiency kgO <sub>2</sub> /kW h	Liquid Temp. °C	Exp. <sup>g</sup> Error <sup>g</sup> + -%
G01	(0.2, 90, 0)	9.5	7.09	19	0.68	13	0.16	4.48	-	35.1
G02	(0.2, 90, 0)	9.5	8.87	35	0.84	25	0.23	3.34	19	31.9
G03	(0.2, 90, 0)	9.5	11.08	65	1.05	48	0.51	3.76	19	14.3
G04	(0.2, 90, 0)	22.2	4.89	55	1.08	23	0.304	4.85	-	18.7
G05	(0.2, 90, 0)	22.2	6.50	116	1.44	53	0.64	4.28	-	8.4
G06	(0.2, 90, 0)	22.2	6.84	119	1.51	62	0.67	3.88	28	11.9
G07	(0.2, 90, 0)	22.2	11.33	482	2.51	282	2.57	3.29	34	4.2
G08	(0.2, 90, 0)	22.2	11.35	367	2.52	283	3.43	4.35	-	3.8
G09	(0.2, 90, 0)	28.6	3.15	46	0.90	10	0.091	3.26	17	51.3
G10	(0.2, 90, 0)	28.6	4.13	91	1.18	23	0.28	4.44	-	20.4
G11	(0.2, 90, 0)	28.6	4.33	72	1.24	26	0.21	2.92	25	15.6
G12	(0.2, 90, 0)	28.6	5.22	160	1.49	46	0.47	3.72	19	15.6
G13	(0.2, 90, 0)	28.6	6.36	239	1.81	83	0.58	2.54	25	3.8

<sup>a</sup> H denotes the height of nozzle exit from liquid surface in m,  $\theta$  is the jet angle to liquid surface in degrees, and R is the off-centricity of jet in m.

<sup>b</sup> Velocity of jet at nozzle end ( $d_j = d_n$ ).

<sup>d</sup> Based on nozzle diameter.

<sup>c</sup> Power measured by measuring the static heads at inlet and outlet of the pump rate can be calculated by adding to the tabulated value the oxygen transfer through tank liquid surface and jet surface which is given by  $(3.63 \times 10^{-6} + 1.31 \times 10^{-5} d_n^{-5} d_n l_j)$  where  $d_n$  (nozzle dia.) and  $l_j$  (jet length) are in m.

<sup>f</sup> Aeration efficiency is based on jet power.

<sup>g</sup> Error is within 95% confidence range.



TABLE V.3.G (continued)

Run	Nozzle Position (H, $\theta$ , R) <sup>a</sup>	Nozzle Dia. mm	Jet Velocity $b$ m/s	Measured Power W	Jet Reynolds Number (-) $\times 10^5$	Jet Power W	O <sub>2</sub> Transfer Rate kg/s $\times 10^{-4}$	Aeration Efficiency kgO <sub>2</sub> /kW h	Liquid Temp. °C	Exp. Error <sup>g</sup> ± %
G14	(0.2, 90, 0)	28.6	8.18	466	2.33	175	2.57	5.28	26	10
G15	(0.2, 90, 0)	38.1	2.55	94	0.97	9.4	0.18	6.94	22	36.6
G16	(0.2, 90, 0)	38.1	3.32	162	1.26	21	0.31	5.28	-	19
G17	(0.2, 90, 0)	38.1	3.86	224	1.47	33	0.19	2.03	25	12.8
G18	(0.2, 90, 0)	38.1	4.71	429	1.79	60	0.63	3.79	26	17.8
G19	(0.41, 90, 0)	9.5	8.87	36	0.84	25	0.302	4.38	-	13.6
G20	(0.41, 90, 0)	9.5	11.53	-	1.09	55	0.68	4.49	20	13.01
G21	(0.41, 90, 0)	22.2	3.58	29	0.80	8.9	0.10	4.06	20	24.8
G22	(0.41, 90, 0)	22.2	5.7	86	1.26	36	0.42	4.16	20	8.1
G23	(0.41, 90, 0)	22.2	7.73	192	1.71	90	1.03	4.12	19	11.6
G24	(0.41, 90, 0)	28.6	2.56	32	0.72	5.4	0.064	4.25	20	46.6
G25	(0.41, 90, 0)	28.6	4.04	86	1.15	21	0.37	6.33	-	16.3
G26	(0.41, 90, 0)	28.6	5.62	194	1.60	57	0.84	5.34	20	13.3
G27	(0.41, 90, 0)	38.1	1.88	47	0.72	3.8	0.083	7.89	-	38.3
G28	(0.41, 90, 0)	38.1	2.66	108	1.01	11	0.29	9.86	-	15.9
G29	(0.41, 90, 0)	38.1	3.32	168	1.26	21	0.38	6.54	20	18.7
G30	(0.2, 90, 0.2)	22.2	5.86	89	1.3	39	0.53	5.18	18	20.8
G31	(0.2, 90, 0.2)	22.2	7.82	193	1.73	93	1.02	3.96	-	7.1
G32	(0.2, 90, 0.2)	22.2	9.06	254	2.01	144	1.85	4.63	-	5.6
G33	(0.2, 90, 0.2)	22.2	11.25	459	2.49	276	3.66	4.77	-	3.1
G34	(0.2, 90, 0.41)	22.2	5.88	89	1.3	39	0.35	3.22	-	21.1
G35	(0.2, 90, 0.41)	22.2	7.84	194	1.74	93	1.07	4.12	24	9
G36	(0.2, 90, 0.41)	22.2	8.93	243	1.98	138	1.57	4.11	-	2.6
G37	(0.2, 90, 0.41)	22.2	10.95	453	2.43	254	2.71	3.84	-	4.5
G38	(0.2, 40, 0)	22.2	3.09	20	0.69	5.7	0.063	3.96	20	50.9
G39	(0.2, 40, 0)	22.2	5.9	39	1.31	40	0.404	3.66	18.5	23.5
G40	(0.2, 40, 0)	22.2	6.34	90	1.41	50	0.35	2.55	-	14.8
G41	(0.2, 40, 0)	22.2	7.82	194	1.73	93	0.78	3.03	-	7.5

TABLE V.3.G (continued)

Run	Nozzle Position (H, $\theta$ , R) a	Nozzle Dia. mm	Jet b Velocity m/s	Measured Power c W	Jet Reynolds Number d (-) $\times 10^5$	Jet Power	O <sub>2</sub> Transfer Rate e kg/s $\times 10^{-4}$	Aeration f Efficiency kgO <sub>2</sub> /kW h	Liquid Temp. °C	Exp. g Error + - %
G42	(0.2, 40, 0)	22.2	9.17	262	2.03	150	1.19	2.85	24	27
G43	(0.2, 40, 0)	22.2	11.35	467	2.52	283	2.3	2.92	25	6
G44	(0.2, 60, 0)	22.2	3.09	20	0.69	5.7	0.031	1.92	23	28.3
G45	(0.2, 60, 0)	22.2	4.07	38	0.90	13	0.16	4.35	23	43.3
G46	(0.2, 60, 0)	22.2	5.62	71	1.25	34	0.46	4.82	18	12.6
G47	(0.2, 60, 0)	22.2	5.86	91	1.3	39	0.44	4.07	24	7.1
G48	(0.2, 60, 0)	22.2	7.82	192	1.73	93	1.08	4.19	23	26.3
G49	(0.2, 60, 0)	22.2	10.42	303	2.31	220	1.58	2.6	20	9.7
G50	(0.2, 80, 0)	22.2	5.86	89	1.3	39	0.43	3.97	-	13.9
G51	(0.2, 80, 0)	22.2	7.82	191	1.73	93	1.3	5.06	-	10.5
G52	(0.2, 80, 0)	22.2	8.81	229	1.95	132	1.38	3.75	24	3.4
G53	(0.2, 80, 0)	22.2	11.25	467	2.49	276	2.21	2.89	24	3.9
G54	(0.2, 40, 0.2)	22.2	4.56	48	1.01	18	0.59	11.56	-	42.2
G55	(0.2, 40, 0.2)	22.2	4.9	54	1.09	22	0.304	4.96	24	45.4
G56	(0.2, 40, 0.2)	22.2	6.51	126	1.44	54	0.71	4.76	-	31.3
G57	(0.2, 40, 0.2)	22.2	7.74	165	1.72	90	0.62	2.48	32	12.3
G58	(0.2, 40, 0.2)	22.2	7.98	203	1.77	98	1.08	3.95	-	10.
G59	(0.2, 40, 0.2)	22.2	9.76	313	2.16	180	1.01	2.01	34	9.3
G60	(0.2, 40, 0.2)	22.2	11.15	462	2.42	269	2.23	2.99	26	11.6
G61	(0.2, 60, 0.2)	22.2	6.19	104	1.38	46	0.55	4.28	-	13.6
G62	(0.2, 60, 0.2)	22.2	7.82	201	1.73	93	1.41	5.47	-	9.7
G63	(0.2, 60, 0.2)	22.2	9.42	287	2.09	162	1.92	4.26	35	3.5
G64	(0.2, 60, 0.2)	22.2	11.15	447	2.47	269	2.82	3.78	30	3.8
G65	(0.2, 80, 0.2)	22.2	5.99	77	1.33	42	0.32	2.80	24	7.7
G66	(0.2, 80, 0.2)	22.2	7.82	193	1.73	93	1.27	4.93	-	16.9
G67	(0.2, 80, 0.2)	22.2	8.68	222	1.92	127	1.24	3.52	24	2.7
G68	(0.2, 80, 0.2)	22.2	11.35	472	2.52	283	2.55	3.24	-	9.9



TABLE V.3.H Experimental Results on Aeration of Sulphite System  
in a Plunging Jet Reactor with Annular Jets.

Liquid volume -  $0.9 \text{ m}^3$ , Jet angle -  $90^\circ$ , Jet length -  $6.35 \times 10^{-2} \text{ m}$ ,  
 $\text{SO}_3^{=}$  concentration -  $> 0.06 \text{ kmol/m}^3$ ,  $\text{Co}^{++}$  concentration -  $4 \times 10^{-6} \text{ kmol/m}^3$   
 Liquid temp.  $20 \pm 2^\circ \text{C}$

Run	Nozzle Outer Dia. mm.	Nozzle Inner Dia. mm.	Jet Velocity m/s	Measured Power W	Jet Power W	$\text{O}_2$ Transfer Rate <sup>a</sup> kg/s $\times 10^{-4}$	Aeration Efficiency <sup>b</sup> kg $\text{O}_2$ /kW h	Exp. Error $\pm$ %
H01	19.7	15.9	10.4	93	60	1.35	8.15	4.7
H02	19.7	15.9	15.76	237	208	2.33	4.02	6.1
H03	29.2	25.4	10.27	111	88	0.63	2.57	15.6
H04	29.2	25.4	15.06	332	279	2.24	2.89	28.6
H05	29.2	25.4	15.46	335	302	2.88	3.43	0.7
H06	33	25.4	5.50	60	29	0.60	7.37	41.1
H07	33	25.4	9.49	235	149	1.6	3.86	3.7
H08	38.1	25.4	3.78	64	17	0.10	2.15	19.24
H09	38.1	25.4	5.84	178	63	0.85	4.87	8.2
H10	38.1	25.4	6.39	254	82	1.21	5.3	5.1
H11	38.1	25.4	7.92	404	157	1.96	4.5	7.7
H12	38.1	25.4	7.81	281	151	1.96	4.7	5.2

<sup>a</sup> Measured (total) oxygen transfer rate can be calculated by adding to  
 tabulated value  $(3.63 \times 10^{-6} + 1.31 \times 10^{-5} l_j (d_{jo} + d_{ji}))$   
 where  $l_j$ ,  $d_{ji}$ ,  $d_{jo}$  are in m.

<sup>b</sup> Based on jet power.

TABLE V.3.I                      Experimental Results for the Effect of Jet  
   Length on Oxygen Transfer

Cylindrical nozzle dia. 22.2 mm

Annular nozzle: Inner dia. - 25.4 mm                      Jet angle - 90°  
                         Outer dia. - 33. mm                      Liquid temp. 23 ± 1 °C

Run	Nozzle	Jet Length	Jet Velocity	Oxygen Transfer Rate <sup>a</sup>
		m	m/s	kg/s x 10 <sup>-4</sup>
I01	Cylindrical	( 0.046	11	1.35
I02		( 0.076	11	1.83
I03		( 0.102	11	2.35
I04		( 0.152	11	4.16
I05		( 0.406	11	3.32
I06		( 0.508	11	3.88
I07		( 0.700	11	4.49
I08	Annular	( 0.025	11.2	3.71
I09		( 0.102	11.57	3.28
I10		( 0.203	11.21	3.89
I11		( 0.406	11.45	4.10

<sup>a</sup> Oxygen transfer due to entrainment.



A Computer Print Out for the Experimental Results  
on Re-aeration of Biological System

Important Notations:

X is time in seconds

Y is per cent dissolved oxygen concentration

K is oxygen transfer coefficient in  $1/s$

S.E. is standard error

D.F. is degrees of freedom

M.S. is mean square

E(Y) is estimated value of Y.

## TIME NOW MEASURED IN MINUTES

$$Y = A + B \cdot R^{**}X \quad R = \text{EXP}(-K)$$

	PARAMETER	S.E.	CORRELATIONS
1	R	0.74943	1.0000
2	B	-0.49724	-0.4085 1.0000
3	A	0.75922	0.8909 -0.7031 1.0000
	K	0.28845	0.01151

	X	Y	E(Y)	WTD. RES.	S.E.
0.0000	0.2700	0.2620	0.0080	0.0054	
0.5000	0.3300	0.3288	0.0012	0.0037	
1.0000	0.3800	0.3866	-0.0066	0.0028	
1.5000	0.4300	0.4366	-0.0066	0.0026	
2.0000	0.4700	0.4800	-0.0100	0.0027	
2.5000	0.5100	0.5175	-0.0075	0.0028	
3.0000	0.5600	0.5499	0.0101	0.0028	
3.5000	0.5800	0.5780	0.0020	0.0028	
4.0000	0.6130	0.6024	0.0106	0.0027	
5.0000	0.6500	0.6417	0.0083	0.0024	
6.0000	0.6710	0.6711	-0.0001	0.0024	
7.0000	0.6910	0.6932	-0.0022	0.0027	
8.0000	0.7060	0.7097	-0.0037	0.0031	
9.0000	0.7200	0.7221	-0.0021	0.0036	
10.0000	0.7300	0.7314	-0.0014	0.0042	

RESIDUAL N.S.      0.000052      D.F.      12

TABLE V.4.J Experimental Results on Re-aeration of De-oxygenated Biological System

Run	Nozzle Dia. mm.	Jet Liquid Flow Rate $m^3/s \times 10^{-3}$	Jet Velocity m/s	Barometric Pressure mm Hg	Liquid Temp. °C	Jet Power W	Equilibrium $O_2$ Saturation Conc. %	Respiration Rate $kg/s \times 10^{-5}$	$O_2$ Transfer Coeff.(K) <sup>b</sup> $1/s \times 10^{-2}$	$O_2$ Transfer Rate $kg/s \times 10^{-4}$	Aeration Efficiency $kgO_2/kW h$	Exp. Error ±%
J01	12.7	1.47	11.64	744	8	100	66	-	0.63	0.68	2.45	17.4
J02	12.7	2.03	16	750	8	259	77.5	-	1.14	1.23	1.71	2.9
J03	12.7	2.10	16.61	756	24	290	64	1.6	1.13	0.83	1.03	2.8
J04	12.7	2.10	16.61	744	8	290	79	-	1.13	1.22	1.51	6.3
J05	12.7	2.40	18.89	750	8	427	83	-	2.24	2.41	2.04	6.4
J06	12.7	2.39	18.90	760	25	427	98	-	1.84	1.32	1.11	7.8
J07	12.7	2.83	22.37	756	24	708	96	1.1	1.78	1.31	0.67	15.1
J08	12.7	3.06	24.14	760	25	890	100	1.4	2.74	1.97	0.80	10.
J09	12.7	3.11	24.56	756	24	938	100	-	2.25	1.66	0.64	15.
J10	12.7	3.37	26.58	757	24	1189	100	1.2	2.49	1.84	0.56	19.4
J11	12.7	3.51	27.72	750	7.5	1348	82.5	-	2.97	3.24	0.86	4.
J12	12.7	3.65	28.83	760	25.	1517	100	1.3	5.68	4.07	1.00	24.
J13	12.7	3.74	29.55	756	25.2	1633	100	2.2	3.53	2.53	0.56	37.
J14	22.2	2.65	6.84	755	27.5	62	18	4.7	1.51	1.02	6.0	26.4
J15	22.2	2.95	7.60	755	27.5	85	29	4.7	1.83	1.24	5.25	-
J16	22.2	3.51	9.06	756	28.	144	46	-	1.29	0.86	2.16	9.4
J17	22.2	3.56	9.18	755	26.	150	96	4.5	2.35	1.65	4.0	6.2
J18	22.2	3.96	10.21	755	29	206	100	-	3.89	2.55	4.45	14.6
J19	22.2	4.28	11.05	756	28	261	75	3.2	2.93	1.96	2.7	16.6
J20	22.2	4.44	11.45	755	26	291	100	3.6	1.79	1.26	1.56	4.5
J21	22.2	4.55	11.74	755	26	313	100	5.	4.26	2.99	3.44	10.7
J22	22.2	4.73	12.21	755	26	353	100	4.65	4.22	2.97	3.03	6.2
J23	22.2	4.98	12.84	756	28	410	90	3.18	1.98	1.33	1.17	13.

a Respiration rate in nearly quiescent tank liquid - after the termination of aeration.

b Oxygen transfer coefficient (K) at the liquid temperature.

c Oxygen transfer rate - corrected to 20°C and 760 mm Hg pressure.

d Aeration efficiency based on jet power.



TABLE V.4.J. (continued)

Run	Nozzle Dia. mm.	Jet Flow Rate $\text{m}^3/\text{s} \times 10^{-3}$	Jet Velocity m/s	Barometric Pressure mm Hg.	Liquid Temp. $^{\circ}\text{C}$	Jet Power W	Equilibrium $\text{O}_2$ Saturation Conc. %	Respiration Rate $\text{kg/s} \times 10^{-5}$	$\text{O}_2$ Transfer Coeff. (K) $\text{l/s} \times 10^{-2}$	$\text{O}_2$ Transfer Rate $\text{kg/s} \times 10^{-4}$	Aeration Efficiency $\text{kg O}_2/\text{kW h}$	Exp. Error $\pm \%$
J24	28.6	2.65	4.14	760	27	35	60	1.1	0.36	0.25*	2.57	10
J25	28.6	2.83	4.42	760	25.5	28	73	0.9	0.48	0.34	4.45	8.2
J26	28.6	3.26	5.09	760	24.	42	70	-	0.38	0.28	2.4	12
J27	28.6	3.37	5.25	760	27	46	72	1.6	0.52	0.36	2.78	6.7
J28	28.6	4.12	6.43	760	27.2	85	96	1.6	1.06	0.72	3.05	14.4
J29	28.6	4.16	6.5	760	23	88	90	-	2.09	1.58	6.46	8
J30	28.6	4.66	7.27	760	27.2	123	99	1.4	1.87	1.27	3.73	9
J31	28.6	4.91	7.66	760	23	144	100	-	2.52	1.90	4.77	15
J32	28.6	5.01	7.82	760	23	153	100	-	2.65	2.	4.69	7
J33	28.6	5.01	7.82	760	27.2	153	98	1.4	2.29	1.56	3.68	5.4
J34	38.1	3.06	2.68	760	23.5	11	46	-	0.79	0.59	19.2	12.
J35	38.1	3.91	3.44	760	25	23	75	1.1	0.94	0.68	10.56	5.
J36	38.1	4.44	3.9	760	23.5	34	87	2.0	1.01	0.76	8.05	3.6
J37	38.1	5.04	4.43	760	25.	49	90	1.1	1.41	1.01	7.38	6.
J38	38.1	5.08	4.46	760	23	50	86	2.0	0.99	0.75	5.36	4.9

e Experimental error within 95% confidence range. For example, for Run J01 the oxygen transfer coefficient (K) is  $6.3 \times 10^{-3} \text{ l/s}$  and its standard error is  $5.34 \times 10^{-4}$  with 33 degrees of freedom. The value of t at 5% probability and 33 degrees of freedom is 2.04. Therefore error

$$= \frac{5.34 \times 10^{-4} \times 2.04 \times 100}{6.30 \times 10^{-3}} = \pm 17.4\%$$

\* Oxygen transfer rate by steady state method (Equation 6.11, page 90.) is  $0.25 \times 10^{-4} \text{ kg/s}$ .



TABLE V.5.K Experimental Results on Continuous Biological Reactor with 28 Hours Retention Time

Run K01, Nozzle diameter ~ 22.2 mm, Jet velocity ~ 11 m/s

Day	C O D (mg/l <sub>t</sub> . x 10 <sup>4</sup> )			B O D (mg/l <sub>t</sub> .x 10 <sup>4</sup> )			Suspended Solids (mg/l <sub>t</sub> . x 10 <sup>4</sup> )		Dry Matter (%)			
	Total		Liquid <sup>a</sup>		Total				Total		Liquid <sup>a</sup> Product	
	Feed	Product	Feed	Product	Feed	Product	Feed	Product	Feed	Product		
1	5.44	4.88	2.4	0.9	3.1	1.25	2.32	1.84	4.5	4.39	2.6	2.1
2	4.22	3.2	-	0.66	2.5	1.55	1.5	1.8	4.23	4.5	-	2.1
5	6.16	3.36	2.9	-	3.7	1.98	2.78	2.2	4.85	4.15	0.1	-
6	8.62	5.92	2.7	1.2	2.5	-	-	-	4.26	4.34	0.9	0.9
7	8.16	4.56	-	0.76	3.3	1.22	3.36	2.72	4.32	4.22	-	-
12	8.38	3.28	3.3	0.8	3.05	1.13	2.28	3.2	5.05	5.35	-	-
13	7.74	5.2	2.06	0.98	3.68	1.1	2.7	2.52	4.68	5.02	-	-

<sup>a</sup> Tabulated values have been multiplied by dilution factor 10.

TABLE V.5.1

Experimental Results on Continuous Biological Reactor with 10 Days Retention Time

Run L01, Nozzle diameter - 38.1 mm, Jet Velocity - 2.33 m/s, Liquid feed rate - 0.91 lt/0.5 h, Liquid volume - 0.87 m<sup>3</sup>

Day	C O D (mg/lt. x 10 <sup>4</sup> )				B O D (mg/lt. x 10 <sup>4</sup> )				Suspended Solids (mg/lt. x 10 <sup>4</sup> )		Dry Matter (%)			
	Total		Liquid <sup>a</sup>		Total		Liquid <sup>a</sup>		Feed	Product	Total		Feed	Product
	Feed	Product	Feed	Product	Feed	Product	Feed	Product			Feed	Product		
1	3.46 3.68	-	2.5 2.2	-	2.4	-	1.6	-	1.97	-	1.9	-	-	-
2	-	1.22 1.06	-	0.9* 1.6*	-	0.31	-	-	-	1.22	-	0.6*	-	-
5	3.7 3.38	2.76 2.68	2.11 1.9	-	-	-	1.2	2.16	1.43	0.76	-	-	-	-
6	3.16 3.14	1.24 1.19	1.6 1.6	0.6*	1.9	0.45	-	-	1.39	0.71	1.1	-	-	-
7	-	0.95 0.89	-	0.4*	-	-	-	0.62	-	0.3	-	-	-	-
12	-	0.76 0.75	-	0.35 0.36	0.075	-	-	0.22	-	0.82	-	-	-	-
13	3.38 3.36	0.75 0.66	1.7 1.8	0.27 0.29	-	-	1.18	0.26	1.74	0.69	0.7	0.45	-	-
14	3.1 3.3	0.85 0.85	2.1 2.1	0.33 0.43	-	-	1.0	0.45	1.25	0.01	-	-	-	-

<sup>a</sup> Tabulated values for feed and product have been multiplied by dilution factors 10 and 5 respectively; however product values marked \* have been multiplied by 10.

TABLE V.5.L (continued)

Day	C O D (mg/lt. x 10 <sup>4</sup> )				B O D (mg/lt. x 10 <sup>4</sup> )				Suspended Solids (mg/lt. x 10 <sup>4</sup> )				Dry Matter (%)			
	Total		Liquid <sup>a</sup>		Total		Total		Total		Total		Total		Total	
	Feed	Product	Feed	Product	Feed	Product	Feed	Product	Feed	Product	Feed	Product	Feed	Product	Feed	Product
19	3.75 3.96	1.99 2.26	2.2 2.0	0.48 0.40	2.0	0.43	1.44 0.84	1.34 1.1	2.0	-	-	-	-	-	-	-
20	3.32 3.44	2.42 2.16	2.0 2.1	0.36 0.32	-	-	1.64 1.00	1.52 1.60	-	2.49	1.2	0.65				
21	4.28 3.98	2.36 2.28	2.2 2.2	0.45 0.40	-	-	0.92 1.12	1.32 1.40	1.7	1.97	-	-				
22	-	2.10 2.18	-	0.50 0.51	-	-	-	1.52 1.52	-	1.15	-	0.6				
23	3.76 3.74	2.45 2.27	2.2 2.0	0.5 0.45	-	-	1.33 1.23	1.47 1.27	1.22	1.44	1.5 0.8	0.45 0.80				
26	3.64 3.86	2.67 2.94	2.3 2.1	0.6 0.7	-	-	1.03 1.23	1.27 1.40	-	1.72	0.8	0.9				
27	3.41 3.15	2.0 2.1	2.0 2.1	0.65 0.55	1.75	0.95	-	1 1.03	1.65	1.72	0.9	0.95				
30	3.82 3.94	1.69 1.35	2.0	0.43 0.43	-	-	1.32 1.52	1 0.9	1.81	1.48	-	1.0				



TABLE V.5.M      Daily Variations (from Continuous Records) in Liquid Temperature, Dissolved Oxygen Concentration and Ambient Temperature in Continuous Biological Reactor, at 28 Hours Retention Time.

Day	Temperature (°C)		Dissolved O <sub>2</sub> Concentration % Saturation	Remarks
	Ambient	Liquid		
1	2	22-25	0-43 (1% for 15 min, 0% for 15 min.) <sup>b</sup>	45 minutes aeration, and 15 minutes defoaming.
2	9 <sup>a</sup> (4)	23-27	0-22 (1% for 22 min, 0% for 15 min.)	
3	7	25-31	0-40 (1% for 26 min, 0% for 15 min.)	
4	7	22-31	0-62 (1% for 11 min., 0% for 15 min.)	
5	5	27-31	0-64 (1% for 8 min., 0% for 15 min.)	
6	5	26-29	0-48 (0% for 35 min.)	
7	3	27-30	0-30 (0% for 45 min.)	Plant shut down for repair and modification to spray system.
9	5	10	34-100	
10	10	29	0-68 (1% for 19 min., 0% for 15 min.)	Re-start: 45 minutes aeration and 15 minutes defoaming.
11	6	25-28	0-40 (1% for 22 min., 0% for 15 min.)	
12	6	23-29	0-72 (1% for 15 min., 0% for 15 min.)	
13	1.5	23-27	0-72 (1% for 15 min., 0% for 15 min.)	

<sup>a</sup> The bracketed value is the maximum or the minimum temperature recorded between the two days.

<sup>b</sup> 0-43 (1% for 15 min., 0% for 15 min.) means, the dissolved oxygen concentration is 1% for 15 minutes and 0% for 15 minutes during its cycle variation from 0 to 43% at the end of each hour.



TABLE V.5.N Daily Variations (from Continuous Records) in Liquid Temperatures Dissolved Oxygen Concentration and Ambient Temperature in Continuous Biological Reactor at 10 Days Retention Time.

Day	Temperature °C		Dissolved O <sub>2</sub> Concentration % Saturation	Remarks
	Ambient	Liquid		
1	7	17	68 (2) <sup>b</sup>	29 minutes aeration, 1 minute defoaming.
2	—	17	— *	
3	—	17	— *	
4	—	17	— *	
5	—	19	— *	
6	—	19	— *	
7	0	14	104	
8	2(o) <sup>a</sup>	13	104	
9	3	13	104	
10	6(-5)	16	106	
11	6	19	106	
12	2.5	15	106	
13	3	13	104	
14	6	16	104	
15	5	—	— *	
16	5	—	— *	
17	—	—	— *	
18	—	—	— *	
19	2.5	7	60(20)	
20	3	8	40(2)	

<sup>a</sup> The bracketed value is the maximum or the minimum temperature recorded between the two days.

<sup>b</sup> The dissolved oxygen concentration drops to bracketed value during defoaming.

\* Dissolved oxygen meter probe was found faulty.

TABLE V.5.N (continued)

Day	Temperature °C		Dissolved O <sub>2</sub> Concentration % Saturation	Remarks
	Ambient	Liquid		
21	0	4	58 (26)	23 minutes aeration, 7 minutes defoaming.
22	4	6	76 (4)	
23	4	12	76(10)	
24	8	13	70(10)	
25	7.5	12	104 (68)	
26	6.4	13	104 (72)	

TABLE V.5.0

Variation in pH, Ammonia and Nitrate  
Nitrogen Concentration in Continuous  
Biological Reactor at 10 days  
Retention Time.

Day	pH	Nitrogen (mg/lt.)			
		Ammonia		Nitrate	
		Feed	Product	Feed	Product
1	7.8	1400	-	16	-
2	7.7	-	300	-	42
5	7.1	-	-	-	-
6	7.0	-	305	-	65
7	6.9	-	340	-	57
12	7.3	-	450	-	94
13	7.3	-	-	-	-
14	-	1475	640	39	136
19	-	1400	720	40	50
20	7.95	-	-	-	-
21	8.1	-	-	-	-
22	-	-	700	-	80
23	7.75	-	580	-	26
26	6.4	-	400	-	83

APPENDIX VI.

PLATES



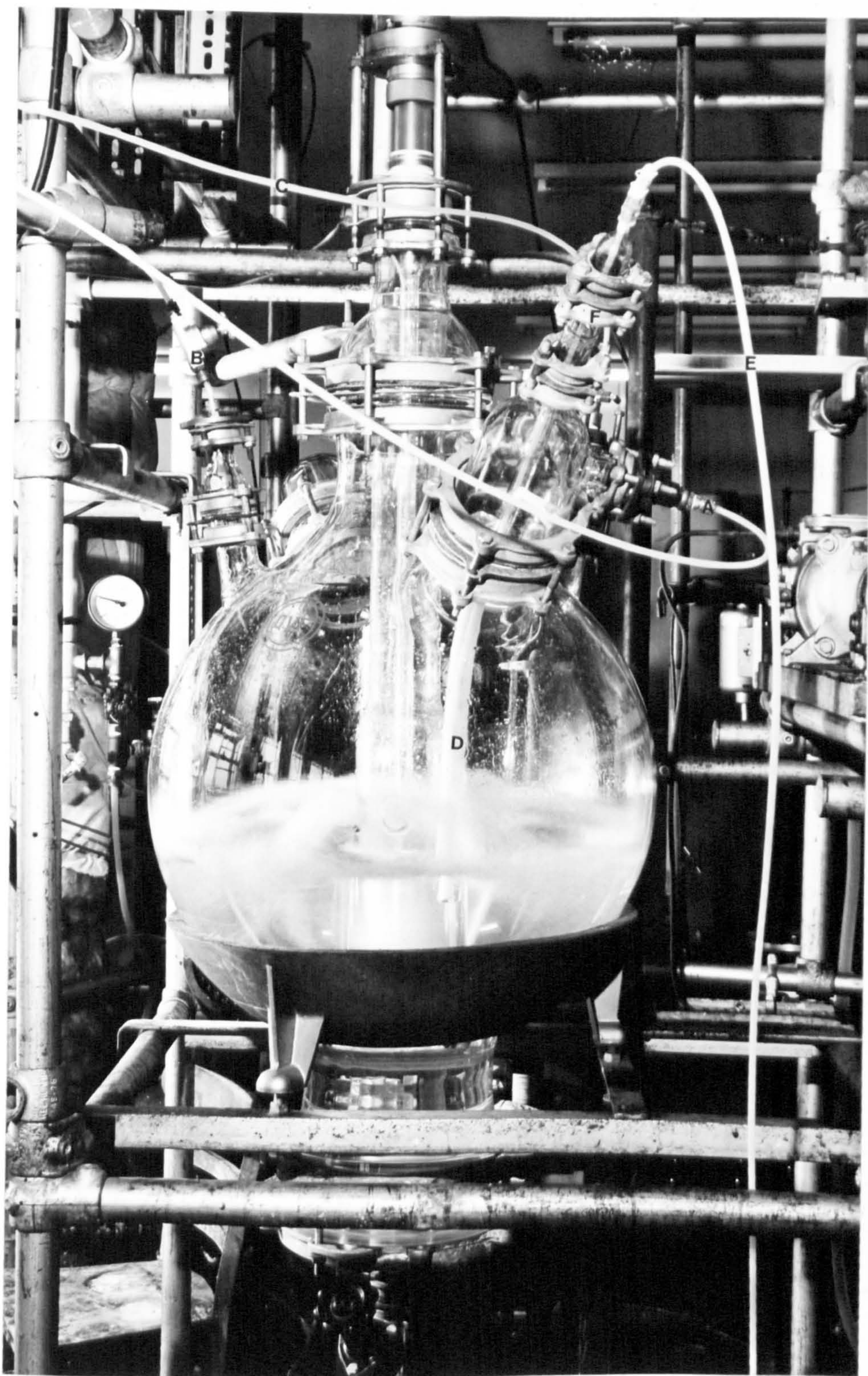


PLATE I. 100 litres QVF Vessel with mixing unit.





PLATE II. Experimental set up for plunging jet aeration experiments.



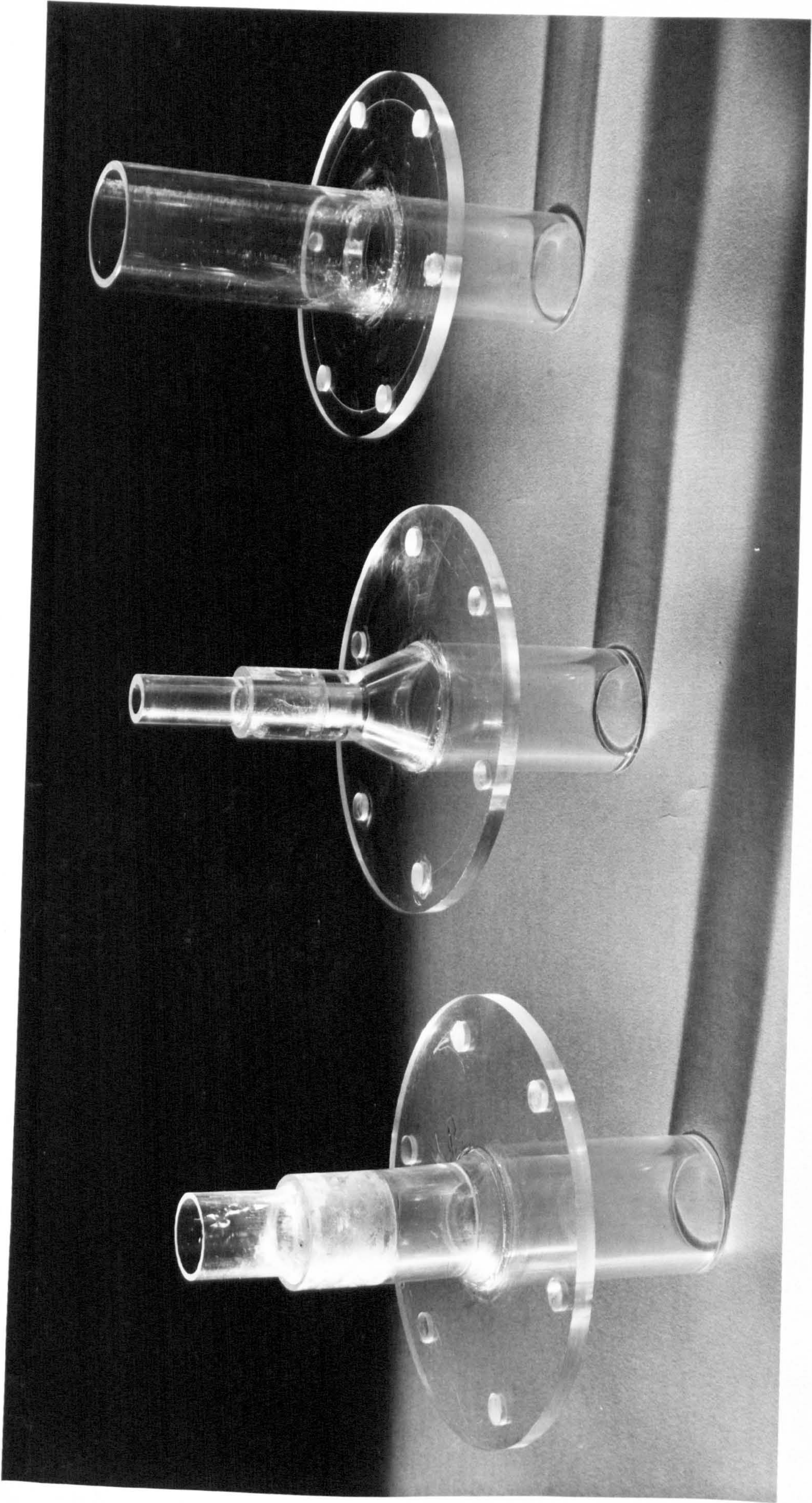


PLATE III. Typical cylindrical jet nozzle designs made of perspex.



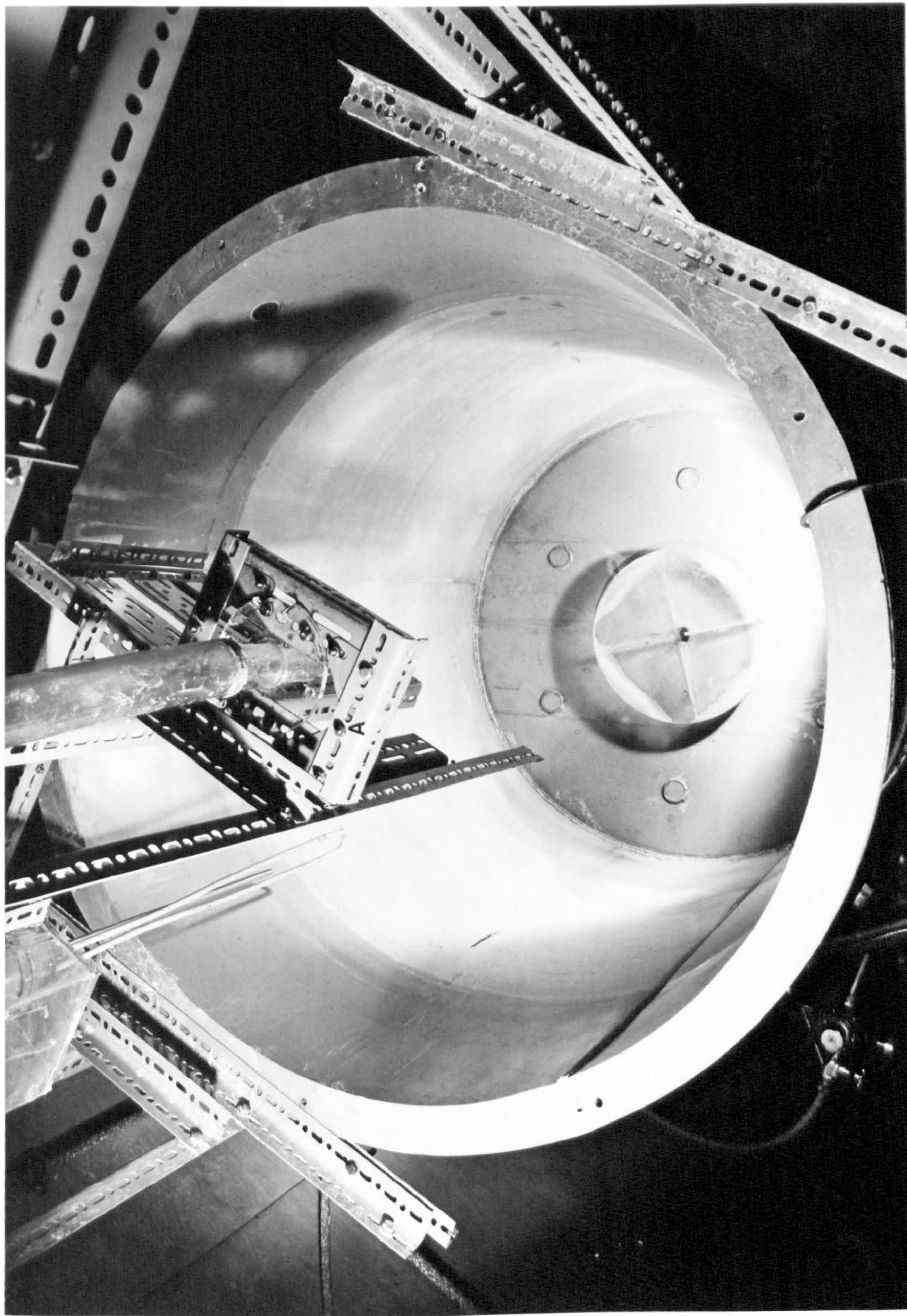


PLATE IV. Photograph showing the nozzle holder (A) and the baffle plate at the tank bottom.



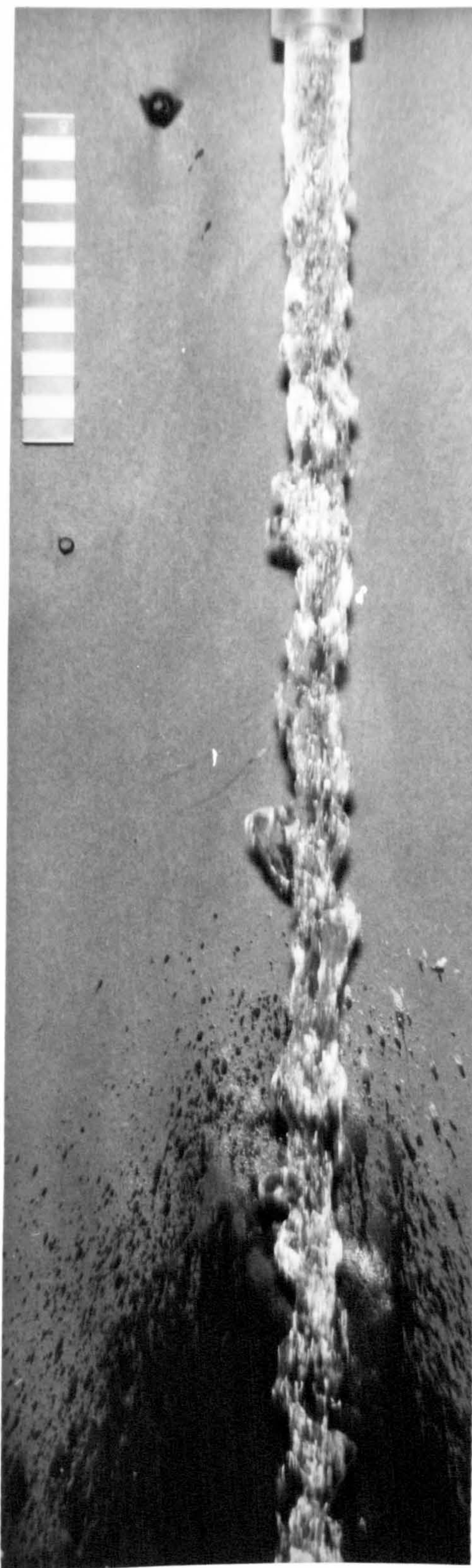


PLATE V. Low velocity jet from 28.6 mm diameter nozzle showing protuberances on the surface due to inertia and surface tension effects.

$$V_j = 3.15 \text{ m/s}$$

$$We = 6.$$



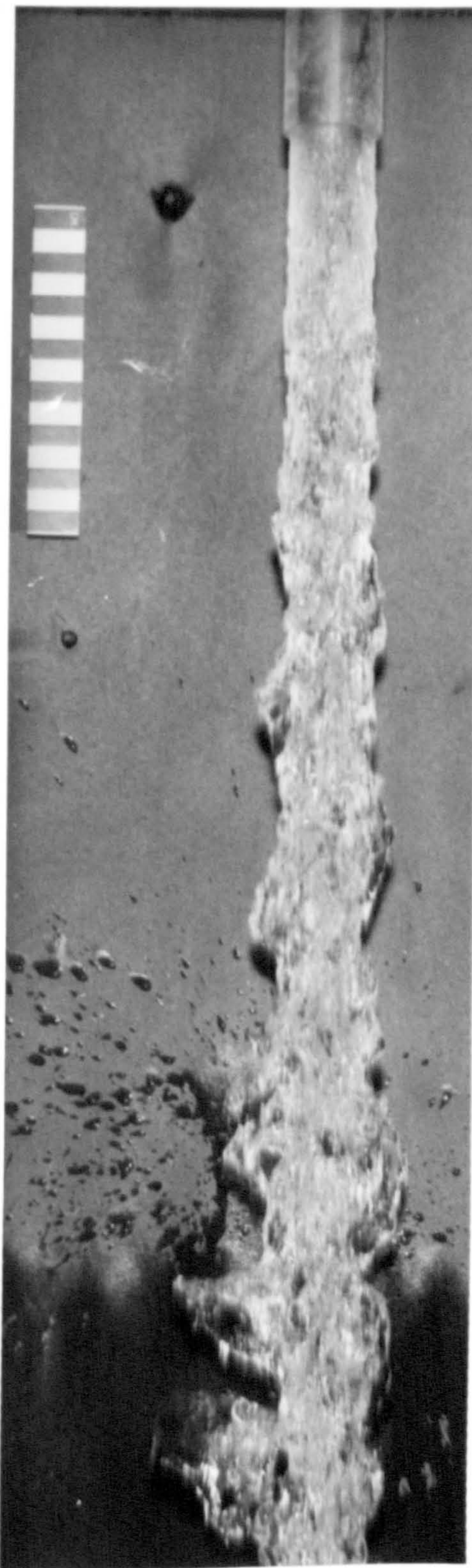


PLATE VI. Jet issuing from 38.1 mm diameter nozzle -  
spreading of jet is ill-defined

$$V_j = 4.25 \text{ m/s}$$

$$We = 11$$



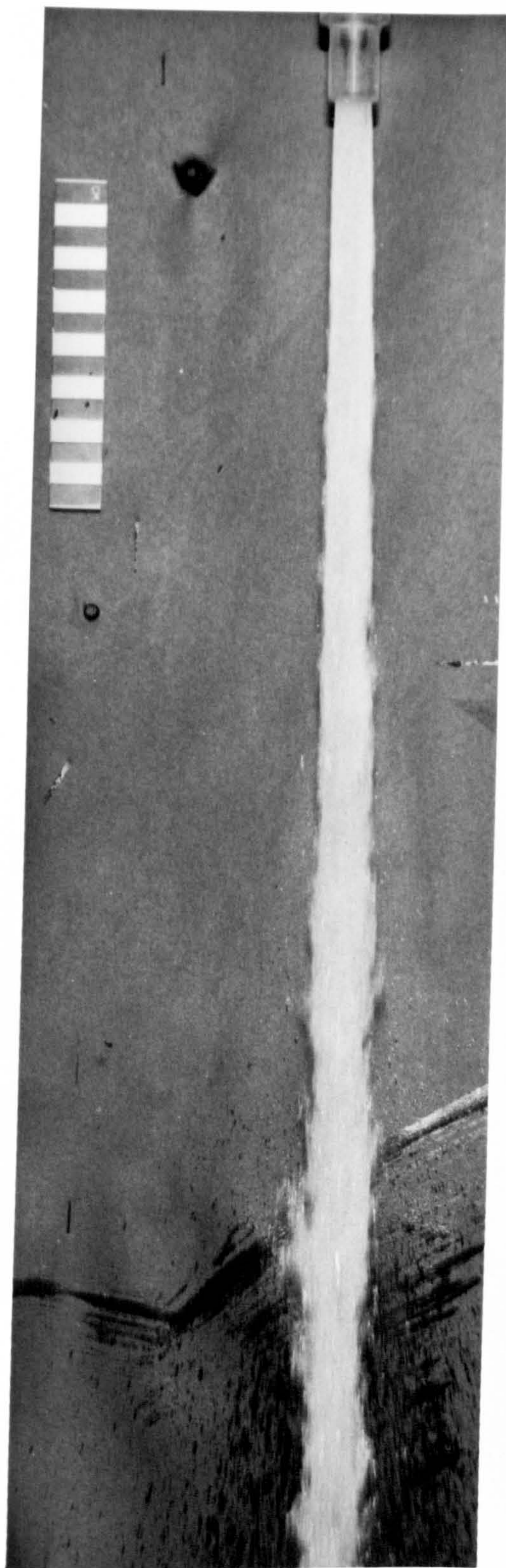


PLATE VII. High velocity jet issuing from 12.7 mm diameter nozzle. Jet spreads uniformly due to air friction forces and turbulence. At long jet length train of drops appears from the jet surface.

$$V_j = 31.5 \text{ m/s} \quad We \gg 10$$



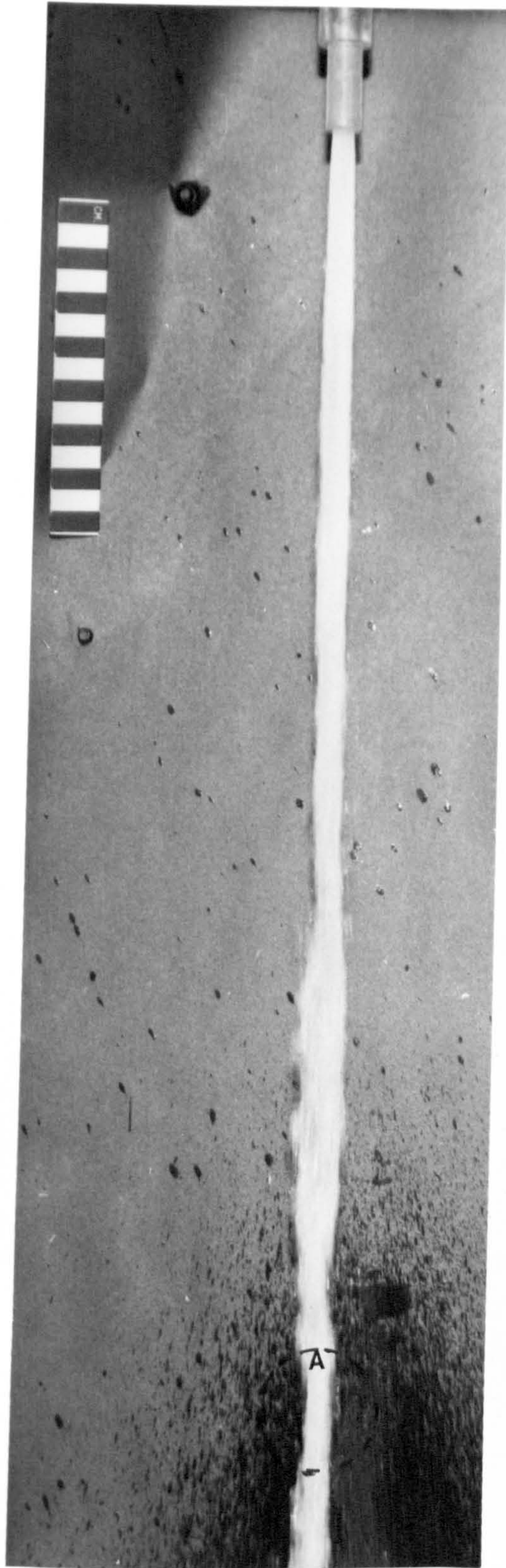


PLATE VIII. High velocity jet issuing from 9.5 mm diameter nozzle. Jet spreads due to air friction forces and turbulence. Circle A shows the central core of the jet.

$$V_j = 23.5 \text{ m/s}$$

$$We \gg 10$$



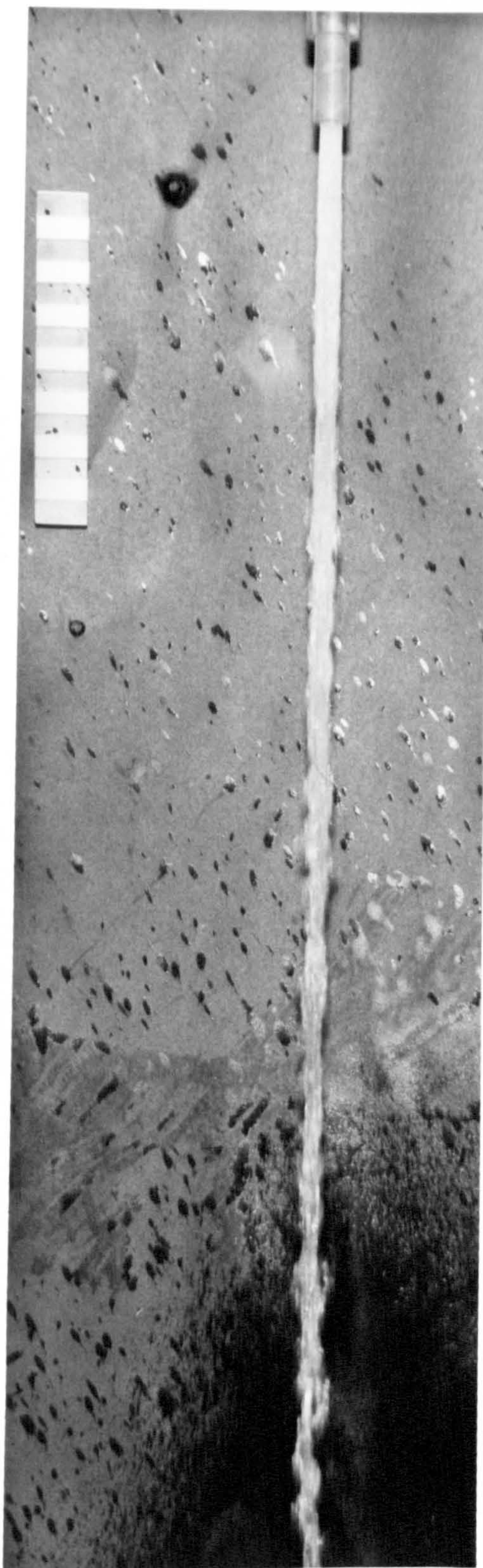


PLATE IX. High velocity jet issuing from 9.5 mm diameter nozzle. Photographs clearly show the superimposition of disturbances on the central core of the jet.

$$V_j = 9.3 \text{ m/s} \quad We \gg 10$$



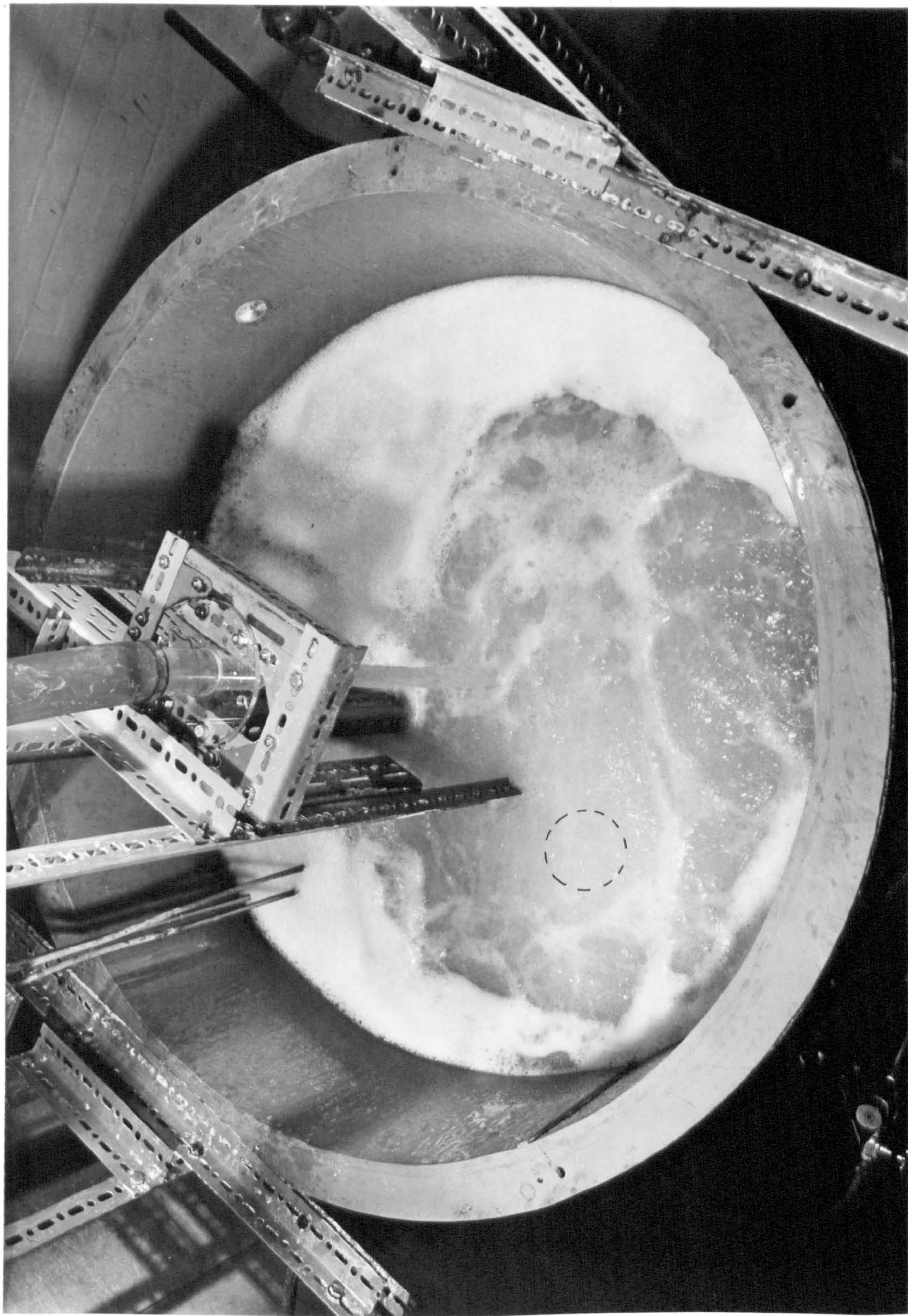


PLATE X. Photograph showing vertical plunging jet and the bubbling region circled by dotted line.



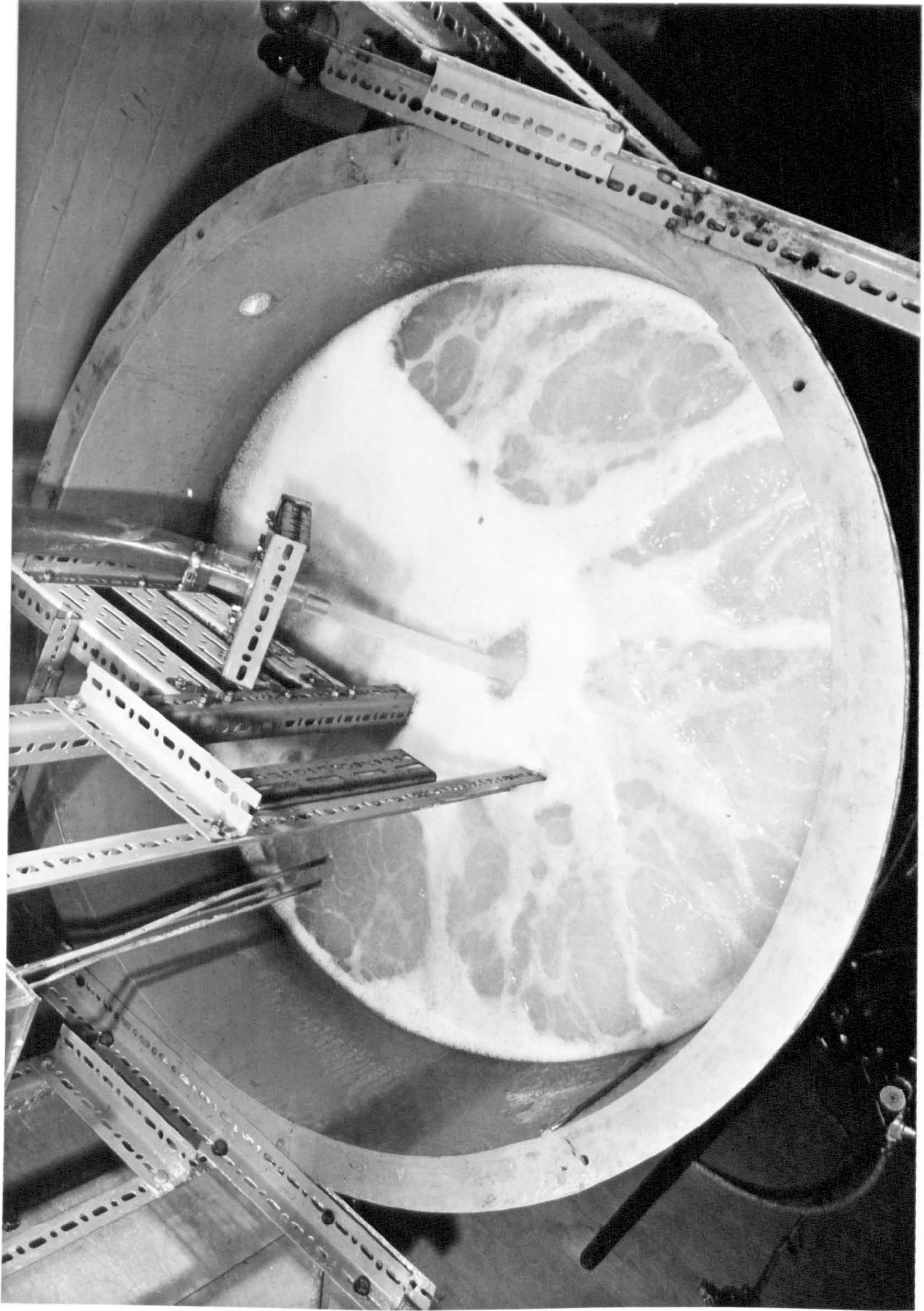


PLATE XI. Photograph showing the adjustment of angular jet and the surface waves in the tank liquid.



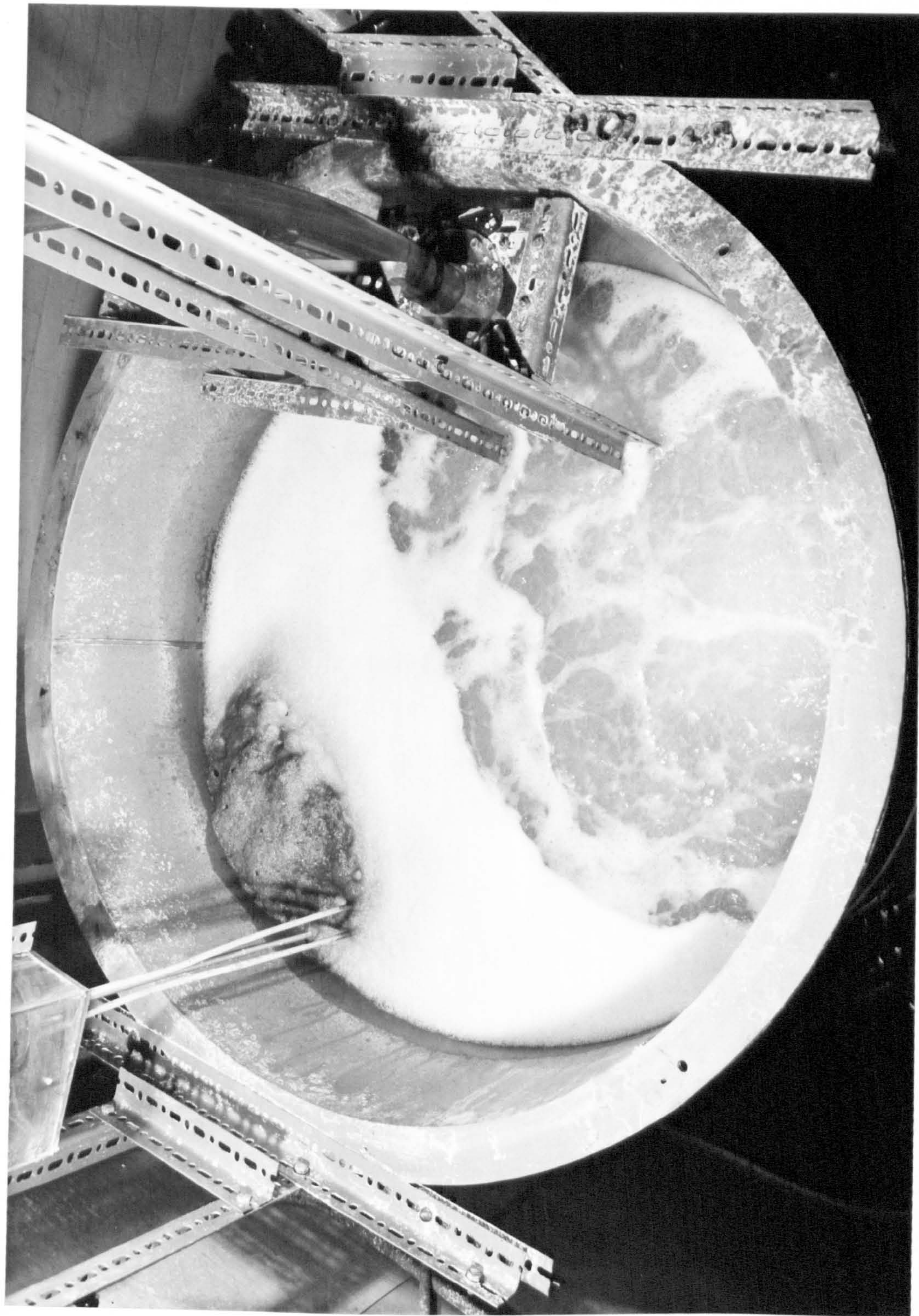


PLATE XII. Photograph showing the vertical off centre jet and surface waves in the tank.



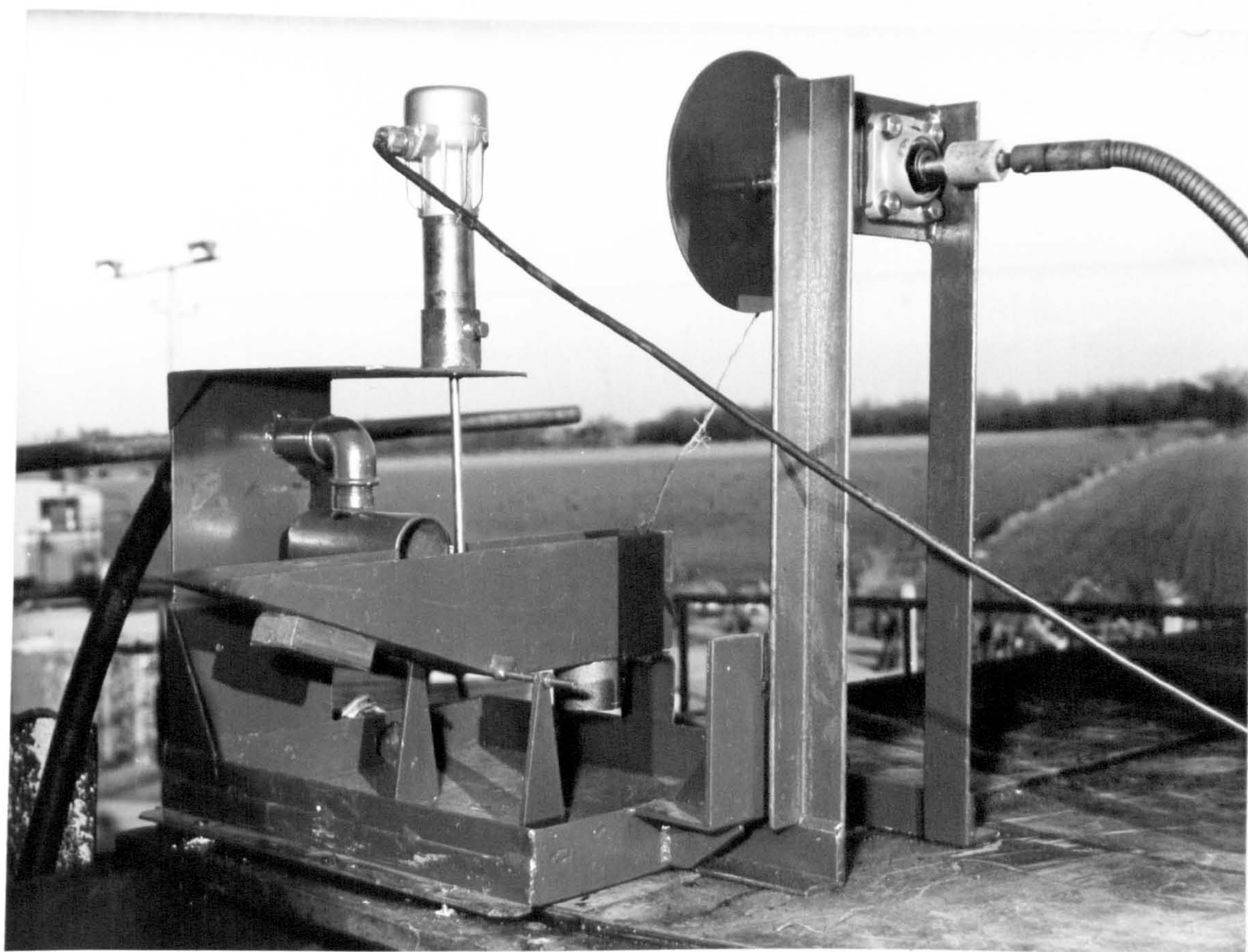


PLATE XIII.

Tipping bucket.



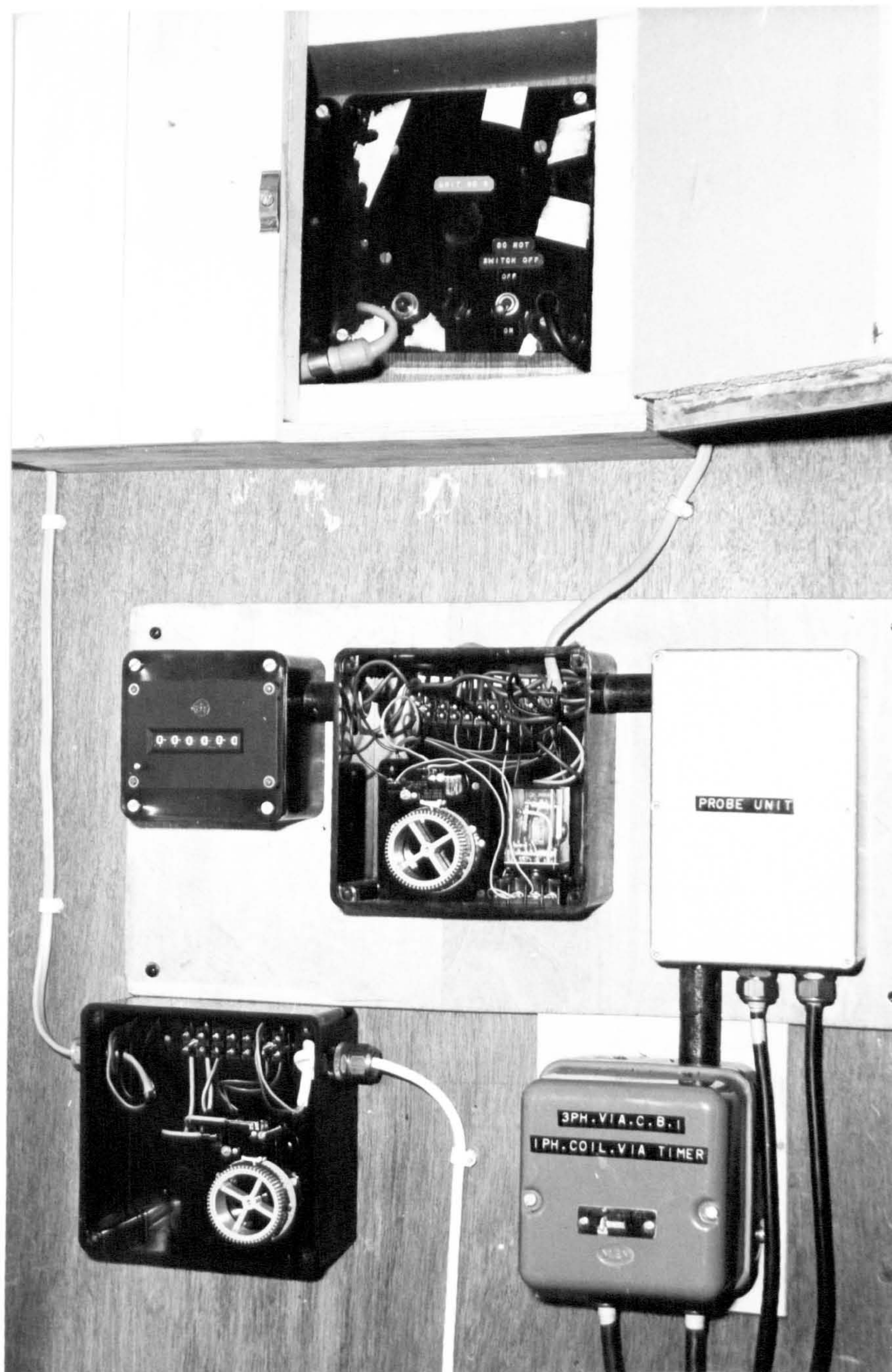


PLATE XIV. Control unit for foam control and continuous feeding system showing drum timers and probe unit.